TAMPEREEN TEKNILLINEN YLIOPISTO
TAMPERE UNIVERSITY OF TECHNOLOGY

Samuli Ollila

Lateral Pressure in Lipid Membranes and Its Role in Function of Membrane Proteins

Julkaisu 937 • Publication 937

Tampere 2010

Tampereen teknillinen yliopisto. Julkaisu 937
Tampere University of Technology. Publication 937

Samuli Ollila

Lateral Pressure in Lipid Membranes and Its Role in Function of Membrane Proteins

Thesis for the degree of Doctor of Science in Technology to be presented with due permission for public examination and criticism in Sähkötalo Building, Auditorium S4, at Tampere University of Technology, on the 26th of November 2010, at 12 noon.

Tampereen teknillinen yliopisto - Tampere University of Technology
Tampere 2010

Supervisor	Professor Ilpo Vattulainen Department of Physics Tampere University of Technology Tampere, Finland
Pre-examiners	Professor Olle Edholm Department of Theoretical Physics Royal Institute of Technology (KTH) Stockholm, Sweden
	Professor Derek Marsh Max Planck Institute for Biophysical Chemistry Göttingen, Germany
Opponent	Professor Robert Cantor Department of Chemistry Dartmouth College Hanover, NH, USA

ISBN 978-952-15-2480-6 (printed)
ISBN 978-952-15-2500-1 (PDF)
ISSN 1459-2045

ABSTRACT

A very important component of cells is the cell membrane separating the contents of a cell from the outside world. The cell membrane contains membrane proteins which, for example, regulate permeation of molecules through the cell membrane. This regulation is essential for functions of cells. Meanwhile, increasing experimental evidence shows that there is a connection between physical properties of the cell membrane and membrane protein functionality. However, this connection is not fully understood. One hyphothesis is that the so-called lateral pressure profile arising from the inhomogeneous nature of a lipid bilayer would regulate membrane protein functionality. The main difficulties in testing this hyphothesis are that experimental measurements of the lateral pressure and the cross sectional area profiles are very difficult to carry out.

This issue is considered in this thesis by calculating theoretical lateral pressure profiles of lipid bilayers, using data obtained via molecular dynamics simulations. The results are then compared to available experimental data. The insight gained in this manner is used to make predictions for membrane protein functionality.

The results presented in this thesis suggest that the theoretical pressure profiles are in relatively good agreement with the available experimental results, and that changes in lipid composition can have a major effect on the pressure profile of a lipid bilayer. What is more, the results suggest that these changes have a significant influence on membrane protein functionality. We also show that the shape of a protein embedded in a membrane, especially in the interfacial region between hydrophobic and hydrophilic regions, is a very important player in gating of mechanosensitive channels.

Preface

This thesis has been conducted in Biological and Soft Matter Physics Group in Tampere University of Technology. The thesis was done during the transition period when the group was moving from the department of physics in Helsinki University of Technology to Tampere, so in practice I have worked in both departments. I am thankful to the leaders and personnel of both departments for allowing this flexible arrangement.

I am thankful to professor Ilpo Vattulainen for giving me the opportunity to work in this very interesting field. Next I would like to thank Marja Hyvönen and Perttu Niemelä for teaching me the art of molecular dynamics simulations of lipid bilayers. I am also grateful to professor Siewert-Jan Marrink and his MD group in the university of Groningen where I spent the most useful time during my PhD studies. Especially I would like to thank Martti Louhivuori and Jelger Risselada for extremely fruitful collaboration.

I would like to thank Tomasz Rog, Emma Terämä, Emppu Salonen, Erik Lindahl and Mikko Karttunen for their help in the publications in this thesis. I am also thankful to Derek Marsh and Olle Edholm whose comments during the pre-examination process improved the thesis.

In addition to this I would like to thank all my other collaborators, present and previous members of Biological and Soft Matter Group at TTY, and Computational Soft Matter Research Group at TKK for all scientific and non-scientific discussions. Especially I want to acknowledge Antti Lamberg for several important discussions and Teemu Murtola for providing a figure for the thesis.

The work was financed by the The Finnish National Graduate School in Nanoscience.

The Finnish IT center for science (CSC) and the HorseShoe (DCSC) supercluster facility at the University of Southern Denmark are acknowledged for providing the computing resources. The Finnish cultural foundation and Väisälä foundation are acknowledged for travel funding.

Finally I want to thank all my friends and Anni for support.

Helsinki, November 2010

Samuli Ollila

Contents

Preface **5**

Contents **7**

List of Publications **9**

Author's contribution **11**

List of Abbreviations **13**

1 Introduction **15**

2 Background **18**

2.1 Physical properties of lipid bilayers 18

2.2 Elastic properties of lipid bilayers 22

2.3 Lateral pressure profile in lipid bilayers 24

2.4 Modeling lipid bilayers using molecular dynamics simulations 28

3 Theoretical concepts **34**

3.1 Local pressure in pointwise particle models 34

3.2 Calculation of lateral pressure profile from simulations 36

3.3 Pressure tensor in planar geometry and connection to elastic properties 37

3.4 Pressure tensor and membrane protein inclusion 39

3.5 Interplay of pressure profile and membrane protein activation 40

3.6 Technical details and complications in implementation of local pressure calculation 44

4 Gauging pressure profiles **48**

5 Dependence of pressure profile on molecular composition **54**

5.1 Dependence on unsaturation level 54

5.2 Effects of different sterols in two-component membranes 56

5.3 Pressure profiles in three-component bilayers 58
5.4 Implications of anesthetics on pressure profile 60

6 Physical implications from pressure profiles 65
6.1 Elastic properties calculated from lateral pressure profile 65
6.2 Bilayer mechanical energy in protein activation 69

7 Conclusions 75

References 77

Appendix A Properties of pressure tensor in planar homogenuous bilayer in liquid phase

List of Publications

This thesis consists of an overview and of the following publications which are referred to in the text by their Roman numerals.

I Ollila, S., Hyvönen, M.T., and Vattulainen, I., Polyunsaturation in lipid membranes - dynamic properties and lateral pressure profiles, Journal of Physical Chemistry B 111, 3139-3150 (2007).

II Ollila, O. H. S., Rog, T., Karttunen, M., and Vattulainen, Role of sterol type on lateral pressure profiles of lipid membranes affecting membrane protein functionality: Comparison between cholesterol, desmosterol, 7-dehydrocholesterol and ketosterol,Journal of Structural Biology, 159,311-323 (2007)

III Niemelä, P. S., Ollila, S., Hyvönen, M. T., Karttunen, M., and Vattulainen, I., Assessing the nature of lipid raft membranes, PLoS Computational Biology 3, 304-312 (2007).

IV Terama, E., Ollila, O. H. S., Salonen, E., Rowat, A., Trandum, C., Westh, P., Patra, M., Karttunen, M., and Vattulainen, I., Influence of ethanol on lipid membranes: rrom lateral pressure profiles to dynamics and partitioning, Journal of Physical Chemistry B 112, 4131-4139 (2008).

V Ollila, O. H. S., Risselada, J., Louhivuori, M., Lindahl, E., Vattulainen, I., and Marrink, S. J., 3D Pressure field in lipid membranes and membrane-protein complexes, Physical Review Letters 102, 078101 (2009).

VI Ollila, O. H. S., Louhivuori, M., Marrink, S. J., and Vattulainen, I.,Protein shape change has a major effect on the gating energy of a mechanosensitive channel, submitted (2010)

Additionally, the author of this thesis has been a co-author in a number of other publications, which, however, are not discussed in the present thesis:

VII Kupiainen, M., Falck, E., Ollila, S., Niemelä, P., Gurtovenko, A. A., Hyvönen, M. T., Patra, M., Karttunen, M., and Vattulainen, I., Free volume properties of sphingomyelin, DMPC, DPPC, and PLPC bilayers, Journal of Computational and Theoretical Nanoscience 2, 401-413 (2005).

VIII Lahdesmaki, K., Ollila O. H. S., Koivuniemi, A., Kovanen, P. T., and Hyvonen, M. T., Membrane simulations mimicking acidic pH reveal increased thickness and negative curvature in a bilayer consisting of lysophosphatidylcholines and free fatty acids, BIOCHIMICA ET BIOPHYSICA ACTA-BIOMEMBRANES 1798, 938-946 (2010).

IX O. H. S. Ollila and I. Vattulainen, Lateral pressure profiles in Lipid Membranes: Dependence on molecular composition, in Molecular Simulations and Biomembranes: From Biophysics to Function, edited by Mark Sansom and Philip Biggin, RSCpublishing 2010

Author's contribution

The author has played an active role in all stages of the research reported in this thesis. He has ran all the simulations, performed all the analysis, and written the first version of publication I. In publications II, III, and IV the author has planned and performed all the analysis related to the lateral pressure profile. In publications II and IV the author has also written the parts which discuss lateral pressure profiles. The author had the main responsibility for the planning, execution, and writing of publications V and VI.

List of Abbreviations

PC phosphatidylcholine

PE phosphatiethanolamine

DPPC dipalmitoyl-PC

POPC palmitoyl-oleoyl-PC

DOPC dioleoyl-PC

PLPC palmitoyl-linoleoyl-PC

PAPC palmitoyl-arachidonic-PC

PDPC palmitoyl-docosahexaenoic-PC

SDPC stearoyl-docosahexaenoic-PC

DOPE di-oleoyl-PE

DMPC di-myristoyl-PC

DPPE dipalmitoyl-PE

DOPE dioleoyl-PC

DLPE di-linoleoyl-PE

DLPC di-linoleoyl-PC

POPE palmitoyl-oleoyl-PE

eth ethanol

SM sphingomyelin

PSM palmitoyl-SM

CHOL cholesterol

DESMO desmosterol

7-DHC 7-dehydrocholesterol

KETO ketosterol

MscL mechanosensitive channel with large conductance

CTP cytidine triphosphate

CG coarse-grained

MD molecular dynamics

PME Particle-Mesh Ewald

NMR nuclear magnetic resonance

DPA docosapentaenoic acid

DHA docosahexaenoic acid

GABA gamma-aminobutyric acid

FRAP fluorescence recovery after photobleaching

SPT single particle tracking

1 Introduction

Almost all living beings consist of cells. A very important component of cells is the cell membrane separating the contents of a cell from the outside world. The basic building blocks of cell membranes are lipids, which form the so called lipid bilayer, which acts as an impermeable barrier for many molecules. In most cells the cell membrane contains, in addition to lipids, also the so called cytoskeleton as well as numerous other molecules like proteins, carbohydrates and sugars. A schematic presentation of a cell membrane is shown in Fig. 1.1.

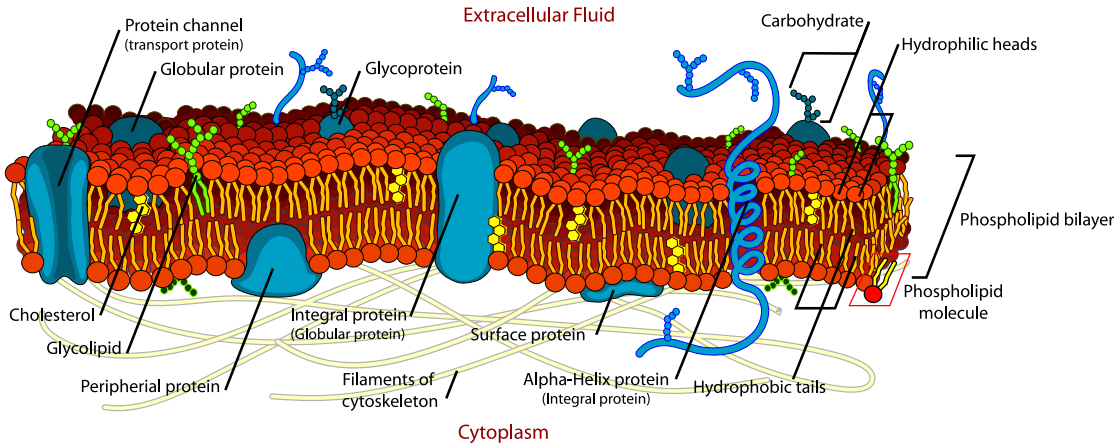

Figure 1.1: Schematic presentation of a cell and a cell membrane. Adapted from http:\\upload.wikimedia.org\wikipedia\commons\d\da\Cell_membrane_detailed_diagram_en.svg

The central component of cell membranes is a lipid bilayer, where two monolayers comprised of lipids are attached together such that the hydrophilic acyl chains of lipids face each other. Membrane proteins attached to, or associated with the lipid bilayer are responsible for many of cells' functions.

In this thesis we concentrate on lipid bilayers and their interplay with membrane

proteins. This is especially interesting because membrane proteins regulate many of the biological processes taking place in cells. For example, signaling in nerve cells is based on channel proteins which can open a pore into a cell membrane, allowing permeation of ions and changing the electrostatic potential across a cell membrane. As another example, include mechanosensitive channels can release osmotic pressure by opening themselves due to the tension in a membrane, thus releasing the osmotic gradient. Energetics of the mechanosensitive channel opening is also studied in this thesis.

In the examples above as well as in many other biological processes, proteins are the main actors. However, increasing evidence is showing that the lipid content also affects the functionality of some proteins. For example, the functionality of rhodopsin and mechanosensitive channels has been shown to depend on lipid membrane content [1, 2]. While some of these cases can be explained by specific interactions between lipids and proteins, in some situations, also the physical properties of lipid bilayers play a significant role [3, 4]. For example, membrane thickness, curvature and elastic properties have been suggested to affect membrane protein functionality [4, 5]. Mechanical coupling between membrane proteins and lipid bilayers has also been formulated in a more rigorous way by using the so called lateral pressure profile [6]. The lateral pressure profile describes an inhomogeneous stress inside a bilayer arising from hydrophobic, electrostatic and steric interactions (a more detailed description is given in section 2.3).

In this thesis, we discuss lateral pressure profiles for various bilayers using data based on molecular dynamics simulations. We also discuss their possible influence on membrane protein energetics. We show that pressure profiles are significantly different for lipid bilayers containing polyunsaturated lipids (publication I) or cholesterol (publication II) compared to saturated lipid bilayers. Furthermore, different pressure profiles are found for raft like bilayers (publication III) and bilayers containing ethanol (publication IV). We also suggest that these changes may be significant

for membrane protein energetics. To this end, in publications V and VI we develop a method which allows more rigorous studies of membrane protein energetics and apply this to consider a model of the large mechanosensitive channel. In publication VI it is shown that the shape change together with the lateral pressure profile is an important player in the gating energy as suggested by Cantor [6]. In addition, an extensive comparison to experiments is attempted.

2 Background

2.1 Physical properties of lipid bilayers

Lipid bilayers are formed of lipid molecules due to their amphiphilic nature. A typical lipid molecule has a polar hydrophilic headgroup and a nonpolar hydrophobic hydrocarbon region, see Fig. 2.1. The nonpolar hydrocarbon tail does not have

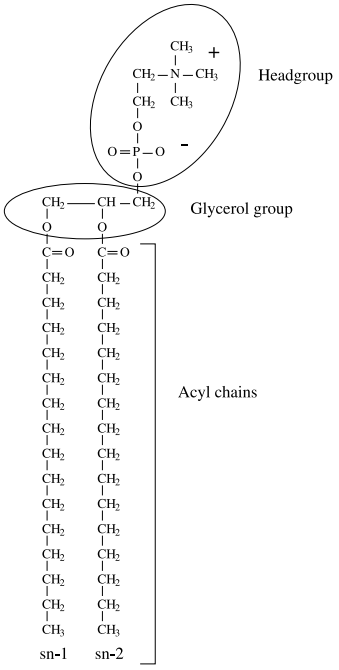

Figure 2.1: Chemical structure of dipalmitoylphosphatidylcholine (DPPC).

significant electrostatic interactions with a polar solute, such as water, in contrast to the polar part. Consequently, mixing the nonpolar part with water disturbs the structure of water, leading to an increase in free energy due to a decrease in entropy. In contrast, electrostatic interactions between water and the hydrophilic part of a lipid lead to a decrease in free energy. Due to these properties amphiphilic lipids self assemble in water such that the contact between hydrophopic chains and water

is minimized, while the contact between headgroup and water is maximized. Due to this tendency these molecules can form various different minimum energy configurations depending on the molecular properties and external conditions. Examples of typical structures are presented in Fig. 2.2.

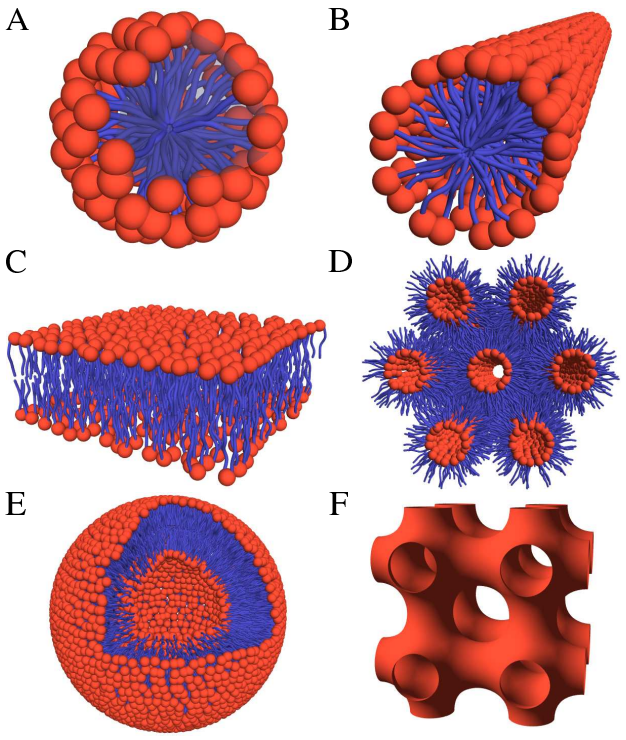

Figure 2.2: Different topological phases formed by amphiphilic lipids. Hydrophilic headgroups are red and hydrophopic tails are blue. A) A *spherical micelle* B) a *cylindrical micelle* C) a *bilayer* D) an *inverted hexagonal* phase, E) a bilayer bent to a *vesicle*, and F) a *bicubic phase*. Figure adapted from [7] (courtesy of T. Murtola).

In this thesis we concentrate on planar lipid bilayers illustrated in Fig. 2.2 C. Planar lipid bilayers have several different lateral phases, which are often divided to the *solid ordered* (gel), the *liquid ordered*, and the *liquid disordered* phases. In the solid ordered phase, lipids have 2D order in the plane of the membrane (hexagonal packing) and also significant conformational ordering of the acyl chains. In the liquid ordered phase the 2D order is lost but the chains are still ordered, and in the liquid disordered phase there is neither translational order nor lipid conformational

order.

Basic structural properties of planar lipid bilayers have been determined using mainly X-ray and neutron scattering techniques. With these techniques, relatively detailed information about thickness, area per molecule and electron density distribution of lipid bilayers have been achieved [8, 9]. All of these properties depend somewhat on the chemistry of lipid molecules forming the bilayer. For example, recent values for thickness and area per molecule for a bilayer formed of DPPC lipids in the liquid disordered phase are 2.84 nm and 0.631 $(\mathrm{nm})^2$, respectively [10].

More structural information have been achieved using deuterium nuclear magnetic resonance (^{2}H NMR) to measure the deuterium order parameters S_{CD} for carbons in hydrocarbon tails [11]. The deuterium order parameter is defined as

$$S_{\mathrm{CD}} = \frac{1}{2}\langle 3\cos^2\theta - 1\rangle, \tag{2.1}$$

where θ is the angle between the bilayer normal and the C-H bond vector, and the brackets denote an average over time and all lipids. In practice the deuterium order parameter is zero if the C-H bond vector is randomly oriented, -1/2 if it is all the time perpendicular to the membrane normal, and 1 if it is all the time parallel to the membrane normal. Thus it gives information of acyl chain ordering with respect to membrane normal. Deuterium order parameters have also been often calculated from atomistic molecular dynamics simulations and compared to experimental values. For example, Fig. 5 in publication I illustrates deuterium order parameters calculated from molecular dynamics simulations compared to experimental values for bilayers formed by lipids with a different number of double bonds. From the results two general conclusions can be drawn: the order decreases towards bilayer center, and double bonds decrease order. Further discussion can be found from publication I.

The techniques discussed above give information about static properties of lipid bilayers. However, lipids in lipid bilayers are in constant motion due to thermal

fluctuations. A great number of different timescales and characteristics are required to describe lipid bilayer dynamics completely. However, to get some view about the dynamics in membranes, one can consider the following five processes: flip-flops of molecules from one membrane leaflet to another; lateral diffusion of molecules in the bilayer plane; rotational motions of lipids; movements of hydrocarbon chains, and vertical movements of molecules leading to bilayer undulations. The timescales associated with these processes span a wide range from picoseconds to minutes, thus several experimental and theoretical methods are needed to study the different dynamical processes.

Flip-flop rates of molecules can be studied, e.g., using radioactive lipids, and the results vary between 10^{-3} and 10^{-6} 1/s per molecule [12]. Sizes and dynamics of undulations have been determined using their relation to the elastic properties of bilayers together with microscopical methods. Reported values vary from a few nanometers to ~ 10 μm for the sizes, and from less than a nanosecond to several milliseconds for the periods of the undulations [13, 14, 15]. The lateral diffusion of lipid molecules in a bilayer can be described using the lateral diffusion coefficient D [16]. The fluorescence recovery after photobleaching (FRAP), single particle tracking (SPT) and NMR techniques have been profitable methods to measure the lateral diffusion coefficient for lipid bilayers [16, 17, 18]. For the ordered gel phase, reported values vary between $D \approx 10^{-11}$ cm^2/s and $D \approx 10^{-16}$ cm^2/s, while for the disordered fluid phase, typical values are between $D \approx 10^{-7}$ cm^2/s and $D \approx 10^{-8}$ cm^2/s [16, 18].

Rotational motions of lipids and the dynamics of hydrocarbon chains can be measured by NMR techniques and through fluorescence probes. Typical time scales for the rotational dynamics of lipid molecules in a bilayer range between $\sim 10^{-11}$ and $\sim 10^{-9}$s [12].

Dynamical properties like hydrocarbon chain dynamics and lateral diffusion have

been successfully calculated also from MD simulations. The results are usually in good agreement with available experiments, see for example publication I and [19].

2.2 Elastic properties of lipid bilayers

Free energy per unit area of deformation in a lipid bilayer can be written, according to Helfrich, as [20]

$$g(c_1, c_2) = \frac{1}{2}K_A(\frac{\Delta a}{a})^2 + \frac{1}{2}\kappa(c_1 + c_2 - c_0)^2 + \bar{\kappa}c_1c_2, \tag{2.2}$$

where K_A is the area compressibility modulus, a is the area per molecule and Δa is the deformation from the equilibrium value a. κ is the bending modulus, c_0 is the spontaneous curvature, c_1 and c_2 are local principal curvatures, and $\bar{\kappa}$ is the Gaussian bending modulus. The area compressibility modulus can be measured using the micro-pipette aspiration method. Values for bilayers containing lipids with different tail lengths and a different number of double bonds in liquid disordered phase vary between 230-265mN/m [21]. The larger area stretching modulus has been found in lipid bilayers that are in solid-ordered phase, and in bilayers with cholesterol [22, 23]. On the other hand, for example insertion of alcohols has been found to decrease the stretching modulus [22, 24].

The bending modulus κ can be measured with several different techniques, but the resulting value seems to depend on technique used [25, 26]. Values for a pure bilayers in liquid disordered phase vary roughly between $(6 - 14) \times 10^{-20}$ J, while the values for bilayers in solid ordered phase or in cholesterol containing saturated bilayers are higher. Addition of alchohol into a bilayer has been found to lower also the bending modulus [24, 25]. Further, recently it has been found that cholesterol does not increase the bending rigidity of unsaturated bilayers [27, 28] but instead may even decrease bending moduli when cholesterol is embedded in a sphingomyelin bilayer [29]. Generally the bending rigidity moduli are smaller than the area stretching

moduli, which means that it is easier to bend the membrane than to stretch it.

Values for spontaneous curvatures are available for some lipids measured from inverted phases [30, 31, 32]. With the common sign convention, the negative spontaneous corresponds to inverted phase and *vice versa*. Generally it is known that smaller headgroups (PE, cholesterol etc.) prefer more negative curvature and larger headgroup (lysolipids etc.) prefer more positive curvature. However, dependence on lipid type might be far from trivial especially if counterions screen the interactions between headgroups. Values for most bilayer forming lipids are found to be negative [30, 31, 32].

As far as the author knows, there is no direct method to measure the Gaussian bending modulus. However, the ratio between the bending modulus and the Gaussian bending modulus for lipid monolayers has been measured and the results vary from $\bar{\kappa}^m/\kappa^m \approx -0.75$ to -0.9 [25, 33].

It is evident that the elastic properties of lipid bilayers depend on the properties of lipid molecules forming the bilayer. This relation is not completely understood, although a connection between macroscopic properties and packing of lipids has been suggested [34]. On the other hand, the curvature elastic constants κ, $\bar{\kappa}$ and the spontaneous curvature c_0 can be connected to the moments of the lateral pressure profile [35]. This dependence can be studied using the lateral pressure profile calculated from simulation data of model systems. These kind of studies can give insight, for example, on dependence of elastic properties of a lipid bilayer on chemistry of lipid molecules. This connection is discussed in section 3.3 and the elastic properties calculated from lateral pressure profiles are discussed in section 6.1.

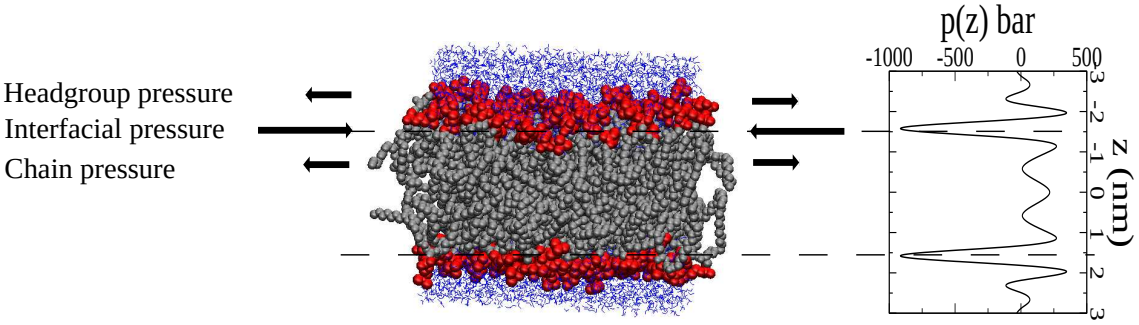

Figure 2.3: The lateral pressure profile in a DPPC lipid bilayer calculated from atomistic molecular dynamics simulations in publication I. The membrane normal coordinate is denoted by z.

2.3 Lateral pressure profile in lipid bilayers

Figure 2.3 illustrates a typical situation in a lipid membrane under zero tension. The interfacial tension between the polar membrane-water region and the hydrophopic acyl chain region is trying to minimize membrane area, creating a negative pressure at the interface. Meanwhile, the repulsive components due to electrostatic and steric interactions in the headgroup and tail regions oppose the interfacial attraction [36, 37, 38]. This inhomogeneous pressure distribution across a membrane is often called the *lateral pressure profile* [1, 6, 38, 39, 40, 41]. The lateral pressure profile is a very important property of lipid membranes because it is related to the elastic properties of lipid bilayers [35, 42] and also to membrane protein functionality [1, 6, 38, 40, 41, 43, 44].

The connection between the lateral pressure profile and membrane protein functionality has been discussed rather extensively elsewhere [6, 38, 41, 43, 44, 45, 46]. In the early 1990s, Brown et al.[1, 40] discussed the role of curvature stress on rhodopsin activity. In the late 1990s, Robert Cantor presented related views in a more concrete framework by formulating a theoretical connection between membrane protein functionality and the lateral pressure profile [6, 41, 43, 44]. His theoretical calculations

for model systems demonstrated that the contribution of the lateral pressure profile for the total free energy barrier of protein (de)activation can be significant. Many experimental studies have used these ideas to interpret their findings. For example, Perozo et al. [47] found that the large mechanosensitive channel (MscL) can be opened without external pressure by adding lyso-PC molecules asymmetrically in only one of the two leaflets in a bilayer (see Fig. 2.4). Meanwhile, symmetric addition of lyso-PCs was not found to open the channel. Related studies by other authors are also in favor of an idea that the lateral pressure profile may be involved in the opening of MscL [48, 49]. More recently, it has been found [50, 51] that addition of short-chain alcohols into a membrane resulted in dissociation of a membrane protein complex (KcSa), and the results were interpreted in terms of changes in the pressure profile induced by alcohol. Findings of similar nature, favoring a view that changes in lateral pressure profile have a role to play in protein functionality have been made for the activation of rhodopsin [1, 52] and the modulation of CTP:phosphocholine cytidylyltransferase [53, 54].

The first and second moment of the pressure profile can be connected to the elastic coefficients for bending, Gaussian bending, and the topological phase behavior of membranes [35, 42, 55]. It has also been shown that the dependence of membrane protein functionality on lateral pressure profile can be written as a function of elastic constants [44, 45]. Connection between lateral pressure profile and elastic properties is discussed in section 3.3 and connection between lateral pressure profile and membrane protein functionality is discussed in section 6.2.

Considering the above examples, it would be of profound interest to understand the relation between the lateral pressure profile and the molecular composition of a membrane. Unfortunately, doing this is not a simple feat. Experimental determination of the lateral pressure profile is exceptionally difficult, because one should measure local pressure differences inside a membrane in a scale that is less than 1 nm. Pyrene probes with different lengths have been used to gauge the pressure in

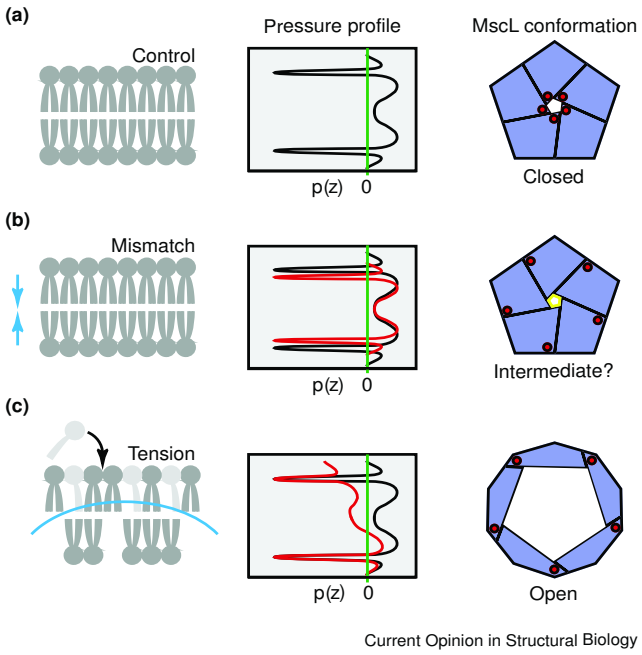

Figure 2.4: Schematic view of how an asymmetric distribution of lipids in the two leaflets of a membrane can result in lateral stress, which may be decisive for the opening of MscL. Shown here are plots for the type of membrane perturbation (left), the estimated transmembrane pressure profile (middle) and the corresponding state of MscL regarding its functionality. Of interest here is the case (c) shown at the bottom, describing the possibility that asymmetric distribution of cone-shaped lipids would alter the pressure profile, favoring the open state of the channel. Figure adapted from Ref. [47]. Copyright granted by Elsevier.

different parts of the acyl chain region (see Fig. 2.5) [56, 57]. However, this technique allows one to measure only relative pressures. What is even more problematic in the use of probes, however, is the fact that their effects on the resulting pressure profile and the exact location in a bilayer are unknown. Atomistic simulations have shown [58] that pyrenes disturb the packing and dynamics of lipids in the vicinity of the probe, the perturbations being significant within a few nanometers around the probe, but their effect on the pressure profile has not been elucidated yet.

As an alternative means, different approaches have been used to characterize the negative peak at the interface of polar and non-polar regions, the peak arising from

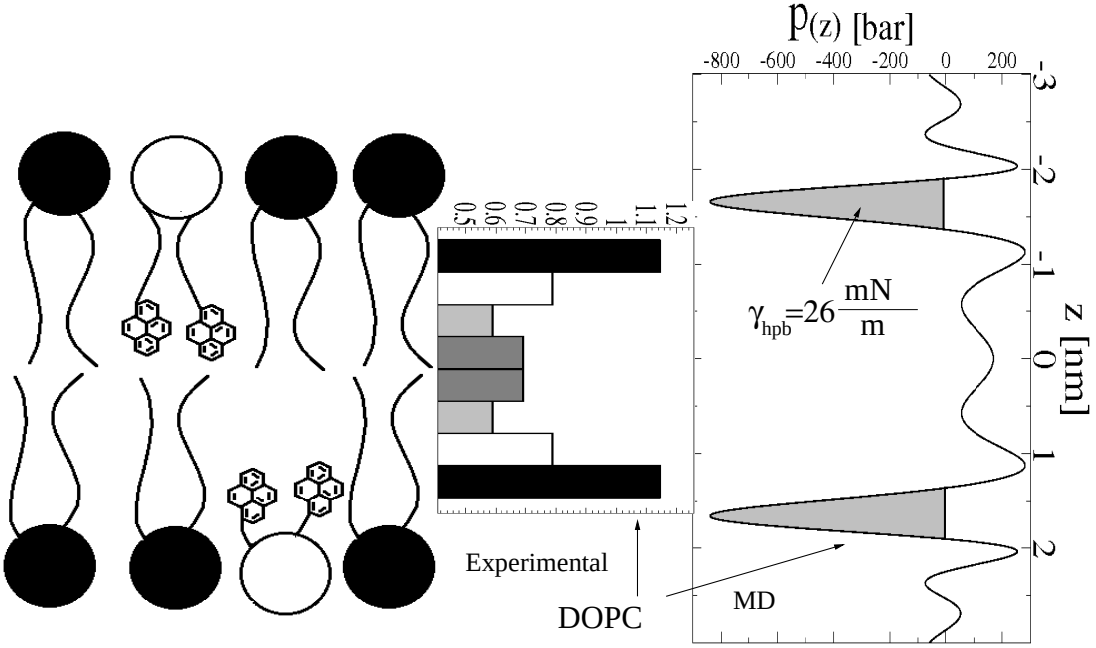

Figure 2.5: Illustration of the pressure distribution for DOPC bilayer measured by pyrene probes [56] (middle) and atomistic simulation from publication II (right). The drawing showing the use of pyrene probes has been adapted from Ref. [57] (left). Experimental and simulated profiles are in agreement in the acyl chain region (further discussion in the text). Interfacial energy density has been calculated integrating over the shaded area in the profile.

the hydrophobic free energy density γ_{hpb}. Using thermodynamic measurements it has been approximated that $\gamma_{\mathrm{hpb}} \approx (30 - 35)\,\mathrm{mN\,/\,m}$ [38]. The relation between surface pressure in monolayer experiments $\Pi(A)$ and the hydrophobic free energy is still under discussion [38, 59, 60, 61], but it is often concluded that $\gamma_{\mathrm{hpb}} \approx \Pi(A_0)$, where A_0 is the equilibrium area of the bilayer. This would allow comparison between the lateral pressure profile and the surface pressure determined from Langmuir monolayer experiments.

Given the difficulties to measure pressure profiles through experiments, computational and theoretical techniques have been applied to complement experiments. As a matter of fact, since atomistic and coarse-grained (CG) model simulations are an exceptionally useful approach to deal with atomistic and molecular aspects of membrane systems in (sub)nanoscopic detail, most of the lateral pressure profile studies reported by far have been based on atomistic and CG simulations. Pressure distributions in the acyl chain region have been determined using mean field theory, statistical thermodynamics calculations, and Monte Carlo methods [43, 62, 63, 64]. The pressure profiles in the whole bilayer region have been studied using dissipative particle dynamics simulations or other coarse grained approaches [65, 66] as well as atom-scale and coarse-grained molecular dynamics simulations in publications I, II, III, IV, V, VI and Refs. [67, 68, 69, 70, 71, 72, 73, 74]. Recent studies have concentrated mainly on four topics: the dependence of pressure distribution on lipid composition (publications I, II, III and Refs. [67, 72]), influence of anesthetics on membranes (publication IV and Refs. [75, 76]), connection between pressure profiles and elastic constants (publication II and Refs. [73, 74, 77]), and the interplay between protein structure and the lateral pressure profile (publications II, III and VI and Ref. [76]).

2.4 Modeling lipid bilayers using molecular dynamics simulations

As already mentioned above the molecular dynamics simulation method is the method of choice in most of the recent pressure profile studies as well as in all publications in this thesis. For this reason, we shortly review here the molecular dynamics simulation method for lipid bilayers. An up-to-date and extensive description of the method can be found, for example, from Ref. [78]. The actual pressure profile calculation is discussed in more detail in sections 3.1 and 3.2.

The basic idea of molecular dynamics (MD) simulations is to solve the Newtons

equations of motion

$$m_i \frac{\mathrm{d}^2 \mathbf{r}_i}{\mathrm{d}t^2} = \mathbf{F}_i = -\nabla_{\mathbf{r}_i} V(\mathbf{r}_1, ..., \mathbf{r}_N), \tag{2.3}$$

where m_i and $\mathbf{r}_i$ are the mass and the position of particle i, respectively. $\mathbf{F}_i$ is the force acting on particle i, and $V(\mathbf{r}_i, ..., \mathbf{r}_N)$ is the potential energy function of the system. The mathematical form of this potential energy function together with its parameters is called a force field. When the potential energy function $V(\mathbf{r}_i, ..., \mathbf{r}_N)$ and the locations of the particles are known, one can calculate the forces acting on each particle by calculating the derivative. Then, the trajectory of each particle can be solved numerically using a discretized form of Eq. (2.3). Several different discretizations have been introduced but in the simulations presented in this work we use the so called leap frog algorithm [79, 80, 81, 82]. Using the particle trajectories and the potential energy function $V(\mathbf{r}_i, ..., \mathbf{r}_N)$, several interesting physical properties of the system can be calculated, such as the local pressure distribution as described in sections 3.1 and 3.2. For a more detailed discussion on the molecular dynamics method and its applications, see for example Ref. [78] or [83].

Based on the above discussion it is obvious that all molecular dynamics simulation results depend on the initial structure and the potential function $V(\mathbf{r}_i, ..., \mathbf{r}_N)$ describing the interactions between particles. In atomic scale systems, the interactions are, in principle, determined by quantum mechanical laws. Nevertheless, under certain conditions atomic interactions can be approximated by classical potentials without losing essential properties of the system [78, 84]. There are many different ways to define the forms of the potentials and the parameters used in a force field. Different force fields are discussed for example in Ref. [78]. Here we concentrate on the framework used in the molecular dynamics simulation package GROMACS [79, 80, 81, 82], which is used in all calculations in this thesis. The potential function is then written as

$$\begin{aligned} V(\mathbf{r}_i, ..., \mathbf{r}_N) = \textstyle\sum_{i<j} V_{coulomb}(\mathbf{r}_{ij}) + \sum_{i<j} V_{Lennard-Jones}(\mathbf{r}_{ij}) \\ + \textstyle\sum_{Bonds} V_{Bond}(\mathbf{r}_{ij}) + \sum_{Angles} V_{Angle}(\theta_{ijk}) + \sum_{Dihedrals} V_{Dihedrals}(\phi_{ijkl}), \end{aligned} \tag{2.4}$$

where $\mathbf{r}_{ij}$ is the vector from atom i to atom j, θ_{ijk} is the angle between the vectors from atom j to atom i and from atom j to atom k, and ϕ_{ijkl} is the angle between the normals of the planes defined by atoms ijk and jkl.

The first two components on the right hand side of Eq. (2.4) describe so-called non-bonded interactions resulting from electrostatic interactions. The first component is just the familiar Coulomb potential

$$V_{coulomb}(\mathbf{r}_{ij}) = \frac{q_i q_j}{4\pi\epsilon\epsilon_0|\mathbf{r}_{ij}|}, \tag{2.5}$$

where q_i is the charge of an atom i, and ϵ and ϵ_0 are the relative dielectric constant and the dielectric constant of vacuum, respectively.

The second component is the so-called Lennard-Jones potential which combines a van der Waals type dispersion force at larger distances with a repulsive force due to the overlap of electron clouds at short distances:

$$V_{Lennard-Jones}(\mathbf{r}_{ij}) = \frac{A_{ij}}{\mathbf{r}_{ij}^{12}} - \frac{B_{ij}}{\mathbf{r}_{ij}^{6}}. \tag{2.6}$$

Here A_{ij} and B_{ij} are constants whose values depend on the pair of atoms interacting with each other.

The last three components of Eq.(2.4) are so-called bonded interactions. A covalent bond between two atoms is described by a harmonic potential

$$V_{Bond}(\mathbf{r}_{ij}) = \frac{1}{2}k_{ij}^{b}(r_{ij} - b_{ij}^{0})^2, \tag{2.7}$$

where the parameters k_{ij}^{b} and b_{ij}^{0}, describing the stiffness and the length of a bond, depend on the pair of atoms connected by the bond. However, often in atomistic simulations the harmonic covalent bond potential is replaced by constraining the bond length, which usually allows two times longer time step to be used in simulation [85]. This is done also in atomistic simulations in this work.

The potential associated with an angle between two consecutive bonds is described by

$$V_{Angle}(\theta_{ijk}) = \frac{1}{2}k^{\theta}_{ijk}(\theta_{ijk} - \theta^{0}_{ijk})^2, \tag{2.8}$$

where the parameters k^{θ}_{ijk} and θ^{0}_{ijk} depend on the three atoms connected by bonds.

Torsional potentials are described either by a periodic potential

$$V_{Diherals}(\phi_{ijkl}) = k^{\phi}_{ijkl}(1 + \cos(n\phi_{ijkl} - \phi^{0}_{ijkl})), \tag{2.9}$$

or in the case of, e.g., a double bond by a harmonic potential

$$V_{Dihedrals}(\phi_{ijkl}) = \frac{1}{2}\tilde{k}^{\phi}_{ijkl}(\phi_{ijkl} - \phi^{0}_{ijkl})^2. \tag{2.10}$$

In both cases the parameters k^{ϕ}_{ijkl}, $\tilde{k}^{\phi}_{ijkl}$, ϕ^{0}_{ijkl} and n depend on the atoms involved in the torsional interaction. There is reason to stress that the force field of any molecule or molecular system is defined not only by Eqs. (2.4)-(2.10), but also by values of the parameters associated with these equations, including some of the numerical methods used in the calculations. For example, if the Lennard-Jones interactions are truncated at some fixed cut-off distance r_{cut}, then the value of r_{cut} is part of the force field, i.e., changing r_{cut} also changes the force field.

Defining the parameters in Eqs. (2.4)-(2.10) is crucial for the validity of a simulation. Parametrization of biological macromolecules started in the 1970s and is still an active field of research [86, 87, 88, 89, 90, 91, 92]. For lipid bilayers there are different force fields available with different levels of accuracy [86, 88, 90]. In some force fields all atoms are described explicitly, e.g. in the CHARMM force field [86, 87], while for example in the so-called Berger force field [93], hydrogens are described together aliphatic carbons. This kind of description is called a united atom model. In more coarse grained models even more atoms are described as one bead. For example, in the so called MARTINI model approximately four heavy atoms are described by one bead [73, 94, 95].

Slightly different parametrization procedures and methods are used in all different force field developments, for reviews see [86, 88, 89, 90]. However, the rough idea in all force fields is to calculate feasible properties from *ab initio*, revise those against available experimental data and then adjust the rest of the parameters such that the force field reproduces chosen experimentally available data. Usually parameters for bonded potentials (Eqs. (2.7)-(2.10)) are accessible from *ab initio* calculations or from spectroscopy. Also partial charge distributions can be based on *ab initio* calculations but also fully empirical partial charges are used in some force fields. After these parameters have been fixed, usually some experimental property is chosen to fit the Lennard-Jones and the dihedral parameters such that the chosen property will match the experimental data.

For example, in the case of the Berger force field, the standard parameters of the OPLS are modified such that they reproduce the density and the heat vaporization for pentadecane [93]. Then the partial charges are taken from the work by Chiu et al. [96] and the GROMOS parameters are used for bonded potentials. This combination of parameters reproduce the experimental value for the area per molecule of a DPPC bilayer [93] and also several experimental properties of many pure lipid bilayers [88, 90, 93]. However, there are serious compatibility problems with some force fields [88, 90]. For example, Tieleman et al. demonstrated that inclusion of peptides into a bilayer modelled by the Berger force field causes significant over-condensation of a bilayer due to a relatively too strong attraction between lipids and a peptide when the standard Berger parameters are used with GROMOS [90]. The same problem is most likely present in simulations of publications II and III, where the cholesterol force field by Höltje et al. [97] was used, in the sense that the attraction between cholesterol and lipids is likely too strong compared to lipid-lipid interactions. Fortunately these problems are known nowadays and a significant effort is being made to develop better force fields for lipid and protein simulations [91, 92].

In the latest coarce grained MARTINI model beads are divided to four main type

depending on their polarity and charge [73]. Furthermore each of the types has 18 subtypes describing the hydrogen bonding capabilities. The beads are bonded to each others always with the same spring constant and the molecular properties are then fitted to atomistic model by modifying the angle potentials. The parametrization of the non-bonded interactions is then done by calculating the free energy of hydration, the free energy of vaporization, and the partitioning free energies between water and number of organic phases [73, 95]. The MARTINI model reproduces remarkably well many experimental properties of lipid bilayers, e.g., area per molecule, elastic properties and topological phase behaviour [73, 94].

The Berger force field is used in publications I, II, III and IV and the MARTINI model in publications V and VI. More details about the used force fields are given in the publications.

In simulations reported in this thesis the temperature was kept constant using Berendsen [98] or Nose-Hoover [99, 100] coupling. Temperature was set either to 310 K or 323 K such that the all the systems were studied above the liquid-gel phase transition temperature. The temperature differences most likely does not effect results in this thesis thus the details can be found from publications. In publications I, II, III and IV the pressure was maintained in 1 bar by the Parrinello-Rahman coupling [101]. In publications V and VI the systems were coupled to different tensions by the Berendesen scheme [98].

3 Theoretical concepts

3.1 Local pressure in pointwise particle models

The pressure for an inhomogeneous system is represented by a tensor $\mathbf{P}(\mathbf{r})$ that depends on the location $\mathbf{r}$. This can be written as a sum of two components

$$\mathbf{P}(\mathbf{r}) = -\sigma_K(\mathbf{r}) - \sigma_C(\mathbf{r}). \tag{3.1}$$

The kinetic contribution of the local stress tensor σ_K is defined as [102]

$$\sigma_K^{\alpha\beta}(\mathbf{r}, t) = -\sum_i m_i v_i^\alpha v_i^\beta \delta(\mathbf{r} - \mathbf{r}_i), \tag{3.2}$$

where m_i, v_i, and $\mathbf{r}_i$ refer to the mass, velocity, and location of atom i. The second component in Eq. (3.1), that is, the configurational part of the local stress tensor σ_C, is defined as [65, 102]

$$\sigma_C^{\alpha\beta}(\mathbf{r}, t) = \textstyle\sum_i \sum_{j<i} \mathbf{F}_{ij} \times \oint_{C_{ij}} \mathrm{d}l^\beta \delta(\mathbf{r} - \mathbf{l}), \tag{3.3}$$

where C_{ij} is a contour from the particle i to the particle j, and $\mathbf{F}_{ij}$ is the force exerted by the particle j on i. For the total pressure this definition is equal to the virial definition [78, 102]. However in inhomogeneous medium, the pressure distribution depends on the used contour, whose correct definition under these conditions is still under discussion [78, 102, 103, 104, 105, 106, 107, 108].

Traditionally two different contours have been suggested: the Irving–Kirkwood contour, which is a straight line between the particles [109], and the Harasima contour, which goes along the coordinate axes [110]. Schofield and Henderson have shown that the choice of contour is arbitrary and thus physical quantities should not depend on that [102]. This view is supported by Rowlinson [111]. The starting point for a study by Schofield and Henderson was the connection between pressure and momentum flux density [102]. On the other hand there is also an independent proof

starting from the derivative of free energy with respect to a deformation and ending to the Irwing-Kirkwood contour (straight line) [103]. The latter work has usually been ignored in the literature [78, 104, 106, 107, 108] and the general opinion in the field is that the issue is still unsolved [112]. Also some more recent studies show theoretical justifications for the Irving–Kirkwood contour [105, 106], while the Harasima contour has been shown to give unphysical results in spherical systems [104]. On the other hand, Sonne et al. showed that long-range interactions treated through Ewald summation techniques can be included in the local pressure calculation using the Harasima contour in simulations of planar lipid bilayers, and that this approach yields a practically identical result [68] compared to the Irwing-Kirkwood contour.

In this thesis, the local pressure is used to calculate elastic properties of lipid bilayers and mechanical energy changes of a lipid bilayer due to inclusions. These calculations are based on the assumption that the local pressure tensor is a derivative of free energy with respect to a deformation [6, 35, 44]. Thus we assume that the proof by Mistura is correct [103] and use the Irwing-Kirkwood contour. Also in all other MD studies of lipid membranes conducted by now, except for the studies by Sonne et al. [68] and Orsi et al. [74], the Irving–Kirkwood contour has been the method of choice.

Equations (3.1), (3.2), and (3.3) give the continuous pressure distribution for a pointwise particle model with pairwise interactions. In this thesis, we use molecular dynamics simulations yielding coordinates and velocities of particles to calculate the pairwise forces $\mathbf{F}_{ij}$. Then we consider the system on a grid and calculate the pressure tensor for each grid element V by taking an average over the volume $\mathbf{P}_V(t) = \int_V \mathrm{d}\mathbf{R}\, \mathbf{P}(\mathbf{R}, t)/V$. More implementation details are given in sections 3.2 and 3.6, in publications I and V, and in reference [69].

3.2 Calculation of lateral pressure profile from simulations

The lateral pressure profile calculations for planar lipid bilayers are traditionally implemented by dividing the membrane system into thin slices perpendicular to the membrane normal, and calculating the local pressure tensor in each slice as in publications I, II, III, IV and Refs. [65, 68, 69, 71]. To this end, Eqs. (3.2) and (3.3) are modified such that the Dirac delta function in Eq. (3.2) and the contour in Eq. (3.3) are discretized. The forces between particles are calculated using potentials for m-body interactions (i.e. pair interactions, three-body interactions, etc.) and summation over pairs is made over clusters formed by the many types of interactions [65, 69, 113] as follows:

$$\begin{aligned}\mathbf{P}^{\alpha\beta}(\mathbf{R},t) &= \textstyle\sum_{i\in\text{slice}} m_i v_i^\alpha v_i^\beta \\ &+ \textstyle\sum_m \frac{1}{mV_{\delta z}} \sum_{\langle j\rangle} \sum_{\langle k,l\rangle} (\nabla_{j_k}^\alpha U^m - \nabla_{j_l}^\alpha U^m) r_{j_k j_l}^\beta f(z_{j_k}, z_{j_l}, z_s).\end{aligned} \tag{3.4}$$

Here, $f(z_{j_k}, z_{j_l}, z_s) = 0$ if particles are on the same side of the slice, $f(z_{j_k}, z_{j_l}, z_s) = 1$ if both particles are inside the slice, $f(z_{j_k}, z_{j_l}, z_s) = \frac{\delta_z}{|z_{j_k} - z_{j_l}|}$ if particles are on different sides of the slice, and $f(z_{j_k}, z_{j_l}, z_s) = \frac{d_z}{|z_{j_k} - z_{j_l}|}$ if only one of the particles is inside the slice. The d_z is the distance from a given particle inside the slice to the wall of the slice separating the two particles, and δ_z and $V_{\delta z}$ are the thickness and the volume of the slice, in respective order. The notion $\langle j\rangle$ stands for summation over all m-clusters in the system, and $\langle k,l\rangle$ describes summation over all possible pairs of particles within a given m-cluster. The form of the local pressure tensor in Eq. (3.4), derived by Goetz and Lipowsky [65], is very practical in calculations from simulations. For example, it overcomes the problem of decomposing angle and dihedral potentials to pairwise interactions.

In publication V is presented a new discretization scheme in which the system is divided to a 3D grid and the pressure tensor is calculated for each element V as a

function of all coordinates:

$$p_V^{\alpha\beta} = \frac{1}{V}\sum_{i\in V} m_i v_i^\alpha v_i^\beta + \\ \sum_n \frac{1}{nV}\sum_{\langle j\rangle}\sum_{\langle k,l\rangle}(\nabla_{j_k}^\alpha U^n - \nabla_{j_l}^\alpha U^n) \times \frac{r_{j_l j_k}^\beta}{N}\sum_{\lambda=0}^{N} f_V(\mathbf{r}_{j_l} + \frac{\lambda}{N}\mathbf{r}_{j_l j_k}), \tag{3.5}$$

where $f_V(\mathbf{r}) = 1$, if $\mathbf{r} \in V$, and zero otherwise. Each vector $\mathbf{r}_{j_l j_k} = \mathbf{r}_{j_k} - \mathbf{r}_{j_l}$ is divided into N parts and the contribution of a given part λ is added only if the contour goes through V, i.e., if $f_V = 1$. The advantage of this discretization is that it allows the local pressure calculation for arbitrary geometry while the traditional discretization, Eq. (3.4), assumes planar symmetry when a system is divided into slices. In publication V the new discretization is applied to a membrane protein system, a phase separated bilayer, and a lipid vesicle, which are important applications without planar symmetry. In this thesis, we concentrate on an application for a membrane protein system discussed in publications V and VI.

3.3 Pressure tensor in planar geometry and connection to elastic properties

As explained above the local pressure can be presented as a tensor and can be calculated for slices in planar symmetry and for volume elements in the general case. In publication V also spherical geometry is considered but in this thesis we consider only planar geometry. In fluid bilayers the non-diagonal components are zero and thus in a planar geometry the pressure tensor can be written as, see Appendix A and Ref. [111],

$$\mathbf{P}(\mathbf{r}) = \mathbf{e_x}\mathbf{e_x}p_{xx}(\mathbf{r}) + \mathbf{e_y}\mathbf{e_y}p_{xx}(\mathbf{r}) + \mathbf{e_z}\mathbf{e_z}p_{zz}(\mathbf{r}). \tag{3.6}$$

If we define z as a normal direction for a planar bulk bilayer, then $p_L(z) = p_{xx}(z) = p_{yy}(z)$ depend only on z and we can write $\mathbf{P}(z) = (\mathbf{e_x}\mathbf{e_x} + \mathbf{e_y}\mathbf{e_y})p_L(z) + \mathbf{e_z}\mathbf{e_z}p_{zz}(z)$. Traditionally the lateral pressure profile in lipid bilayers is then defined as [35, 38,

111]

$$p(z) = p_L(z) - p_{zz}(z). \tag{3.7}$$

From the condition of mechanical equilibrium $\nabla \cdot \mathbf{P} = 0$, it follows that for a surface with planar symmetry the normal pressure p_{zz} is constant, see Appendix A and [111].

The definition (3.7) for the lateral pressure profile is chosen because then the moments are related to the surface tension γ and the elastic constants of a bilayer [35],

$$\gamma = \int_{-h}^{h} p(z)\,\mathrm{d}z \tag{3.8}$$

$$\kappa_m c_0^m = \int_0^h (z-\delta)p(z)\,\mathrm{d}z = \tau_m^{(1)} \tag{3.9}$$

$$\bar{\kappa}_m = \int_0^h (z-\delta)^2 p(z)\,\mathrm{d}z = \tau_m^{(2)}, \tag{3.10}$$

where z is the normal coordinate of the layer and δ is the position of the monolayer neutral plane. Here we define $z = 0$ to be the center of the bilayer and h to be the thickness of the monolayer. c_0^m, κ_m and $\bar{\kappa}_m$ refer to the properties of the monolayer. Thus equations (3.9) and (3.10) give elastic properties of a monolayer in the bilayer. The first and second moments are denoted by $\tau_m^{(1)}$ and $\tau_m^{(2)}$, respectively. These are written for a monolayer because the first moment would be zero for a symmetric bilayer because the spontaneous curvature would be zero. However, for a monolayer in a bilayer it is not necessarily zero as seen in section 6.1.

The moments and elastic properties of lipid monolayers described in these equations have been studied earlier using analytical theory [114], statistical thermodynamics calculations [44], coarse grained molecular dynamics simulations [73, 74, 115], and atomistic molecular dynamics simulations in publication II. The results are discussed and extended in section 6.1.

3.4 Pressure tensor and membrane protein inclusion

If a protein is embedded into a membrane or if there is a phase separation taking place in a membrane, then the planar symmetry is lost and P_{xx} is no longer equal to P_{yy}. However, the system can still be divided to bulk (where $P_{xx} = P_{yy}$) and interfacial regions. For example, Markin and Sachs have divided an ideal system to bulk bilayer, interface and bulk protein [116]. In this case there is a different surface tension in the lipid region γ_{lipid}, and in the protein region $\gamma_{protein}$, and the line tension between the regions f, can be defined as

$$f = R(\gamma_{lipid} - \gamma_{protein}), \tag{3.11}$$

where R is the radius of the protein [116]. However, two complications arise if this is applied to a real protein inclusion: First the protein region is too inhomogeneous and complex to be considered as bulk, and second the radius of the protein is difficult to determine explicitly. In publication V is calculated the surface tension as a function of distance from the center of the protein. This is shown in Fig. 3.1. The tension has a clear plateau when the distance is larger than 3 nm from the center, while inside the protein no clear plateau is found. Thus we cannot see a well defined bulk region inside the protein. Despite these complications a rough estimate for the line tension can be made by approximating from Fig. 3.1 that inside the protein the tension is roughly 0 mN/m while in the bulk bilayer it is roughly 40 mN/m. The protein radius can also be approximated to be 2 nm. Substituting these values into Eq. (3.11), one finds $f \approx 80$ pN for the line tension between a lipid bilayer and MscL.

Nevertheless the above complications are avoided in publication VI by considering the protein as an inclusion embedded in a bulk bilayer, characterized by a bulk bilayer pressure profile. In a bulk bilayer $P_{xx} = P_{yy}$, thus the lateral force is equal in each direction and we do not have to take the direction of the boundary excplicitly into account in publication VI. Using these assumptions the mechanical energy

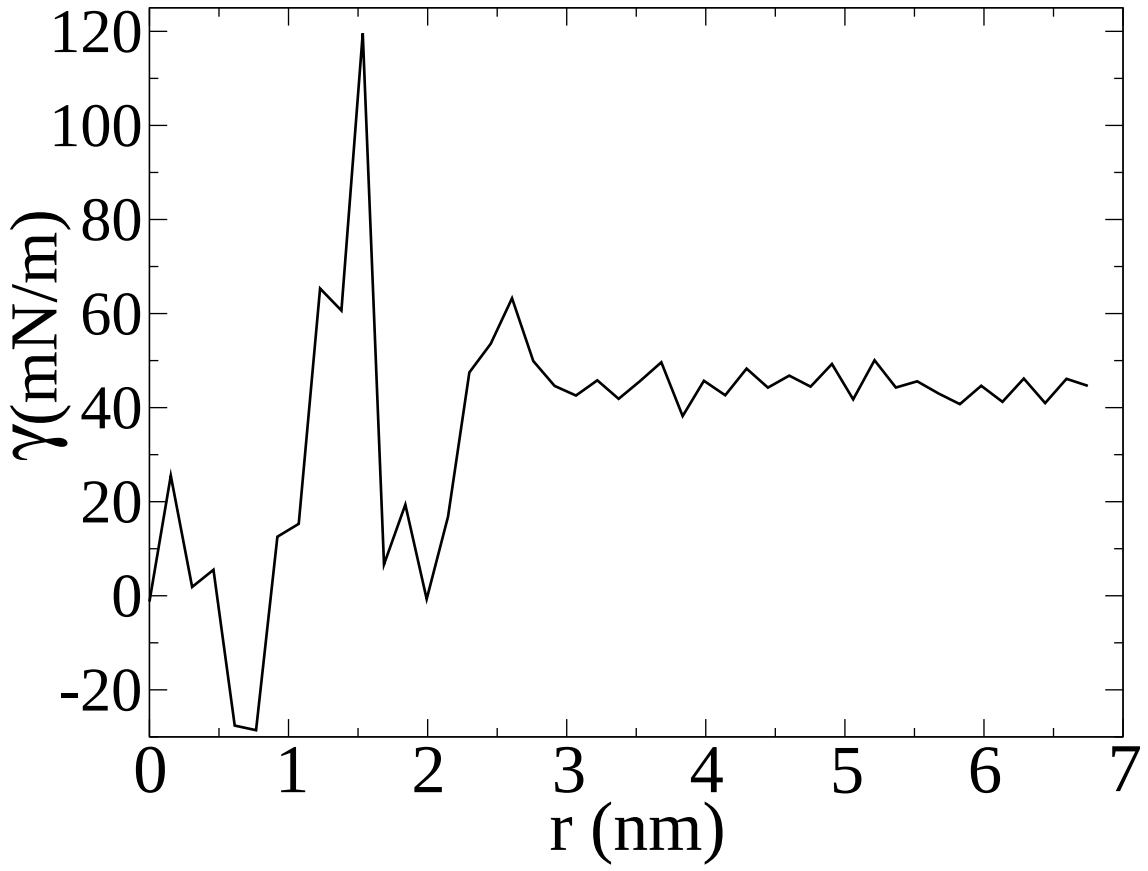

Figure 3.1: Surface tension as a function of distance from the center of the protein for MscL from publication V.

change of a bilayer is calculated when the protein goes from one state to another as explained in section 3.5.

3.5 Interplay of pressure profile and membrane protein activation

Influence of the lateral pressure profile on protein configurational energies can be approximated by calculating the mechanical work needed to create a cavity for the

protein inclusion into the membrane [44]

$$W = -\int_{-h}^{h} p(z)A(z)\,\mathrm{d}z, \tag{3.12}$$

where $A(z)$ is the area of the protein. z and h are as in the previous section, thus integration goes now over the bilayer. The mechanical energy difference between two different conformational states of the protein embedded into a bilayer with pressure profile $p(z)$ is then

$$\Delta E = \int_{-h}^{h} p(z)\Delta A(z)\,\mathrm{d}z, \tag{3.13}$$

where $\Delta A(z)$ is the difference in area between the states. The work can be connected to measurable quantities by expanding the protein cross-sectional area profile $A(z)$ using the Taylor expansion [44, 45]

$$A(z) = A(0) + a_1 z + a_2 z^2 + \cdots. \tag{3.14}$$

If we ignore higher order terms and substitute this to Eq. (3.12), we get

$$W = -a_1 \int_{-h}^{h} z\,p(z)\,\mathrm{d}z - a_2 \int_{-h}^{h} z^2\,p(z)\,\mathrm{d}z. \tag{3.15}$$

The moments of the pressure profile are connected to elastic constants through Eqs. (3.9) and (3.10), thus we get [45]

$$W = (a_1 + 2a_2\delta)\kappa_b c_0^b - a_2\bar{\kappa}_b. \tag{3.16}$$

Here c_0^b, κ_b, and $\bar{\kappa}_b$ refer to the properties of a bilayer, and δ to the neutral surface of the bilayer. From Eq. (3.16) one can see that the effect due to the pressure profile on changes in membrane protein shape can be written using elastic constants for bending and Gaussian bending. This means that the dependence of membrane protein functionality on membrane elasticity and the changes in pressure profile are related.

Mechanical energy differences between two conformational states in different lipid environments have been calculated using Eq. (3.13) in publications II and III and

in Refs. [44, 71, 76, 117]. In these studies the pressure profile is taken from molecular dynamics simulations or some other computational results and the protein is assumed to undergo some simple conformational change. The results and further details are discussed in section 6.2.

Effect of bilayer mechanical properties on membrane proteins have also been studied using elastic deformation models for lipid bilayers [4, 5, 118, 119, 120, 121, 122]. In these models bilayer deformation energies have been usually divided to thickness deformations due to hydrophobic mismatch, area dilation component, midplane bending and curvature frustration components [4, 119, 120]. As seen from Eq. (3.16) the elastic deformation model is just a lower order approximation from the pressure profile model [44, 45, 120]. However, the advantage of the elastic deformation model is that the deformation energy is related to the elastic constants of a lipid bilayer, which are measurable quantities [25, 26]. In this thesis we do not discuss these models in more detail.

In all models discussed above a simple approximation for a conformational change of membrane protein was used. In publication VI we overcome this approximation by simulating the mechanosensitive channel in closed and open states in a DOPC bilayer. Then the idea in Eq. (3.12) is exploited to calculate the mechanical energy change in mechanosensitive channel gating ΔE. The energy change is also divided into contributions from size and shape changes of the protein.

First, the cross sectional area of the protein $A(z)$ is decomposed into two components: a constant average area A_0 and a z-dependent shape variation $\delta A(z)$ around A_0,

$$A(z) = A_0 + \delta A(z). \tag{3.17}$$

Inserting this decomposition into Eq. (3.12) we get

$$\begin{aligned} W &= \int p(z)[A_o + \delta A(z)]\,\mathrm{d}z \\ &= A_o \int p(z)\,\mathrm{d}z + \int p(z)\delta A(z)\,\mathrm{d}z. \end{aligned} \tag{3.18}$$

Using the connection between pressure profile of a membrane and total surface tension from Eq. (3.8), and defining $W_{shape} = \int p(z)\delta A(z)\mathrm{d}z$, we get a useful decomposition

$$W = -\gamma A_0 + W_{shape}(\gamma). \tag{3.19}$$

The first term on the right hand side describes the work done against a cylindrical inclusion with area A_0, and the second term describes the work done against shape variations $\delta A(z)$. It should be noted, though, that since both $A(z)$ and $p(z)$ depend on the total tension γ, also W_{shape} depends implicitly on γ.

To estimate ΔE we first calculate the mechanical work of insertion for closed and open states separately using Eq. (3.12):

$$\begin{aligned} W_{closed} &= \int p_{closed}(z) A_{closed}(z)\mathrm{d}z. \\ W_{open} &= \int p_{open}(z) A_{open}(z)\mathrm{d}z. \end{aligned} \tag{3.20}$$

Then we approximate ΔE by first calculating the work done when the closed state is removed from a membrane, and next calculating the work when the open state is inserted back into the membrane. Thus we get the approximation

$$\Delta E = W_{open}(\gamma) - W_{closed}(\gamma) = -\gamma \Delta A_0 + \Delta E_{shape}(\gamma), \tag{3.21}$$

where the decomposition (3.19) is applied and $\Delta E_{shape}(\gamma)$ is the mechanical energy change due to the shape change. Now we see that ΔE contains the area dilation term $-\gamma \Delta A_0$ and the term arising from the shape change $\Delta E_{shape}(\gamma)$. The second term $\Delta E_{shape}(\gamma)$ corresponds to the curvature frustration term in elastic models. In publication VI both terms and the total mechanical energy difference are calculated under different tensions for a mechanosentive channel using pressure profiles and

cross sectional area profiles calculated from molecular dynamics simulation models. The results are discussed in section 6.2.

3.6 Technical details and complications in implementation of local pressure calculation

In papers I, II, III, IV and other published studies of pressure profiles of planar lipid bilayers using atomistic molecular dynamics [67, 68, 69, 70, 71, 72, 75, 76], the bilayer is usually divided into slabs approximately 0.1 nm thick. The implementation of the pressure profile calculation is largely similar in all publications, though some details differ. The basic idea is to calculate pairwise forces and distances for each atom pair using the molecular dynamics simulation data and potential function (Eq. (2.4)) and then substitute these into Eq. (3.4).

The most evident difference between different implementations concerns the treatment of long-range electrostatic interactions. Using truncation for electrostatic interactions causes severe artifacts in lipid bilayer simulations [123, 124, 125], which can be corrected using, e.g., Ewald summation methods. However, in Ewald summation techniques, forces cannot be divided into pairwise forces and, thus, Eq. (3.4) can no longer be used. This problem is usually handled by running the actual simulations using Particle-Mesh Ewald summation (PME) for Coulombic interactions, and calculating the pressure profile from the obtained simulation results (trajectories) by using a long cut-off distance (typically about 2 nm) for long-range interactions. The error in this case is systematic, not cumulative as it would be if also the simulation were done with truncation. The lateral pressure profiles from atomistic simulations in publications I, II, III and IV are calculated using this method. This is a reasonably good approximation for comparing pressure profiles of different systems, since the systematic error is then almost identical in all the cases. However, a different

treatment of electrostatics in the simulation and in the pressure profile calculation leads to a non-zero integral of pressure profile even in cases where the system is simulated in zero tension. This must be taken into account in calculations of moments in section 6.1. In papers V and VI the coarse grained MARTINI model is used in which electrostatic interactions are handled using a shift function with cutoff 1.2 nm [73], thus it can be normally included in the pressure calculation.

Rather recently, Sonne et al. [68] introduced a method to include Ewald summation in pressure distribution calculation using the Harasima contour. They showed that PME and truncation yield qualitatively similar results for pressure profiles, if the truncation distance is larger than about 2.0 nm.

More complications arise if bond constraints are used in simulation, which is often the case in atomistic molecular dynamics simulations. If bond lengths were described by a stiff harmonic potential, then the time step should be short enough to prevent the crash of a simulation. To allow the use of a longer time step, the bond lengths are often kept constant by adding Lagrange multipliers into the equation of motion [84, 126]. Different methods to solve the equation of motion with constraints have been proposed [84, 126, 85] but in none of these the actual forces arising from constraints are calculated. However, the use of equation (3.4) requires pairwise forces. The constraint forces can be calculated using the Lagrange coefficients in the constrained equation of motion as demonstrated earlier by the author of this thesis [113]. In all publications in this work the method presented in [113] is applied to calculate the constraint forces, and these are then embedded into Eq. (3.4) in pressure profile calculation. In other studies using atomistic molecular dynamics, some other methods have been used to calculate the contribution from constraints, but the details have not always been reported [68, 69, 71, 72].

It is also important to note that the kinetic contribution of the pressure tensor is not constant in inhogoneneous systems due to two reasons: the density is inho-

mogeneous, and the contribution from bond length vibrations is included in the component which arises from the constraints (if they are used).

As mentioned in section 3.3 the normal component of pressure tensor p_{zz} should be constant to satisfy the mechanical stability condition in a homogeneous planar bilayer [111]. However, it has been found to be non-constant in atomistic simulations [113, 127], while in coarse grained simulations it is mostly constant as in Fig. 4 in publication V and in Ref. [127]. In both works which have reported non-constant normal components the GROMACS simulation package has been used, but the pressure profile calculation implementation has been different. In the earlier work it was demonstrated that running simulations without constraints yielded a constant normal component, thus it was suggested that there is some problem in the calculation of pressure from constraints [113]. In the latter work it was suggested that if bonds with constraints orient, then they produce a non-constant normal pressure [127]. However, recently the author has run longer atomistic simulations without constraints and observed a non-constant normal component also in this case. In all tests made by the author a long cut-off was used for electrostatics due to the complications in calculations of local pressure from PME. Similar non-constant normal component was found in both cases, thus the treatment of electrostatics is most likely not the reason for the non-constant normal component. Other possible reason might be the choice of contour in the definition of local pressure (Eq. (3.3)). However, the normal component is constant when the MARTINI model is used together with the same contour, thus this is most likely not the reason either. Also, as far as the author knows, simulations with different simulation packages but with the same contour give a constant normal component [68, 71].

In general the reason for this non-physical behavior of atomistic simulations is not known. Based on studies by far it seems that the reason is a technical problem related to the implementation of molecular dynamics simulations or pressure calculations. In principle, this artifact questions the pressure profile results of the

atomistic simulations reported in publications I, II, IV and III. However, in practice the interpretation of all the results has been done such that this artifact should not influence the results. Also in pressure profiles shown it is assumed that the normal component is constant. In coarse grained simulations this issue does not exist.

The author's opinion is that this issue should be resolved before more pressure profile calculations are performed with these methods from atomistic molecular dynamics simulations.

4 Gauging pressure profiles

As mentioned in section 2.3, several theoretical and computational methods have been used to calculate the lateral pressure profile in planar lipid bilayers [43, 62, 63, 64, 65, 66, 67, 68, 69, 70, 71, 72, 73, 74] including papers I, II, III and IV. By far, the most successful technique has been molecular dynamics since it allows the pressure to be calculated in almost atomic detail, providing at least semi-quantitative insight into the pressure distribution inside membranes (see Refs. [67, 68, 69, 70, 71, 72, 73, 74] and papers I, II, III and IV). Below we compare the lateral pressure profiles obtained from atomistic and in part also coarse-grained molecular dynamics simulations applied to a variety of different models. These results are compared to experiments, when appropriate.

Let us first discuss how reliably one can determine the pressure profiles on the whole, since a variety of different force fields are available for any lipid system, and it is likely that the pressure profile depends at least to some extent on the force field used. Figure 4.1A depicts a comparison of pressure profiles for a DPPC bilayer found in four different atomistic models, see Refs. [68, 71, 72] and paper I. All profiles portray similar features, though some details are different. The differences arise likely from differences in the force fields as well as from differences in the implementation of the lateral pressure profile calculation. In publication I and the study by Patra [72], the model and simulation protocols (using GROMACS [81]) are essentially identical but the implementation of the lateral pressure profile calculation is different. Yet, the only difference between the profiles found in these studies is the height of the interfacial and headgroup peaks, which likely results from different averaging schemes: in publication I the pressure was calculated from configurations which were saved every 10 ps from molecular dynamics simulations, while in the study by Patra the run was continued for 4 ps from each saved configuration and the pressure was calculated from the last 2 ps of each short run. The profiles found by

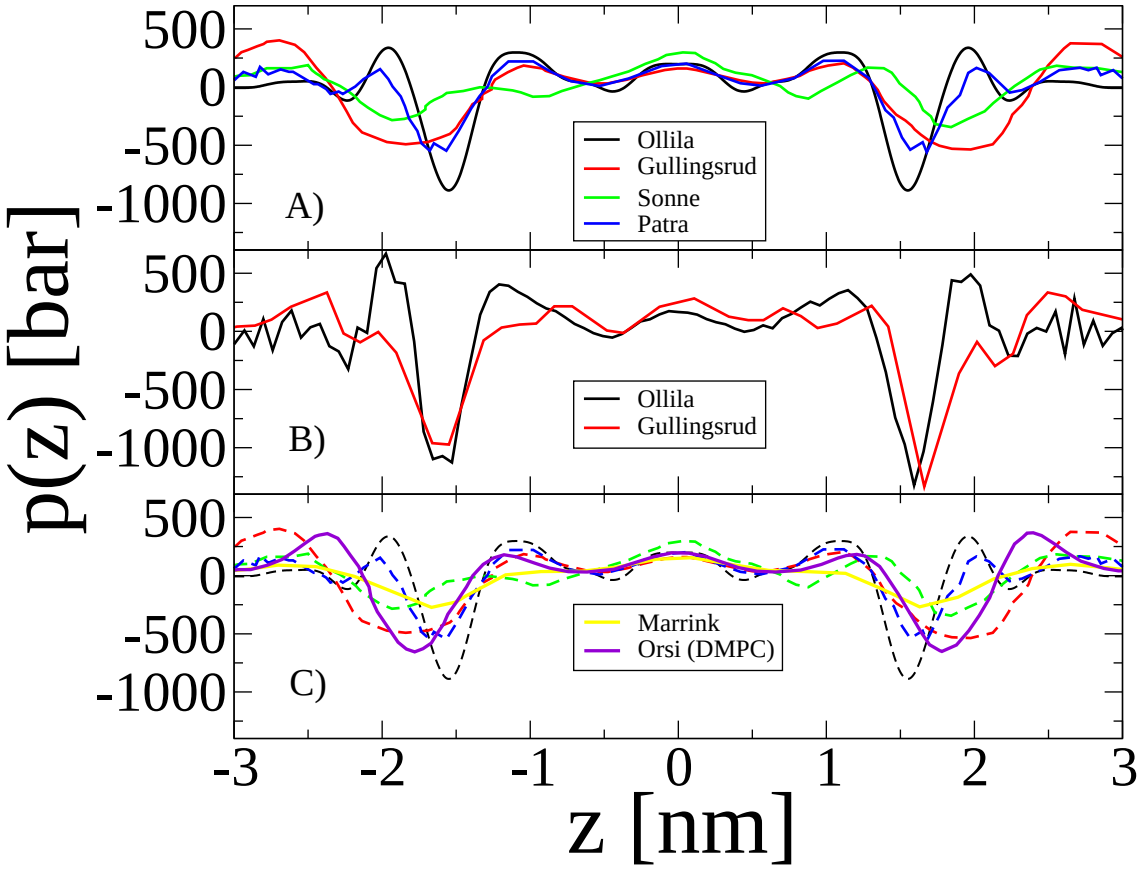

Figure 4.1: Comparison between lateral pressure profiles found by a number of different force fields for bilayer models. A) Atomistic simulations for a DPPC bilayer; B) atomistic simulations for a POPC bilayer; and C) coarse-grained simulations for DPPC and DMPC (atomistic data shown with dashed lines for comparison). See text for discussion. The data is taken from publication I (referred as Ollila in the picture), Ref. [71] (Gullingsrud), Ref. [68] (Sonne), Ref. [72] (Patra), Ref. [73] (Marrink) and Ref. [74] (Orsi).

Gullingsrud et al. [71] and Sonne et al. [68] were calculated with the same simulation protocol (using NAMD/CHARMM) but with different force field parameters for the DPPC bilayer. The profiles calculated using NAMD/CHARMM [68, 71] seem to be broader than the results calculated by GROMACS and related force fields, see Ref. [72] and publication I. In both studies by NAMD/CHARMM the running average is taken over the profile, which suppresses the peaks, while in publication I the spline fitting is used. This difference may be due to the averaging schemes or

due to the differences in the models.

Figure 4.1B compares the lateral pressure profiles for a POPC bilayer calculated using the NAMD/CHARMM [71] and GROMACS protocols from publication I. In these profiles the interfacial peaks are in good agreement, which likely results from the fact that here both profiles are pure data, not smoothed by running averages or related schemes. However, the positive peaks in the acyl chain region, close to the interface and headgroup regions, are in somewhat different locations.

In Fig. 4.1C, we compare the pressure profiles found through two coarse-grained models: the MARTINI model [73, 94] and the model by Orsi et al. [74]. Generally speaking, the features of both models are similar to those found in atomistic models that are also shown in the same figure. In the MARTINI model [73], the heights of the interfacial and headgroup peaks seem to be small, but actually they are comparable to the profiles given by the atomistic study of Sonne et al. [68].

In general, while some details of the pressure profiles (such as the height of the peaks) may vary quite a lot, it is important to keep in mind that physical properties arising from the pressure profile are dictated by its moments (see Secs. 2.2 and 3.5), thus the moments are likely more important than the actual form of the profile. We will discuss this issue in more detail in section 6.1.

Experimental determination of the lateral pressure profile is very difficult, because one should measure local pressure differences in nanometer scale. Templer et al. [56] used pyrene probes to measure pressure at different depths inside a DOPC bilayer using four probes with different chain lengths. Kamo et al. [57] have also used a technique of similar nature. The results by Templer et al. are shown and compared to computational results from publication II in Fig. 2.5. It is evident that experiments and simulations yield the same general form for the pressure profile in the acyl chain region: pressure decreases as one moves ahead from the interfacial region

towards membrane center, but then there is a peak in the center of the bilayer. This peak was not found in earlier models that were based on simplified descriptions of lipids [43, 62, 63, 65, 66, 114], but it is evident in all atomistic simulations [67, 68, 69, 70, 71, 72] including publications I, II, III and IV, recent coarse-grained simulations [73, 74], and also in recent theoretical studies [64]. However, it is important to notice that the technique based on probes to measure pressure allows only relative pressures to be measured, the exact location of probes in a bilayer is not known, and the effects of probes on the pressure profile are not understood.

The origin of the pressure profile peak in the membrane center has been discussed quite extensively [51, 64, 74], including publication I. The most obvious explanations would be the larger density in the membrane center compared to the acyl chain region, or interdigitation of the leaflets [51]. However, in computer simulations where the peak in the pressure profile has been observed, there is no pronounced density in the middle of a membrane as seen in publication I. Also it has been found that the peak in the pressure profile disappears with increasing unsaturation, while interdigitation remains essentially unchanged as in publication I. Mukhin and Baoukina suggested that the origin of the peak is related to increasing configurational freedom of the chains in the center of the bilayer, which hints at the possibility of entropic origin [64]. In publication I, this idea was used to explain the disappearance of the pressure profile peak in the membrane center due to increasing number of double bonds in acyl chains. In figure 4.2 is presented an intuitive explanation for the central peak. However, this idea is suggestive and more studies are needed to resolve this issue.

The above indicates that, despite their limitations, experiments based on the use of fluorescent probes seem to be consistent with atomistic simulations and to yield some insight into the pressure distribution inside membranes. Another connection to experimental data can be done through hydrophobic free energy density γ_{hpb}, see Fig. 2.5. It can be computed from the pressure profile as an integral over the negative

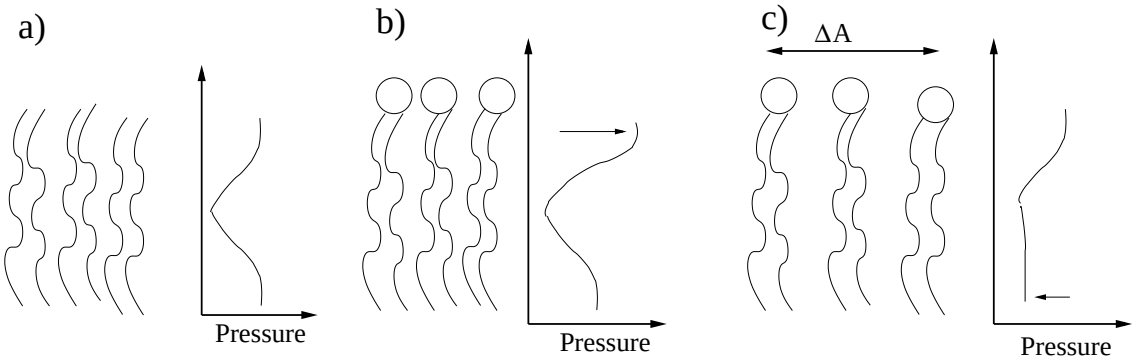

Figure 4.2: Origin of the central peak in a bilayer can be explained by configurational entropy of lipid chains. A) Polymer chains organized to an ordered layer tend to maximize the area in the chain end region because of configurational entropy. Chain ends are the least restricted to bonds with other particles in a chain, thus they tend to expand the area due to entropic reasons: Chain ends need more space compared to the center to sample through all possible configurational states. This tendency leads to a larger pressure in the chain end region. B) In the case of lipids, the headgroup restricts the movement of the other end. This restriction of movement leads to an even higher pressure as illustrated in the figure. C) If the area per molecule is increased, the repulsive pressure is decreases especially in the chain's free end region since they now have more space. However, the repulsive pressure remains in the other end since the headgroup restricts the movement despite the increase of area.

peak in the interfacial region and measured with some degree of approximation using e.g. thermodynamical and Langmuir monolayer experiments [38]. While simulations give $\gamma_{\mathrm{hpb}} \approx 26\,\mathrm{mN\,/\,m}$, experimental values for γ_{hpb} range over $(30-35)\,\mathrm{mN\,/\,m}$ [38], in reasonably good agreement with simulations. While the relation between the surface pressure in monolayer experiments $\Pi(A)$ and the hydrophobic free energy is under discussion [38, 59, 60, 61], it is rather widely accepted that γ_{hpb} and $\Pi(A_0)$ are related (A_0 being the equilibrium area of the bilayer). This suggests that qualitative comparison between lateral pressure profiles and surface pressures measured through Langmuir monolayer film experiments is possible. There have been recent studies going to that direction [128, 129], but the connection is still not fully understood.

Acyl chain order parameters, S_{CD}, determined through deuterium ^{2}H NMR mea-

surements have also been suggested to be related to the lateral pressure profile [130]. The idea is that small order parameters would refer to large repulsive pressure. As S_{CD} often relates to the average area per lipid in a membrane, a more complex relation to describe the dependence of the lateral pressure profile on the area per molecule has also been suggested in publication I and in Ref. [74]. These propositions are essentially similar to the suggestion that pressure profiles depend on bending rigidity and the occupied area of acyl chains [64]. Further, properties of the inverted hexagonal phase have also been used to approximate the intensities of different components in the lateral pressure profile [131]. While none of the above suggestions have been systemically tested, recent progress in computational resources together with validated force fields hints that it will soon be possible.

5 Dependence of pressure profile on molecular composition

5.1 Dependence on unsaturation level

It has been suggested that inclusion of polyunsaturated lipids in lipid membranes could affect protein activity through changes in lateral pressure profile or consequent changes in elastic properties [1, 43, 44, 52, 130, 132]. Especially, an increase in the fraction of the MII state of rhodopsin has been suggested to follow from an altered pressure profile [1, 40]. To corroborate these views, it is necessary to understand the dependence of the lateral pressure profile on the level of unsaturation.

Dependence of lateral pressure profile on unsaturation level has been studied through statistical thermodynamics calculations [43] and atomistic molecular dynamics simulations in publication I and in Ref. [67]. The statistical thermodynamics calculations by Cantor suggest that pressure in the acyl chain region is shifted towards the interfacial region with increasing number of double bonds [43]. Tripp et al. [67] studied pressure profiles in one-component membranes comprised of polyunsaturated lipids (with DPA or DHA chains) using atomistic simulations. They showed that even though DPA and DHA differ only by one double bond, there is a clear change in the lateral pressure profile, in line with the prediction of Cantor [43]. Their results are shown in Fig. 5.1.

Publication I focused on the effect of double bonds on the lateral pressure profile using atom-scale molecular dynamics simulations by comparing membranes where the number of double bonds in a lipid hydrocarbon chain varied from zero to six. The results are shown in Fig. 5.1. The most pronounced effect found was the reduction of the central peak for increasing number of double bonds. The reduction

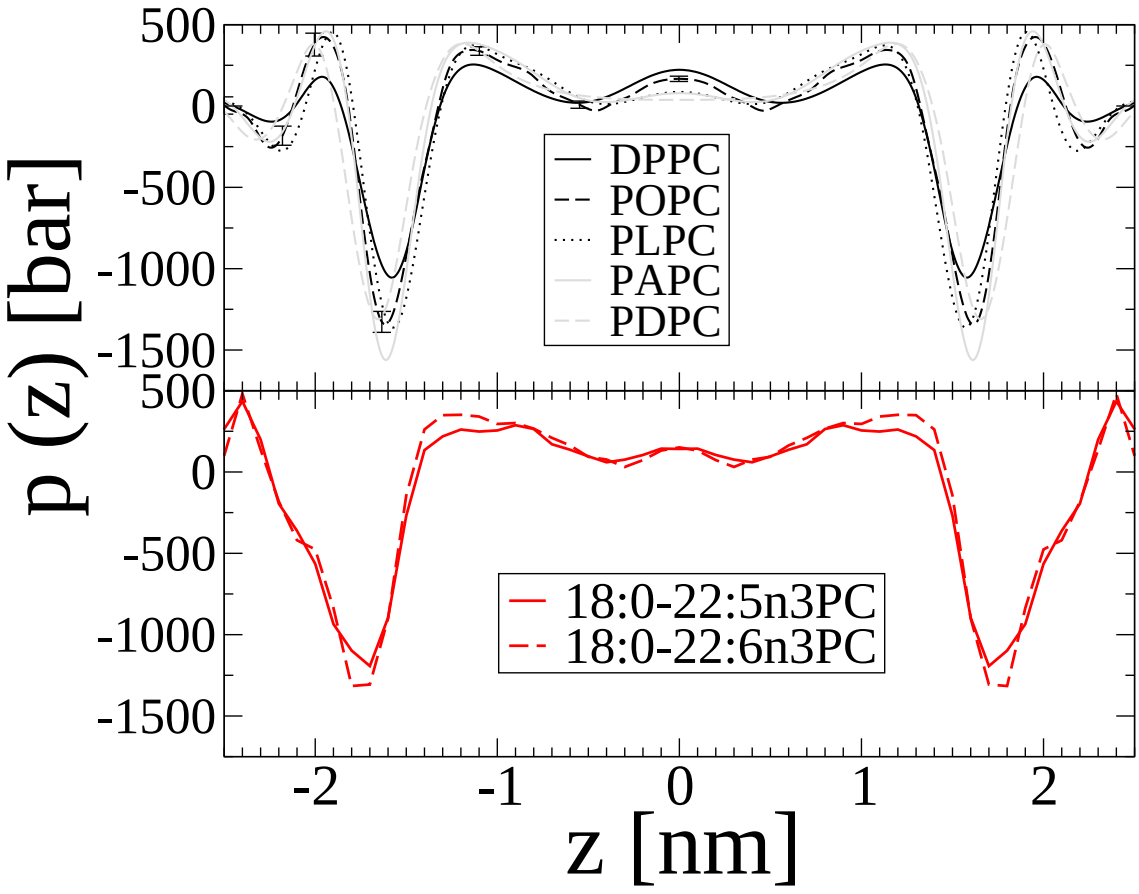

Figure 5.1: Top: Dependence of the lateral pressure profile on the number of double bonds: DPPC, POPC, PLPC, PAPC, and PDPC bilayers, having zero, one, two, four, and six double bonds, in respective order. The data from publication I. Bottom: Influence of adding one extra double bond (from five to six) by Tripp et al. [67].

in pressure in the membrane center was found to be accompanied by an increase in pressure in the headgroup and interfacial regions.

Both simulation studies therefore support the prediction by Cantor that double bonds shift repulsive pressure from the acyl chain region towards the interfacial area. Besides that, they suggest a slight increase in surface free energy and in the headgroup peaks of the pressure profile.

Further analysis and possible simulations with rhodopsin embedded in a membrane are needed to find out if the reported changes in the pressure profile could explain the dependence of rhodopsin functionality on the level of unsaturation in a membrane.

5.2 Effects of different sterols in two-component membranes

Cholesterol (CHOL) is one of the most important lipid components of biological membranes, thus its effect on the lateral pressure profile is also of profound interest. Interestingly, concerning the above mentioned dependence of rhodopsin activity on lipid composition, the fraction that rhodopsin spends in the MII state decreases with increasing cholesterol concentration [133, 134], in contrast to the trend observed with polyunsaturated lipids [132]. One way to explain this difference might be the difference in lateral pressure profiles in the two cases.

The effect of cholesterol on the lateral pressure profile in two-component membranes has been studied using statistical thermodynamic calculations [43] as well as through atomistic molecular dynamics simulations in publication II and in Refs. [67, 72]. Also, the effects of other sterols (such as desmosterol, 7-dehydrocholesterol and ketosterol) in varying lipid matrices is studied in publication II and the effect of cholesterol as a function of its concentration in Ref. [72]. All these investigations support the view that inclusion of cholesterol and other sterols in a membrane is associated with a significant change in the lateral pressure profile.

Simulation studies indicate additional peaks to emerge in the bilayer interior region due to cholesterol, see Fig. 5.2. The relative significance of additional peaks increases for increasing cholesterol concentration at least until 50 mol% [72]. Studies of saturated (DPPC) and diunsaturated (DOPC) membranes have shown peaks associated with headgroup repulsion and interfacial energy to increase substantially due to cholesterol, see [72] and publication II. In polyunsaturated membranes with

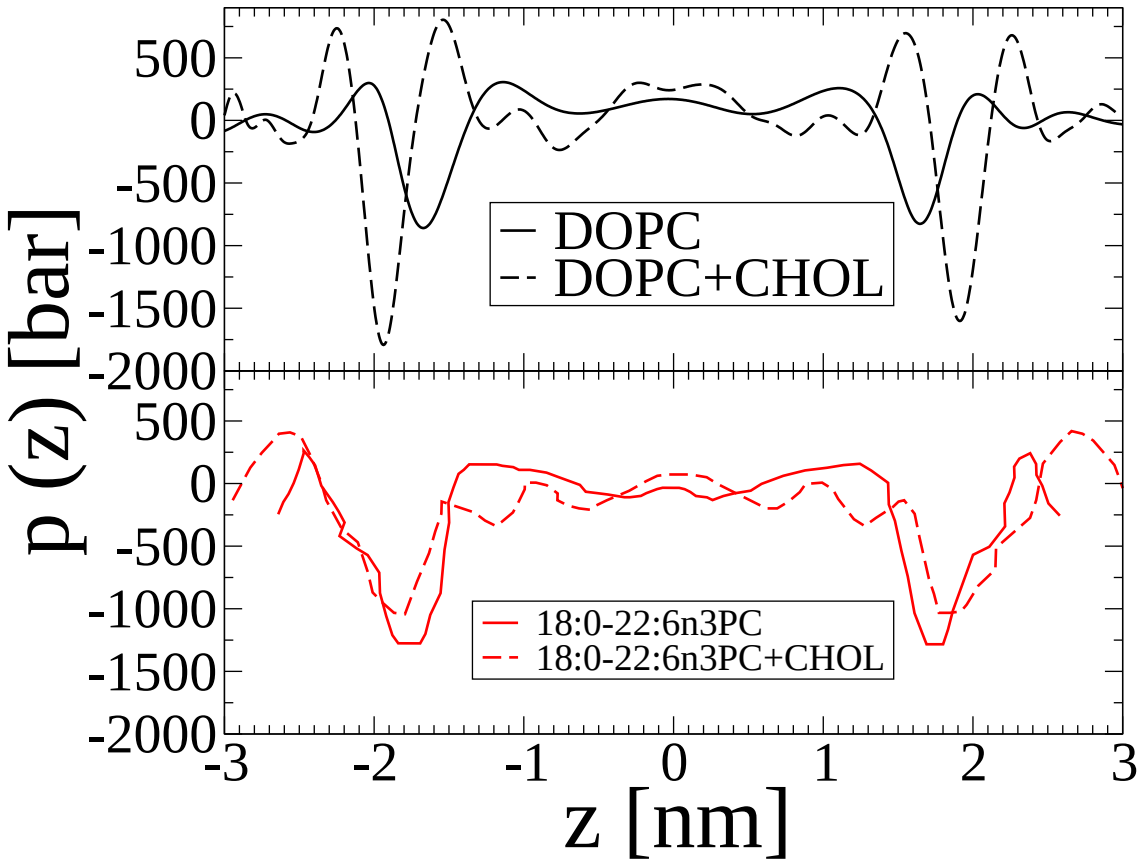

Figure 5.2: Effect of cholesterol on the lateral pressure profile in unsaturated membranes. Top: DOPC and DOPC/CHOL from publication II; Bottom: SDPC and SDPC/CHOL [67].

cholesterol, a small increase has been found in the headgroup peak, accompanied by a small decrease in the interfacial peak [67], opposite to conclusions reported in other simulation studies for saturated or diunsaturated membranes (see Fig. 5.2). While the difference could be due to different force fields or different simulation protocols (GROMACS with constant pressure in publication II and NAMD/CHARMM with constant area in [67]), it could also be due to double bonds that are known to play an important role in membranes. In polyunsaturated membranes, in particular, the effect of cholesterol on membrane structure and ordering has been shown to be distinctly different compared to saturated lipid bilayers [135].

Interestingly, peaks in the bilayer interior region have been found in all simulation studies of lipid bilayers with cholesterol in publication II and Refs. [67, 72], for many different sterols in publication II, and also with different lipid matrices in publication II and Ref. [67]. The results from publication II are shown in Fig. 5.3. Thus, it seems evident that these peaks are characteristic to all sterols. The origin of these peaks is likely related to the ordering effect of the rigid ring structure in sterols. This explanation is supported by similar peaks found in the pressure profiles associated with gel phase membranes in publication V. The fine structures slightly differentiating the pressure profiles of the different sterols probably arise from the chemical details such as the number and the locations of methyl groups and double bonds in the sterol structure.

It is also notable that the pressure becomes negative in the location of ring structures in all the simulation results discussed here. The reason for this is most likely the cohesive interaction between cholesterol and phospholipids.

The data in publication II support the view that the effect of sterols on the lateral pressure profile is the strongest in saturated membranes, see Fig. 5.3. In a similar fashion, also the differences in pressure profiles between the many sterols have been shown to be the strongest in saturated bilayers. For increasing level of unsaturation, the role of sterols in the pressure profile becomes weaker.

5.3 Pressure profiles in three-component bilayers

Biological membranes typically consist of hundreds of different lipid types, thus it is crucial to understand how membrane properties emerge from their molecular composition in many-component systems. On a general level, the nature of fluid-like membranes can be classified to two types: strongly disordered membranes comprised of polyunsaturated lipids, and raft-like membrane domains with pronounced

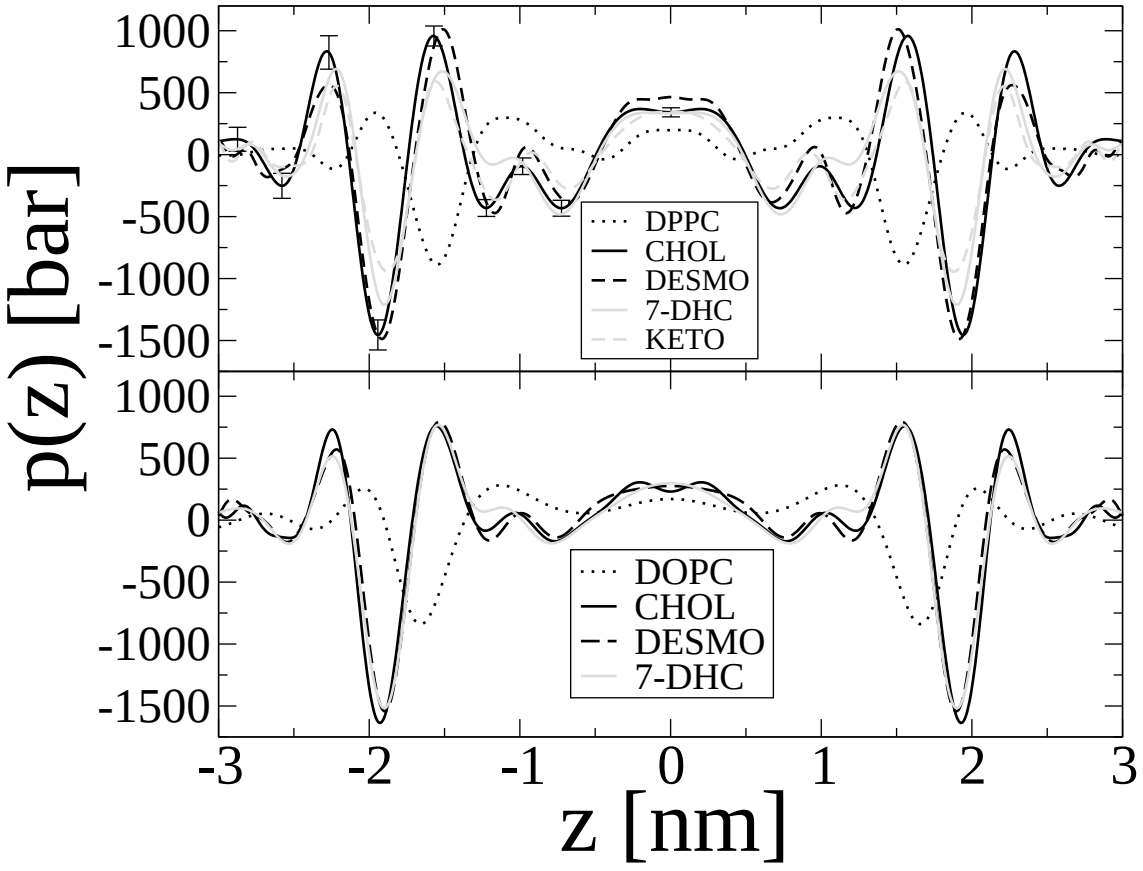

Figure 5.3: Top: Lateral pressure profiles of DPPC, DPPC/CHOL, DPPC/DESMO, DPPC/7-DHC, and DPPC/KETO bilayers. Statistical errors are presented for one leaflet of the DPPC/CHOL system, in which the fluctuations were the largest. Error bars in other systems were smaller. Bottom: Lateral pressure profiles of DOPC, DOPC/CHOL, DOPC/DESMO, and DOPC/7-DHC bilayers. Statistical errors are presented for one leaflet of the DOPC/CHOL system. Error bars in other systems were smaller. Adapted from publication II.

order characteristic to the liquid-ordered phase. The lateral pressure profiles for the latter, raft-like membrane domains have been studied in publication III in which three-component membrane systems containing POPC, cholesterol, and palmitoylsphingomyelin (PSM) with two different concentration ratios for POPC:CHOL:PSM (1:1:1 and 2:1:1) are studied.

The pressure profiles calculated from these simulations are presented in Fig. 5.4.

For comparison, the pressure profiles of single-component POPC and PSM bilayers and of two-component DPPC/CHOL systems are also presented. Comparison of the lateral pressure profiles of three- and two-component systems reveals that the general features remain the same: all peaks common to the one-component cases remain but become higher, though additional peaks are also found in the acyl chain region. For the three-component systems the additional negative peaks in the acyl chain region are even more pronounced. This is logical if we look at the lateral pressure profile of a pure PSM bilayer which also has lower values in the acyl chain region compared to the POPC bilayer. Thus, the high peaks in the acyl chain region in the three-component system could be understood in generic sense to arise from the ordering of the bilayer rather than from any specific property of cholesterol.

5.4 Implications of anesthetics on pressure profile

One of the greatest mysteries in medical sciences is general anesthetics. Despite the fact that anesthetics have been used successfully for more than 150 years, the molecular mechanisms of how anesthetic molecules bring about their effects are not understood. The discussion on mechanism of action of anesthetics has given rise to two schools and the debate is still going on [136, 137, 138]. According to the "direct interaction school" the anesthetics modify protein functions by directly binding to those [136], while according to the "lipid school" anesthetics modify lipid bilayer properties, thus leading to changes in protein functions [41, 137, 139] or directly disturbing the signaling [138].

In the late 1990s, Cantor suggested that anesthetics might change the lateral pressure profile of a lipid bilayer and thus affect membrane protein functionality as explained in section 3.5 [6, 41, 139]. This idea, as all lipid related ideas, seems reasonable since it is well known that the action of an anesthetic correlates with its partitioning between oil (membrane) and water: the larger the partitioning coeffi-

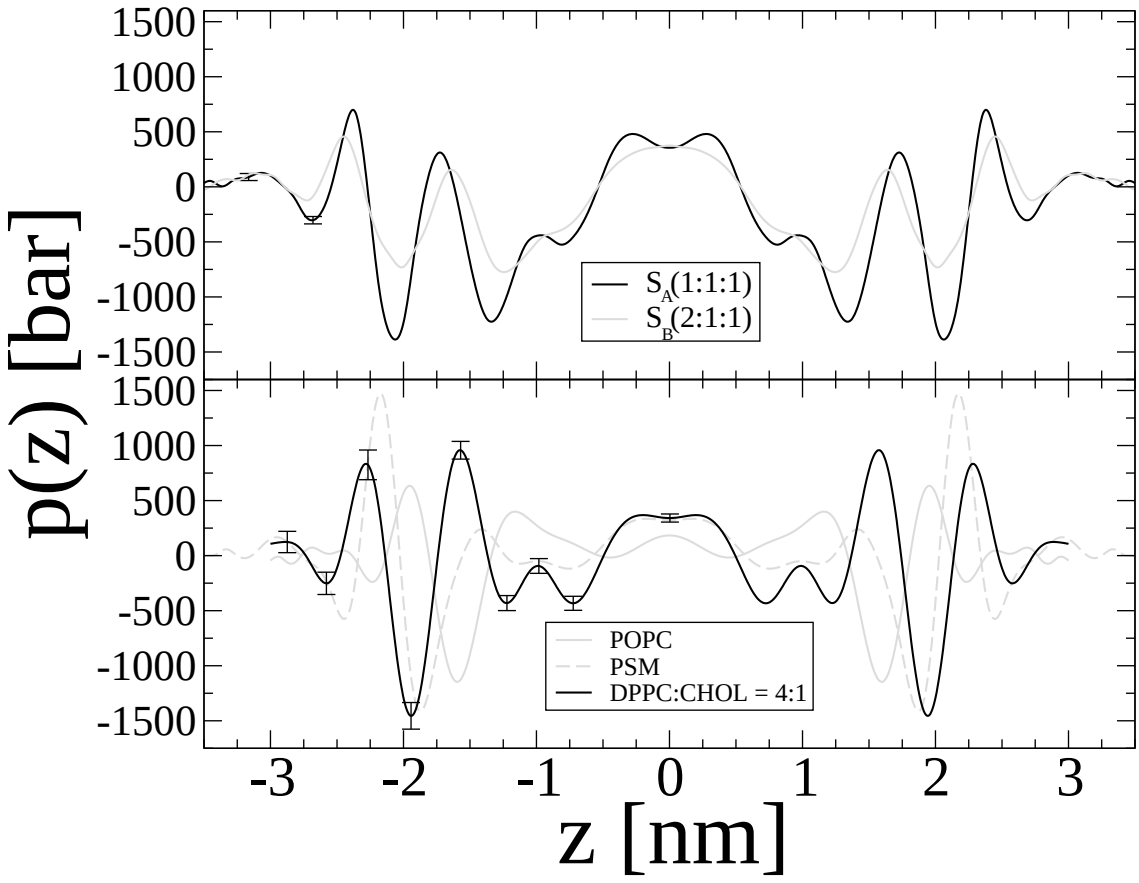

Figure 5.4: (Top) Lateral pressure profiles of the raft-like systems POPC:CHOL:PSM = 1:1:1 (S_A) and 2:1:1 (S_B). (Bottom) Pressure profiles for pure POPC and PSM single-component systems and a binary DPPC/CHOL membrane. The center of the membrane is at $z = 0$. Adapted from publication III.

cient for membrane, the stronger are also the effects of the given anesthetic. Direct experimental verification of Cantor's view is difficult because lateral pressure profiles or protein cross sectional areas cannot be measured easily, as explained in section 4. However, there are indirect studies in which this idea has been used to interpret experiments with known and unknown anesthetics [129, 140, 137].

Considering experimental difficulties to measure lateral pressure profiles and especially changes in the profile due to anesthetics, it is positive that theoretical and computational approaches have been able to shed some light on this issue. Re-

garding theoretical studies, the effect of alkanols with different chain lengths on the lateral pressure profile has been studied by Cantor [41]. He found that short-chain alkanols change the pressure profile close to the interfacial region, and long-chain alkanols in the membrane center. Frischknecht and Frink [141] studied the pressure profiles as a function of ethanol, butanol and hexanol concentrations using coarse-grained molecular dynamics simulations and found that the peaks in the pressure profile decrease with increasing alcohol concentration. In publication IV the effect of ethanol on the pressure profile of DPPC and PDPC bilayers is studied using atomistic molecular dynamics simulations and it is found that ethanol reduces the peaks in the headgroup and interfacial regions, see Fig. 5.5. Recent data by Griepernau and Böckmann [75] is somewhat different. They found an insignificant decrease in the interfacial region and significant changes in the acyl chain region. They suggest that the difference is due to different force fields and electrostatic interaction treatments in pressure profile calculation. In addition to this, the difference might arise from the non-constant normal component issue discussed in section 3.6. In publication IV only $p_L(z)$ is shown because the normal component should be constant and 1 bar, which is negligible. However, as discussed in section 3.6, in atomistic simulations the normal component is not constant due to an unknown reason. Thus, if Griepernau and Böckmann have actually plotted the difference $p_L(z) - p_N(z)$, the difference might arise from this source.

Summarizing the present theoretical and simulation studies, they predict that the peaks in the pressure profile in the headgroup and interfacial regions are reduced due to alcohol, while changes in the acyl chain region are weaker. The decrease in the interfacial region is in agreement with conclusions drawn from micropipette aspiration studies [24, 142].

The results above seem to indicate that ethanol and other short-chain alcohols decrease the hydrophobic free energy density γ_{hpb}. This may have implications on membrane protein functionality, especially when combined to the results in publi-

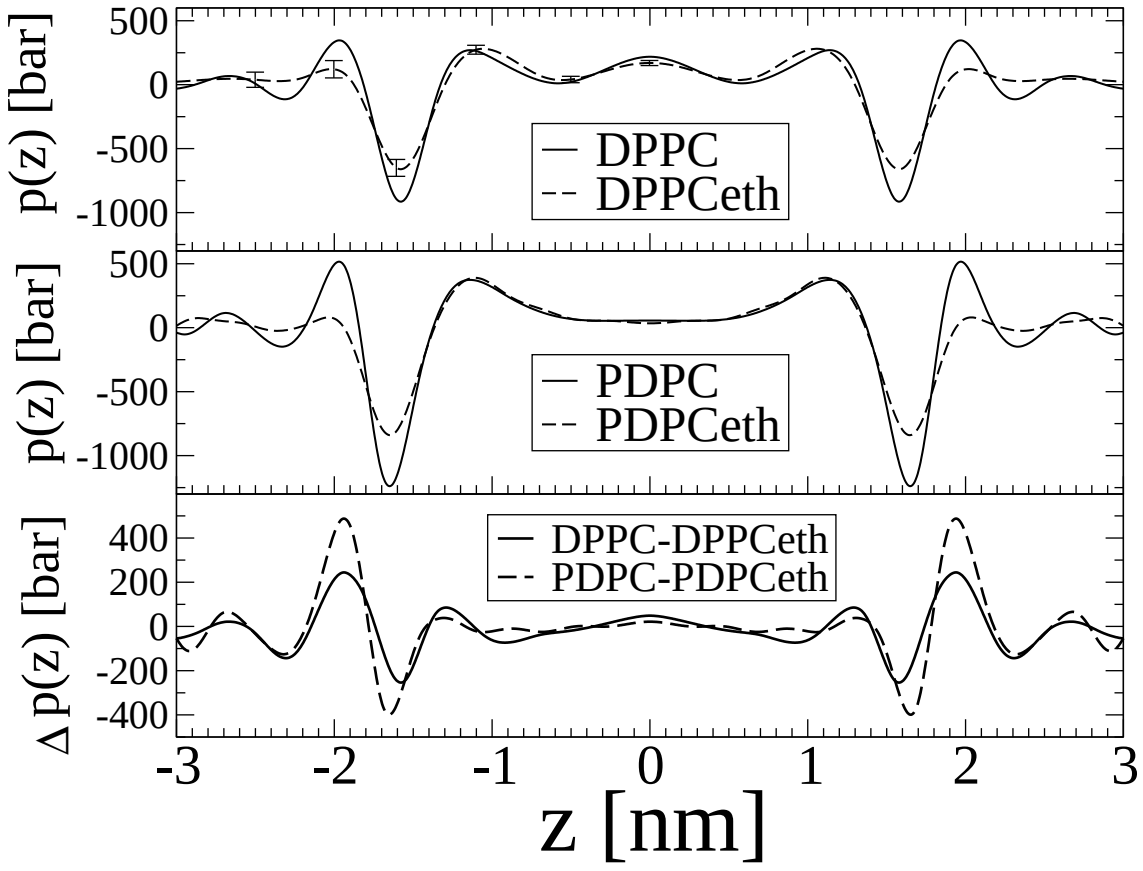

Figure 5.5: Lateral pressure profiles across a membrane for pure DPPC and PDPC bilayers, and for the same bilayer under the influence of ethanol (DPPCeth and PDPCeth). Adapted from publication IV.

cation VI where it is shown that largest mechanical energy differences between the protein states arise from the boundary region. However, the results have to be interpreted with some caution because the model used in publication IV is known to produce a too high partitioning of ethanol into the bilayer, which may exaggerate the effect.

Most studies of pressure profiles with anesthetic molecules have been done with alcohols as reviewed above. An exception is a recent study by Jerabek et al. who calculated pressure profiles with ketamine imbedded into a bilayer [76]. They also found significant changes in the pressure profile but in the acyl chain region instead

of the interfacial region. They also assumed possible shape changes for membrane channels in gating and showed that changes in pressure profile might have a significant influence on channel functionality with physiological concentrations of an anesthetic.

6 Physical implications from pressure profiles

6.1 Elastic properties calculated from lateral pressure profile

As discussed in section 2.2, the Gaussian bending modulus $\bar{\kappa}$, and the product of the bending modulus κ and the spontaneous curvature c_0 of a monolayer are connected to the lateral pressure profile through Eqs. (3.9) and (3.10). Further, the spontaneous curvature, as well as the bending and Gaussian bending moduli of a monolayer are related, e.g., to topological phase behavior [55], stalk formation [55, 143, 144], and membrane pore formation [145]. The product κc_0 is also interesting as such because it has been connected to the CTP activity [53, 54] and membrane protein activity [45] (see Eq. (3.16)).

Experimental values for the bending modulus for different bilayers have been published [25, 26] but experimental or theoretical estimates for spontaneous curvatures and Gaussian bending moduli are rare [25, 143, 144, 146]. Consequently, it is interesting to calculate the spontaneous curvatures using Eq. (3.9) and the Gaussian bending moduli using Eq. (3.10), see below.

Recently spontaneous curvatures for monolayers have been determined by calculating the first moment of the pressure profile, thus finding the bending modulus with another approach and calculating the spontaneous curvature from Eq. (3.9) $c_0^m = \tau_m^{(1)}/\kappa_m$ [73, 74]. Marrink et al. [73] used experimental estimates for the bending modulus of a bilayer $\kappa_b \approx (6-14) \times 10^{-20}$ J, and Orsi et al. [74] calculated the bending modulus from simulations and obtained $\kappa_b = (9.2 \pm 0.8) \times 10^{-20}$ J. The bending moduli for monolayers are then obtained by dividing these by two, that is, $\kappa_m = \kappa_b/2$ [25].

Table 6.1 summarizes the published elastic properties calculated from the pressure

profiles obtained through atomistic and coarse-grained molecular dynamics simulations. Spontaneous curvatures c_0 and Gaussian bending moduli $\bar{\kappa}$ are calculated also from pressure profiles in publications I, II, III and IV. To calculate the values of spontaneous curvatures we used experimental values for the bending modulus. However, this is not straightforward since the actual values vary significantly between different methods used [25, 26]. We have chosen the most representative values for each lipid by comparing the values gathered in two publications [25, 26]. Then error bars are chosen such that most of the reported values are inside the error (the most extreme values reported might be beyond the error bars). For DPPC, POPC and DOPC there was experimental data available. For PLPC, PAPC and PDPC experimental data was not available thus data available for other polyunsaturated lipids was used instead. Similarly for DPPC-cholesterol mixtures, we used the available data for mixtures of saturated lipid and cholesterol was used. For DOPC-cholestrol mixtures, the value has been measured to be independent of the amount of cholesterol, thus the pure DOPC value was employed [27, 28]. In the systems with ethanol the measured 20% decrease in the bending modulus was taken into account [24].

The Gaussian bending modulus is calculated directly from Eq. (3.10). The location of the neutral surface, i.e., the surface where stretching and bending deformation are energetically uncoupled is not excatly known [147, 148]. However, the location of the pivotal plane, i.e., the surface where the area per molecule remains constant when curvature is changed in the inverted phase, is known to reside close to the polar/apolar interface [30, 146, 149]. More precisely, Templer et al. [146] located the pivotal plane to the first maximum of the pressure profile after the interfacial peak in the acyl chain region. On the other hand, Orsi et al. [74] have defined the neutral surface to locate at the interfacial minimum of the pressure profile. Our results have been calculated using the surface in the middle of these two locations, and the error bars have been determined using the locations employed in previous studies. In principle, the first moment $\tau_m^{(1)}$ is independent of the location of the neutral plane in zero tension [25], which is the case in all simulations analyzed in

table 6.1. However, the integral over the pressure profile (surface tension) is not exactly zero because of numerical inaccuracy and the approximation of PME by the use of cutoff in the pressure profile calculation. Thus also the error in the first moment is approximated by using different locations for the neutral plane.

Table 6.1 presents the moments and elastic constants calculated from pressure profiles for bilayers with several different compositions. The data from coarse-grained studies are from publications by Marrink et al. [73] and Orsi et al. [74], and data from atomistic simulations are from publications I, II, III and IV. While moments of the pressure profile and their dependence on lipid content have also been studied by Cantor [44, 117], these results are difficult to compare with simulations because Cantor's statistical thermodynamic calculations included only the acyl chain region explicitly, thus we concentrate here on molecular dynamics simulation results presented in Table 6.1.

Comparison between calculated and experimental values for spontaneous curvature shows that the coarse-grained simulations by Marrink et al. [73] are in good agreement with experimental values for DOPC, while atomistic simulations yield somewhat larger values. Meanwhile, for a DOPE bilayer the coarse-grained simulations give smaller values than experimental studies. For a DOPC/CHOL mixture, atomistic values are in good agreement with experiments. In general all the simulation results produce negative spontaneous curvatures corresponding preference for the inverted phase, which is in agreement with experiments [30, 31, 32].

Even though quantitative data for spontaneous curvatures of different monolayers are sparse, the qualitative dependence is better known based on topological phase transitions [130]. Double bonds, small headgroups like PE, and cholesterol have been found to promote inverted phases [130]. Thus, inclusion of these lipids induces negative spontaneous curvature, while the effect of ethanol has been found to be the opposite [130]. From Table 6.1 one can see that the spontaneous curvatures

are more negative for polyunsaturated bilayers (about $-0.8\,\mathrm{nm}^{-1}$ for PLPC, PAPC, and PDPC) than for saturated ones ($-0.2\,\mathrm{nm}^{-1}$ for DPPC), calculated from publication I. Comparing the spontaneous curvatures determined from the coarse-grained study by Marrink et al. [73] for DOPC and DOPE bilayers, we see, as expected, that the spontaneous curvature is more negative with the PE headgroup. However, the effect of cholesterol on spontaneous curvature is more difficult to realize from the simulation results. Spontaneous curvatures for DOPC/cholesterol mixtures are slightly more negative than for pure DOPC, while for DPPC/cholesterol mixtures the trend is the opposite. Ethanol seems to have a different effect on saturated and polyunsaturated monolayers: for DPPC it induces more negative curvature while for PDPC the effect is negligible. In general, all the above findings are in qualitative agreement with topological phase studies except for the case where cholesterol was included in a DPPC bilayer.

However, in the above comparisons, there is reason to keep in mind that the error bars are relatively high due to the uncertainty in the bending modulus. Further, the numerical values for the bending modulus depend on experimental method used [25, 26], thus the values used here are suggestive. Due to these approximations, there is reason to consider these results with some caution. To improve the analysis, one could calculate the bending modulus from simulations and use that value to calculate the spontaneous curvature. This is likely soon feasible despite large system sizes needed for that purpose [150, 151].

Experimental measurements of the Gaussian bending modulus are sparse [25, 143, 146] and only the ratio with bending modulus has been reported [25]. Gaussian bending moduli for different bilayers calculated from molecular dynamics simulations are presented in Table 6.1. The coarse-grained study by Orsi et al. [74] suggests that the relation between the Gaussian bending modulus and the bending modulus is $\bar{\kappa}/\kappa \approx -0.5$, which is close to the experimental result $\bar{\kappa}/\kappa \approx -0.8$ [25]. The calculation of this ratio is not reasonable from other simulation results presented in

Table 6.1, because the value of the bending modulus is uncertain. However, qualitative predictions can be made. Gaussian bending moduli for polyunsaturated bilayers seem to be lower than for saturated bilayers, although the difference is within error bars. Respectively, Gaussian bending moduli for DPPC-cholesterol and DOPC-cholesterol mixtures are larger compared to pure bilayers, and the largest bending modulus is found for the pure sphingomyelin bilayer. This is in agreement with a picture that bending is generally more difficult for bilayers with high order. Inclusion of ethanol does not seem to have influence on the Gaussian bending modulus.

6.2 Bilayer mechanical energy in protein activation

Lateral pressure profiles determined from atomistic molecular dynamics simulations have been used to calculate mechanical energy differences associated with conformational changes of membrane proteins in publications II and III and in reference [71]. The studies have typically used simplified models for structures of proteins in two possible states (active vs. inactive), to describe a transition where a protein essentially changes structure from cylindrical to conical shape. As an example, consider Fig. 6.1 which describes a simplified transition of a membrane channel. The radius of the cone in the center of the bilayer (R) is kept constant, and the radius as a function of the normal coordinate z is then written as $r(z) = R + sz$, where s is the slope of the cone. For $s = 0$ one finds a cylinder, while a choice like $s = 0.2$ describes conical shape. Substituting these into Eq. (3.13) one gets

$$\begin{aligned} \Delta E = \textstyle\int_{-h}^{h} p(z)(\pi R^2 - \pi(R + sz)^2)\,\mathrm{d}z = \\ -2\pi R s \tau_b^{(1)} - \pi s^2 \tau_b^{(2)}. \end{aligned} \tag{6.1}$$

This description has been discussed as a simple model for MscL [71]. Note that in this case for a symmetric pressure profile ($p(z) = p(-z)$) the first moment $\tau^{(1)}$ vanishes, while the second moment $\tau^{(2)}$ is non-zero. Thus, for this kind of model the free energy difference of a conformational change between two states is small

Lipid	Reference	$\tau^{(1)} = \kappa c_0$ [10^{-12} J/m]	κ_m^{expt} [10^{-20} J]	c_0 [nm^{-1}]	c_0 [nm^{-1}] (Expt)	$\tau^{(2)} = \bar{\kappa}$ [10^{-20} J]
DPPC	I,II	-11 ± 1	5 ± 2	-0.2 ± 0.1		-1.1 ± 0.5
	[73] CG		5 ± 2	-0.02 to -0.05		
DMPC	[74] CG	-0.8 ± 0.1	4.6 ± 0.4	-0.018 ± 0.003		-2.3 ± 0.1
POPC	I	-12 ± 1	4 ± 2	-0.3 ± 0.2		-0.8 ± 0.5
DOPC	II	-16 ± 2	5 ± 2	-0.3 ± 0.2	-0.05 to -0.11 [30, 31]	-1.1 ± 0.8
	[73] CG		5 ± 2	-0.07 to -0.15		
	II	-16 ± 2	4 ± 2	-0.4 ± 0.2		-1.1 ± 0.8
PLPC	I	-15 ± 2	2 ± 1	-0.8 ± 0.5		-0.5 ± 0.5
PAPC	I	-14 ± 2	2 ± 1	-0.7 ± 0.5		-0.7 ± 0.5
PDPC	I	-15 ± 2	2 ± 1	-0.8 ± 0.5		-0.5 ± 0.5
DPPE	[73] CG		5 ± 2	-0.12 to -0.28		
DOPE	[73] CG		5 ± 2	-0.15 to -0.35	-0.35 to -0.37 [30, 32]	
DPPC/CHOL	II	-7 ± 2	12 ± 3	-0.1 ± 0.1		-2.3 ± 0.2
DPPC/DESMO	II	-20 ± 2	12 ± 3	-0.2 ± 0.1		-2.8 ± 0.8
DPPC/7-DHC	II	-8 ± 2	12 ± 3	-0.1 ± 0.1		-1.9 ± 0.3
DPPC/KETO	II	-9 ± 2	12 ± 3	-0.1 ± 0.1		-1.9 ± 0.3
DOPC/CHOL	II	-19 ± 2	4 ± 2	-0.5 ± 0.3	-0.37 [30]	-2.6 ± 0.6
DOPC/DESMO	II	-18 ± 2	4 ± 2	-0.5 ± 0.3		-2.8 ± 0.7
DOPC/7-DHC	II	-19 ± 2	4 ± 2	-0.5 ± 0.3		-2.2 ± 0.6
DPPCeth	IV	-15 ± 2	4 ± 2	-0.4 ± 0.2		-1.1 ± 0.7
PDPCeth	IV	-13 ± 2	2 ± 1	-0.7 ± 0.4		-1.0 ± 0.7
SM	III	-14 ± 2	5 ± 2	-0.3 ± 0.2		-3.2 ± 0.6

Table 6.1: Elastic coefficients calculated from lateral pressure profiles for several fluid-like pure and planar bilayers, PC-sterol binary systems, and the influence of ethanol. "CG" stands for coarse grained, "expt" stands for experiment, and "eth" refers to ethanol. The data given correspond to atomistic simulations, unless mentioned otherwise. Roman numbers refer to publications related to the thesis and Arabic numbers to references. Suggestive values for the bending modulus κ^{expt} are approximated from experimental values reported in [25, 26].

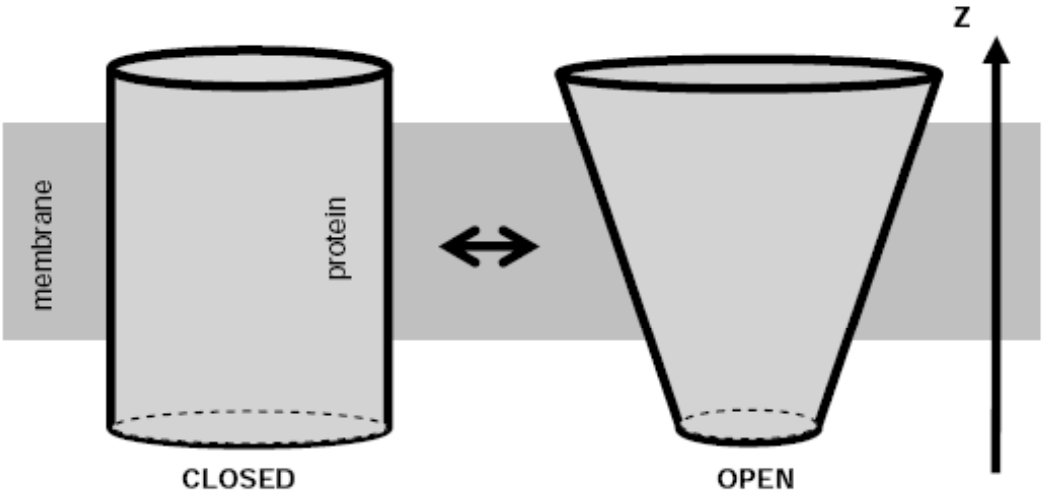

Figure 6.1: Schematic description of the two conformational states of MscL using a cone model. Adapted from [152].

compared, for example, to hour-glass shape where also the first moment would be non-zero. Hence, energies calculated for these kinds of models likely underestimate the free energy contribution due to the pressure profile.

Gullingsrud et al. [71] used this model together with lateral pressure profiles determined from atomistic molecular dynamics simulations to study the dependence of ΔE on lipid composition using DLPE, DLPC, POPE, and POPC lipid matrices. They concluded that changes between these lipid types yield a change of $(2-4)\,k_BT$ to energy differences between different conformations. Publication II considered changes in energy differences in DPPC/sterol and DOPC/sterol bilayers with a number of different sterols. In publication III this change was calculated in POPC/CHOL/SM ternary membranes. Energy differences in PC bilayers with different sterols varied between $(0.8-3.3)\,k_{\mathrm{B}}T$, while in the ternary mixtures they were considerably larger, about $(4-11)\,k_{\mathrm{B}}T$.

In recent publications also different models for ion channels have been discussed and

the calculated changes in energy difference between states due to the pressure profile have been found to be similar to previous studies [76, 153]. In the most recent study it was also demonstrated that ketamine, a well known anesthetic drug, can have a significant influence on ion channel equilibrium conformations through the pressure profile, also with realistic concentrations [76].

A shortcoming of all the above results for membrane protein gating energy is that they are based on an idealistic model used for the protein gating, as noted in publication II. In publication VI this approximation is avoided by simulating the mechanosensitive channel separately in the closed and open states embedded in a DOPC bilayer using molecular dynamics simulations and the MARTINI force field. The cross sectional area profiles and pressure profiles for a protein are then calculated explicitly. The pressure profile was calculated using Eq. (3.5) for each volume element. Then an average over a bulk bilayer was taken and it was assumed that the protein inclusion feels this pressure. The cross sectional area profiles and the pressure profile exerted against the protein in the open and closed states under different tensions are shown in Fig. 6.2.

The first observation is that in all states the largest cross sectional area is found from the location of the interfacial peak in the pressure profile. A plausible explanation for this is that the protein adapts the pressure distribution from a bilayer by expanding itself in the interfacial region. The expansion lowers the bilayer energy because the area for a contact between hydrophobic chains and water is smaller. A similar protein shape with maximum cross sectional areas in the interfacial region has been found also in studies of Ca^{2+}-ATPase [154].

The bilayer mechanical energy in gating, divided to the area dilation and shape contributions according to Eq. (3.21), is shown in Fig. 6.3 From the figure we see that the energy release in gating increases approximately linearly with increasing tension, as also found in patch clamp experiments [155, 156]. The total mechanical

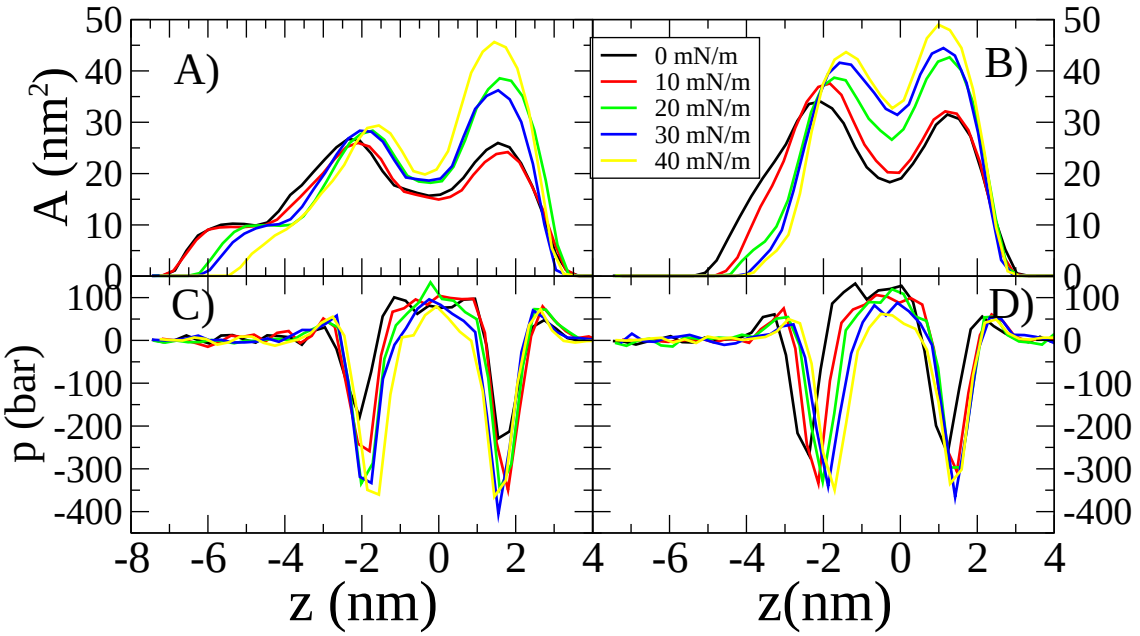

Figure 6.2: A) and B) Area profiles for the closed and open channel under different tensions, respectively. C) and D) Pressure profiles felt by the closed and open channel under different tensions, respectively. Negative z values area on the cytoplasmic side.

work done by the bilayer is always negative because the energy for the open state is always lower compared to the closed state in Fig. 6.3. Thus, the bilayer energy is in every case favorable for the open state, even under zero tension. The preference in zero tension is 30 k_BT which is significantly higher than previous estimates varying between 0-10 k_BT, see publications II and III and references [71, 76, 120, 121]. The main reason for the difference is that in previous studies one assumed simple shape transitions from a cylinder to a cone. However, in our simulations we see large area changes in the location of the surface between the hydrophobic interior of the bilayer and water. When the area of the protein is increased in this region, it reduces the contact area between water and the hydrophobic phase of the bilayer, reducing the hydrophobic energy. This energy release can be large because the hydrophobic surface energy is huge in nanoscale.

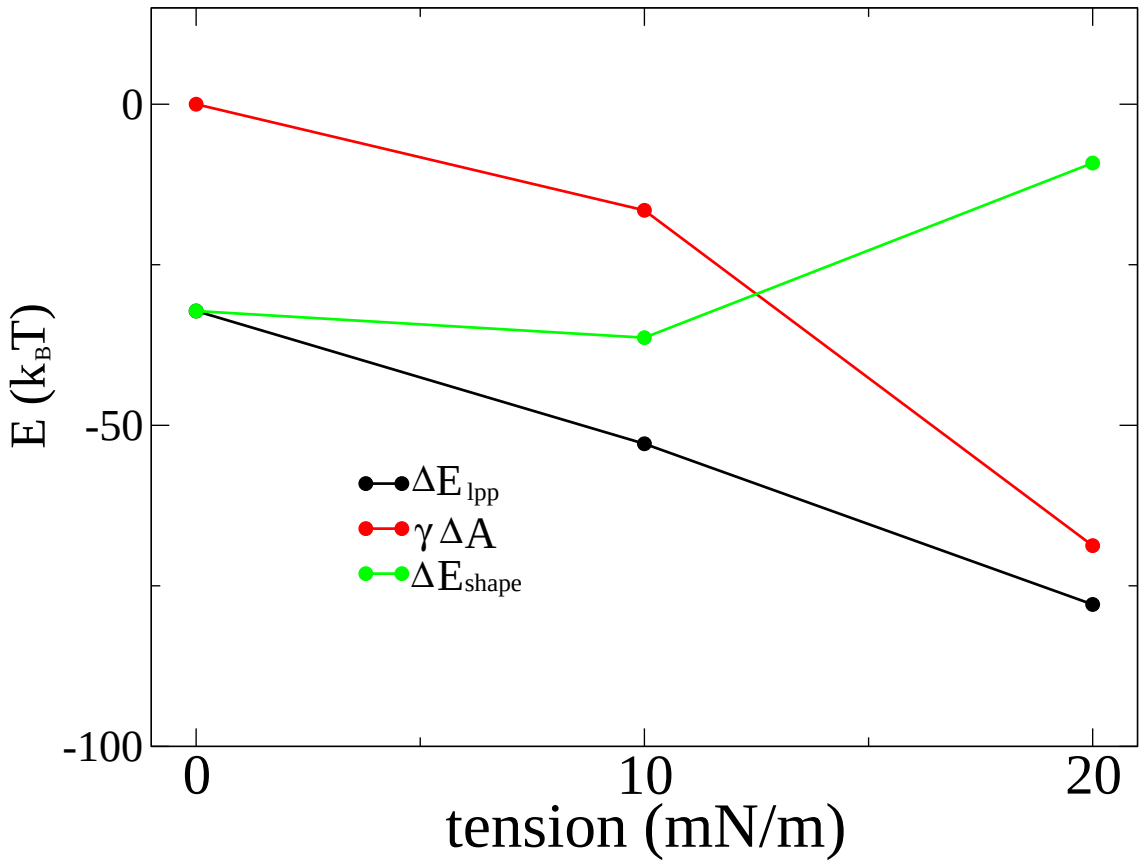

Figure 6.3: Energy release of a bilayer in gating, ΔE, divided to the area contribution $\gamma \Delta A$ and to the shape contribution ΔE_{shape} according to Eq. (3.21).

To give an order of magnitude estimate for the hydrophobic energy change with a realistic area change, we calculate the energy release when the area of a surface having a surface tension of 30 mN/m is decreased by 5 nm^2. 30mN/m is a reasonable approximation for the hydrophobic energy density at a hydrocarbon-water interface [38] and 5 nm^2 is realistic for the local change of the protein area (see our results above and [155, 156]). The released energy can be simply approximated as $\Delta E_{area} = -\gamma \Delta A \approx -30\text{mN/m} \times 5\text{nm}^2 \approx -35\, k_B T$. This demonstrates that small area changes in the location of an interface can have a significant energetic effect. This is not surprising because surface tension is known to have macroscopically measurable effects [36]. Thus, it is reasonable that it can also have significant effects in the length scale of proteins and membranes.

7 Conclusions

In this thesis, we have shown that changes in lipid composition can have major effect on the pressure profile of a lipid bilayer. We have also shown that these changes may be important in membrane protein functionality, creating 0-10 k_BT changes for the energy difference between the different protein states. We have also compared elastic properties calculated from pressure profiles to experimental results. Unfortunately this comparison is incomplete because we were not able to calculate bending moduli from our data and due to the lack of experimental data. However, the results point out that a full comparison is possible later, and an important subject for further studies.

In this thesis it has also been shown that the shape change of a mechanosensitive channel has an important contribution, even 30 k_BT, in the energetics of a gating process. It is suggested that this contribution should be taken into account in interpreting the patch clamp experiments for mechanosensitive channels. Furthermore, the gating energy dependence on protein shape arising from interfacial tension effects is likely a general phenomenon, which renders it relevant also for other proteins.

The main results of this thesis are, in principle, experimentally testable. However, in practice direct measurements are very difficult. For this reason it is very important to perform more complete comparisons between experimentally measured and simulation-based elastic properties. For the same reason it is important to solve the unknown technical problem, which causes the non-constant normal pressure component in atomistic membrane simulations. Before these issues have been solved, the pressure profile results from atomistic simulations have to be interpreted with caution.

Generally the results in this thesis support the idea that the pressure profile of a

lipid bilayer has an influence on protein functionality.

References

[1] M. F. Brown, "Modulation of rhodopsin function by properties of the membrane bilayer," *Chem. Phys. Lipids*, vol. 73, pp. 159–180, 1994.

[2] E. Perozo, A. Kloda, D. M. Cortes, and B. Martinac, "Physical principles underlying the transduction of bilayer deformation forces during mechanosensitive channel gating," *Nature Struct. Biol.*, vol. 9, pp. 696–703, 2002.

[3] A. G. Lee, "How lipids affect the activities of integral membrane proteins," *Biochim. Biophys. Acta - Biomembranes*, vol. 1666, pp. 62–87, 2004.

[4] R. Phillips, T. Ursell, P. Wiggins, and P. Sens, "Emerging roles for lipids in shaping membrane-protein function," *Nature*, vol. 459, pp. 379–385, 2009.

[5] O. S. Andersen and R. E. Koeppe, "Bilayer thickness and membrane protein function: An energetic perspective," *Annu Rev Biophys Biomol Struct.*, vol. 36, pp. 107–130, 2007.

[6] R. S. Cantor, "Lateral pressures in cell membranes: A mechanism fo modulation of protein function," *J. Phys. Chem. B*, vol. 101, pp. 1723–1725, 1997.

[7] T. Murtola, *Systematic Coarse-Graining Using Structural Information: Applications to Lipid Membranes*. PhD thesis, Helsinki University of Technology, 2009.

[8] J. F. Nagle and S. Tristram-Nagle, "Structure of lipid bilayers," *Biochem. Biophys. Acta*, vol. 1469, pp. 159–195, 2000.

[9] G. Pabst, N. Kucerka, M.-P. Nieh, M. Rheinstädter, and J. Katsaras, "Applications of neutron and x-ray scattering to the study of biologically relevant model membranes," *Chem Phys Lipids*, vol. 163, pp. 460 – 479, 2010.

[10] N. Kucerka, J. F. Nagle, J. N. Sachs, S. E. Feller, J. Pencer, A. Jackson, and J. Katsaras, "Lipid bilayer structure determined by the simultaneous analysis of neutron and x-ray scattering data," *Biophys. J.*, vol. 95, pp. 2356 – 2367, 2008.

[11] M. F. Brown and A. A. Nevzorov, "^{2}H-NMR in liquid crystals and membranes," *Colloids Surf., A*, vol. 158, pp. 281 – 298, 1999.

[12] R. B. Gennis, *Biomembranes*. New York: Springer Verlag, 1989.

[13] E. Evans, "Entropy-driven tension in vesicle membranes and unbinding of adherent vesicles," *Langmuir*, vol. 7, pp. 1900–1908, 1991.

[14] E. Lindahl and O. Edholm, "Mesoscopic undulations and thickness fluctuations in lipid bilayers from molecular dynamics simulations," *Biophys. J.*, vol. 79, pp. 426–433, 2000.

[15] O. Edholm, "Time and length scales in lipid bilayer simulations," in *Computational Modeling of Membrane Bilayers* (S. E. Feller, ed.), vol. 60 of *Current Topics in Membranes*, pp. 91 – 110, Academic Press, 2008.

[16] P. Almeida and W. Vaz, "Lateral diffusion in membranes," in *Structure and Dynamics of Membranes - From Cells to Vesicles* (R. Lipowsky and E. Sackmann, eds.), vol. 1, Part 1 of *Handbook of Biological Physics*, pp. 305 – 357, North-Holland, 1995.

[17] A. J. García-Sáez and P. Schwille, "Surface analysis of membrane dynamics," *Biochim. Biophys. Acta - Biomembranes*, vol. 1798, no. 4, pp. 766 – 776, 2010. A Surface View on Membrane Structure, Dynamics and Applications.

[18] G. Lindblom and G. Orädd, "Lipid lateral diffusion and membrane heterogeneity," *Biochim. Biophys. Acta - Biomembranes*, vol. 1788, no. 1, pp. 234 – 244, 2009. Lipid Interactions, Domain Formation, and Lateral Structure of Membranes.

[19] N. V. Eldho, S. E. Feller, S. Tristram-Nagle, I. V. Polozov, and K. Gawrisch, "Polyunsaturated docosahexaenoic vs docosapentaeoic acid-differences in lipid matrix properties from the loss of one double bond," *J. Am. Chem. Soc.*, vol. 125, pp. 6409–6421, 2003.

[20] W. Helfrich, "Elastic properties of lipid bilayers: theory and possible experiments.," *Z Naturforsch C.*, vol. 28, pp. 693–703, 1973.

[21] W. Rawicz, K. C. Olbrich, T. McIntosh, D. Needham, and E. Evans, "Effect of chain length and unsaturation on elasticity of lipid bilayers," *Biophys. J.*, vol. 79, pp. 328–339, 2000.

[22] K. J. Tierney, D. E. Block, and M. L. Longo, "Elasticity and phase behavior of DPPC membrane modulated by cholesterol, ergosterol, and ethanol," *Biophys. J.*, vol. 89, pp. 2481 – 2493, 2005.

[23] W. Rawicz, B. Smith, T. McIntosh, S. Simon, and E. Evans, "Elasticity, strength, and water permeability of bilayers that contain raft microdomain-forming lipids," *Biophys. J.*, vol. 94, pp. 4725 – 4736, 2008.

[24] H. V. Ly and M. L. Longo, "The influence of short-chain alcohols on interfacial tension, mechanical properties, area/molecule, and permeability of fluid lipid bilayers," *Biophys. J.*, vol. 87, pp. 1013–1033, 2004.

[25] D. Marsh, "Elastic curvature constants of lipid monolayers and bilayers," *Chem Phys Lipids*, vol. 144, pp. 146 – 159, 2006.

[26] M. Rappolt and G. Pabst, "Flexibility ans structure of fluid bilayer interfaces," in *Structure and dynamics of Memranous Interfaces* (K. Nag, ed.), pp. 45–81, John Wiley Sons, Hoboken (NJ), 2008.

[27] J. Pan, T. T. Mills, S. Tristram-Nagle, and J. F. Nagle, "Cholesterol perturbs lipid bilayers nonuniversally," *Phys. Rev. Lett.*, vol. 100, p. 198103, May 2008.

[28] J. Pan, S. Tristram-Nagle, and J. F. Nagle, "Effect of cholesterol on structural and mechanical properties of membranes depends on lipid chain saturation," *Phys. Rev. E*, vol. 80, p. 021931, Aug 2009.

[29] R. S. Gracia, N. Bezlyepkina, R. L. Knorr, R. Lipowsky, and R. Dimova, "Effect of cholesterol on the rigidity of saturated and unsaturated membranes: fluctuation and electrodeformation analysis of giant vesicles," *Soft Matter*, vol. 6, pp. 1472–1482, 2010.

[30] Z. Chen and R. P. Rand, "The influence of cholesterol on phospholipid membrane curvature and bending elasticity.," *Biophys. J.*, vol. 73, pp. 267–276, 1997.

[31] J. A. Szule, N. L. Fuller, and R. P. Rand, "The effects of acyl chain length and saturation of diacylglycerols and phosphatidylcholines on membrane monolayer curvature," *Biophys. J.*, vol. 83, pp. 977–984, 2002.

[32] E. E. Kooijman, V. Chupin, N. L. Fuller, M. M. Kozlov, B. de Kruijff, K. N. J. Burger, and P. R. Rand, "Spontaneous curvature of phosphatidic acid and lysophosphatidic acid," *Biochemistry*, vol. 44, pp. 2097 – 2102, 2005.

[33] D. P. Siegel, "Determining the ratio of the gaussian curvature and bending elastic moduli of phospholipids from QII phase unit cell dimensions," *Biophys. J.*, vol. 91, pp. 608 – 618, 2006.

[34] A. Ben-Shaul, "Molecular theory of chain packing, elasticity and lipid-protein interaction in lipid bilayers," in *Structure and Dynamics of Membranes - From Cells to Vesicles* (R. Lipowsky and E. Sackmann, eds.), vol. 1, Part 1 of *Handbook of Biological Physics*, pp. 359 – 401, North-Holland, 1995.

[35] S. A. Safran, *Statistical Thermodynamics of Surfaces, Interfaces, and Membranes*. Reading, MA: Addison-Wesley, 1994.

[36] J. N. Israelachvili, *Intermolecular and surface forces*. London: Academic Press, 1985.

[37] J. N. Israelachvili, S. Marcelja, and R. G. Horn, "Physical principles of membrane organization," *Q. Rev. Biophys.*, vol. 13, pp. 121–200, 1980.

[38] D. Marsh, "Lateral pressure in membranes," *Biochim. Biophys. Acta*, vol. 1286, pp. 183–223, 1996.

[39] T. S. Wiedemann, R. D. Pates, J. M. Beach, A. Salmon, and M. F. Brown, "Lipid-protein interactions mediate the photochemical function of rhodopsin," *Biochemistry*, vol. 27, pp. 6469–6474, 1988.

[40] N. J. Gibson and M. F. Brown, "Lipid headgroup and acyl chain composition modulate the MI-MII equilibrium of rhodopsin in recombinant membranes," *Biochemistry*, vol. 32, pp. 2438–2454, 1993.

[41] R. S. Cantor, "The lateral pressure profile in membranes: A physical mechanism of general anesthesia," *Biochemistry*, vol. 36, pp. 2339–2344, 1997.

[42] J. Seddon and R. Templer, "Polymorphism of lipid-water systems," in *Structure and Dynamics of Membranes - From Cells to Vesicles* (R. Lipowsky and E. Sackmann, eds.), vol. 1, Part 1 of *Handbook of Biological Physics*, pp. 97 – 160, North-Holland, 1995.

[43] R. S. Cantor, "Lipid composition and the lateral pressure profile in bilayers," *Biophys. J.*, vol. 76, pp. 2625–2639, 1999.

[44] R. S. Cantor, "The influence of membrane lateral pressures on simple geometric models of protein conformational equilibria," *Chem Phys Lipids*, vol. 101, pp. 45–56, 1999.

[45] D. Marsh, "Lateral pressure profile, spontaneous curvature frustration, and the incorporation and conformation of proteins in membranes," *Biophys. J.*, vol. 93, pp. 3884–3899, 2007.

[46] D. Marsh, "Protein modulation of lipids, and vice-versa, in membranes," *Biochem. Biophys. Acta*, vol. 1778, pp. 1545–1575, 2008.

[47] E. Perozo, "Structure and mechanism in prokaryotic mechanosensitive channels," *Curr. Opin. Struc. Biol.*, vol. 13, pp. 432–442, 2003.

[48] J. H. A. Folgering, J. M. Kuiper, A. H. de Vries, J. B. Engberts, and B. Poolman, "Lipid-mediated light activation of a mechanosensitive channel of large conductance," *Langmuir*, vol. 20, pp. 6985–6987, 2004.

[49] M. Kuiper, *Azobenzene-substituted Phosphate Amphiphiles*. PhD thesis, Rijksuniversiteit Groningen, 2005.

[50] E. van den Brink-van der Laan, V. Chupin, J. A. Killian, and B. de Kruijff, "Small alcohols destabilize the KcsA tetramer via their effect on the membrane lateral pressure," *Biochemistry*, vol. 43, pp. 5937 – 5942, 2004.

[51] E. van den Brink-van der Laan, J. A. Killian, and B. Kruijff, "Nonbilayer lipids affect peripheral and integral membrane proteins via changes in the lateral pressure profile," *Biochim. Biophys. Acta*, vol. 1666, pp. 275–288, 2004.

[52] A. V. Botelho, T. Huber, T. P. Sakmar, and M. F. Brown, "Curvature and hydrophobic forces drive oligomerization and modulate activity of rhodopsin in membranes," *Biophys. J.*, vol. 91, pp. 4464–4477, 2006.

[53] G. S. Attard, R. H. Templer, W. S. Smith, A. N. Hunt, and S. Jackowski, "Modulation of CTP:phosphocholine cytidylyltransferase by membrane curvature elastic stress," *Proc. Natl. Acad. Sci. USA*, vol. 97, pp. 9032–9036, 2000.

[54] G. Shearman, G. Attard, A. Hunt, S. Jackowski, M. Baciu, S. Sebai, X. Mulet, J. Clarke, R. Law, C. Plisson, C. Parker, A. Gee, O. Ces, and R. Templer, "Using membrane stress to our advantage," *Biochem. Soc. Trans.*, vol. 35, pp. 498–501, 2007.

[55] J. M. Seddon, "Structure of the inverted hexagonal (hii) phase, and non-lamellar phase transitions of lipids," *Biochim. Biophys. Acta - Reviews on Biomembranes*, vol. 1031, no. 1, pp. 1 – 69, 1990.

[56] R. H. Templer, S. J. Castle, A. R. Curran, G. Rumbles, and D. R. Klug, "Sensing isothermal changes in the lateral pressure profile in model membranes using di-pyrenol phosphatidylcholine," *Faraday Discuss.*, vol. 111, pp. 41–53, 1999.

[57] T. Kamo, M. Nakano, Y. Kuroda, and T. Handa, "Effects of an amphipathic α-helical peptide on lateral pressure and water penetration in phosphatidylcholine and monoolein mixed membranes," *J. Phys. Chem. B*, vol. 110, pp. 24987 – 24992, 2006.

[58] J. Curdova, P. Capkova, J. Plasek, J. Repakova, and I. Vattulainen, "Free pyrene probes in gel and fluid membranes: Perspective through atomistic simulations," *J. Phys. Chem. B*, vol. 111, p. 3640, 2007.

[59] S.-S. Feng, "Interpretation of mechanochemical properties of lipid bilayer vesicles from the equation of state or pressure-area measurement of the monolayer at the air-water or oil-water interface," *Langmuir*, vol. 15, pp. 998–1010, 1999.

[60] D. Marsh, "Comment on interpretation of mechanochemical properties of lipid bilayer vesicles from the equation of state or pressure-area measurement of the monolayer at the air-water or oil-water interface," *Langmuir*, vol. 22, pp. 2916 –2919, 2006.

[61] S.-S. Feng, "Reply to comment on interpretation of mechanochemical properties of lipid bilayer vesicles from the equation of state or pressure-area measurement of the monolayer at the air-water or oil-water interface," *Langmuir*, vol. 22, pp. 2920 –2922, 2006.

[62] D. Harries and A. Ben-Shaul, "Conformational chain statistics in a model lipid bilayer: Comparison between mean field and Monte Carlo calculations," *J. Chem. Phys.*, vol. 106, pp. 1609–1619, 1997.

[63] T. Xiang and B. D. Anderson, "Molecular distribution in interphases: Statistical mechanical theory combined with molecular dynamics simulation of a model lipid bilayer," *Biophys. J.*, vol. 66, pp. 561–573, 1994.

[64] S. I. Mukhin and S. Baoukina, "Analytical derivation of thermodynamic characteristics of lipid bilayer from a flexible string model," *Phys. Rev. E*, vol. 71, pp. 061918–061923, 2005.

[65] R. Goetz and R. Lipowsky, "Computer simulations of bilayer membranes: Self-assembly and interfacial tension," *J. Chem. Phys.*, vol. 108, pp. 7397–7409, 1998.

[66] M. Venturoli and B. Smit, "Simulating the self-assembly of model membranes," *Phys. Chem. Comm.*, vol. 2, pp. 45–49, 1999.

[67] M. Carrillo-Tripp and S. E. Feller, "Evidence for a mechanism by ω-3 polyunsaturated lipids may affect membrane protein function," *Biochemistry*, vol. 44, pp. 10164–10169, 2005.

[68] J. Sonne, F. Y. Hansen, and G. H. Peters, "Methological problems in pressure profile calculations for lipid bilayers," *J. Chem. Phys.*, vol. 122, p. 124903, 2005.

[69] E. Lindahl and O. Edholm, "Spatial and energetic-entropic decomposition of surface tension in lipid bilayers from molecular dynamics simulations," *J. Chem. Phys.*, vol. 113, pp. 3882–3893, 2000.

[70] J. Gullingsrud and K. Schulten, "Gating of MscL studied by steered molecular dynamics," *Biophys. J.*, vol. 85, pp. 2087–2099, 2003.

[71] J. Gullingsrud and K. Schulten, "Lipid bilayer pressure profiles and mechanosensitive channel gating," *Biophys. J.*, vol. 86, pp. 3496–3509, 2004.

[72] M. Patra, "Lateral pressure profiles in cholesterol-DPPC bilayers," *Eur. Biophys. J.*, vol. 35, pp. 79–88, 2005.

[73] S. Marrink, H. Risselada, S. Yefimov, D. Tieleman, and A. de Vries, "The MARTINI forcefield: coarse grained model for biomolecular simulations.," *J. Phys. Chem. B*, vol. 111, pp. 7812–7824, 2007.

[74] M. Orsi, D. Y. Haubertin, W. E. Sanderson, and J. W. Essex, "A quantitative coarse-grain model for lipid bilayers," *J. Phys. Chem. B*, vol. 112, pp. 802–815, 2008.

[75] B. Griepernau and R. A. Böckmann, "The influence of 1-alkanols and external pressure on the lateral pressure profiles of lipid bilayers," *Biophys. J.*, vol. 95, pp. 5766 – 5778, 2008.

[76] H. Jerabek, G. Pabs, M. Rappolt, and T. Stockner, "Membrane-mediated effect on ion channels induced by the anesthetic drug ketamine," *J. Am. Chem. Soc.*, vol. 132, pp. 7990–7997, 2010.

[77] K. Lähdesmäki, O. S. Ollila, A. Koivuniemi, P. T. Kovanen, and M. T. Hyvönen, "Membrane simulations mimicking acidic ph reveal increased thickness and negative curvature in a bilayer consisting of lysophosphatidylcholines and free fatty acids," *Biochim. Biophys. Acta - Biomembranes*, vol. 1798, no. 5, pp. 938 – 946, 2010.

[78] H. J. C. Berendsen, *Simulating physical world*. Cambridge University Press, 2007.

[79] H. J. C. Berendsen, D. van der Spoel, and R. van Drunen, "GROMACS: A message-passing parallel molecular dynamics implementation.," *Comput. Phys. Commun.*, vol. 91, pp. 43–56, 1995.

[80] E. Lindahl, B. Hess, and D. van der Spoel, "Gromacs 3.0: a package for molecular simulation and trajectory analysis," *J. Mol. Model.*, vol. 7, pp. 306–317, 2001.

[81] D. van der Spoel, E. Lindahl, B. Hess, B. Groenhof, A. E. Mark, and H. J. C. Berendsen, "Gromacs: Fast, flexible and free," *J. Comp. Chem.*, vol. 26, pp. 1701–1718, 2005.

[82] B. Hess, C. Kutzner, D. van der Spoel, and E. Lindahl, "Gromacs 4: Algorithms for highly efficient, load-balanced, and scalable molecular simulation," *J. Chem. Theory Comput.*, vol. 4, pp. 435–447, 2008.

[83] D. Frenkel and B. Smit, *Understanding molecular simulation.* Academic Press, 2002.

[84] M. P. Allen and D. J. Tildesley, *Computer simulation of liquids.* Oxford: Oxford University Press, 1989.

[85] B. Hess, H. Bekker, H. J. C. Berendsen, and J. G. E. M. Fraaije, "LINCS: a linear constraint solver for molecular dynamics simulations," *J. Comput. Chem.*, vol. 18, pp. 1463–1472, 1997.

[86] J. B. Klauda, R. M. Venable, A. D. M. Jr., and R. W. Pastor, "Considerations for lipid force field development," in *Computational Modeling of Membrane Bilayers* (S. E. Feller, ed.), vol. 60 of *Current Topics in Membranes*, pp. 1 – 48, Academic Press, 2008.

[87] J. B. Klauda, R. M. Venable, J. A. Freites, J. W. O'Connor, D. J. Tobias, C. Mondragon-Ramirez, I. Vorobyov, A. D. M. Jr, and R. W. Pastor, "Update of the CHARMM all-atom additive force field for lipids: Validation on six lipid types," *J. Phys. Chem. B*, vol. 114, pp. 7830–7843, 2010.

[88] N. Sapay and D. P. Tieleman, "Molecular dynamics simulation of lipid-protein interactions," in *Computational Modeling of Membrane Bilayers* (S. E. Feller,

ed.), vol. 60 of *Current Topics in Membranes*, pp. 111 – 130, Academic Press, 2008.

[89] S. A. Pandit, S. wing Chiu, E. Jakobsson, and H. L. Scott, "Atomistic and mean field simulations of lateral organization in membranes," in *Computational Modeling of Membrane Bilayers* (S. E. Feller, ed.), vol. 60 of *Current Topics in Membranes*, pp. 281 – 312, Academic Press, 2008.

[90] D. P. Tieleman, J. L. MacCallum, W. L. Ash, C. Kandt, Z. Xu, and L. Monticelli, "Membrane protein simulations with a united-atom lipid and all-atom protein model: lipid-protein interactions, side chain transfer free energies and model proteins," *J. Phys. Condens. Matter*, vol. 18, no. 28, p. S1221, 2006.

[91] L. Monticelli, E. Salonen, and D. P. Tieleman, "Calgary lipids: A lipid force field for molecular simulations," *Biophys. J.*, vol. 98, pp. 668a – 668a, 2010.

[92] A. H. de Vries, M. Fuhrmans, J. Risselada, M. E. Siwko, V. Knecht, and S. J. Marrink, "Phase transformations of lipid aggregates at molecular resolution," *Biophys. J.*, vol. Suppl. S, pp. 192A–193A, 2007.

[93] O. Berger, O. Edholm, and F. Jähnig, "Molecular dynamics simulations of a fluid bilayer of dipalmitoylphosphatidylcholine at full hydration, constant pressure, and constant temperature," *Biophys. J.*, vol. 72, pp. 2002 – 2013, 1997.

[94] S. Marrink, A. de Vries, and A. E. Mark, "Coarse grained model for semi-quantitative lipid simulations.," *J. Phys. Chem. B*, vol. 108, pp. 750–760, 2004.

[95] L. Monticelli, S. K. Kandasamy, X. Periole, R. G. Larson, D. P. Tieleman, and S.-J. Marrink, "The MARTINI coarse-grained force field: Extension to proteins," *J. Chem. Theor. Comp.*, vol. 4, no. 5, pp. 819–834, 2008.

[96] S. Chiu, M. Clark, V. Balaji, S. Subramaniam, H. Scott, and E. Jakobsson, "Incorporation of surface tension into molecular dynamics simulation of an

interface: a fluid phase lipid bilayer membrane," *Biophys. J.*, vol. 69, pp. 1230 – 1245, 1995.

[97] M. Höltje, T. Förster, B. Brandt, T. Engels, W. von Rybinski, and H.-D. Höltje, "Molecular dynamics simulations of stratum corneum lipid models: fatty acids and cholesterol," *Biochim. Biophys. Acta - Biomembranes*, vol. 1511, no. 1, pp. 156 – 167, 2001.

[98] H. J. C. Berendsen, J. P. M. Postma, W. F. van Gunsteren, A. DiNola, and J. R. Haak, "Molecular dynamics with coupling to an external bath.," *J. Chem. Phys.*, vol. 81, pp. 3684–3690, 1984.

[99] S. Nose, "A molecular dynamics method for simulations in the canonical ensemble.," *Mol. Phys.*, vol. 52, pp. 255–268, 1984.

[100] W. G. Hoover, "Canonical dynamics: Equilibrium phase-space distributions.," *Phys. Rev. A*, vol. 31, pp. 1695–1697, 1985.

[101] M. Parrinello and A. Rahman, "Polymorphic transitions in single crystals: A new molecular dynamics method," *J. Appl. Phys.*, vol. 52, pp. 7182–7190, 1981.

[102] P. Schofield and J. R. Henderson, "Statistical mechanics of inhomogeneous fluids," *Proc. R. Soc. London, Ser. A*, vol. 379, pp. 231–246, 1982.

[103] L. Mistura, "The definition of the pressure tensor in the statistical mechanics of nonuniform classical fluids," *Int. J. Thermophys.*, vol. 8, pp. 397–403, 1987.

[104] B. Hafskjold and T. Ikeshoji, "Microscopic pressure tensor for hard-sphere fluids," *Phys. Rev. E*, vol. 66, p. 011203, 2002.

[105] E. Wajnryb, A. R. Altenberger, and J. S. Dahler, "Uniqueness of the microscopic stress tensor," *J. Chem. Phys.*, vol. 103, no. 22, pp. 9782–9787, 1995.

[106] S. Morante, G. C. Rossi, and M. Testa, "The stress tensor of a molecular system: An exercise in statistical mechanics," *J. Chem. Phys.*, vol. 125, p. 034101, 2006.

[107] R. Lovett and M. Baus, "A molecular theory of the Laplace relation and of the local forces in a curved interface," *J. Chem. Phys.*, vol. 106, pp. 635–644, 1997.

[108] B. D. Todd, D. J. Evans, and P. J. Daivis, "Pressure tensor for inhomogeneous fluids," *Phys. Rev. E*, vol. 52, pp. 1627–1638, Aug 1995.

[109] J. H. Irving and J. G. Kirkwood, "The statistical mechanical theory of transport processes. IV. the equations of hydrodynamics," *J. Chem. Phys.*, vol. 18, pp. 817–829, 1950.

[110] A. Harasima, "Molecular theory of surface tension," *Adv. Chem. Phys.*, vol. 1, pp. 203–237, 1958.

[111] J. S. Rowlinson and B. Widom, *Molecular Theory of Capillarity.* Oxford: Clarendon press, 1982.

[112] "General discussion," *Faraday Discuss.*, vol. 144, pp. 445–466, 2010.

[113] O. H. S. Ollila. Master's thesis, Laboratory of Physics, Helsinki University of Technology, 2006.

[114] I. Szleifer, D. Kramer, A. Ben-Shaul, W. M. Gelbart, and S. A. Safran, "Molecular theory of curvature elasticity in surfactant films," *J. Chem. Phys.*, vol. 92, no. 11, pp. 6800–6817, 1990.

[115] G. Brannigan and F. L. H. Brown, "A consistent model for thermal fluctuations and protein-induced deformations in lipid bilayers," *Biophys. J.*, vol. 90, pp. 1501–1520, 2006.

[116] V. S. Markin and F. Sachs, "Thermodynamics of mechanosensitivity," *Phys. Biol.*, vol. 1, no. 2, p. 110, 2004.

[117] R. S. Cantor, "Size distribution of barrel-stave aggregates of membrane peptides: Influence of the bilayer lateral pressure profile," *Biophys. J.*, vol. 82, pp. 2520–2525, 2002.

[118] P. Wiggins and R. Phillips, "Membrane-protein interactions in mechanosensitive channels," *Biophys. J.*, vol. 88, pp. 880 – 902, 2005.

[119] T. Ursell, J. Kondev, D. Reeves, P. A. Wiggins, and R. Phillips, "The role of lipid bilayer mechanics in mechanosensation," in *Mechanosensitivity in Cells and Tissues 1: Mechanosensitive Ion Channels* (A. Kamkin and I. Kiseleva, eds.), Springer-Verlag, 2008.

[120] D. Reeves, T. Ursell, P. Sens, J. Kondev, and R. Phillips, "Membrane mechanics as a probe of ion-channel gating mechanisms," *Phys. Rev. E*, vol. 78, no. 4, p. 041901, 2008.

[121] T. Ursell, K. C. Huang, E. Peterson, and R. Phillips, "Cooperative gating and spatial organization of membrane proteins through elastic interactions," *PLoS Comput Biol*, vol. 3, no. 5, p. e81, 2007.

[122] M. S. Turner and P. Sens, "Gating-by-tilt of mechanically sensitive membrane channels," *Phys. Rev. Lett.*, vol. 93, no. 11, p. 118103, 2004.

[123] M. Patra, M. Karttunen, M. T. Hyvönen, E. Falck, P. Lindqvist, and I. Vattulainen, "Molecular dynamics simulations of lipid bilayers: Major artifacts due to truncating electrostatic interactions," *Biophys. J.*, vol. 84, pp. 3636–3645, 2003.

[124] M. Patra, M. Karttunen, M. Hyvönen, E. Falck, and I. Vattulainen, "Lipid bilayers driven to a wrong lane in molecular dynamics simulations by subtle changes in long-range electrostatic interactions," *J. Phys. Chem. B*, vol. 108, pp. 4485–4494, 2004.

[125] M. Patra, M. Hyvonen, E. Falck, M. Sabouri-Ghomi, I. Vattulainen, and M. Karttunen, "Long-range interactions and parallel scalability in molecular simulations," *Comput. Phys. Commun.*, vol. 176, pp. 14–22, 2007.

[126] J. P. Ryckaert, G. Ciccotti, and H. J. C. Berendsen, "Numerical integration of the cartesian equations of motion of a system with constrains: Molecular dynamics of *n*-alkanes," *J. Comput. Phys.*, vol. 23, pp. 327–341, 1977.

[127] S. Baoukina, S. J. Marrink, and D. P. Tieleman, "Lateral pressure profiles in lipid monolayers," *Faraday Discuss.*, vol. 144, pp. 393–409, 2010.

[128] V. Belyy, K. Kamaraju, B. Akitake, A. Anishkin, and S. Sukharev, "Adaptive behavior of bacterial mechanosensitive channels is coupled to membrane mechanics," *J Gen Physiol*, vol. 135, pp. 641–652, 2010.

[129] Y. Weng, T. T. Hsu, J. Zhao, S. Nishimura, G. G. Fuller, and J. M. Sonner, "Isovaleric, methylmalonic, and propionic acid decrease anesthetic ec50 in tadpoles, modulate glycine receptor function, and interact with the lipid 1,2-dipalmitoyl-sn-glycero-3-phosphocholine," *Anesth Analg*, vol. 108, pp. 1538–1545, 2009.

[130] K. Gawrisch and L. L. Holte, "NMR investigations of non-lamellar phase promoters in the lamellar phase state," *Chem. Phys. Lipids*, vol. 81, pp. 105–116, 1996.

[131] D. Marsh, "Components of the lateral pressure in lipid bilayers deduced from HII phase dimensions," *Biochim. Biophys. Acta*, vol. 1279, pp. 119–123, 1996.

[132] B. J. Litman and D. C. Mitchell, "A role for phospholipid polyunsaturation in modulating membrane protein function," *Lipids*, vol. 31, pp. S193–S197, 1996.

[133] S.-L. Niu, D. C. Mitchell, and B. J. Litman, "Manipulation of cholesterol levels in rod disk membranes by methyl-beta -cyclodextrin. Effects on receptor activation," *J. Biol. Chem.*, vol. 277, pp. 20139–20145, 2002.

[134] D. C. Mitchell, M. Straume, J. L. Miller, and B. J. Litman, "Modulation of metarhodopsin formation by cholesterol-induced ordering of bilayer lipids," *Biochemistry*, vol. 29, pp. 9143 – 9149, 1990.

[135] S. R. Wassall and W. Stillwell, "Docosahexaenoic acid domains: the ultimate non-raft membrane domain," *Chem Phys Lipids*, vol. 153, no. 1, pp. 57 – 63, 2008.

[136] N. P. Franks, "Molecular targets underlying general anaesthesia," *Br. J. Pharmacol.*, vol. 147, no. S1, pp. S72–S81, 2006.

[137] R. S. Cantor, K. S. Twyman, P. S. Milutinovic, and R. Haseneder, "A kinetic model of ion channel electrophysiology: bilayer-mediated effects of agonists and anesthetics on protein conformational transitions," *Soft Matter*, vol. 5, pp. 3266–3278, 2009.

[138] K. Wodzinska, A. Blicher, and T. Heimburg, "The thermodynamics of lipid ion channel formation in the absence and presence of anesthetics. blm experiments and simulations," *Soft Matter*, vol. 5, pp. 3319–3330, 2009.

[139] R. S. Cantor, "The lateral pressure profile in membranes: a physical mechanism of general anesthesia," *Toxicol. Lett.*, vol. 100-101, pp. 451–458, 1998.

[140] L. Yang and J. M. Sonner, "Anesthetic-like modulation of receptor function by surfactants: A test of the interfacial theory of anesthesia," *ANESTHESIA ANALGESIA*, vol. 107, pp. 868–874, 2008.

[141] A. L. Frischknecht and L. J. D. Frink, "Alcohols reduce lateral membrane pressures: Predictions from molecular theory," *Biophys. J.*, vol. 91, pp. 4081–4090, 2006.

[142] H. V. Ly, D. E. Block, and M. L. Longo, "Interfacial tension effect of ethanol on lipid bilayer rigidity, stability, and area/molecule: A micropipet aspiration approach," *Langmuir*, vol. 18, pp. 8988 – 8995, 2002.

[143] D. P. Siegel and M. M. Kozlov, "The gaussian curvature elastic modulus of n-monomethylated dioleoylphosphatidylethanolamine: Relevance to membrane fusion and lipid phase behavior," *Biophys. J.*, vol. 87, pp. 366–374, 2004.

[144] D. P. Siegel, "The gaussian curvature elastic energy of intermediates in membrane fusion," *Biophys. J.*, vol. 95, pp. 5200 – 5215, 2008.

[145] J. Wohlert, W. K. den Otter, O. Edholm, and W. J. Briels, "Free energy of a trans-membrane pore calculated from atomistic molecular dynamics simulations," *J. Chem. Phys.*, vol. 124, p. 154905, 2006.

[146] R. H. Templer, B. J. Khoo, and J. M. Seddon, "Gaussian curvature modulus of an amphiphilic monolayer," *Langmuir*, vol. 14, pp. 7427–7434, 1998.

[147] M. M. Kozlov and M. Winterhalter, "Elastic-moduli for strongly curved monolayers - position of the neutral surface," *J. Phys. France II*, vol. 1, pp. 1077–1084, 1991.

[148] M. M. Kozlov and M. Winterhalter, "Elastic-moduli and neutral surface for strongly curved monolayers - analysis of experimental results," *J. Phys. France II*, vol. 1, pp. 1085–1100, 1991.

[149] S. Leikin, M. Kozlov, N. Fuller, and R. Rand, "Measured effects of diacylglycerol on structural and elastic properties of phospholipid membranes," *Biophys. J.*, vol. 71, pp. 2623–2632, 1996.

[150] S. Baoukina, L. Monticelli, H. J. Risselada, S. J. Marrink, and D. P. Tieleman, "The molecular mechanism of lipid monolayer collapse," *Proc. Natl. Acad. Sci. USA*, vol. 105, pp. 10803–10808, 2008.

[151] J. Wong-Ekkabut, S. Baoukina, W. Triampo, I.-M. Tang, D. P. Tieleman, and L. Monticelli, "Computer simulation study of fullerene translocation through lipid membranes," *Nature Nanotech.*, vol. 3, pp. 363–368, 2008.

[152] P. S. Niemelä, M. T. Hyvönen, and I. Vattulainen, "Atom-scale molecular interactions in lipid raft mixtures," *Biochim. Biophys. Acta - Biomembranes*, vol. 1788, no. 1, pp. 122 – 135, 2009.

[153] G. Pabst, B. Boulgaropoulos, E. Gander, B. R. Sarangi, H. Amenitsch, V. A. Raghunathan, and P. Laggner, "Effect of ceramide on nonraft proteins," *J. Membr. Biol.*, vol. 231, pp. 125–132, 2009.

[154] M. Musgaard, J. V. Møller, P. Nissen, L. Thøgersen, and B. Schiøtt, "Modeling the membrane role in ca2+-atpase catalytic cycle," *Biophys. J.*, vol. 98, pp. 487a – 487a, 2010.

[155] S. I. Sukharev, W. J. Sigurdson, C. Kung, , and F. Sachs, "Energetic and spatial parameters for gating of the bacterial large conductance mechanosensitive channel, MscL," *J Gen Physiol*, vol. 113, pp. 525–540, 1999.

[156] C.-S. Chiang, A. Anishkin, and S. Sukharev, "Gating of the large mechanosensitive channel in situ: Estimation of the spatial scale of the transition from channel population responses," *Biophys. J.*, vol. 86, pp. 2846–2861, 2004.

[157] L. D. Landau and E. M. Lifshitz, *Theory of Elasticity.* Oxford: Pergamon press, 1970.

Appendix A Properties of pressure tensor in planar homogenuous bilayer in liquid phase

The pressure tensor in general case can be written as

$$\mathbf{P} = \begin{pmatrix} p_{xx} & p_{xy} & p_{xz} \\ p_{yx} & p_{yy} & p_{yz} \\ p_{zx} & p_{zy} & p_{zz} \end{pmatrix}. \tag{A.1}$$

The stability condition for the local pressure tensor $\nabla \cdot \mathbf{P} = 0$ can be written as [111, 157]

$$F_i = \partial p_{ik}/\partial x_k = 0, \tag{A.2}$$

where the Einstein summation convention is used and the F_i is the ith component of the force acting to the volume element. Here we assume that there are no external forces. Practically this condition means that the forces acting to the volume element has to cancel each others in equilibrium [157]. Also the moments of the forces has to cancel in equilibrium which leads to the symmetry of the pressure tensor [157].

Above applies generally for pressure tensors in any solid or liquid systems in equilibrium without external forces. Next we focus on properties of pressure tensor in a lipid bilayer in liquid phase. By expanding Eqs. A.2 we get

$$\begin{aligned} \tfrac{\partial p_{xx}}{\partial x} + \tfrac{\partial p_{xy}}{\partial y} + \tfrac{\partial p_{xz}}{\partial z} &= 0 \\ \tfrac{\partial p_{yx}}{\partial x} + \tfrac{\partial p_{yy}}{\partial y} + \tfrac{\partial p_{yz}}{\partial z} &= 0 \\ \tfrac{\partial p_{zx}}{\partial x} + \tfrac{\partial p_{zy}}{\partial y} + \tfrac{\partial p_{zz}}{\partial z} &= 0 \end{aligned} \tag{A.3}$$

If we assume that the system is homogenuous in xy-plane all the derivates respect to the x or y must be zero. The we get for the pressure tensor

$$\frac{\partial p_{xz}}{\partial z} = 0; \quad \frac{\partial p_{yz}}{\partial z} = 0; \quad \frac{\partial p_{zz}}{\partial z} = 0. \tag{A.4}$$

which means that p_{xz}, p_{yz} and p_{zz} must be independent from the z. On the other hand, in water phase $p_{xz} = p_{yz} = 0$ due to the lack of shear stress in liquid water,

thus they must zero through the whole system. Furthermore, a liquid bilayer does not have a shear stress in plane thus also $p_{xy} = 0$. Consequently we have shown that the pressure tensor is diagonal and the normal component p_{zz} is constant for a planar homogeneous lipid bilayer in a liquid phase.

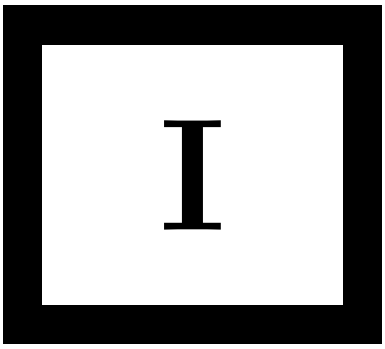

Publication I

Ollila, S., Hyvönen, M.T., and Vattulainen, I., Polyunsaturation in lipid membranes - dynamic properties and lateral pressure profiles, Journal of Physical Chemistry B 111, 3139-3150 (2007).

Polyunsaturation in Lipid Membranes: Dynamic Properties and Lateral Pressure Profiles

Samuli Ollila,[†,‡] Marja T. Hyvönen,[†,§] and Ilpo Vattulainen*[,†,‡,||]

Laboratory of Physics and Helsinki Institute of Physics, Helsinki University of Technology, P.O. Box 1100, FI-02015 HUT, Finland, Institute of Physics, Tampere University of Technology, P.O. Box 692, FI-33101 Tampere, Finland, Wihuri Research Institute, Kalliolinnantie 4, FI-00140 Helsinki, Finland, and Memphys—Center for Biomembrane Physics, Physics Department, University of Southern Denmark, Campusvej 55, DK-5230 Odense M, Denmark

Received: August 22, 2006; In Final Form: December 22, 2006

We elucidate the influence of unsaturation on single-component membrane properties, focusing on their dynamical aspects and lateral pressure profiles across the membrane. To this end, we employ atomistic molecular dynamics simulations to study five different membrane systems with varying degrees of unsaturation, starting from saturated membranes and systematically increasing the level of unsaturation, ending up with a bilayer of phospholipids containing the docosahexaenoic acid. For an increasing level of unsaturation, we find considerable effects on dynamical properties, such as accelerated dynamics of the phosphocholine head groups and glycerol backbones and speeded up rotational dynamics of the lipid molecules. The lateral pressure profile is found to be altered by the degree of unsaturation. For an increasing number of double bonds, the peak in the middle of the bilayer decreases. This is compensated for by changes in the membrane−water interface region in terms of increasing peak heights of the lateral pressure profile. Implications of the findings are briefly discussed.

I. Introduction

The level of unsaturation is a strictly regulated property of all biological membranes, including cell membranes as well as intracellular specialized membranes. Unsaturated lipids are known to play a significant role in membranes, the topical and highly prominent example being the importance of polyunsaturated lipids such as those containing docosahexaenoic acid (DHA); see refs 1−4 and references therein. The lipids containing DHA have been suggested, for example, to modulate the membrane elastic stress and thereby influence the functionality of integral membrane proteins.[5] Long-chain ω-3-polyunsaturated fatty acids are also known to induce various health benefits in terms of preventing cancer and heart diseases, among others.[6]

Nowadays, double bonds are known to affect various structural membrane properties such as the area per lipid and the ordering of the acyl chains.[3,7] Yet it is evident that the ideas of the role of double bonds have changed over time as more data and more qualified methodology has become available. For instance, originally double bonds were considered as rigidifying structures in membranes due to the natural rigidity of a cis type double bond,[8,9] whereas recent studies have revealed unsaturated hydrocarbon chains to be remarkably flexible due to extraordinary isomerization of the single bonds neighboring the double bonds.[4,7,10,11] This recent progress also highlights the fact that, in contrast to the structural properties of unsaturated membranes, much less attention has been paid to understand the influence of double bonds on the dynamic properties of lipids. These effects are discussed in more detail in this article.

An especially interesting and poorly understood property of lipid membranes is the distribution of local pressure inside a bilayer, the so-called lateral pressure profile. The lateral pressure profile is related to many important macroscopic and measurable quantities, such as surface tension, surface free energy, and spontaneous curvature.[12] Furthermore, Cantor has rather recently proposed an interesting idea that changes in the lateral pressure profile may affect the functionality of mechanosensitive proteins in cell membranes,[13] which could explain, for example, the action of general anesthetics[14,15] and the coupling between protein functionality and lipid content.[14,16] It is noteworthy that Cantor's mean-field calculations[14] and atomic-scale molecular dynamics simulations of Carrillo-Tripp and Feller[17] have suggested that double bonds shift repulsive pressure from the middle of the membrane toward the interfacial region. This change has been suggested to lead to the observed increase in rhodopsin activity due to polyunsaturated lipids.[14] Interestingly, the same idea concerning the dependence of rhodopsin activity on unsaturation level has been presented earlier by Brown et al.[18−20] who discussed the role of curvature stress, which in turn is related to the lateral pressure profile and the elasticity of a membrane.

Despite the rather substantial number of studies on unsaturated membranes, it is evident that not even the recent findings do fully explain the functional properties of double bonds in membranes. Of particular interest would be to clarify the interplay between double bonds, lateral pressure, and the dynamics of membranes for varying degrees of unsaturation. That would also render the understanding of protein functionality in unsaturated membranes more comprehensible.

In this work, we present a thorough systematic analysis of unsaturated lipid membranes studied through atomic-scale molecular dynamics simulations, focusing on the dynamics and the lateral pressure profiles. Starting from saturated lipids, we systematically increase the level of unsaturation and end up with

* Author to whom correspondence should be addressed. E-mail: Ilpo.Vattulainen@csc.fi.
† Helsinki University of Technology.
‡ Tampere University of Technology.
§ Wihuri Research Institute.
|| University of Southern Denmark.

10.1021/jp065424f CCC: $37.00
Published on Web 03/03/2007

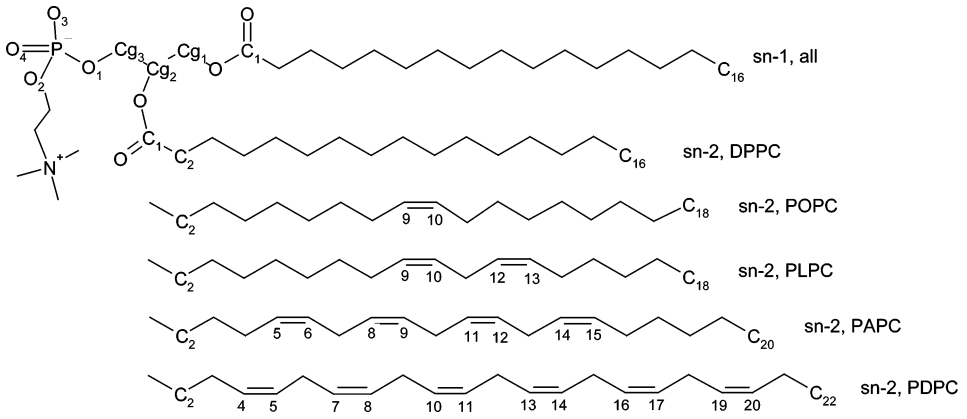

Figure 1. Structures of lipids used in bilayer simulations.

lipids containing DHA; see Figure 1. More specifically, we keep the *sn*−1 chain as well as the glycerol backbone and phosphocholine head group fixed and vary the *sn*−2 chain by considering palmitoyl, oleoyl, linoleoyl, arachidonoyl, and docosahexaenoyl chains. In this fashion, we have analyzed single-component membranes comprised of 1,2-dipalmitoyl-*sn*-glycero-3-phosphatidylcholine (DPPC), 1-palmitoyl-2-oleoyl-*sn*-glycero-3-phosphatidylcholine (POPC), 1-palmitoyl-2-linoleoyl-*sn*-glycero-3-phosphatidylcholine (PLPC), 1-palmitoyl-2-arachidonoyl-*sn*-glycero-3-phosphatidylcholine (PAPC), and 1-palmitoyl-2-docosahexaenoyl-*sn*-glycero-3-phosphatidylcholine (PDPC) lipids, as the number of double bonds in the *sn*−2 chain is increased systematically from zero to six.

The simulation data indicates that an increasing level of unsaturation leads to major changes in structural properties, such as increased area per lipid and conformationally less ordered chains. Similarly, for an increasing degree of unsaturation, we find considerable effects on dynamic properties, such as accelerated dynamics of the phosphocholine head groups and glycerol backbones and speeded up rotational dynamics of the lipid molecules. The lateral diffusion rate of the lipids studied, however, seems to be rather insensitive to the unsaturation level. In addition, we have found that the lateral pressure profile of a saturated DPPC bilayer is characterized by a repulsive peak in the middle of the membrane. For an increasing number of double bonds, the peak in the middle decreases, rendering the profile smoother in the middle of the membrane, while both positive and negative peaks at the membrane−water interface region increase in size. Implications of our findings are briefly discussed at the end of this article.

II. Methods

A. Force Field Parameters. The force field parameters employed in this work are based on a recent study by Bachar et al.[21] They adapted the force field parameters for DPPC[22] and POPC[23] to construct a force field for PLPC. For the double bond region they calculated dihedral angle parameters using ab initio techniques such that the single bonds next to the outermost double bonds as well as the bonds between double bonds are in accordance with skew$^+$ and skew$^-$ states. Further details of these potentials can be found from ref 21.

We used the PLPC force field in our work by varying the number of double bonds in the *sn*−2 hydrocarbon chain. The force field for POPC, available at http://moose.bio.ucalgary.ca/index.php?page=Downloads, was also updated such that the dihedral potentials near double bonds were in line with the ab initio calculations of Bachar et al. Other parts of the model were kept unchanged. The force field, simulation details, and some results of DPPC and PLPC have already been discussed elsewhere.[24−30]

B. Initial Structures. The initial structure for the PLPC bilayer was taken from simulations by Bachar and co-workers,[21] available at http://moose.bio.ucalgary.ca/index.php?page=Downloads. The system was comprised of 128 PLPC and 2453 water molecules. We modified the system by increasing the water/lipid ratio to 28.6 by adding 1202 water molecules to the system. Having done this, we are confident that the bilayer is fully hydrated.

The initial structure for a POPC bilayer structure was taken from the final configuration of our previous work discussed in ref 31. To construct an initial structure for a PAPC bilayer, the structure of the PLPC lipid bilayer was taken, and the two CH_2 groups were added to the *sn*−2 chain. After that, to ensure enough space for the equilibration of the system, the upper and lower monolayers were moved apart by approximately 0.5 nm. The structure was also slightly loosened in the plane of the membrane. The PDPC structure was constructed in a similar way using PAPC as a template. In all cases, the energy of the membrane systems was minimized using the steepest descent method.

C. Simulation Details. Molecular dynamics simulations were run by the GROMACS 3.1.4 simulation package.[32−34] The simulations were performed in the NPT ensemble at 1 bar and 310 K for the unsaturated systems (POPC, PLPC, PAPC, and PDPC), and at 323 K for DPPC. These temperatures are above the main transition temperatures of given lipids; thus the systems were in the fluid (liquid-disordered) phase. The simulations were carried out with the Berendsen thermostat and barostat[35] until the system had equilibrated. After equilibration the Nosé−Hoover temperature coupling[36,37] and Parrinello−Rahman pressure coupling[38,39] were applied. The coupling constant used for pressure was $\tau_p = 1.0$ ps, and for temperature $\tau_t = 0.1$ ps. The lipid bilayer and water were separately coupled to the heat bath, and the semi-isotropic pressure coupling was applied separately in the *xy*-direction (bilayer plane) and the *z*-direction (bilayer normal). The cutoff radius for van der Waals interactions was chosen as 1.0 nm. Particle mesh Ewald (PME) summations[40] were applied for long-range electrostatic interactions with a grid spacing of 0.12 nm, and a cutoff radius of 1.0 nm was employed for real space summation. In previous studies, PME has been shown to do well in membrane simulations.[25,26] The neighbor list update was performed every 10 steps. The time step was 2 fs, using LINCS[41] to constrain all bond lengths of lipids, whereas the SETTLE[42] algorithm was used for the SPC water.[43] The data saving frequency was 0.1 ps^{-1}. In total the systems were

simulated for 50.0 ns, of which the first 10.0 ns were regarded as an equilibration period and not included in analysis.

Below we compare the results of the unsaturated systems to those of a fully saturated DPPC bilayer. The simulation details and some results of the DPPC simulation study have been described elsewhere.[24−27] For this work, we have extended the analysis of the DPPC bilayer, especially in the case of lipid dynamics and the lateral pressure profile.

D. Lateral Pressure Profile. The local pressure for a system consisting of pointwise particles with *m*-body potentials can be defined using the local stress tensor

$$P = -\sigma_K - \sigma_C \tag{1}$$

The kinetic contribution of the local stress tensor σ_K is defined as[44]

$$\sigma_K^{\alpha\beta}(\mathbf{R}, t) = -\sum_i m_i v_i^\alpha v_i^\beta \delta(\mathbf{R} - \mathbf{r}_i) \tag{2}$$

where m_i, v_i, and $\mathbf{r}_i$ refer to the mass, velocity, and location of atom *i*. The definition of the configurational component of the local stress tensor σ_C for the *m*-body potential U^m is[44,45]

$$[\sigma_C^{\alpha\beta}(\mathbf{R}, t)]^{(m)} = \frac{1}{m}\Sigma_{\langle j\rangle}\Sigma_{\langle k,l\rangle}(\nabla_{j_k}^\alpha U^m - \nabla_{j_l}^\alpha U^m)\oint_{C_{jljk}} dl^\beta\, \delta(\mathbf{R} - \mathbf{l}) \tag{3}$$

where C_{jljk} is a contour from the particle j_l to the particle j_k, $\langle j\rangle$ stands for a summation over all *m*-clusters in the system, and $\langle k, l\rangle$ describes summation over all possible pairs of particles within a given *m*-cluster.

The lateral pressure profile $\pi(z)$ is then defined as a difference between the normal and the lateral components of the pressure tensor, that is, $P_N = P_{zz}$ and $P_L = (P_{xx} + P_{yy})/2$

$$\pi(z) = P_L - P_N \tag{4}$$

Qualitatively, this means that a bilayer tends to expand along the membrane plane (*xy*) with positive $\pi(z)$ and contract with negative $\pi(z)$.

The lateral pressure profile calculation is implemented to lipid bilayers by dividing the system into thin slices and calculating the local pressure tensor in each slice.[46−48] The discretization of eqs 2 and 3 leads now to the equation used in the calculations

$$\mathbf{P}^{\alpha\beta}(\mathbf{R}, t) = \Sigma_{i\in\text{slice}}\, m_i v_i^\alpha v_i^\beta + \frac{1}{mV_{\delta z}}\Sigma_{\langle j\rangle}\Sigma_{\langle k,l\rangle}(\nabla_{j_k}^\alpha U^m - \nabla_{j_l}^\alpha U^m) r_{j_k j_l}^\beta f(z_{j_k}, z_{j_l}, z_s) \tag{5}$$

where $f(z_{j_k}, z_{j_l}, z_s) = 0$ if particles are on the same side of the slice, $f(z_{j_k}, z_{j_l}, z_s) = 1$ if both particles are inside the slice, $f(z_{j_k}, z_{j_l}, z_s) = (\delta_z/|z_{j_k} - z_{j_l}|)$ if particles are on different sides of the slice, and $f(z_{j_k}, z_{j_l}, z_s) = (d_z/|z_{j_k} - z_{j_l}|)$ if only one of the particles is inside the slice. Here d_z is the distance between the particle inside the slice and the wall of the slice between the two particles, and δ_z is the thickness of the slice. The $V_\delta z$ is the volume of the slice.

Here, let us briefly comment on the chosen contour. The definition for local pressure presented above is actually unambigous due to the arbitrary contour in eq 3.[44] In practice, there are two feasible contours that can be employed. In the most intuitive and the most generally employed case, one uses the Irving−Kirkwood contour,[49,50] which goes directly from the particle j_l to j_k. A recent study by Morante et al.[51] supports the choice of this contour, too. It allows one to use eq 5, but then the range of interactions has to be finite. In practice, this implies that electrostatic interactions have to be truncated at some cutoff distance r_{cut}. In contrast, if one preferred to employ Ewald-type descriptions for long-range interactions, then the approach in eq 5 could not be used to calculate the local pressure contribution from the reciprocal space part of the Ewald sum.[46,48] Recently, Sonne et al.[48] showed that this contribution can be included using the Harasima contour.[52] Through comparison of different techniques, they concluded that the Irving−Kirkwood contour with truncation and the Harasima contour with PME yield qualitatively similar results provided that $r_{cut} > 1.8$ nm. Here, we have employed the Irving−Kirkwood contour together with truncation of electrostatic interactions at $r_{cut} = 2.0$ nm. Note, however, that while the determination of lateral pressure profiles was conducted by employing truncation via postanalysis, in the actual bilayer simulations the electrostatic interactions were treated by PME.

The practical implementation of calculations is made by dividing the system in 100 slices (approximately 0.07-nm-thick) perpendicular to the normal of the bilayer and then calculating the lateral pressure in each slice using eqs 4 and 5. The analysis is performed as a posttrajectory analysis exploiting the force field and saved locations and velocities. Forces arising from constraints are calculated using a general equation for constrained forces derived by Hess et al.[41] The estimation of statistical error for the lateral pressure profiles is made by calculating the error of the mean in each slice.

The method used here has been validated against the results of Lindahl and Edholm,[46] who used an essentially similar force field for DPPC and who also used the same contour together with the truncation for electrostatics during the pressure profile calculation. Our results for the lateral pressure profile of DPPC were found to be essentially identical.

III. Results and Discussion

A. Structural Properties. Structural properties of unsaturated systems have already been discussed in several simulation and experimental studies. We have found it essential to return to the subject due to the lack of systematic studies considering the level of unsaturation. Here we systematically vary the number of double bonds in the *sn*−2 tail by starting from a saturated palmitoyl chain and ending up in the maximally unsaturated docosahexaenoyl chain. In this fashion, we avoid potential problems due to varying force fields and simulation conditions that might hamper systematic comparison. Structural characterization serves also as a basis for the interpretation of the dynamic properties as well as the lateral pressure profiles.

1. Equilibration and Phase Behavior. As a common practice in simulations of lipid membranes (in the absence of salt), systems are considered to have achieved equilibrium when simulation box dimensions are not drifting. This condition was achieved after 10 ns for POPC, PLPC, PAPC, and PDPC (data not shown). Thereby, all results below have been analyzed over the interval of 10−50 ns of simulation time. For the DPPC bilayer, the analysis is performed over the period of 20−100 ns, which has been analyzed already in earlier studies.[24−27]

For the average area per lipid, we found 0.65 ± 0.01 nm^2 for DPPC, 0.68 ± 0.01 nm^2 for POPC, 0.69 ± 0.01 nm^2 for PLPC, 0.70 ± 0.01 nm^2 for PAPC, and 0.71 ± 0.01 nm^2 for PDPC. As a reminder, DPPC was studied at 323 K and the other systems at 310 K. The results are in good agreement with experiments. For DPPC, Nagle and Tristram-Nagle have reported a value of 0.64 nm^2 at 323 K.[53] For POPC, Kučerka et

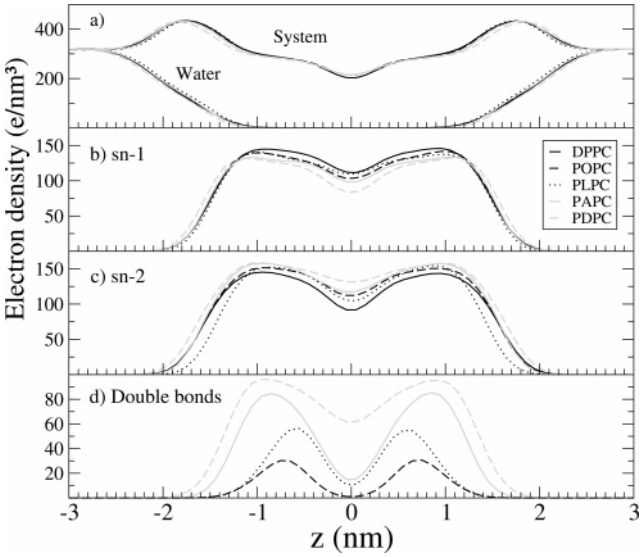

Figure 2. Electron density profiles across the bilayer for (A) the whole system together with the profile for water, (B) *sn*-1 chains, (C) *sn*-2 chains, and (D) double bonds.

al.[54] have found an area of 0.68 nm^2 at 303 K. The simulation results are also in line with the suggested trends based on various experiments:[3] The addition of first and second double bonds clearly increases the area per molecule, but additional double bonds do not seem to have remarkable effect. Additionally, although areas per lipid in monolayers and bilayers are not directly comparable, the simulation-based areas per lipid for POPC, PLPC, and PAPC are remarkably close to the respective measured values for corresponding monolayers: 0.658, 0.677, and 0.700 nm^2 (measured at 40 dynes/cm).[55] Further, our simulations reproduce the experimentally observed increase in the area per lipid from oleoyl-containing PC to arachidonoyl- or docosahexaenoyl-containing PC.[56]

Data for two-dimensional radial distribution functions of the lipid center of mass positions (not shown) indicated clearly that all bilayer systems were in the liquid-disordered phase, as expected.

2. Profiles across Bilayer and Interdigitation. In Figure 2 are shown the total electron densities of the DPPC, POPC, PLPC, PAPC, and PDPC bilayers across the bilayer, together with the separate partial densities of *sn*-1 and *sn*-2 chains and water layers together with the double bonds.

Distances between the main peaks in the total electron density profile, used generally as a measure of bilayer thickness, were for DPPC, POPC, PLPC, PAPC, and PDPC bilayers 3.6, 3.4, 3.5, 3.5, and 3.8 nm, in respective order. The experimentally determined value for the thickness of the DPPC bilayer is 3.83 nm,[53] which is in good agreement with our result. Our results for the thickness of PAPC and PDPC show also good agreement with the very recent small-angle X-ray diffraction study reporting a thickness of 3.5 nm for PAPC and 3.6 nm for PDPC.[57]

Membrane thickness does not seem to have any clear trend with regard to an increasing number of double bonds, which is probably due to the competition between various factors: Although double bonds are thought to increase the amount of tilted conformations, thereby reducing thickness, the length of the *sn*-2 chain is increasing at the same time counteracting the effects of double bonds themselves. A report of Eldho et al.[4] presents electron density curves of the DHA-containing SDPC and some other less unsaturated lipids and ends up with a conclusion that the most prominent feature in a comparison is, if the profiles are arbitrarily normalized to the same peak-to-trough extent, the broader and more shallow methyl trough region in the DHA-containing bilayer. We observe this feature in our data too, which Eldho et al. interpreted to indicate a higher density of saturated stearic acid in the bilayer center. Rajamoorthi et al.[57] interpret their very recent X-ray data for PAPC and PDPC in a similar way, suggesting that in the more unsaturated systems the saturated *sn*-1 chain would be shifted toward the membrane center. However, despite the qualitative similarity of the total electron density curves and the even quantitative agreement of membrane thickness, our simulation data would suggest the contrary: The more unsaturated the membrane, the less the saturated *sn*-1 chain appears in the membrane center; see Figure 2B. It is interesting to note, however, that if we compare just POPC and PLPC systems having *sn*-2 chains of equal lengths in carbon segments, then the density profiles of the *sn*-1 and *sn*-2 chains reproduce qualitatively the findings of the study of Eldho et al.[4]

The investigation of partial density profiles reveals also that water molecules penetrate down to the carbonyl group region (carbonyl profiles not shown), correlating with the thickness of the bilayers. Interestingly, in each system water seems to be in contact also with the hydrocarbon segments of the chains, and the probability for the contacts between water molecules and double bonds is apparently increasing with unsaturation. Unsaturared lipids are considered more susceptiple to lipid peroxidation than saturated lipids.[58] This phenomenon could be explained by the increased probability of contacts observed here. Hypothetically, increased unsaturation could ease up the entering of water-soluble oxidants to the membrane and increase the probability for their contacts with double bonds, the commonly suggested site for the beginning of membrane degrading chain reaction of oxidation.[58]

We also calculated the amount of water molecules inside bilayers, where they reside merely transiently. It can be concluded that there is more water inside a bilayer in the PAPC and PDPC bilayers than in the PLPC and POPC bilayers (data not shown). This is in agreement with the experimentally observed increase of the amount of water inside a bilayer,[3,59] when the number of double bonds is increased. As for the dynamics of water molecules in terms of permeation, during the 50 ns simulations we found only 4, 2, 7, and 6 water molecules to go through the membrane in the POPC, PLPC, PAPC, and PDPC systems, respectively. These numbers are statistically clearly too insignificant to draw any conclusions of the permeation process. After all, water molecules migrate inside bilayers relatively rarely as compared with the time scales of our present simulations. More careful studies of water inside a bilayer are therefore beyond the scope of this work.

To gain insight into the importance of interdigitation in lateral diffusion and lateral pressure profiles discussed later in this work, we quantify interdigitation as follows.[24,28] For each lipid molecule at every moment, we find its minimum and maximum *z*-coordinate, defined by the van der Waals radii of its atoms. The lipid molecule is considered to cover the whole regime between these points. The final profile is constructed by averaging over all configurations and plotting the number of the lipids as a function of the distance from the bilayer center; see Figure 3. In this fashion, one is able to study how lipid molecules in one leaflet extend to the opposite one.

The results in Figure 3 show that the interdigitation in the studied membranes is significant, but the differences between the different membranes are minor. Interdigitation in the saturated *sn*-1 chain follows the order (from largest to smallest) PLPC > DPPC > POPC > PAPC > PDPC, while in the

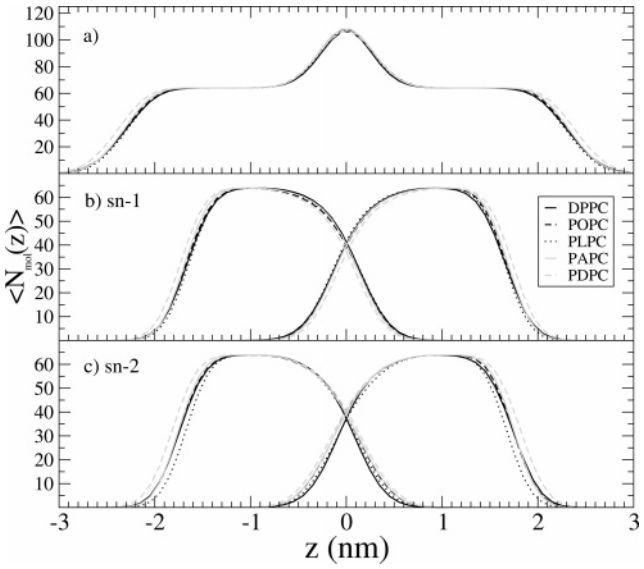

Figure 3. Average number of lipid molecules as function of distance from bilayer center along the bilayer normal. Results are shown for (A) the whole system, (B) the *sn*-1 chain, and (C) the *sn*-2 chain. For comparison, the number of lipids in each leaflet is 64.

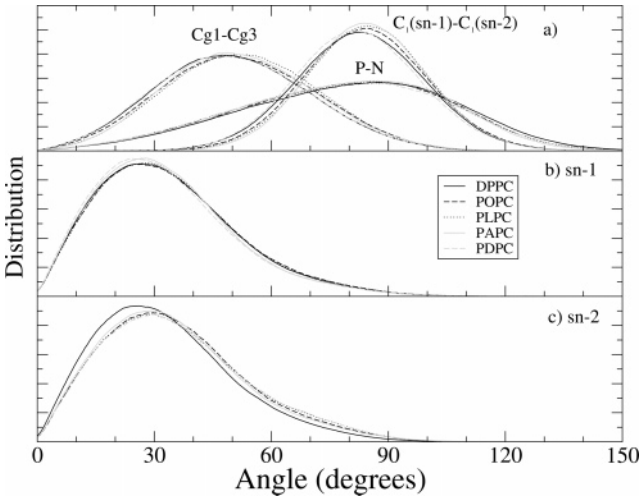

Figure 4. Angular distributions of several vectors characterizing molecular orientations. (A) Head group (P−N vector) and glycerol (Cg1−Cg3) backbone vectors together with the vectors between first carbons of *sn*-2 and *sn*-1 chains (C1(*sn*-1)−C1(*sn*-2)) with respect to the outward bilayer normal. (B) Vector from the first to the last carbon of the *sn*-1 chain with respect to the inward bilayer normal. (C) As in part B, but for the *sn*-2 chain.

unsaturated *sn*−2 chain the order is essentially opposite PDPC > PAPC > POPC > PLPC > DPPC. When it comes to the total interdigitation, it is to some extent enhanced for increasing unsaturation, though the differences are indeed minor.

3. Orientation of the Head Group, Glycerol Backbone, and Hydrocarbon Chains. The angular distributions of various vectors describing the overall structure of the studied unsaturated molecules have been calculated with respect to the bilayer normal and are shown in Figure 4. The broad distributions show that the average orientation angle of the phosphorus−nitrogen (P−N) vector with respect to the outward bilayer normal is practically similar, 78° ± 1°, in all five systems. This agrees well with the experimental estimate of, for instance, 72° by Akutsu and Nagamori.[60] This leads to the conclusion that head groups lie, on average, almost in parallel to the bilayer surface and that unsaturation has only a minor effect on the orientation of the head group. The widths of the distributions demonstrate, however, that the membrane−water interface is subject to considerable fluctuations and rather rough, as the head groups may occasionally point directly toward the water phase and next almost toward the interior of the bilayer.

Figure 4 shows also the angular distributions of the glycerol backbone vector, determined as a vector from the *sn*-1 carbon to the *sn*-3 carbon of the glycerol group. Again there is no significant difference between the different lipids, as the most prevailing orientation angle of the glycerol backbone in the different systems is 48° ± 3°. The angular distribution of the vector from the first carbon of the *sn*-1 chain to the first carbon of the *sn*-2 chain presents also no significant differences between the bilayer systems, showing only that in all systems this vector lies on average almost in parallel to the bilayer surface making the chains to start approximately from the same height. Hence, these distributions do not reveal significant differences in the head group and interfacial regions between the different unsaturated bilayers. The widths of the distributions demonstrate the dynamic nature of the interface.

Figures 4B and 4C depict the angular distributions of the vectors from the first to the last carbons of the hydrocarbon chains and are shown with respect to the inward normal of the bilayer. The most prevailing angles for the *sn*-1 chains of the DPPC, POPC, PLPC, PAPC, and PDPC bilayers are 27°, 25°, 28°, 28° and 24°, respectively, and for the *sn*-2 chain 26°, 30°, 30°, 30°, and 30°. These values are in line with suggestions based on fluorescence emission experiments:[59,61,62] Addition of fthe irst double bond increases the tilt angle, but addition of more double bonds has a minor effect. However, since the observed changes are small, conclusions must be drawn with care as well.

4. Chain Structures. We have determined the deuterium order parameter

$$S_{CD} = \frac{1}{2}\langle 3\cos^2\theta - 1\rangle \qquad (6)$$

where θ is the angle between the bilayer normal and the C−H bond vector and the brackets denote an average over all lipids and different times. To calculate deuterium order parameters from eq 6, the positions of hydrogen atoms had to be included in the simulation trajectories of the system, which was performed by calculating the positions on the basis of the orientation of carbon chains and exploiting tetrahedral symmetry at given sites. A similar approach has been used elsewhere.[27] Figure 5 shows the order parameters of the *sn*-1 and *sn*-2 chains of DPPC, POPC, PLPC, PAPC, and PDPC bilayers. For clarity's sake, error bounds have been calculated for all carbons but plotted only for selected ones.

Order parameters for the *sn*-1 chains of the bilayers with a different level of unsaturation appear to be approximately similar; see Figure 5F. The ^{2}H NMR study of Holte et al.[63] suggests that adding the second and third double bond into the *sn*-2 chain decreases the order of the *sn*-1 chain, but adding further double bonds would not cause a further decrease in ordering. Nevertheless, the observed changes in experiments are also small. Taking into account the experimental uncertainties, simulations and experiments are in good agreement. Especially in the case of the DPPC and POPC bilayers, quantitative agreement with experiments is very good.

For the PLPC bilayer there are no experimental order parameter results available, so the comparison is made mostly for the *sn*-2 linoleate chain. Here, the order parameters are measured for the isolinoleate chain of 1-palmitoyl-2-isolinoleoyl−glycero-3-phosphocholine (PiLPC),[64] in which the loca-

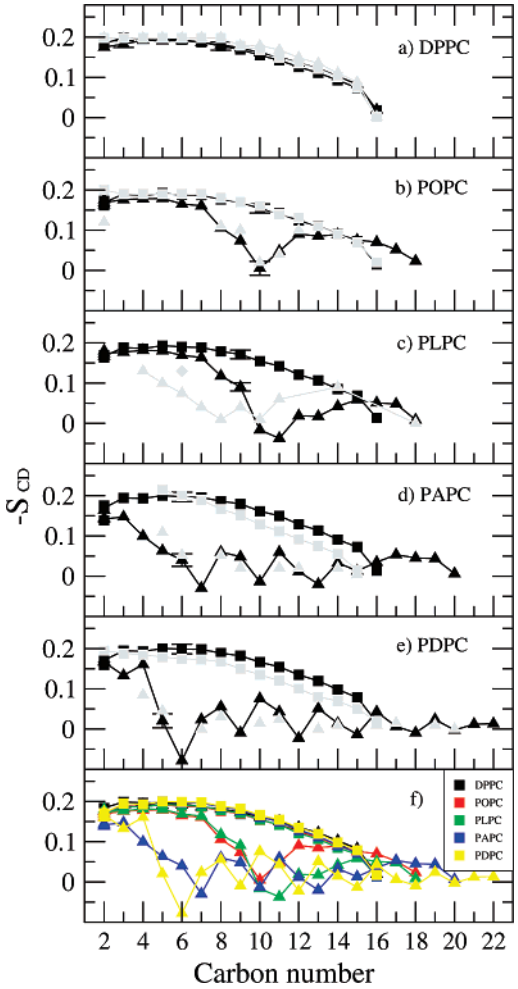

Figure 5. Order parameters for the *sn*-1 (squares) and *sn*-2 (triangles) chains of (A) DPPC, (B) POPC, (C) PLPC, (D) PAPC, and (E) PDPC. Simulation results are shown in full black, and experimental results for comparison in gray. Additionally, part F summarizes the data for all bilayers from the simulations. Experimental order parameters were chosen for comparison as follows. The order parameters for DPPC (T = 323 K) are based on studies by Petrache et al.[98] whereas the experimental S_{CD} values for PDPC and for the *sn*-1 chain of POPC (T = 310 K) are based on studies by Huber et al.[67] For the *sn*-1 chain of PDPC, the data set at 310 K is obtained by linearly interpolating between data at 303 and 323 K, whereas for the *sn*-2 chain the data at 303 K are presented.[67] Experimental values for the *sn*-2 chain of POPC are based on studies by Seelig et al.[99] A single experimental value is available also for the *sn*-2 chain of the PLPC bilayer at 313 K (diamond)[64] to compare with our simulated order parameters for PLPC. Together with PLPC, there are also experimental results for PiLPC (T = 313 K).[64] Experimental order parameters for the *sn*-1 and *sn*-2 chains of PAPC (T = 303 K) are based on quadrupole splittings measured by Rajamoorthi et al.[100] For the *sn*-1 chain the monotonic decrease through the acyl chain is expected. For the *sn*-2 chain, values are fitted such that the agreement is as good as possible.

tion of double bonds is shifted three carbons toward the glycerol backbone. If this shift is taken into account in the comparison together with the fact that the experimental order parameters are absolute values, then the comparison of the profile shapes suggests very good agreement between the simulations and experiments due to two double bonds. This is further supported by the single measurement in the experiments of Baenziger et al.[64] for carbon C6 of the *sn*-2 chain of PLPC, Figure 5C, which agrees with our simulation-based value. Order parameters of the *sn*-1 chain of the PLPC bilayer agree well with simulations by Bachar et al.[21]

In the PAPC and PDPC bilayers, the *sn*-1 chains seem to be more ordered in our simulations than in experiments. However, the assignment of the order parameter from ^{2}H NMR experiments with perdeuterated acyl chains is not segment-specific but assumes monotonically decreasing order toward the chain ends. If this assumption were not done for experimental values, then the experimental order parameter profile would likely be more similar to ours in the beginning of the chains. What is more, in addition to the results presented in Figure 5, the experimental results for the sn-1 chain order parameters of PAPC[65] and PDPC[66] agree with our results. Qualitatively the difference between the *sn*-1 chains of PAPC and PDPC in our simulations is similar to the ^{2}H NMR study[57]of Rajamoorthi et al.: In the same absolute temperatures the order parameters of the *sn*-1 chains of PAPC are closer to zero than those of PDPC.

It is noteworthy that we find nearly identical, almost zero, order parameter values in the last segments of the chains in each bilayer, indicating almost full orientational freedom of the methyl segment in the bilayer center. This is in full agreement with experimental findings, wherever comparison is possible.

As the number of double bonds in the *sn*−2 chain increases, the order parameters at the double bond regions apparently approach zero indicating lower order. Interestingly, Eldho et al.[4] mention in their deuterium NMR study that the order parameters of docosahexaenoyl and docosapentaenoyl chains (in the *sn*-2 position) for carbons in double bonds show higher order at the first carbon in the bond relative to the second. A similar feature is mostly observed also in the order parameter profiles of arachidonoyl and docosahexaenoyl chains as calculated from our simulations. However, the order parameter profile measured for the *sn*-2 docosahexaenoyl chain by Huber et al. for PDPC is much smoother.[67]

In all, the comparison of our simulation-based order parameters with corresponding experimental results shows good agreement, even at a quantitative level, especially taking into account the apparent differences in order parameters between different experimental systems.

The fractions of trans/gauche$^+$/gauche$^-$ or skew$^+$/skew$^-$ states along the chains were calculated for each bond along the chain, depending on the type of the bond (data not shown). In all bonds of *sn*-1 chains the fraction of gauche states is approximately 20−25%, except for the last dihedral, where the amount increases to 30%. However, there is very little variation between different bilayers. The general amount accords with the Fourier transform infrared spectroscopy experiments for a DPPC bilayer.[68] The fraction for skew$^+$ states in *sn*-2 chains is approximately 50% as can be expected from the dihedral potential applied.[21] Trans fractions for saturated regions in *sn*-2 chains are approximately similar to those in *sn*−1 chains, except for a bond closest to the skew-type bonds. In those bonds the amounts of trans states are decreased to approximately 50−65%.

B. Dynamic Properties. *1. Lateral Diffusion.* The lateral diffusion rate of lipid molecules in the plane of the bilayer is described by the lateral diffusion coefficient. Among several experimental methods, the fluorescence recovery after photobleaching, nuclear magnetic resonance, and single-particle tracking have been perhaps the most popular techniques to consider lateral diffusion for lipid bilayers.[69]

The lateral diffusion coefficient D for single-particle motion is defined as

$$D = \lim_{t\to\infty} \frac{1}{2dt}\langle[\vec{r}(t) - \vec{r}(0)]^2\rangle \qquad (7)$$

where $d = 2$ is the dimensionality of the system and $\vec{r}(t)$ is the molecule's center of mass position at time t. Hence, $\langle[\vec{r}(t) - \vec{r}(0)]^2\rangle$ constitutes the mean-squared displacement (MSD) of a single tagged particle, which is then averaged over different time origins and molecules in the bilayer. Importantly, since the center of mass of individual monolayers in a membrane may drift during the simulation, there is reason to consider single-particle motion with respect to the leaflet's center of mass motion. Here, we took this effect into account in a similar fashion as in ref 25.

Having calculated the MSD as a function of time, we determined the diffusion coefficient D from the slope of the MSD over time windows of 2−3 and 5−10 ns. The studied two cases allowed us to estimate the error bounds with reasonable accuracy. The results shown below refer to the longer time scale.

Through this analysis, we found a lateral diffusion coefficient of $(12 \pm 3) \times 10^{-8}$ cm^2/s for DPPC, $(9 \pm 3) \times 10^{-8}$ cm^2/s for POPC, $(13 \pm 3) \times 10^{-8}$ cm^2/s for PLPC, $(9 \pm 3) \times 10^{-8}$cm^2/s for PAPC, and $(11 \pm 3) \times 10^{-8}$ cm^2/s for PDPC. There is reason to keep in mind that the DPPC simulations were carried out at 323 K and the others at 310 K.

The simulations indicate that the studied systems have very similar lateral diffusion coefficients as the differences are within the error bars. Therefore, the data propose that unsaturation in the *sn*-2 chain does not affect lateral diffusion rates in a significant fashion, or if it does, then there are competing mechanisms with opposing trends. For example, one is tempted to assume that increasing unsaturation increases the rate of lateral diffusion, because the area per lipid and hence also the free volume available to diffusion increases; see section III.A.1. However, since in our case the increase in unsaturation is associated to an increase in the length of the *sn*-2 chain, one might expect the increasing interdigitation to slow down diffusion (Figure 3). However, the results shown in Figure 3 indicate only minor differences in interdigitation between the studied membranes. Additionally, what might play a role in lateral diffusion is the effect of entanglements: For long enough chains, their lateral motion is slowed down since they are entangled with other chains, and this effect increases for increasing chain length. It is likely that all these processes contribute to the lateral diffusion studied here, but nevertheless, within the quality of the data, the lateral diffusion rate seems to only rather weakly depend on the unsaturation level.

As for the trend of increasing unsaturation level, comparison to previous simulations and experiments is rather difficult because, to our knowledge, there are no systematic studies available for comparison. The wide range of published values indicates some uncertainty concerning the actual diffusion rate and is likely, in part, due to different experimental techniques considering diffusion phenomena over different scales in space and time. Let us therefore concentrate on the work by Filippov et al., who have systematically used pulsed-field gradient NMR to measure lateral diffusion in several one-component systems. At 323 K, they found 14×10^{-8} cm^2/s for DPPC,[70] and at 313 K a lateral diffusion coefficient of 13.5×10^{-8} cm^2/s for POPC.[71] If one assumes the Arrhenius form to hold and uses the Arrhenius barrier of 28 kcal/mol found by Filippov et al.,[71] then one finds 12.1×10^{-8} cm^2/s for POPC at 310 K. The trend here is in reasonable agreement with our simulation results. Similarly, Vaz et al.[72] used fluorescence recovery after photobleaching and found 12.5×10^{-8} cm^2/s at 323 K for DPPC and 7×10^{-8} cm^2/s at 313 K for POPC. The trends in these results are in agreement with the simulation data, too. For DOPC, Filippov et al.[71] and Ladha et al.[73] found a slightly higher diffusion coefficient than for POPC. As the hydrocarbon chains of POPC and DOPC are almost of equal length and the average area per lipid is slightly larger for DOPC than for POPC,[54] this trend is expected and is in line with the simulation data; see above. Preliminary results of Dustman et al.[74] based on pulsed-field gradient magic-angle spinning NMR experiments have indicated an increase in the diffusion rates upon increasing unsaturation. Mitchell and Litman[59] have reported increased dynamics of the fluorescent diphenylhexatriene (DPH) probe in lipid bilayers for increasing unsaturation, but in this case one has to keep in mind that the results reflect the dynamics of the probe rather than the behavior of the unlabeled lipid molecules.[29,30] Finally, concerning previous simulations, a study by Niemela et al.[75] showed that for sphingomyelin bilayers the monounsaturated lipids expressed faster diffusion than the saturated counterpart. However, they also found that increasing chain length slowed down lateral diffusion. We come back to this issue at the end of this article.

2. Intramolecular Dynamics. The understanding of intramolecular dynamics of lipids is largely based on NMR studies, complemented by computational studies of rotational autocorrelation functions that provide related data for comparison. For this purpose, we consider here the autocorrelation functions of various vectors describing different parts of the lipid molecules: the glycerol region through the vector from the *sn*-1 to the *sn*-3 carbon, the head group region through the P−N vector, and the C−H vector of individual carbon−hydrogen bonds along the hydrocarbon chains (Figure 1). In practice, we employ the second-order reorientational autocorrelation function[27]

$$C_2(t) = \frac{1}{2}\langle 3[\vec{\mu}(t)\cdot\vec{\mu}(0)]^2 - 1\rangle \tag{8}$$

where $\vec{\mu}(t)$ is a unit vector that defines the chosen rotational mode; see above. To characterize the motion of the molecular parts, either the half-times of the decay, $t_{1/2}$, or the effective characteristic times, τ_{eff}, were determined from the autocorrelation functions. The effective characteristic time of the autocorrelation function is defined by

$$\tau_{\mathrm{eff}} = \int_0^\infty \mathrm{d}t\, \frac{C_2(t) - C_2(\infty)}{C_2(0) - C_2(\infty)} \tag{9}$$

where $C_2(\infty)$ is the plateau value of the autocorrelation function at long times and $C_2(0) = 1$ due to normalization. Equation 9 stems from the assumption that the decay of $C_2(t)$ is exponential. Here, the characteristic time is called effective because this is not the case, that is, the autocorrelation functions of the C−H vectors are not truly exponential but rather have several characteristic time scales. This has been shown rather recently in several studies,[4,76,77] which have found evidence for the idea that the decay of $C_2(t)$ follows a power law or stretched exponential, though the present view is inconclusive in the sense that both forms seem to describe the data equally well (and asymptotically one expects exponential decay for a dissipative system). Our results (not shown) support these findings. The relevance of using eq 9 therefore lies in the idea that it allows us to systematically compare the influence of double bonds on the chain dynamics between the many different lipid types. Though these results are suggestive and describe the rate of dynamics in an averaged sense, the effective correlation time grasps the essential behavior.

Figure 6A presents the data for the decay half-times for these autocorrelation functions. Figures 6B and 6C, in turn, show the

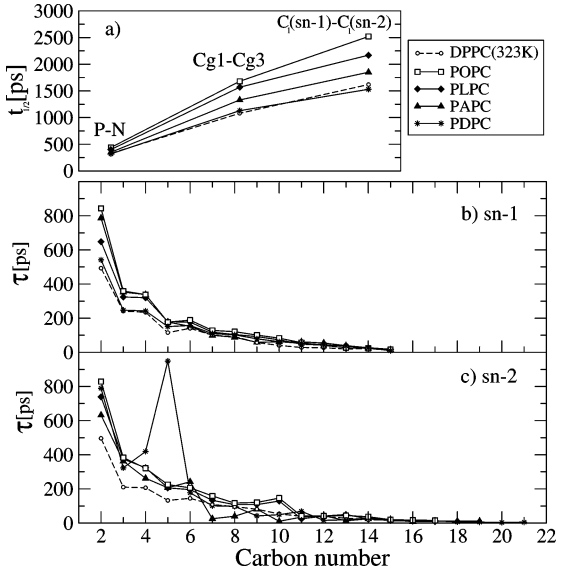

Figure 6. (A) Decay half-times for autocorrelation functions of P−N, Cg1−Cg2, and C1(*sn*-1)−C1(*sn*-2) vectors. Parts B and C show effective characteristic times for autocorrelation functions of C−H vectors along the hydrocarbon chains in different bilayers. Note that the DPPC bilayer was simulated at a higher temperature of 323 K, resulting in the more rapid dynamics seen here.

effective characteristic times for autocorrelation functions of C−H vectors in the acyl chains.

The decay half-times of the reorientational autocorrelation functions of the head group and glycerol backbone vectors together with the C1(*sn*-1)−C1(*sn*-2) vector show that in our model membranes the rotational dynamics of these vectors become faster as the number of double bonds increases from one to six. Autocorrelation functions of these various vectors would indicate the C1(*sn*-1)−C1(*sn*-2) vector to have the slowest motion of the vectors compared here. This is, however hand, natural, as the C1(*sn*-1)−C1(*sn*-2) vector lies on average in the bilayer plane (Figure 4), and the motion therefore represents roughly the rotational motion of the whole molecule, which is expected to be a slow process. It is interesting to note that although we cannot observe a significant trend in the lateral diffusion coefficients along the increasing unsaturation (see discussion above), there seems to be a clear trend of increasing rotational motion in the P−N, Cg1−Cg2, and C1(*sn*-1)−C1-(*sn*-2) vectors for increasing unsaturation.

From Figure 6 one can observe that the rotational dynamics of C−H vectors, for both chains, are considerably slower near the head group than near the bilayer center. This behavior has also been reported based on experiments for both saturated[78] and unsaturated[4,7] chains. Unsaturation does not seem to have a significant effect on the rotational dynamics of C−H vectors in the *sn*-1 chain in our simulation time scale, except for faster dynamics in the three first carbons.

The profile of the effective characteristic times for the *sn*-2 chains suggests that the rotational dynamics of the carbon segments are significantly increased after each double bond toward the methyl end. In most cases this leads to exceptionally rapid rotational motions between the double bonds, while the dynamics of the double-bonded carbons might be relatively slow. This observation is in line with various experiments.[4,7,79]

Rotational autocorrelation functions of C−H vectors can be compared with the spin lattice relaxation times from ^{2}H NMR and ^{13}C NMR experiments according to the procedure presented, e.g., in refs 4 and 76. Here we have made this comparison to ensure that our dynamics are in agreement with experimental results. We have determined the spectral densities by fitting the four exponential sums on the autocorrelation functions as in ref 4 and then applied the equations in ref 76. All available spin lattice relaxation times increase toward the end of the acyl chain.[4,57,78,80] For carbons 2−14 in the *sn*-2 chain of DPPC, spin lattice relaxation times between 0.5−1.7 and 0.02−0.1 s are obtained from ^{13}C NMR (conducted at 126 MHz, 323 K)[80] and ^{2}H NMR (54.4 MHz, 324 K)[78] experiments, respectively. In our analysis, spin lattice relaxation times have been calculated from simulation data using the same NMR frequencies as used in experiments. The experimental results are then found to be in good agreement with our results giving 0.1−1.7 and 0.003−1.4 s, in respective order. According to ^{13} C NMR (125.7 MHz, 303 K) results[4,7,81] for a bilayer containing DHA chains, the spin lattice relaxation times are approximately between 0.3 and 2 s for carbon numbers 2−17, increasing stepwise from one double bond to another toward the methyl end. According to the same studies, ^{13}C NMR spin lattice relaxation times for carbons 19−22 in the DHA chain are between 3 and 5 s. Our simulations give spin lattice relaxation times between 0.29 and 5 s for carbons 2−17, having a similar stepwise increase, and times between 9 and 22 s for carbons 19−22. In general, the qualitative and even quantitative agreement between experiments and our simulations is good.

For the purpose of completeness, we also analyzed the transition rates between gauche and trans states in the single bonds and between skew$^+$ and skew$^-$ states in the single bonds next to the double bonds (data not shown). For this purpose, due to remarkably high transition rates, each system was simulated for an extra 1 ns with a greater data saving frequency of 50 ps^{-1} to be able to determine reliable transition rates. The transition rates in the bonds of the chains range between 20 and 450 transitions per nanosecond; see below.

Transition rates for *sn*-1 chains of the unsaturated lipids do not appear to vary significantly between the different unsaturated systems. The rates increase from the beginning of the *sn*-1 chain toward their end, being approximately 35−45 ns^{-1} until the bond C12−C13, after which the rate increases to a value of 65 ns^{-1} in the bond C14−C15. In the *sn*-1 chain of the DPPC system, the behavior is similar to other systems, but the number of transitions is increased by approximately 10 ns^{-1} for each bond, probably due to the higher simulation temperature.

A similar increase of transition rates toward the bilayer center is found also in the *sn*-2 chain. The exception to this behavior concerns the transition rates for the skew-type bonds next to the double-bonded regions, where the rates are especially large, larger than 350 ns^{-1}, while in the region between the double bonds the rate is roughly twice the normal value of single bonds, i.e., approximately 100 ns^{-1}. Similar trends have been seen in CHARMM simulations of Hyvönen et al.,[11,82] though there the rates were clearly smaller than in our present simulations. These variations may be due to a different data saving frequency or differences in force fields. Interestingly, Gawrisch et al.[7] and Eldho et al.[4] have proposed that the increased flexibility in bilayers with an increasing number of double bonds may be caused by conformational freedom and structural transition rates near double bond regions. They assumed, however, that the dynamics of all skew-type bonds would be equally fast, both at the edges and inside the double bond regions. Simulation studies would suggest, though, that the profoundly high transition rate would take place only at the edges of the double bond regions, although the rate would be significantly increased also in the skew-type single bonds between the double bonds. This type of behavior would guarantee, altogether, a very flexible nature

for the highly unsaturated bilayers, especially those containing DHA, as has been suggested also based on solid-state NMR experiments.[7]

Taken together, we find good agreement with the corresponding dynamic properties in related experimental systems, whenever comparison is possible. This lays sound background for the interpretation of our other results for which experimental data does not exist, such as the lateral pressure profiles discussed below.

C. Lateral Pressure Profiles. The concept of lateral pressure profile, $\pi(z)$, arises from local forces acting inside a lipid bilayer in the direction of the membrane plane; see section II.D.

In equilibrium, to guarantee mechanical stability of the membrane, the integrated lateral pressure profile across the membrane should be zero. Yet the profile may spatially express different behaviors due to different interaction types. Traditionally three different regimes have been identified: a repulsive contribution arising from hydrophilic head groups due to electrostatic and steric interactions and hydration repulsion; an attractive contribution due to the interfacial energy between the water and the hydrocarbon phase, trying to minimize the surface area; and a repulsive contribution from the hydrophopic chains due to steric interactions.[83−85] These forces are assumed to create a nonuniform lateral component of local pressure inside a bilayer.[85,86]

Previous atomistic simulation studies[17,46−48,87] have shown that the lateral pressure profile depends on the lipid composition of the membrane and is characterized by narrow local peaks on the order of 1000 bar. Mean-field analytical predictions[14] and simulations of coarse-grained model systems[45,88] have provided support for these conclusions. On the basis of these exceptional properties, it has been suggested that the functioning of certain membrane proteins is influenced by the lateral pressure profile,[13] and it may even provide a mechanism for the action of anesthetics affecting the state of membrane proteins such as ion channels. However, the lateral pressure profile is extremely difficult to measure experimentally. To our knowledge, there is only one rather recent study[89] in which fluorescent probes were utilized to gauge the lateral pressure at several places in the hydrocarbon part of a membrane to determine the qualitative form of the pressure profile. In general, the atomic-scale molecular dynamics method seems to provide the most accurate means to elucidate lateral pressure profiles.

Here we employ the atomic-scale simulation data to systematically analyze the dependence of lateral pressure profiles on the unsaturation level. The results are presented in Figure 7. For clarity, the profiles have been smoothed by adaptive high order spline fitting[90] and averaged over the two monolayers. Original data are presented in the Supporting Information.

The lateral pressure profile found for DPPC is in good agreement with earlier atomic-scale simuations.[46,48,87] Considering the present case, the profile is most importantly characterized by the negative peak at the boundary between the water and hydrophopic phases and by the shallow peak in the middle of the bilayer. The origin of the latter is still under debate;[91] see below.

We find that the main effect of increasing the number of double bonds is the decrease of the lateral pressure in the middle of the membrane, for $|z| < 0.5$ nm. The largest difference at this region, 180 bar, is obtained between DPPC (saturated) and PDPC (six double bonds), though the effect due to increasing unsaturation seems to be most pronounced when the first two double bonds are incorporated into the *sn*-2 chain. We also find that the reduction of lateral pressure in the membrane center is

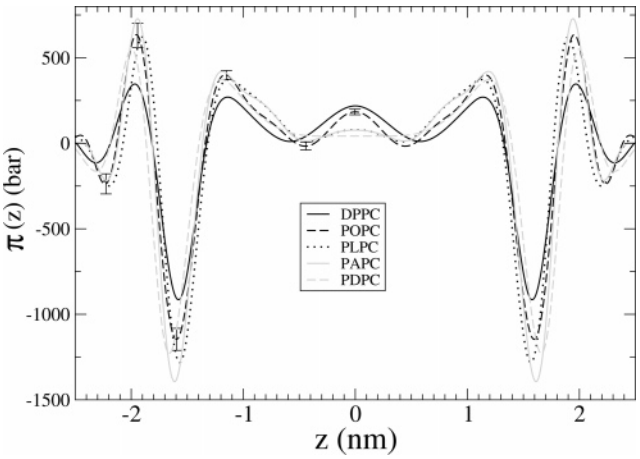

Figure 7. Lateral pressure profiles of DPPC, POPC, PLPC, PAPC, and PDPC bilayers, having zero, one, two, four, and six double bonds, in respective order. Statistical errors are presented for one leaflet of the POPC system. Error bars in the other leaflet and in other systems are similar.

partly compensated for by an increase of lateral pressure on both sides of the membrane−water interface, but these changes are not as systematic as in the middle of the bilayer.

Previously, the peak in the middle of the bilayer has been suggested to emerge from interdigitation of the two leaflets.[91] To consider this possibility, we analyzed the interdigitation in a similar manner as in ref 75 and found that the interdigitation does not significantly change when the number of double bonds is increased; see Figure 3. This result suggests that the disappearance of the peak in the membrane center in Figure 7 cannot be explained straightforwardly by interdigitation.

Carrillo-Tripp and Feller[17] have calculated lateral pressure profiles from atomistic molecular dynamics simulations for lipid bilayers having six and five double bonds in the *sn*-2 chain, with equal chain lengths (18:0−22:6n3PC and 18:0−22:5n6PC). Their main result was that the addition of a double bond increases the pressure near the interfacial region, which is in agreement with lattice thermodynamics calculations of Cantor.[14] They did not, however, observe a change in the middle of the bilayer. Furthermore, according to ref 17, the repulsive chain pressure follows the distribution of the polyunsaturated acyl chain segments. Figures 2 and 7 indicate that we find somewhat different behavior, especially in the middle of the bilayer, where the density of the unsaturated chains increases, the pressure decreases contrary to the suggestion of ref 17. We think that the reasons for these differences with respect to our work are partly methodological and subject to the lipids studied. First, the area of the bilayer was held constant during the simulations in ref 17, and this area was also identical in the simulations of the two different unsaturated bilayers (18:0−22:6n3PC and 18:0−22:5n6PC). This does not allow the system to find its equilibrium area with zero surface tension (see section III.A.1). Second, Carrillo-Tripp and Feller compared only lipids that have equal chain lengths, but a different number of double bonds. This is also the case between POPC and PLPC systems, but those include, however, only one and two double bonds and thus are not fully comparable with the systems of ref 17. In most of the systems studied here, both the number of double bonds and the chain length are varied.

The relation between the deuterium order parameter and the lateral pressure has been discussed rather recently, but no general consensus has been achieved.[16,92] Gawrisch and Holte have observed that an increase of temperature, chain length, or level of unsaturation promotes the formation of an inverse lamellar

phase and decrease lipid ordering. Thus, they have suggested that a decrease in the order of the hydrocarbon chains increases the lateral pressure in the acyl chain region.[92] From Figures 5 and 7 it can be seen that near the interfacial region the absolute value of the deuterium order parameter decreases due to double bonds, but the lateral pressure remains almost unchanged. At the same time, in the middle of the bilayer the lateral pressure decreases due to double bonds, but the deuterium order parameter is only weakly affected. Thus, our results do not suggest any clear-cut relation between the deuterium order parameter and the lateral pressure.

In fact, all of the above-mentioned results[14,16,17,92] also agree with our results, which is, however, not trivial. First, in our simulations as well as in experimental results the order remarkably decreases near the interfacial region for increasing unsaturation. On the basis of the above suggestion, the repulsive pressure is expected to increase in that region. This increase would lead to an increase in the area per lipid, which has been observed in experiments[7] and our simulations. However, the order in the middle of the bilayer is not significantly changed due to unsaturation, and thus, according to the suggestion above, the repulsive pressure in that region is expected to be approximately equal in all systems regardless of the number of double bonds. This argument leads to a conclusion that the lateral pressure in the middle of the bilayer is decreased due to polyunsaturation, because the area per molecule increases accordingly. Furthermore, the maximum in the middle of a saturated or monounsaturated membrane can be explained by reduced ordering in the middle of the membrane compared with the interfacial region. This idea is in good agreement with the suggestion of Mukhin and Baoukina[93] who have proposed that the peak in the middle of the bilayer is induced by increased configurational entropy due to the low order.

Quantitatively, the differences between the lateral pressure profiles of saturated and polyunsaturated lipid bilayers in the middle of the bilayer are approximately a few hundred bars. The change is substantial, and approximately 15% of the peak value is close to the membrane−water interface. It is likely that changes of this size may play a role in membrane protein functionality. This is substantiated by the theory of Cantor, which predicts that changes in the lateral pressure profile affect exponentially the ratio of concentrations of conformational (functional) states of mechanosensitive proteins.[13] Furthermore, it has been suggested that changes in the lateral pressure profile are involved in increasing rhodopsin activity with increasing level of unsaturation.[14,20,94] Being more specific, this proposition was first made in terms of curvature stress by Brown et al.[18−20] and later extended more explicitly by Cantor.[14] Our results support this view, because double bonds seem to systemically decrease the repulsive pressure in the middle of the bilayer. It also seems evident that the active state of rhodopsin has a larger volume than the inactive state.[95] In addition, the crystal structure of rhodopsin[96] suggests that the retinal, the origin of the activation, locates rather close to the center of the bilayer. Cholesterol, in turn, has been observed to decrease rhodopsin activity,[94] while the atomic-scale molecular dynamics calculations of several authors[17,87,97] suggest that cholesterol increases the repulsive pressure in the middle of the bilayer. These results encourage us to hypothesize that the activity of membrane proteins such as rhodopsin is affected by changes in the lateral pressure profile in the middle of the membrane. More direct studies including proteins embedded in membranes would be most welcome to validate this idea.

IV. Concluding Remarks

Here, we have employed atomistic molecular dynamics simulations to thoroughly elucidate the effects of unsaturation on lipid bilayer properties. The *sn*-1 chain in phosphatidylcholines was held fixed (palmitoyl), while the *sn*-2 chain was varied systematically by changing its unsaturation level and length. In this fashion, we analyzed single-component membranes comprised of DPPC, POPC$^{\Delta 9}$, PLPC$^{\Delta 9,12}$, PAPC$^{\Delta 5,8,11,14}$, and PDPC$^{\Delta 4,7,10,13,16,19}$. The focus of the study was on the dynamics and lateral pressure profiles and in particular on the changes in system properties as the level of unsaturation was varied systematically in a controlled manner.

First, as for structural properties, one of the most obvious effects found in the fluid (liquid-disordered) phase is the increase in the area per lipid, which is most prominent after the incorporation of the first double bond, that is, the area per lipid is increased in the POPC bilayer as compared with saturated DPPC. This results in many other structural effects in quantities such as the ordering of lipid hydrocarbon chains, membrane thickness, and density profiles across the membrane.

Recently, it has been proposed[4,5,57] that there would be an uneven distribution of density in DHA-containing bilayers as compared with less unsaturated ones: The saturated *sn*-1 chain would be displaced toward the bilayer center whereas the *sn*-2 polyunsaturated chain would be shifted toward the bilayer−water interface. This kind of conclusion cannot directly be drawn from our simulations, if the PDPC bilayer is compared with PAPC, as was done by Rajamoorthi et al.[57] However, this type of distributional difference can be interpreted to appear when comparison is made between POPC and PLPC bilayers, having chains with an equal number of carbon segments like in the comparison carried out in the study of Eldho et al.[4]

No major differences were found to appear in the orientational distributions of the head groups or vectors of the interfacial regions with respect to the bilayer plane; the head groups lie on average parallel to the membrane surface. Incorporation of double bonds into the fatty acyl chains naturally affects their structural properties. In our simulations the effects on the order parameters of the *sn*-1 chains were found to be minor, but in the case of unsaturated *sn*-2 chains the order parameters are strongly reduced locally at the regions of the double bonds. Close to the last carbon segments in the tails of the chains, the order parameter is essentially zero in all systems and for both chains indicating full orientational freedom. Overall, our simulation data for the order parameters of acyl chains are in good agreement with NMR measurements.

Second, concerning dynamics of the membranes, the lateral diffusion coefficients in the studied systems were observed to lie in the range $(9-13) \times 10^{-8}$ cm ^{2}/s, in good accordance with the few and varying experimental values available. However, as far as we know, no systematic reports appear to exist yet for the effect of unsaturation on lateral diffusion in the lipid bilayer systems. The present results seem to indicate that unsaturation plays a minor role for lateral diffusion. However, this conclusion should be taken with a grain of salt, since in the lipids considered in this work both the number of double bonds and the length of the hydrocarbon chains were varied. As the area per lipid increases for increasing unsaturation, one expects the lateral diffusion to speed up, too. However, this holds only for chains of equal length. If the length of the hydrocarbon chains increases, then entanglement effects become more prominent, and interdigitation may increase as well. These effects are expected to counter-balance the effect of increasing area per lipid and to slow down diffusion. To fully elucidate the effect

of unsaturation on lateral diffusion, further comparative studies with lipids of equal length would be most welcome. NMR, in particular, might be the method of choice to clarify this issue.

Though no clear trend in lateral diffusion was found due to unsaturation, the analysis of the autocorrelation functions of intramolecular vectors revealed that the rotational dynamics increase due to unsaturation. This increase was found essentially in every part of the molecules. The interfacial vector between the first carbons of the fatty acyl chains is the most slowly rotating vector in these molecules, describing the rotational motion of the whole molecule. This vector was found to lie, on average, parallel to the membrane surface. The rotational motion of C−H bonds was found to increase strongly along the chains toward the methyl end. The increase is most prominent in the next carbons from the double bonds toward the methyl end. This is most likely related to the recently found extraordinary flexibility of the single bonds in the neighborhood of double bonds; in the case of a chain containing six double bonds, the flexibility becomes more prominent toward the ends of the chains.

When it comes to the lateral pressure profiles in the simulated systems, it can be first concluded that we were able to reproduce the main features of the profile for saturated DPPC, in agreement with earlier molecular dynamics simulation studies.[46,48,87] Interestingly, there was a shallow peak of pressure in the middle of the DPPC bilayer, which, however, disappeared gradually in POPC, PLPC, PAPC, and PDPC bilayers. This peak has also been observed in other atomic-scale computational studies for DPPC and in the theoretical model of Mukhin and Baoukina.[93] The experiment conducted by Templer et al.[89] also suggests the existence of the peak. We could ensure from the simulation data that the disappearance of the peak in the membrane center was not related to changes in the interdigitation of the acyl chains, which was earlier suggested to explain the emergence of the peak in the interior of a DPPC bilayer.[91] Alternatively, Gawrisch and Holte[92] have suggested that decrease in the order of the hydrocarbon chains would be related to an increase in the lateral pressure profile. This would not, however, directly explain the disappearance of the central pressure peak, as in the middle of all of the bilayers the order parameters are almost zero. Though, ordering could explain the change in the central region indirectly, as due to unsaturation there appears to be a strong decrease of ordering toward the glycerol region of the chains. It is plausible that this would lead to an increase in the area per lipid, which would, in turn, lead to a conclusion that the lateral pressure in the middle of the bilayer is decreased due to polyunsaturation.

Overall, the results are in line with previous suggestions of the effects of membrane composition on, e.g., lipid−rhodopsin interactions[18−20] and the gating of mechanosensitive channels such as MscL.[13,91] Both ideas are essentially based on the concept of the lateral pressure profile. Interestingly, it was formulated already approximately two decades ago in terms of spontaneous curvature and curvature stress in the context of rhodopsin−lipid interactions.[18−20] The present work has shown that the lateral pressure profile indeed depends rather strongly on the unsaturation level of the lipid matrix. The role of the lateral pressure profile has also been discussed in relation to the mechanism of general anesthesia, which has been an open question for a long time in the field of membrane biophysics. In the late 1990s, Robert Cantor presented a simple model suggesting that incorporation of amphiphilic or other interfacially active solutes into the bilayer increases the interfacial lateral pressure, which then results in the decreased lateral pressure in the center of the bilayer. In case of ion channels, this redistribution of lateral pressure would cause a shift of the protein conformational equilibrium toward a closed state, resulting in a possible mechanism for general anesthesia.[15]

Summarizing, including the present data, there now seems to be a reasonable amount of evidence suggesting that the molecular composition of membranes affects the lateral pressure profile[17,46−48,87] exerted on membrane proteins. This would affect its structure and hence its activity. However, due to the lack of complete studies of lateral pressure profiles in the presence of membrane proteins, this intriguing hypothesis remains to be fully validated.

Acknowledgment. We thank Jarmila Repáková for providing the simulation trajectory of the DPPC system, Arvi Rauk and Michal Bachar for correspondence, and Perttu Niemelä for fruitful discussions. This work has, in part, been supported by the Academy of Finland (M.T.H. and I.V.), the Academy of Finland Center of Excellence Program (S.O. and I.V.), and the Jenny and Antti Wihuri Foundation (M.T.H.). We further acknowledge the Finnish IT Center for Science and the HorseShoe (DCSC) supercluster computing facility at the University of Southern Denmark for computer resources.

Supporting Information Available: Additional plot to illustrate the original raw data (prior to spline-based smoothing) for the lateral pressure profiles presented in the article. This material is available free of charge via the Internet at http://pubs.acs.org.

References and Notes

(1) Hooper, L.; Thompson, R. L.; Harrison, R. A.; Summerbell, C. D.; Ness, A. R.; Moore, H. J.; Worthington, H. V.; Durrington, P. N.; Higgins, J. P. T.; Capps, N. E.; Riemersma, R. A.; Ebrahim, S. B. J.; Smith, G. D. *BMJ* **2006**, *332*, 752−760.

(2) Feller, S. E.; Gawrisch, K. *Curr. Opin. Struct. Biol.* **2005**, *15*, 416−422.

(3) Stillwell, W.; Wassall, S. R. *Chem. Phys. Lipids* **2003**, *126*, 1−27.

(4) Eldho, N. V.; Feller, S. E.; Tristram-Nagle, S.; Polozov, I. V.; Gawrisch, K. *J. Am. Chem. Soc.* **2003**, *125*, 6409−6421.

(5) Mihailescu, M.; Gawrisch, K. *Biophys. J.* **2006**, *90*, L04−L06.

(6) Wassall, S. R.; Brzustowicz, M. R.; Shaikh, S. R.; Cherezov, V.; Caffrey, M.; Stillwell, W. *Chem. Phys. Lipids* **2004**, *132*, 79−88.

(7) Gawrisch, K.; Eldho, N. V.; Holte, L. L. *Lipids* **2003**, *38*, 445−452.

(8) Seelig, A.; Seelig, J. *Biochemistry* **1977**, *16*, 45−50.

(9) Hyvönen, M. T.; Ala-Korpela, M.; Vaara, J.; Rantala, T. T.; Jokisaari, J. *Chem. Phys. Lett.* **1995**, *246*, 300−306.

(10) Salmon, A.; Dodd, S. W.; Williams, G. D.; Beach, J. M.; Brown, M. F. *J. Am. Chem. Soc.* **1987**, *109*, 2600−2609.

(11) Hyvönen, M. T.; Kovanen, P. T. *Eur. Biophys. J.* **2005**, *34*, 294−305.

(12) Safran, S. A. *Statistical Thermodynamics of Surfaces, Interfaces, and Membranes*; Addison-Wesley: Reading, MA, 1994.

(13) Cantor, R. S. *J. Phys. Chem. B* **1997**, *101*, 1723−1725.

(14) Cantor, R. S. *Biophys. J.* **1999**, *76*, 2625−2639.

(15) Cantor, R. S. *Biochemistry* **1997**, *36*, 2339−2344.

(16) Kuiper, M. Azobenzene-Substituted Phosphate Amphiphiles. Ph.D. Thesis, Rijksuniversiteit Groningen, Groningen, The Netherlands, 2005.

(17) Carrillo-Tripp, M.; Feller, S. E. *Biochemistry* **2005**, *44*, 10164−10169.

(18) Wiedmann, T. S.; Pates, R. D.; Beach, J. M.; Salmon, A.; Brown, M. F. *Biochemistry* **1988**, *27*, 6469−6474.

(19) Gibson, N. J.; Brown, M. F. *Biochemistry* **1993**, *32*, 2438−2454.

(20) Brown, M. F. *Chem. Phys. Lipids* **1994**, *73*, 159−180.

(21) Bachar, M.; Brunelle, P.; Tieleman, D. P.; Rauk, A. *J. Phys. Chem. B* **2004**, *108*, 7170−7179.

(22) Tieleman, D. P.; Berendsen, H. J. C. *J. Chem. Phys.* **1996**, *105*, 4871−4880.

(23) Tieleman, D. P.; Berendsen, H. J. C. *Biophys. J.* **1998**, *74*, 2786−2801.

(24) Falck, E.; Patra, M.; Karttunen, M.; Hyvönen, M. T.; Vattulainen, I. *Biophys. J.* **2004**, *87*, 1076−1091.

(25) Patra, M.; Karttunen, M.; Hyvönen, M.; Falck, E.; Vattulainen, I. *J. Phys. Chem. B* **2004**, *108*, 4485−4494.
(26) Patra, M.; Karttunen, M.; Hyvönen, M. T.; Falck, E.; Lindqvist, P.; Vattulainen, I. *Biophys. J.* **2003**, *84*, 3636−3645.
(27) Niemelä, P.; Hyvönen, M.; Vattulainen, I. *Biophys. J.* **2004**, *87*, 2976−2989.
(28) Kupiainen, M.; Falck, E.; Ollila, S.; Niemelä, P.; Gurtovenko, A. A.; Hyvönen, M. T.; Patra, M.; Karttunen, M.; Vattulainen, I. *J. Comput. Theor. Nanosci.* **2005**, *2*, 401−413.
(29) Repáková, J.; Čapková, P.; Holopainen, J. M.; Vattulainen, I. *J. Phys. Chem. B* **2004**, *108*, 13438−13448.
(30) Repáková, J.; Holopainen, J. M.; Morrow, M. R.; McDonald, M. C.; Čapkova, P.; Vattulainen, I. *Biophys. J.* **2005**, *88*, 3398−3410.
(31) Patra, M.; Salonen, E.; Terämä, E.; Vattulainen, I.; Faller, R.; Lee, B. W.; Holopainen, J.; Karttunen, M. *Biophys. J.* **2006**, *90*, 1121−1135.
(32) der Spoel, D. V.; Lindahl, E.; Hess, B.; van Buuren, A. R.; Meulenhoff, E. A. P. J.; Tieleman, D. P.; Sijbers, A. L. T. M.; Feenstra, K. A.; van Drunen, R.; Berendsen, H. J. C. *GROMACS User Manual*, version 3.2.; 2004.
(33) Berendsen, H. J. C.; van der Spoel, D.; van Drunen, R. *Comput. Phys. Commun.* **1995**, *91*, 43−56.
(34) Lindahl, E.; Edholm, O. *Biophys. J.* **2000**, *79*, 426−433.
(35) Berendsen, H. J. C.; Postma, J. P. M.; van Gunsteren, W. F.; DiNola, A.; Haak, J. R. *J. Chem. Phys.* **1984**, *81*, 3684−3690.
(36) Hoover, W. G. *Phys. Rev. A* **1985**, *31*, 1695−1697.
(37) Nosé, S. *Mol. Phys.* **1984**, *52*, 255−268.
(38) Nosé, S.; Klein, M. *Mol. Phys.* **1983**, *50*, 1055−1076.
(39) Parrinello, M.; Rahman, A. *J. Appl. Phys.* **1981**, *52*, 7182−7190.
(40) Essman, U. L.; Perera, M. L.; Berkowitz, M. L.; Larden, T.; Lee, H.; Pedersen, L. G. *J. Chem. Phys.* **1995**, *103*, 8577−8592.
(41) Hess, B.; Bekker, H.; Berendsen, H. J. C.; Fraaije, J. G. E. M. *J. Comput. Chem.* **1997**, *18*, 1463−1472.
(42) Miyamoto, S.; Kollman, P. A. *J. Comput. Chem.* **1992**, *13*, 952−962.
(43) Berendsen, H. J. C.; Postma, J. P. M.; van Gunsteren, W. F.; Hermans, J. In *Intermolecular Forces*; Pullman, B., Ed.; Reidel: Dordrecht, The Netherlands, 1981; pp 331−342.
(44) Schofield, P.; Henderson, J. R. *Proc. R. Soc. London, Ser. A* **1982**, *379*, 231−246.
(45) Goetz, R.; Lipowsky, R. *J. Chem. Phys.* **1998**, *108*, 7397−7409.
(46) Lindahl, E.; Edholm, O. *J. Chem. Phys.* **2000**, *113*, 3882−3893.
(47) Gullingsrud, J.; Schulten, K. *Biophys. J.* **2004**, *86*, 3496−3509.
(48) Sonne, J.; Hansen, F. Y.; Peters, G. H. *J. Chem. Phys.* **2005**, *122*, 124903.
(49) Kirkwood, J. G.; Buff, F. P. J. *J. Chem. Phys.* **1949**, *17*, 338−343.
(50) Irving, J. H.; Kirkwood, J. G. *J. Chem. Phys.* **1950**, *18*, 817−829.
(51) Morante, S.; Rossi, G. C.; Testa, M. *J. Chem. Phys.* **2006**, *125*, 034101.
(52) Harasima, A. *Adv. Chem. Phys.* **1958**, *1*, 203−237.
(53) Nagle, J. F.; Tristram-Nagle, S. *Biochem. Biophys. Acta* **2000**, *1469*, 159−195.
(54) Kučerka, N.; Tristam-Nagle, S.; Nagle, J. F. *J. Membr. Biol.* **2005**, *208*, 193−202.
(55) Ghosh, D.; Tinoco, J. *Biochim. Biophys. Acta* **1972**, *266*, 41−49.
(56) Brockman, H. L.; Applegate, K. R.; Momsen, M. M.; King, W. C.; Glomset, J. A. *Biophys. J.* **2003**, *85*, 2384−2396.
(57) Rajamoorthi, K.; Petrache, H. I.; McIntosh, T. J.; Brown, M. F. *J. Am. Chem. Soc.* **2005**, *127*, 1576−1588.
(58) Brodnitz, M. H. *J. Agric. Food Chem.* **1968**, *16*, 994−999.
(59) Mitchell, D. C.; Litman, B. J. *Biophys. J.* **1998**, *74*, 879−891.
(60) Akutsu, H.; Nagamori, T. *Biochemistry* **1991**, *30*, 4510−4516.
(61) van Langen, H.; van Ginkel, G.; Shawn, D.; Levine, Y. K. *Eur. Biophys. J.* **1989**, *17*, 37−48.
(62) Stubbs, C. D.; Kouyama, T.; Kinosita, K.; Ikegami, A. *Biochemistry* **1981**, *20*, 4257−4262.
(63) Holte, L. L.; Peter, S. A.; Sinnwell, T. M.; Gawrisch, K. *Biophys. J.* **1995**, *68*, 2396−2403.
(64) Baenziger, J. E.; Jarrel, H. C.; Hill, R. J.; Smith, I. C. P. *Biochemistry* **1991**, *30*, 894−903.
(65) Drobnies, A. E.; van der Ende, B.; Thewalt, J. L.; Cornell, R. B. *Biochemistry* **1999**, *38*, 15606−15614.
(66) Petrache, H. I.; Salmon, A.; Brown, M. F. *J. Am. Chem. Soc.* **2001**, *123*, 12611−12622.
(67) Huber, T.; Rajamoorthi, K.; Kurze, V. F.; Beyer, K.; Brown, M. F. *J. Am. Chem. Soc.* **2002**, *124*, 298−309.
(68) Mendelsohn, R.; Davies, M. A.; Schuster, H. F.; Xu, Z.; Bittman, R. *Biochemistry* **1991**, *30*, 8558−8563.
(69) Vattulainen, I.; Mouritsen, O. G. In *Diffusion in Condensed Matter: Methods, Materials, Models*; Heitjans, P., Karger, J., Eds.; Springer: Berlin, 2004.
(70) Lindblom, G.; Orädd, G.; Filippov, A. *Chem. Phys. Lipids* **2006**, *141*, 179−184.
(71) Filippov, A.; Orädd, G.; Lindblom, G. *Biophys. J.* **2003**, *84*, 3079−3086.
(72) Vaz, W. L. C.; Clegg, R. M.; Hallmann, D. *Biochemistry* **1985**, *24*, 781−786.
(73) Ladha, S.; Mackie, A. R.; Harvey, L. J.; Clark, D. C.; Lea, E. J. A.; Brullemans, M.; Duclohier, H. *Biophys. J.* **1996**, *71*, 1364−1373.
(74) Dustman, J. M.; Casas, R. S.; Scheidt, H. A.; Eldho, N. V.; Teague, W. E.; Gawrisch, K. *Biophys. J.* **2005**, *88*, 27a.
(75) Niemelä, P.; Hyvönen, M. T.; Vattulainen, I. *Biophys. J.* **2006**, *90*, 851−863.
(76) Lindahl, E.; Edholm, O. *J. Chem. Phys.* **2001**, *115*, 4938−4950.
(77) Wohlert, J.; Edholm, O. *J. Chem. Phys.* **2006**, *125*, 204703.
(78) Brown, M. F.; Seelig, J.; Häberlen, U. *J. Chem. Phys.* **1979**, *70*, 5045−5053.
(79) Baenziger, J. E.; Jarrel, H. C.; Smith, I. C. P. *Biochemistry* **1992**, *31*, 3377−3385.
(80) Brown, M. F. *J. Chem. Phys.* **1984**, *80*, 2808−2831.
(81) Feller, S. E.; Gawrisch, K.; MacKerell, A. D., Jr. *J. Am. Chem. Soc.* **2002**, *124*, 318−326.
(82) Hyvönen, M. T.; Rantala, T. T.; Ala-Korpela, M. *Biophys. J.* **1997**, *73*, 2907−2923.
(83) Israelachvili, J. N. *Intermolecular and Surface Forces*; Academic Press: London, 1985.
(84) Israelachvili, J. N.; Marcelja, S.; Horn, R. G. *Q. Rev. Biophys.* **1980**, *13*, 121−200.
(85) Marsh, D. *Biochim. Biophys. Acta* **1996**, *1286*, 183−223.
(86) Seddon, J. M.; Templer, R. H. In *Structure and Dynamics of Membranes*; Lipowsky, R., Sackmann, E., Eds.; Elsevier: Amsterdam, 1995; pp 97−160.
(87) Patra, M. *Eur. Biophys. J.* **2005**, *35*, 79−88.
(88) Venturoli, M.; Smit, B. *Phys. Chem. Commun.* **1999**, *2*, 45−49.
(89) Templer, R. H.; Castle, S. J.; Curran, A. R.; Rumbles, G.; Klug, D. R. *Faraday Discuss.* **1998**, *11*, 41−53.
(90) Thijsse, B. J.; Hollanders, M. A.; Hendrikse, J. *Comput. Phys.* **1998**, *12*, 393−399.
(91) van den Brink-van der Laan, E.; Killian, J. A.; Kruijff, B. *Biochim. Biophys. Acta* **2004**, *1666*, 275−288.
(92) Gawrisch, K.; Holte, L. L. *Chem. Phys. Lipids* **1996**, *81*, 105−116.
(93) Mukhin, S. I.; Baoukina, S. *Phys. Rev. E* **2005**, *71*, 061918−061923.
(94) Litman, B. J.; Mitchell, D. C. *Lipids* **1996**, *31*, S193−S197.
(95) Attwood, P. V.; Gutfreund, H. *FEBS Lett.* **1980**, *119*, 323−326.
(96) Sakmar, T. P.; Menon, S. T.; Marin, E. P.; Awad, E. S. *Annu. Rev. Biophys. Biomol. Struct.* **2002**, *31*, 443−484.
(97) Ollila, S.; Rog, T.; Karttunen, M.; Vattulainen, I. *J. Struct. Biol.*, in press.
(98) Petrache, H. I.; Dodd, S. W.; Brown, M. F. *Biophys. J.* **2000**, *79*, 3172−3192.
(99) Seelig, J.; Waespe-Sarcevic, N. *Biochemistry* **1978**, *17*, 3310−3315.
(100) Rajamoorthi, K.; Brown, M. F. *Biochemistry* **1991**, *30*, 4204−4212.

II

Publication II

Ollila, O. H. S., Rog, T., Karttunen, M., and Vattulainen, Role of sterol type on lateral pressure profiles of lipid membranes affecting membrane protein functionality: Comparison between cholesterol, desmosterol, 7-dehydrocholesterol and ketosterol,Journal of Structural Biology, 159,311-323 (2007)

Available online at www.sciencedirect.com
ScienceDirect
Journal of Structural Biology 159 (2007) 311–323
Journal of Structural Biology
www.elsevier.com/locate/yjsbi

Role of sterol type on lateral pressure profiles of lipid membranes affecting membrane protein functionality: Comparison between cholesterol, desmosterol, 7-dehydrocholesterol and ketosterol

O.H. Samuli Ollila [a,b], Tomasz Róg [c,d], Mikko Karttunen [e], Ilpo Vattulainen [a,b,f,*]

[a] Institute of Physics, Tampere University of Technology, P.O. Box 692, FI-33101 Tampere, Finland
[b] Laboratory of Physics and Helsinki Institute of Physics, Helsinki University of Technology, P.O. Box 1100, FI-02015 HUT, Finland
[c] Biophysics and Statistical Mechanics Group, Laboratory of Computational Engineering, Helsinki University of Technology, P.O. Box 9203, FI–02015 HUT, Finland
[d] Department of Biophysics, Faculty of Biotechnology, Jagiellonian University, Krakow, Poland
[e] Department of Applied Mathematics, University of Western Ontario, Middlesex College, 1151 Richmond Street North, London, Ont., Canada N6A 5B7
[f] Memphys–Center for Biomembrane Physics, Physics Department, University of Southern Denmark, Campusvej 55, DK–5230 Odense M, Denmark

Received 14 September 2006; received in revised form 19 January 2007; accepted 22 January 2007
Available online 1 February 2007

Abstract

Lateral pressure profiles have been suggested to play a significant role in many cellular membrane processes by affecting, for example, the activation of membrane proteins through changes in their conformational state. This may be the case if the lateral pressure profile is altered due to changes in molecular composition surrounding the protein. In this work, we elucidate the effect of varying sterol type on the lateral pressure profile, an issue of topical interest due to lipid rafts and their putative role for membrane protein functionality. We find that the lateral pressure profile is altered when cholesterol is replaced by either desmosterol, 7-dehydrocholesterol, or ketosterol. The observed changes in the lateral pressure profile are notable and important since desmosterol and 7-dehydrocholesterol are the immediate precursors of cholesterol along its biosynthetic pathway. The results show that the lateral pressure profile and the resulting elastic behavior of lipid membranes are sensitive to the sterol type, and support a mechanism where changes in protein conformational state are facilitated by changes in the lateral pressure profile. From a structural point of view, the results provide compelling evidence that despite seemingly minor differences, sterols are characterized by structural specificity.

Keywords: Lateral pressure profile; Lipid membrane; Lipid raft; Sterol; Molecular dynamics simulation

1. Introduction

A major fraction of proteins on cellular level are embedded in or attached to cellular membranes. This highlights the importance of understanding the structures and consequent functions of membrane proteins. Recent progress in resolving their structures (Bowie, 2005; White, 2004) has paved way for a better understanding of a variety of cellular functions. At the same time, however, it has become clear that membrane proteins do not work alone but rather in conjunction with the membrane, which often facilitates or even governs the functioning of membrane proteins. Here, the composition of the membrane plays an important role.

Various eukaryotic cellular membranes, and in particular the plasma membrane are rich in cholesterol. It comprises about 30 mol% of molecules in the plasma

* Corresponding author. Address: Institute of Physics, Tampere University of Technology, P. O. Box 692, FI-33101 Tampere, Finland.
E-mail address: Ilpo.Vattulainen@csc.fi (I. Vattulainen).

1047-8477/$ - see front matter © 2007 Elsevier Inc. All rights reserved.
doi:10.1016/j.jsb.2007.01.012

membrane and is present in large amounts in other cellular membranes, reaching up to 70 mol% in the ocular lens membrane. Cholesterol affects various physical properties of lipid membranes, such as ordering of lipid hydrocarbon chains, packing of lipids in a membrane, lateral diffusion in the membrane plane, and permeation rates of small molecules across membranes. Cholesterol is known to induce a so-called liquid-ordered phase in model membranes, characterized by a liquid-like behavior in the membrane plane, but significant conformational ordering of lipid hydrocarbon chains and tight packing of lipids.

The recently proposed lipid raft model (Simons and Ikonen, 1997) for the structure and biological relevance of lipid membranes is largely based on the role of cholesterol, as rafts have been found to be rich in cholesterol, sphingomyelin, and saturated phospholipids. Rafts have been found to play a major role in a number of cellular processes, including membrane trafficking and signal transduction (Simons and Ikonen, 1997; Edidin, 2003; Pike, 2004), and the role of cholesterol seems to be crucial in many of them. For example, if cholesterol is replaced by desmosterol, its immediate precursor in the biosynthetic pathway, the activation of certain proteins such as insulin receptors has been found to be affected in a significant manner (Vainio et al., 2006). This, too, highlights the idea that the lipid composition in a membrane does influence the functionality of integral membrane proteins (Mihailescu and Gawrisch, 2006), though the related mechanisms are not well understood.

Almost ten years ago, Robert Cantor proposed the interesting idea that changes in the lateral pressure profile of a lipid membrane may affect the functionality of membrane proteins such as mechanosensitive channels (Cantor, 1997). The lateral pressure profile (Marsh, 1996) describes the distribution of local pressure inside a lipid bilayer, and it underlies many important macroscopic and measurable membrane properties, such as surface tension, surface free energy, and spontaneous curvature (Safran, 1994). In a way, the lateral pressure profile describes the local force exerted on a protein embedded in a membrane. Since the local pressure inside a membrane can be as high as of the order of 1000 bar (Lindahl and Edholm, 2000a), it is evident that it might be able to affect protein structure by favoring a certain conformational state. The concept of the lateral pressure profile is very appealing, since if it plays a significant biological role, it could explain, for example, the coupling between protein functionality and lipid content (Cantor, 1999a) and even play a role in such phenomena as general anesthesia (Cantor, 1997; Eckenhoff, 2001).

The problem is that the lateral pressure profile is not easy to gauge. At the moment, to our knowledge, there is only one experimental attempt to measure the profile (Templer et al., 1999). That study employed probes, thus the measured system was not a native one, as would have been preferred. Computational studies based on atomistic models of lipid bilayers have shed light on this issue, though. Several studies have confirmed that the shape of the lateral pressure profile is rather complex and characterized by pressures of the order of 1000 bar (Carrillo-Tripp and Feller, 2005; Lindahl and Edholm, 2000a; Sonne et al., 2005; Gullingsrud and Schulten, 2004; Patra, 2005; Ollila et al., 2007). Moreover, it has been found that bilayers composed of saturated lipids and those rich in cholesterol have distinctly different pressure profiles (Patra, 2005). Also, lateral pressure profiles of membranes comprised of polyunsaturated lipids are markedly different from profiles found in membranes with saturated lipids (Carrillo-Tripp and Feller, 2005; Ollila et al., 2007). What comes to biological relevance, a number of studies have indeed indicated that the functionality of membrane proteins depends on the lipid composition of a membrane. As an example, the activity of rhodopsin has been found to be affected by lipid composition (Litman and Mitchell, 1996). Recent studies by van den Brink-van der Laan et al. (2004a,b) also propose that the lateral pressure profile is involved in the stability and activation of membrane protein complexes, and Hong and Tamm (2004) suggested on the basis of their experiments that nonspecific physical interactions and lipid packing are more important in determining membrane protein stability than specific lipid interactions (see also discussion in (Bowie, 2005)). Further support is given by recent studies, which have suggested (Mihailescu and Gawrisch, 2006) that membrane elastic stress modulates the functions of integral receptor proteins like rhodopsin, and that the binding of amphipathic peptides such as melittin to lipid bilayers decreases with increasing bilayer compressibility modulus (Allende et al., 2003).

On the basis of the above discussion, it is appealing to consider the possibility that the lateral pressure profile could serve as a generic means in mediating interactions between lipids and proteins, and hence in facilitating changes in protein conformation. Further, due to the exceptional importance of cholesterol in cellular membranes and ordered membrane domains (rafts), one is tempted to think that the lateral pressure profile would provide insight for a better understanding of the essentially unique structure-function relationship of cholesterol. After all, it is still a challenge to understand why cholesterol, only one of numerous sterols found in nature, is the most abundant one in eukaryotic cells.

In this work, we focus on the above issues and study systematically a variety of sterols, their influence on the lateral pressure profile, and the implications of sterol specificity on a few issues related to membrane protein functions. To this end, we employ atomic-scale molecular dynamics simulations to study nine different membrane systems comprised of phosphatidylcholines (PCs) and sterols. For the PC component, we have chosen a saturated dipalmitoylphosphatidylcholine (DPPC) or an unsaturated dioleoylphosphatidylcholine (DOPC). That allows us to assess the influence of unsaturation. The sterols comprising 20 mol% of membrane composition, in turn, include cholesterol (CHOL), desmosterol (DESMO), 7-dehydrocholesterol (7-DHC), and ketosterol (KETO). As discussed above, CHOL is known as the "raft" sterol because of its

prominent capability to promote the ordering of lipid hydrocarbon chains and the formation of ordered lipid domains. DESMO and 7-DHC are interesting since they are immediate precursors in CHOL's biosynthetic pathway. Finally, KETO is fascinating due to its structural similarity to CHOL, the only difference being the ketone group replacing the hydroxyl group in CHOL.

Our results indicate that the lateral pressure profiles of different lipid-sterol systems are largely similar concerning their qualitative form, but quantitatively there are notable differences. These differences are surprisingly large considering that desmosterol and 7-dehydrocholesterol deviate from cholesterol only by a single double bond. The differences in the lateral pressure profiles are particularly pronounced in a saturated lipid bilayer and are manifested in many quantities analyzed in this work, such as variations in membrane elasticity and changes in the free energy associated with membrane protein conformational change. Implications of our findings are briefly discussed at the end of this work.

The rest of this paper is organized as follows: In the next section we describe computational details, methods, and the lateral pressure profile calculation. In Section 3 we present results; for structural properties in Section 3.1, the lateral pressure profiles are given in Section 3.2, and Section 3.3 focuses on the implications of the lateral pressure profiles in terms of membrane elasticity. Finally, Section 4 summarizes our conclusions.

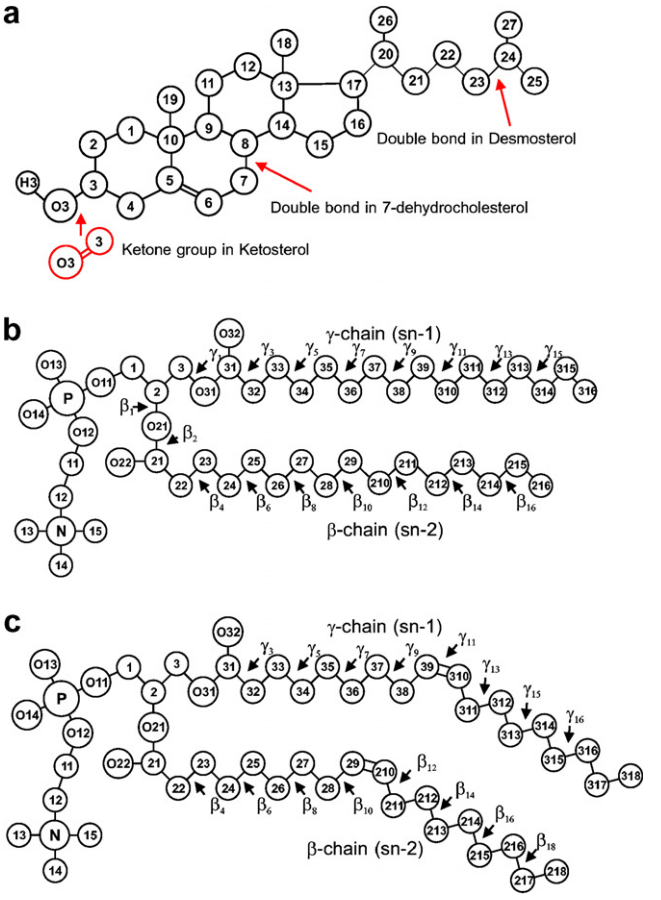

Fig. 1. (a) Structures of the sterols studied in this work. The structure of cholesterol is shown in full. For other sterols, only the changes with respect to cholesterol are given. (b) DPPC showing also the numbering of atoms and dihedral angles. (c) DOPC in a similar manner.

2. Methods

2.1. System descriptions and force fields

We have performed atomic-scale molecular dynamics (MD) simulations of nine different membrane systems. For each system, the simulations were conducted over a time scale of about 100 ns. The total simulation time was almost 1 μs.

First, for the purpose of comparison, we considered two single-component bilayers consisting of 128 phosphatidylcholine (PC) lipid molecules, either the saturated DPPC or the monounsaturated DOPC. Second, we considered a variety of different two-component lipid bilayers comprised of 128 DPPCs and 32 sterol molecules. That constitutes a molar fraction of 20% for sterols. The sterols (see Fig. 1) used here were cholesterol (CHOL), desmosterol (DESMO), 7-dehydrocholesterol (7-DHC), and ketosterol (cholesterol from which the hydroxyl group is substituted by a ketone group) (KETO). Third, we considered the effect of unsaturation by studying three systems composed of 128 DOPC and 32 sterol molecules, using the sterols CHOL, DESMO, and 7-DHC. All of the bilayers were hydrated with ~3500 water molecules.

The initial structures of pure PC and PC/CHOL bilayers were obtained by arranging the PC molecules in a regular array in the bilayer plane (xy-plane) with an initial surface area of 0.64 nm^2 per PC molecule. The z-axis then corresponds to the membrane normal direction. An equal number of sterol molecules were inserted regularly into each leaflet. The remaining sterol systems were obtained by transforming the cholesterol molecules into the desired sterol type in PC/CHOL bilayers which had already been equilibrated through a 100 ns simulation. Prior to the actual MD simulations, the steepest-descent algorithm was used to minimize the energies of the initial structures (Murzyn et al., 2001; Patra et al., 2003). The simulations were performed using the GROMACS software package (der Spoel et al., 2004; Berendsen et al., 1995; Lindahl and Edholm, 2000b).

All the MD simulations were carried out in the NpT ensemble over a time scale of 100 ns. The first 20 ns were considered as an equilibration period (Falck et al., 2004), and only the last 80 ns of each trajectory were analyzed. Fig. 1 shows the structure, the numbering of atoms, and the torsion angles in DPPC, DOPC and sterol molecules.

We used the standard united-atom force field parameters for DPPC molecules (Berger et al., 1997), where the partial charges were taken from the underlying model description (Tieleman and Berendsen, 1996). For DOPC molecules we used the same force field supplemented with

a double bond as described in (Marrink et al., 1998). For the sterol force field, we used the cholesterol description of Holtje et al. (2001) which is based on the GROMACS force field. Thus any modifications within sterols were parameterized consistently using this force field. For water, we employed the SPC (Simple Point Charge) model (Berendsen et al., 1981).

Periodic boundary conditions with the usual minimum image convention were used in all three directions. The LINCS algorithm (Hess et al., 1997) was used to preserve the bond lengths in the sterol hydroxyl groups, and SETTLE (Miyamoto and Kollman, 1992) was used for water. The time step was set to 2 fs. The simulations were carried out at constant pressure (1 atm) and temperature (323 K), which is above the main phase transition temperature of DPPC and DOPC (Vist and Davis, 1990). The temperature and pressure were controlled using the Berendsen method (Berendsen et al., 1984) with relaxation times set to 0.6 and 1.0 ps, respectively. The temperatures of the solute and solvent were controlled independently, and the pressure was controlled semi-isotropically. The Lennard–Jones interactions were cut off at 1.0 nm without shift or switch functions. For the electrostatic interactions we employed the particle-mesh Ewald method (PME) (Essman et al., 1995) with a real space cut-off of 1.0 nm, spline interpolation (of order five), and direct sum tolerance of 10^{-6}. In previous studies, PME has been shown to do well in membrane simulations (Patra et al., 2003, 2004, 2006a). The list of non-bonded pairs was updated every 10 time steps. The simulation protocol used in this study has been successfully applied in various MD simulation studies of lipid bilayers, such as studies of the influence of sterols on lipid bilayers (Vainio et al., 2006; Falck et al., 2004), ion leakage and pore formation mechanisms in lipid membranes (Gurtovenko and Vattulainen, 2005), and partitioning of small molecules such as alcohols and fluorescent probes in to lipid bilayers (Patra et al., 2006b; Repakova et al., 2005, 2006; Lee et al., 2004).

2.2. Lateral pressure profile

The local pressure for a system consisting of particles with many-body potentials can be defined using the local stress tensor. The lateral pressure profile $p(z)$ is then defined as a difference between the normal (along the membrane normal direction) and the lateral components of the pressure tensor, that is, $P_N = P_{zz}$ and $P_L = (P_{xx} + P_{yy})/2$:

$$p(z) = P_L - P_N. \quad (1)$$

Qualitatively, this means that a bilayer tends to expand along the membrane xy-plane with positive $p(z)$ and contract with negative $p(z)$.

In practice, lateral pressure profiles were determined using an approach similar to the ones presented and validated by several authors elsewhere (Carrillo-Tripp and Feller, 2005; Lindahl and Edholm, 2000a; Sonne et al., 2005; Gullingsrud and Schulten, 2004; Patra, 2005; Ollila et al., 2007). More details of our method are available in (Ollila et al., 2007). Here, we summarize the most essential points of the calculation.

The lateral pressure was calculated using the Irving–Kirkwood (IK) contour (Kirkwood and Buff, 1949; Irving and Kirkwood, 1950) dividing the systems in ~0.1 nm thick slabs. Here, it should be pointed out that while the actual simulations were conducted by PME for long-range interactions, the post-trajectory analysis of simulation trajectories for lateral pressure profiles was carried out by truncating the long-range interactions, because otherwise the IK contour can not be employed in the analysis. Nevertheless, the choice of the IK contour is supported by a recent study by Morante et al. (2006) and by the recent calculations by Sonne et al. (2005). Sonne et al. showed that the IK contour provides the correct behavior for pressure profiles in lipid membranes provided that the truncation distance (during post-trajectory analysis) for long-range interactions is $r_{cut} > 1.8$ nm. Here, we have employed $r_{cut} = 2.0$ nm. Pairwise forces during the pressure calculation were computed from the force field description and MD trajectory. Constrained forces arising from SETTLE and LINCS were calculated from the general equation by Hess et al. (1997). Statistical error for the lateral pressure profiles was estimated by calculating the error of the mean in each slice. For each system, the lateral pressure profile was calculated exactly similarly.

The method used here has been validated against the results of (Lindahl and Edholm, 2000a), who used an essentially similar force field for DPPC, and who also used the same contour together with the truncation for electrostatics during the pressure profile calculation. Our results for the lateral pressure profile of DPPC were found to be essentially identical. Similarly, our results for the DPPC/CHOL system (below) are consistent with those of Patra (2005), whose model is largely similar to ours.

3. Results

The main objective of this article is to elucidate the effects of sterol type on the lateral pressure profile across a membrane. For this purpose, we consider two different lipid matrices (DPPC, DOPC) and several different sterols. In this fashion, all the systems are described on an equal footing because the force fields are based on the same underlying description. We only vary those details of the force field which differentiate the lipids and sterols from one another. However, before discussing the results for lateral pressure profiles, let us briefly assess some of the relevant structural properties needed to interpret the lateral pressure profile data. It is worthwhile to mention that the models for DPPC/CHOL and DPPC/DESMO have been previously validated and discussed elsewhere (Falck et al., 2004; Vainio et al., 2006). The lateral pressure profiles of these systems have not been reported previously except for the DPPC/CHOL system (Patra, 2005). As for 7-dehydrocholesterol and ketosterol, we are not aware of any previous computational studies of these systems.

3.1. Structural properties

3.1.1. Area per lipid

The results in Table 1 show clearly the exceptional nature of cholesterol as a molecule able to enhance the packing of saturated lipids in a bilayer, and hence to decrease the average area per PC. For other sterols, we find a similar but less pronounced effect. In the unsaturated DOPC bilayer, the differences are considerably smaller and the effect of cholesterol is less significant than in the case of DPPC. This behavior is consistent with experimental studies (Warschawski and Devaux, 2005), which have indicated that the influence of cholesterol on the packing and ordering of lipids becomes less prominent as lipid unsaturation increases. The differences between the different sterols hence seem to be strongest in bilayers composed of saturated lipids. This is in full agreement with the fact the lipid rafts have been found to be rich in saturated rather than unsaturated lipids (Simons and Ikonen, 1997).

The results are in good agreement with experiments. For DPPC, Nagle and Tristram-Nagle have reported a value of 0.64 nm^2 at 323 K (Nagle and Tristram-Nagle, 2000). For DOPC, experiments have yielded values of 0.72 nm^2 at 303 K (Tristram-Nagle et al., 1998; Kučerka et al., 2005). For increasing cholesterol concentration, experiments have shown a decrease in the average area per lipid, and the changes are of the same size as in the present work (see (Falck et al., 2004) and references therein). For other sterols, to our knowledge, experimental data is not available.

3.1.2. Lipid chain order parameters

We have determined the deuterium order parameter

$$S_{CD} = \tfrac{1}{2}\langle 3\cos^2\theta - 1\rangle, \quad (2)$$

where θ is the angle between the bilayer normal and the C–H bond vector and the brackets denote an average over all lipids and different times. To calculate the deuterium order parameters from Eq. (2), the positions of the hydrogen atoms had to be included in the simulation trajectories of the system. That was performed by calculating the positions on the basis of the orientation of the carbon chains and exploiting the tetrahedral symmetry at given sites. Similar approach has been used elsewhere (Niemelä et al., 2004). Using S_{CD}, we define the molecular order parameter $S_{mol} = 2S_{CD}$ whose maximum value is one in a fully ordered all-trans configuration. When S_{mol} is calculated separately for each CH_2 group in the acyl chain, one obtains the order parameter profile along the hydrocarbon chain, separately for the *sn*–1 and *sn*–2 chains, see e.g. (Falck et al., 2004).

In Table 1, we summarize the results for S_{mol} averaged over all carbons in the two acyl chains. This averaged quantity characterizes the average conformational order of the lipid acyl chains and is essentially the same as the M_1 order parameter (first moment of the NMR profile) obtained through NMR experiments. The results in Table 1 show that in the saturated DPPC bilayer, cholesterol is superior in terms of promoting ordering of the lipid acyl chains, followed by 7-DHC, KETO, and DESMO, in order of decreasing ordering capability. In the unsaturated DOPC matrix, the different sterols are essentially identical in terms of their ordering properties. For comparison, let us briefly point out that the simulation results for CHOL and DESMO have been previously validated to be in line with experiments (Falck et al., 2004; Vainio et al., 2006).

Results for the average sterol tilt support the recent findings that the tilt of a sterol is coupled to its capability to order acyl chains in its immediate vicinity (Vainio et al., 2006; Aittoniemi et al., 2006). For sterols characterized by a large order parameter, the average sterol tilt angle is small, and vice versa. What is more, recent studies (Aittoniemi et al., 2006) have proposed that this also holds for the instantaneous angle of the sterol: for sterols whose orientation with respect to membrane normal fluctuates a lot, the ordering of neighboring acyl chains is affected in a similar manner, decreasing the average conformational order of acyl chains.

3.1.3. Density profiles across bilayer

Figs. 2 and 3 show the density profiles of several molecular groups in the studied membranes. Results for membrane thickness determined from electron density profiles and shown in Table 1 are consistent with the above

Table 1
Summary of the structural results for the studied PC/sterol systems

Bilayer	Area/PC (nm^2)	Thickness (nm)	Averaged S_{mol}	Sterol tilt (°)
DPPC	0.66	3.92	0.29	—
DPPC/CHOL	0.60	4.69	0.57	19.8
DPPC/DESMO	0.65	4.22	0.46	26.9
DPPC/7-DHC	0.62	4.49	0.53	21.9
DPPC/KETO	0.63	4.38	0.50	28.1
DOPC	0.69	3.97	0.27	—
DOPC/CHOL	0.65	4.54	0.36	24.7
DOPC/DESMO	0.65	4.54	0.36	24.9
DOPC/7-DHC	0.66	4.54	0.35	25.8

The error bounds are ±0.01 nm^2 for area/PC, ±0.02 nm for membrane thickness, ±0.01 for the lipid chain order parameter S_{mol}, and ±0.2° for sterol tilt. Note that the area is computed by dividing the average area of the bilayer by the number of PCs in a leaflet (not accounting for sterols). Membrane thickness is determined from the electron density profile by considering the distance between the phosphorus-rich head group peaks. The sterol tilt was defined as the angle between the C3–C17 vector (see Fig. 1) and the bilayer normal.

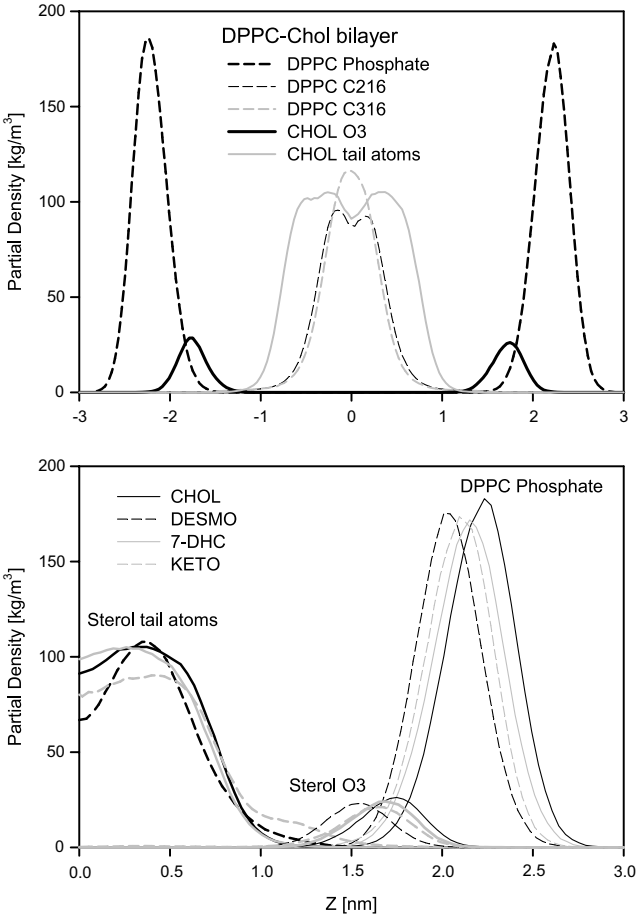

Fig. 2. Density profiles of the DPPC/sterol systems studied in this work. Shown here are the profiles of phosphor in the PC head group and the terminal CH_3 group in the two acyl chains. Also given are the profiles of the oxygens in the OH and ketone groups of sterols, and the profiles of their short hydrocarbon chain. For numbering of atoms, see Fig. 1.

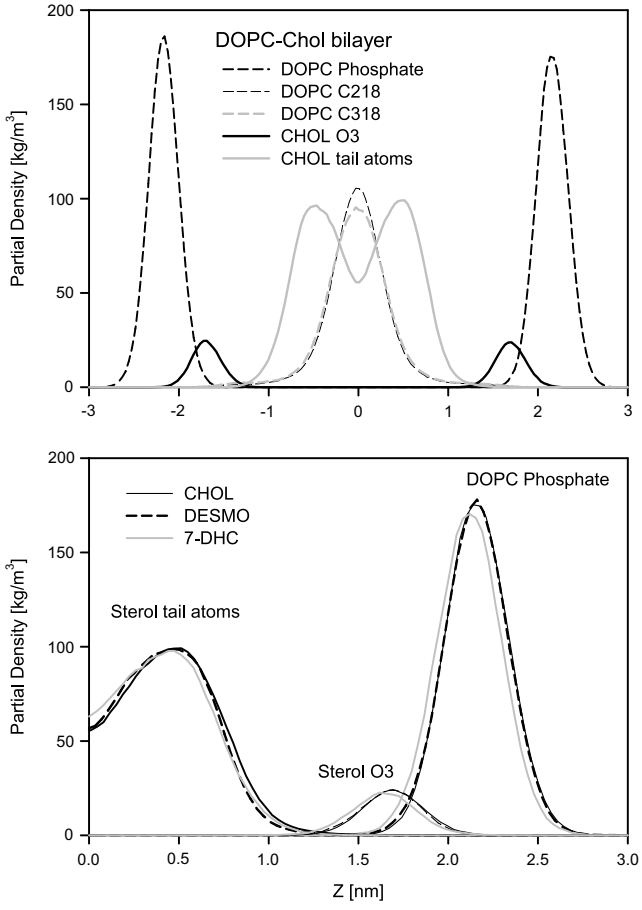

Fig. 3. Density profiles of the DOPC/sterol systems studied in this work, as in Fig. 2 but here for the unsaturated case.

findings. The thickness of the DPPC-CHOL system is largest, reflecting the prominent ordering of lipid acyl chains, while other sterol/PC mixtures are thinner, following the same order as for the acyl chain order parameter. The membrane thickness of 3.9 nm for a pure DPPC bilayer is consistent with electron density profile experiments, which have yielded 3.83 nm at 323 K (Nagle and Tristram-Nagle, 2000). For DOPC, related electron density profile studies have given 3.69 nm at 303 K (Nagle and Tristram-Nagle, 2000) (here, we have 323 K). As for sterol-induced effects, addition of cholesterol, ergosterol, and lanosterol is known to increase membrane thickness above the main transition temperature (Pencer et al., 2005), and a similar conclusion is expected for other sterols, too.

Additionally, for the purpose of comparing structural data with the lateral pressure profiles discussed below, we also show the density profiles for phosphorus (P) in the PC lipid head groups, the terminal CH_3 groups of the acyl chains, the short hydrocarbon chain of the sterols, and the OH or ketone group of the sterols studied here. We discuss the details of these density profiles below, together with the results for the lateral pressure profiles.

3.2. Lateral pressure profiles

The lateral pressure profile, $p(z)$, arises from local forces acting inside a lipid bilayer in the direction of the membrane plane. The condition for mechanical stability and equilibrium requires that the integrated lateral pressure profile across the membrane vanishes. Nevertheless, the profile may display different behavior in different regions in the membrane due to a variety of interactions whose relative importance varies across the membrane. Traditionally, three different regimes have been identified: (1) a repulsive contribution in the hydrophilic head group region due to electrostatic and steric interactions and hydration repulsion; (2) an attractive contribution at the membrane-water interface due to the interfacial energy between the water and the hydrocarbon phase, trying to minimize the surface area; and (3) a repulsive contribution inside the membrane due to steric interactions between hydrophobic chains (Israelachvili et al., 1980; Israelachvili, 1985; Marsh, 1996). These forces are assumed to create a non-uniform lateral component of local pressure inside a bilayer (Seddon and Templer, 1995; Marsh, 1996). The details may vary considerably from one system to another.

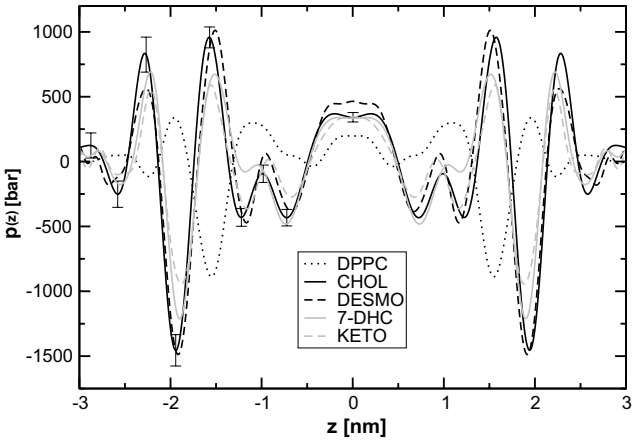

Fig. 4. Lateral pressure profiles of DPPC, DPPC/CHOL, DPPC/DESMO, DPPC/7-DHC, and DPPC/KETO bilayers. Statistical errors are presented for one leaflet of the DPPC/CHOL system, in which the fluctuations were the largest. Error bars in other systems were smaller.

Here, we employ atom-scale simulations to systematically analyze the dependence of lateral pressure profiles on the sterol type. The results are presented in Figs. 4 and 5. For clarity, the profiles have been smoothed by adaptive high order spline fitting (Thijsse et al., 1998) and averaged over the two monolayers. The error bounds shown in the plots demonstrate fluctuations of the data.

The lateral pressure profile found for the pure DPPC bilayer (see Fig. 4) is in good agreement with earlier atomic-scale simulations (Lindahl and Edholm, 2000a; Sonne et al., 2005; Patra, 2005). Considering the present case, the profile is most importantly characterized by a positive peak at the head group region, a negative peak at the boundary between the water and hydrophobic hydrocarbon regions, and by a shallow peak in the middle of the bilayer. The peak heights are notable and of the order of 1000 bar. Let us next consider the influence of sterols on the two different cases, where the matrix is either a saturated or an unsaturated lipid bilayer.

3.2.1. Influence of sterols on a saturated DPPC bilayer

Let us first consider the *saturated* DPPC matrix. Fig. 4 demonstrates that CHOL has a major impact on the lateral pressure profile, in agreement with an earlier study by Patra (2005). In the presence of CHOL, the lateral pressure profile becomes broader than the corresponding one of pure DPPC, because CHOL increases membrane thickness. More importantly, however, CHOL affects the qualitative nature of the profile. It increases the number of peaks and increases their heights by a factor of two. Indeed, the maximum values of the lateral pressure profile are about 1000 bar (attractive component) and 1500 bar (repulsive component) in the presence of cholesterol. We discuss the energy scale related to these pressures below. Here we rather note that, despite their seemingly larger values, lateral pressures of this magnitude have been predicted previously on the basis of the thickness of the membrane-water interface and the interfacial tension associated with this region (Cantor, 1997, 1999a). In the region where the rigid steroid structure is located ($z \approx 1$–1.5 nm), the lateral pressure profile displays fine details not present in the DPPC bilayer. In the membrane center the lateral pressure is increased substantially in comparison with the profile of a pure DPPC membrane.

What comes to the differences between the different PC-sterol systems, we find that the main features of the lateral pressure profiles are largely the same, but the quantitative details vary. Cholesterol gives rise to peaks whose magnitudes are typically about 200 bar larger than for other sterols. Largest differences are found in the peak heights close to the membrane-water interface ($z \approx 2$–2.5 nm), where the head group of the lipids is located. The pressures in this region may differ by as much as about 500 bar. Significant differences are also observed in the region where the rigid steroid structures are located (z around 1 nm), and where the additional double bonds reside ($z \approx 1.2$ nm for 7-DHC and $z \approx 0.5$ nm for DESMO, see Figs. 2 and 3). In part, these findings are rather obvious since the tilts of the sterols differ from one sterol to another (see Table 1). Hence, the packing of molecules differs correspondingly, implying that the strengths of interactions such as van der Waals forces are also varied among the different systems.

A comparison between the different DPPC/sterol systems indicates that the lateral pressure profile of 7-DHC differs most from the profile of cholesterol. For 7-DHC, the pressure close to its additional double bond in the steroid moiety at about $z = 1.2$ nm from membrane center has a clear fingerprint, as it is about 400 bar larger than for other sterols.

3.2.2. Influence of sterols on an unsaturated DOPC bilayer

Fig. 5 depicts the data in the unsaturated DOPC bilayer. It demonstrates that in this case the differences between the

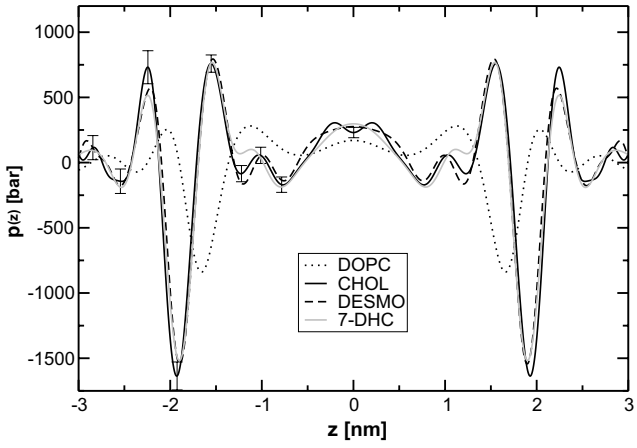

Fig. 5. Lateral pressure profiles of DOPC, DOPC/CHOL, DOPC/DESMO, and DOPC/7-DHC bilayers. Statistical errors are presented for one leaflet of the DOPC/CHOL system, in which the fluctuations were the largest. Error bars in other systems were smaller.

sterols are much smaller than in a saturated DPPC membrane. The deviations of PC/sterol systems from DOPC/CHOL are essentially everywhere less than 200 bar, and hence minor compared with the differences observed in the saturated systems. Nevertheless, the fingerprint of 7-DHC at about $z = 1.2$ nm is still evident.

3.3. Implications of lateral pressure profiles

Let us discuss the implications of the above results by considering the effect of lateral pressure profiles on membrane elasticity and the energetics related to interactions with membrane proteins. As the first and simplest example, let us relate the magnitude of lateral pressures to the thermal energy k_BT, which is the driving force of all soft matter systems.

The maximum value of the lateral pressure profile is of the order of 1500 bar. What does this mean in practice? Some insight is provided by considering a simplified model where we describe an integral protein as a cylinder of radius 2 nm, and then calculate the force due to the lateral pressure profile exerted on a thin strip of height 0.1 nm on the surface of the protein. Then the force acting on the strip is $F = 1500\ \text{bar} \times 4\pi \times 10^{-19}\ \text{m}^2$, which yields ~190 pN. If this force displaces the protein (or some of its structural units) in the membrane normal direction by 0.2 nm, then the corresponding energy is roughly $9k_BT$. In brief, this implies that the energies related to the lateral pressure profile, as they do work to influence membrane protein conformations, are of the order of thermal energy. The local effects due to lateral pressures hence can not be washed out by thermal fluctuations. On larger scales the importance of lateral pressures is even more evident, because the lateral pressure profile is at the core of many elastic coefficients of membranes. That will be discussed next.

Cellular membranes are essentially soft interfaces, whose elasticity is related to their structural properties such as undulations, compressibility, and bending rigidity. We now consider how the subtle changes in sterol structure are manifested in elastic coefficients determined from the lateral pressure profile: the point is that many membrane elastic coefficients (such as the bending modulus κ, the spontaneous curvature c_0, and the saddle splay modulus $\bar{\kappa}$) can be determined when the lateral pressure profile is known (Safran, 1994). However, in practice this is not straightforward. For example, in order to find the bending modulus, one has to compute derivatives of the lateral pressure profile with respect to the area per molecule. That is not a simple feat as it requires several extensive simulations to be made with different values for the area per molecule. Here, we consider a more feasible case and focus on the product of the bending modulus and the spontaneous curvature for a monolayer, which can be defined as the first moment of the lateral pressure profile $p(z)$,

$$\kappa c_0 = \int_0^h (z - z^*) p(z) \mathrm{d}z, \tag{3}$$

where h is the thickness of the monolayer, and z^* is the location of the pivotal surface of the monolayer (Cantor, 1999a). Here, we define the pivotal surface of a monolayer to correspond to the local maximum of the lateral pressure profile in the hydrophobic region close to the interface. A similar definition has been made, for example, by Chen and Rand (1997). Then we can calculate the product κc_0 using Eq. 3. Results for the different systems are presented in Table 2.

Chen and Rand measured $\kappa c_0 = -6.6 \times 10^{-12}$ J/m for a DOPC/CHOL mixture (20 mol% of cholesterol), which is larger than our result $\kappa c_0 = -19.2 \times 10^{-12}$ J/m for DOPC/CHOL. However, a quantitative comparison is not particularly meaningful because the experiment was carried out for monolayers in the inverted hexagonal phase, while our results have been determined from a flat lipid bilayer by rather crudely truncating the system into two halves. Despite this, our results are in agreement with the qualitative trend found by Chen and Rand (1997). They observed that the product κc_0 increased for increasing cholesterol concentration, and the relative increase is in line with our data: we found an increase of 20% in the value of κc_0 when cholesterol molar concentration increased from 0 to 20 mol%, while the data by Chen and Rand indicates an increase of about 25%.

For the saturated DPPC-sterol bilayers, we find that the result of desmosterol is considerably and that of ketosterol slightly larger than the coefficient given by cholesterol. This is mainly due to the larger pressures in these systems in the hydrophobic region. 7-Dehydrocholesterol, in turn, yields a coefficient which is almost identical with that of cholesterol: the lateral pressure profiles of DPPC/CHOL and DPPC/7-DHC systems are different, but the differences largely cancel each other (see the linear dependence of κc_0 on the pressure profile in Eq. 3). For comparison, in the DOPC matrix the results for different sterols are practically identical within error bounds.

The elasticity of membranes depends on their sterol content, and in a saturated bilayer in particular the minor structural differences between the sterol types give rise to

Table 2
Elastic coefficient κc_0 determined from the lateral pressure profiles

	κc_0 [10^{-12} J/m]	ΔW [k_BT]
DPPC	−11.0	−1.2
DPPC/CHOL	−6.7	−1.0
DPPC/DESMO	−20.4	−3.3
DPPC/7-DHC	−7.6	−0.8
DPPC/KETO	−9.2	−1.8
DOPC	−16.1	−2.2
DOPC/CHOL	−19.2	−3.1
DOPC/DESMO	−18.3	−1.9
DOPC/7-DHC	−18.9	−3.3

The error bound associated with this product is ±20%. Also, we show data for the energy ΔW associated with a change in model protein structure due to the lateral pressure profile, see discussion in the text. The error bounds associated with ΔW are ±20%.

observable differences in membrane elasticity. The question is, could that play a role in membrane protein functionality. The results by Cantor (1997, 1999a) are in favor of this idea and suggest that the inhomogeneous lateral pressure within a membrane can affect the equilibrium distribution of conformations of membrane proteins, if the difference in cross-sectional area between two conformations varies with depth.

To consider the above idea, we finish with a discussion of possible implications of the lateral pressure profiles on protein structure by calculating the lateral pressure profile component for the energy between tilted (open) and non-tilted (closed) protein conformations following the approach of Cantor (1999a), later also used by Gullingsrud and Schulten (2004) who employed the same approach to analyze atomistic simulation data for single-component lipid bilayers. We hence adopt the simplest nontrivial model for the shape of an ion channel, in this case the mechanosensitive channel MscL, and represent the protein as a truncated cone with radius $r(z)$ and slope s interacting with a lateral pressure profile $p(z)$, see Gullingsrud and Schulten (2004). In this model, the slope s is zero for the closed and non-zero for the open state. We define $z = 0$ to be in the middle of the bilayer (Gullingsrud and Schulten, 2004) and calculate the first (M_1) and the second moment (M_2) of the lateral pressure profile over the whole bilayer. The $\Delta W = W_{\text{non-tilted}} - W_{\text{tilted}}$ is the energy between tilted and non-tilted states. The energy of the tilted state, W_{tilted}, is then

$$\int \mathrm{d}z p(z) A(z) = \pi \int \mathrm{d}z p(z)[r(z)]^2 \tag{4}$$

$$= \pi \int \mathrm{d}z p(z)(R + sz)^2, \tag{5}$$

and hence

$$\Delta W = 2\pi R s M_1 + \pi s^2 M_2. \tag{6}$$

The radius of the closed state was chosen as $R = 2.5$ nm and the slope as $s = 0.2$. Gullingsrud et al. used identical values (Gullingsrud and Schulten, 2004). For the non-tilted state, $r(z) = R$ and hence constant.

Before presenting the results, there is reason to stress why the reference level $z = 0$ is here defined to be in the middle of the bilayer. Doing so implies that the cross-sectional area of the channel is fixed in the middle of the membrane. Another and perhaps an intuitively more appropriate possibility would be to use a condition where the reference level $z = 0$ is set to be outside the bilayer, such that the cross-sectional area for one end of the channel would be fixed at that point. However, the latter choice would increase the error due to fluctuations in $p(z)$ rather substantially because of the z^2 dependence in W_{tilted}, see above. This was confirmed through additional studies. In essence, this implies that setting the reference level in the middle of the membrane is more robust and less sensitive to errors than having the reference level outside the membrane. This choice is also supported by the considerations of Gullingsrud and Schulten (2004), who used the same approach. Hence, the results shown below are comparable to those reported previously (Gullingsrud and Schulten, 2004).

First, the result of $\Delta W = -2.2 k_B T$ for pure DOPC is in reasonable agreement with the study of Gullingsrud and Schulten (2004), who found about $-(0.9–2.0)\ k_B T$ for POPC for varying values of area per lipid. We also analyzed our recent simulation data for a one-component POPC bilayer at 323 K (Ollila et al., 2007) and found $\Delta W = -(1.9 \pm 0.2) k_B T$.

The energy ΔW characterizes the work done against the lateral pressure profile to alter the shape of the membrane cavity occupied by a protein, as it changes its conformation from the closed to an open state. This can be compared with the free energy difference of about 20–50 $k_B T$ (Sukharev et al., 1999; Gullingsrud and Schulten, 2004) between the open and closed states. On the basis of Table 2, the contribution due to the pressure profile ranges from about 0.8 to 3.3 $k_B T$ depending on lipid content. The influence of sterols on the found values is larger in saturated bilayers. In unsaturated bilayers the differences between the different sterol types are smaller. For comparison, significantly larger values have been found recently in simulations of a lipid raft-like bilayer (Niemelä et al., 2007) for an equimolar mixture of cholesterol, sphingomyelin, and POPC. For that system a similar analysis yielded $\Delta W \approx 11\ k_B T$. Using a simplified lattice model, the theoretical study by Cantor, 1999a) resulted in values which were of the same order of magnitude. Further, in a recent theoretical study, Wiggins and Phillips (2005) found that the free energies associated with elastic bilayer deformations for the MscL channel are also of the order of 10 $k_B T$. As a number of elastic coefficients of membranes can be determined from the lateral pressure profile, this further highlights the significance of lateral pressures in this context. Summarizing, we find that the seemingly minor structural differences between the sterols are manifested as observable differences in ΔW. This is most evident in saturated bilayers and supported by significant effects in very compact raft-like bilayers (Niemelä et al., 2007).

Here, we have considered the case where the lateral pressure profiles have been determined from protein-free lipid bilayers. One may ask whether the insertion of a protein into a membrane would affect the lateral pressure profile and hence its action on the protein. According to the recent atomic-scale study (Gullingsrud et al., 2006), there seems to be some local changes in the lateral pressure profile due to a protein. It is likely, though, that the lipid composition surrounding the protein does matter considerably. This is particularly evident from (Niemelä et al., 2007) and Table 2, which highlight the difference between varying lipid compositions in bilayer systems.

We would like to stress that the value of the energy ΔW found through this analysis depends on the shape of the model protein. By varying $r(z)$, one can assess the impact of different regions in the lateral pressure profile. Here we

do not discuss this issue further, but rather conclude that the results provide strong evidence that the lateral pressure profile has a clear importance. Changes in the pressure profile can give rise to energetic changes in ΔW to be approximately 1–10 k_BT, and this amounts to a significant fraction of the free energy cost between the open and closed states of a membrane protein.

4. Discussion and concluding remarks

Here, we have employed atomistic molecular dynamics simulations to unravel the effects of different sterol types on lateral pressure profiles (Marsh, 1996) in saturated and unsaturated lipid bilayers. We have used two different phospholipid compositions, a saturated DPPC bilayer and an unsaturated DOPC membrane. For sterols, we used cholesterol, desmosterol, 7-dehydrocholesterol, and ketosterol. Since all the molecular models are based on the same underlying force field, and only the details differentiating the sterols from one another have been varied, this study has indeed been performed in systematic and controlled manner.

First, as for structural properties, we found that cholesterol is superior in terms of the capability to order saturated lipid hydrocarbon chains and to enhance packing of lipids. This is manifested in many structural properties such as membrane thickness and the average area per lipid. In this regard, cholesterol was followed by 7-DHC, KETO, and DESMO, the last one being the least efficient in terms of ordering. The behavior in the unsaturated DOPC bilayer was different. There, the differences between all the studied sterol/DOPC systems were found to be marginal. Our results clearly show that the ordering properties of sterols are primarily directed towards saturated chains. In unsaturated systems the sterol type is of less importance as far as the ordering of hydrocarbon chains is concerned.

Next, we turned our attention to lateral pressure profiles. First, we validated our method against the few existing studies for saturated DPPC and DPPC/CHOL (Lindahl and Edholm, 2000a; Sonne et al., 2005; Patra, 2005; Ollila et al., 2007) and found full agreement. For other systems, no data for comparison exists.

We have found that the lateral pressure profile is altered when cholesterol in the saturated DPPC bilayer is replaced by either desmosterol, 7-dehydrocholesterol, or ketosterol. Bearing in mind that desmosterol and 7-dehydrocholesterol are the immediate precursors of cholesterol along its biosynthetic pathways, and that their structures differ from cholesterol only by one additional double bond, the observed changes in the lateral pressure profile are somewhat surprisingly significant.

First, the height of the pressure profile depends on the sterol due to changes in membrane thickness. For proteins embedded in a membrane, this implies that in membranes containing different sterol types, the largest pressures are exerted on different regions of the protein. Second, the minor structural differences between cholesterol and other sterols give rise to observable differences in the lateral pressure profile. In the case of KETO, the pressure profiles of DPPC/CHOL and DPPC/KETO systems deviate in the head group region, as expected. For DESMO and 7-DHC, the changes are observed mainly close to the additional double bond (in the steroid structure for 7-DHC, and in the membrane center for DESMO). These changes manifest themselves in variations in membrane elastic coefficients. More importantly, though, if we consider the work needed to be done against the lateral pressure in order to reshape the cavity of a protein in the bilayer, we find that it varies by several k_BT, depending on the sterol type. Further studies have shown that in lipid raft-like bilayer compositions the same quantity is about $11k_BT$ (Niemelä et al., 2007). While these results are suggestive and concern only the mechanosensitive channel MScL studied here as an example, they demonstrate that the contribution due to the lateral pressure profile may correspond to a significant fraction of the free energy cost between the open and closed states of a membrane protein. In practice, the sterol type, or more generally the lipid content around a given protein may either stabilize or destabilize the state of the protein.

The finding that the differences due to the sterols in the unsaturated DOPC bilayer are considerably smaller than in a saturated one are consistent with the general understanding that the role of cholesterol is most prominent in bilayers composed of saturated chains. This is the case in lipid rafts rich in cholesterol, sphingomyelin (SM), and saturated phospholipids. Cholesterol, in particular, has been found to promote the formation of ordered domains in model membranes, while for other sterols this property seems to be less evident. For example, while lanosterol has been found to induce domain formation in DOPC/SM/CHOL mixtures, the same study concluded that ketosterol could not induce a phase separation at any of the sterol concentrations considered (Bacia et al., 2005). Also, it has been found that if cholesterol is depleted from membranes and replaced with desmosterol, the ordering of the acyl chains decreases and the activation of an insulin receptor is altered (Vainio et al., 2006). In a recent work dealing with three-component model membranes with DOPC, sterol, and varying amounts of other lipids such as DPPC, SM, or ceramide, desmosterol has also been found to stabilize domain formation weakly (Megha et al., 2006). For 7-DHC, the same study found an intriguing result that 7-DHC promotes domain (raft) formation more strongly than cholesterol (Megha et al., 2006; Xu et al., 2001). At the same time, our results propose that the ordering capability of 7-DHC is not as good as that of cholesterol, though this study is for two-component model membranes. It seems evident that formation of ordered raft-like domains is affected by the interplay of several lipid components, of which the sterol is one of the important ones. Given this data, it is likely that the lateral pressure profiles of the sterols studied here would be different in raft-like bilayers enriched by saturated PCs and SMs, too.

The above-discussed finding that the sterol type affects membrane elasticity, the lateral pressure profile, and consequently the force exerted by the lipids on a membrane protein forces one to pose the question, whether this issue is biologically relevant, and whether it has been observed in experiments. The relevance has been discussed by Cantor, who proposed that changes in the lateral pressure profile influence exponentially the ratio of concentrations of the conformational states of, e.g. mechanosensitive proteins (Cantor, 1997). In that regard, the present results give support to the suggestion (Cantor, 1999b; Brown, 1994; Gibson and Brown, 1993; Wiedmann et al., 1988) that changes in the lateral pressure profile are involved in increasing rhodopsin activity with increasing level of unsaturation, and in decreasing rhodopsin activity with increasing amount of cholesterol (Litman and Mitchell, 1996). This issue is further discussed in a recent work (Mihailescu and Gawrisch, 2006), which also proposed that membrane elastic stress would modulate the functions of integral receptor proteins like rhodopsin. Recent studies by van den Brink-van der Laan et al. (2004a,b) also propose that the lateral pressure profile is involved in the stability and activation of membrane protein complexes. Nevertheless, there is reason for care before conclusions are being drawn, since unfortunately, to our knowledge, there is only one experimental study which has tried to gauge the lateral pressure profile inside a lipid membrane (Templer et al., 1999). The study found essentially the same form for the pressure profile as our simulations for pure PC bilayers. However, since the experiments employed probes which unavoidably perturb membrane structure (Repakova et al., 2004, 2005, 2006; Curdova et al., 2007), the final view remains to be established.

The results of this work show that the lateral pressure profile, the resulting elastic behavior of lipid membranes, and the energies involved in changes of protein conformational states are sensitive to the sterol content of lipid membranes. The results hence support a mechanism where changes in protein conformational state are facilitated by changes in the lateral pressure profile. From a structural point of view, the results provide compelling evidence that despite seemingly minor differences, sterols are characterized by structural specificity.

Acknowledgments

We thank Perttu Niemelä and Marja Hyvönen for fruitful discussions. This work has, in part, been supported by the Academy of Finland, the Jenny and Antti Wihuri Foundation, the Emil Aaltonen Foundation, and the Natural Sciences and Engineering Research Council of Canada (NSERC). Tomasz Róg holds a Marie Curie Intra-European Fellowship '024612-Glychol'. We further acknowledge the Finnish IT Center for Science, the HorseShoe (DCSC) supercluster computing facility at the University of Southern Denmark, and the Shared Hierarchical Academic Research Computing Network (SHARCNET:www.sharcnet.ca) for computer resources.

References

Aittoniemi, J., Róg, T., Niemela, P., Pasenkiewicz-Gierula, M., Karttunen, M., Vattulainen, I., 2006. Tilt: Major factor in sterols' ordering capability in membranes. J. Phys. Chem. B Lett. 110, 25562–25564.

Allende, D., Vidal, A., Simon, S.A., McIntosh, T.J., 2003. Bilayer interfacial properties modulate the binding of amphipathic peptides. Chem. Phys. Lipids 122, 65–76.

Bacia, K., Schwille, P., Kurzchalia, T., 2005. Sterol structure determines the separation of phases and the curvature of the liquid-ordered phase in model membranes. Proc. Natl. Acad. Sci. USA 102, 3272–3277.

Berendsen, H.J.C., Postma, J.P.M., van Gunsteren, W.F., Hermans, J., 1981. Intermolecular Forces. In: Pullman, B. (Ed.). Reidel, Dordrecht, pp. 331–342.

Berendsen, H.J.C., Postma, J.P.M., van Gunsteren, W.F., DiNola, A., Haak, J.R., 1984. Molecular dynamics with coupling to an external bath. J. Chem. Phys. 81, 3684–3690.

Berendsen, H.J.C., van der Spoel, D., van Drunen, R., 1995. GROMACS: a message-passing parallel molecular dynamics implementation. Comput. Phys. Commun. 91, 43–56.

Berger, O., Edholm, O., Jahnig, F., 1997. Molecular dynamics simulations of a fluid bilayer of dipalmitoylphosphatidylcholine at full hydration, constant pressure, and constant temperature. Biophys. J. 72, 2002–2013.

Bowie, J.U., 2005. Solving the membrane protein folding problem. Nature 438, 581–589.

Brown, M.F., 1994. Modulation of rhodopsin function by properties of the membrane bilayer. Chem. Phys. Lipids 73, 159–180.

Cantor, R.S., 1997. The lateral pressure profile in membranes: a physical mechanism of general anestasia. Biochemistry 36, 2339–2344.

Cantor, R.S., 1999a. The influence of membrane lateral pressures on simple geometric models of protein conformational equilibria. Chem. Phys. Lipids 101, 45–56.

Cantor, R.S., 1999b. Lipid composition and the lateral pressure profile in bilayers. Biophys. J. 76, 2625–2639.

Carrillo-Tripp, M., Feller, S.E., 2005. Evidence for a mechanism by ω-3 polyunsaturated lipids may affect membrane protein function. Biochemistry 44, 10164–10169.

Chen, Z., Rand, R.P., 1997. The influence of cholesterol on phospholipid membrane curvature and bending elasticity. Biophys. J. 73, 267–276.

Curdova, J., Capkova, P., Plasek, J., Repakova, J., Vattulainen, I., 2007. Free pyrene probes in gel and fluid membranes: perspective through atomistic simulations. J. Phys. Chem. B, in press.

der Spoel, D.V., Lindahl, E., Hess, B., van Buuren, A.R., Apol, E., Meulenhoff, P.J., Tieleman, D.P., Sijbers, A.L.T.M., Feenstra, K.A., van Drunen, R., Berendsen, H.J.C., 2004. GROMACS User Manual Version 3.2.

Eckenhoff, R.G., 2001. Promiscuous ligands and attractive cavities. How do the inhaled anesthetics work? Mol. Interv. 1, 258–268.

Edidin, M., 2003. The state of lipid rafts: from model membranes to cells. Annu. Rev. Biophys. Biomol. Struct. 32, 257–283.

Essman, U.L., Perera, M.L., Berkowitz, M.L., Larden, T., Lee, H., Pedersen, L.G., 1995. A smooth particle mesh ewald potential. J. Chem. Phys. 103, 8577–8592.

Falck, E., Patra, M., Karttunen, M., Hyvönen, M.T., Vattulainen, I., 2004. Lessons of slicing membranes: interplay of packing, free area, and lateral diffusion in phospholipid/cholesterol bilayers. Biophys. J. 87, 1076–1091.

Gibson, N.J., Brown, M.F., 1993. Lipid headgroup and acyl chain composition modulate the MI–MII equilibrium of rhodopsin in recombinant membranes. Biochemistry 32, 2438–2454.

Gullingsrud, J., Schulten, K., 2004. Lipid bilayer pressure profiles and mechanosensitive channel gating. Biophys. J. 86, 3496–3509.

Gullingsrud, J., Babakhani, A., McCammon, J.M., 2006. Computational investigation of pressure profiles on lipid bilayers with embedded proteins. Mol. Simul. 32, 831–838.

Gurtovenko, A.A., Vattulainen, I., 2005. Pore formation coupled to ion transport through lipid membranes as induced by transmembrane ionic charge imbalance: atomistic molecular dynamics study. J. Am. Chem. Soc. 127, 17570–17571.

Hess, B., Bekker, H., Berendsen, H.J.C., Fraaije, J.G.E.M., 1997. LINCS: a linear constraint solver for molecular dynamics simulations. J. Comput. Chem. 18, 1463–1472.

Holtje, M., Forster, T., Brandt, B., Engels, T., von Rybinski, W., Holtje, H.-D., 2001. Molecular dynamics simulations of stratum corneum lipid models: fatty acids and cholesterol. Biochim. Biophys. Acta 1511, 156–167.

Hong, H.D., Tamm, L.K., 2004. Elastic coupling of integral membrane protein stability to lipid bilayer forces. Proc. Natl. Acad. Sci. USA 101, 4065–4070.

Irving, J.H., Kirkwood, J.G., 1950. The statistical mechanical theory of transport processes. IV. The equations of hydrodynamics. J. Chem. Phys. 18, 817–829.

Israelachvili, J.N., 1985. Intermolecular and Surface Forces. Academic Press, London.

Israelachvili, J.N., Marcelja, S., Horn, R.G., 1980. Physical principles of membrane organization. Q. Rev. Biophys. 13, 121–200.

Kirkwood, J.G., Buff, F.P.J., 1949. The statistical mechanical theory of surface tension. J. Chem. Phys. 17, 338–343.

Kučerka, N., Tristam-Nagle, S., Nagle, J.F., 2005. Structure of fully hydrated fluid phase lipid bilayers with monounsaturated chains. J. Membr. Biol. 208, 193–202.

Lee, B.W., Faller, R., Sum, A.K., Vattulainen, I., Patra, M., Karttunen, M., 2004. Structural effects of small molecules on phospholipid bilayers investigated by molecular simulations. Fluid Phase Equil. 225, 63–68.

Lindahl, E., Edholm, O., 2000a. Spatial and energetic-entropic decomposition of surface tension in lipid bilayers from molecular dynamics simulations. J. Chem. Phys. 113, 3882–3893.

Lindahl, E., Edholm, O., 2000b. Mesoscopic undulations and thickness fluctuations in lipid bilayers from molecular dynamics simulations. Biophys. J. 79, 426–433.

Litman, B.J., Mitchell, D.C., 1996. A role for phospholipid polyunsaturation in modulating membrane protein function. Lipids 31, S193–S197.

Marrink, S.-J., Berger, O., Tieleman, P., Jahnig, F., 1998. Adhesion forces of lipids in a phospholipid membrane studied by molecular dynamics simulations. Biophys. J. 74, 931–943.

Marsh, D., 1996. Lateral pressure in membranes. Biochim. Biophys. Acta 1286, 183–223.

Megha, Bakht, O., London, E., 2006. Cholesterol precursors stabilize ordinary and ceramide-rich ordered lipid domains (lipid rafts) to different degrees. J. Biol. Chem. 281, 21903–21913.

Mihailescu, M., Gawrisch, K., 2006. The structure of polyunsaturated lipid bilayers important for rhodopsin function–a neutron diffraction study. Biophys. J. 90, L04–L06.

Miyamoto, S., Kollman, P.A., 1992. SETTLE: an analytical version of the shake and rattle algorithm for rigid water models. J. Comput. Chem. 13, 952–962.

Morante, S., Rossi, G.C., Testa, M., 2006. The stress tensor of a molecular system: an exercise in statistical mechanics. J. Chem. Phys. 125, 034101.

Murzyn, K., Róg, T., Jezierski, G., Takaoka, Y., Pasenkiewicz-Gierula, M., 2001. Effects of phospholipid unsaturation on the membrane/water interface: a molecular simulation study. Biophys. J. 81, 170–183.

Nagle, J.F., Tristram-Nagle, S., 2000. Structure of lipid bilayers. Biochem. Biophys. Acta 1469, 159–195.

Niemelä, P., Hyvönen, M., Vattulainen, I., 2004. Structure and dynamics of sphingomyelin bilayer: insight gained through systematic comparison to phosphatidylcholine. Biophys. J. 87, 2976–2989.

Niemelä, P., Ollila, S., Hyvönen, M., Karttunen, M., Vattulainen, I., 2007. Assessing the nature of lipid raft membranes (PLoS Computational Biology (2007); dx.doi.org/10.1371/journal.pcbi.0030034.eor).

Ollila, S., Hyvönen, M.T., Vattulainen, I., 2007. Polyunsaturation in lipid membranes–dynamic properties and lateral pressure profiles. J. Phys. Chem. B, in press.

Patra, M., 2005. Lateral pressure profiles in cholesterol-DPPC bilayers. Eur. Biophys. J. 35, 79–88.

Patra, M., Karttunen, M., Hyvönen, M.T., Falck, E., Lindqvist, P., Vattulainen, I., 2003. Molecular dynamics simulations of lipid bilayers: major artifacts due to truncating electrostatic interactions. Biophys. J. 84, 3636–3645.

Patra, M., Karttunen, M., Hyvönen, M., Falck, E., Vattulainen, I., 2004. Lipid bilayers driven to a wrong lane in molecular dynamics simulations by subtle changes in long-range electrostatic interactions. J. Phys. Chem. B 108, 4485–4494.

Patra, M., Hyvonen, M., Falck, E., Sabouri-Ghomi, M., Vattulainen, I., Karttunen, M., 2006a. Long-range interactions and parallel scalability in molecular simulations. Comput. Phys. Commun. 176, 14–22.

Patra, M., Salonen, E., Terama, E., Vattulainen, I., Faller, R., Lee, B.W., Holopainen, J.M., Karttunen, M., 2006b. Under the influence of alcohol: the effect of ethanol and methanol on lipid bilayers. Biophys. J. 90, 1121–1135.

Pencer, J., Nieh, M.-P., Harroun, T.A., Krueger, S., Adams, C., Katsaras, J., 2005. Bilayer thickness and thermal response of dimyristoylphosphatidylcholine unilamellar vesicles containing cholesterol, ergosterol and lanosterol: a small-angle neutron scattering study. Biochim. Biophys. Acta 1720, 84–91.

Pike, L.J., 2004. Lipid rafts: heterogeneity on the high seas. Biochem. J. 378, 281–292.

Repakova, J., Capkova, P., Holopainen, J., Vattulainen, I., 2004. Distribution, orientation, and dynamics of DPH probes in DPPC bilayer. J. Phys. Chem. B 108, 13438–13448.

Repakova, J., Holopainen, J.M., Morrow, M.R., McDonald, M.C., Capkova, P., Vattulainen, I., 2005. Influence of DPH on the structure and dynamics of a DPPC bilayer. Biophys. J. 88, 3398–3410.

Repakova, J., Holopainen, J.M., Karttunen, M., Vattulainen, I., 2006. Influence of pyrene-labeling on fluid lipid membranes. J. Phys. Chem. B 110, 15403–15410.

Safran, S., 1994. Statistical Thermodynamics of Surfaces, Interfaces, and Membranes. Addison-Wesley, New York.

Seddon, J.M., Templer, R.H., 1995. Structure and Dynamics of Membranes. In: Lipowsky, R., Sackmann, E. (Eds.). Elsevier, Amsterdam, pp. 97–160.

Simons, K., Ikonen, E., 1997. Functional rafts in cell membranes. Nature 387, 569–571.

Sonne, J., Hansen, F.Y., Peters, G.H., 2005. Methodological problems in pressure profile calculations for lipid bilayers. J. Chem. Phys. 122, 124903.

Sukharev, S.I., Sigurdson, W.J., Kung, C., Sachs, F., 1999. Energetic and spatial parameters for gating of the bacterial large conductance mechanosensitive channel, MscL. J. Gen. Physiol. 113, 525–540.

Templer, R.H., Castle, S.J., Curran, A.R., Rumbles, G., Klug, D.R., 1999. Sensing isothermal changes in the lateral pressure in model membranes using di-pyrenyl phosphatidylcholine. Faraday Discuss. 111, 41–53.

Thijsse, B.J., Hollanders, M.A., Hendrikse, J., 1998. A practical algorithm for least-squares spline approximation of data containing noise. Computers in Physics 12, 393–399.

Tieleman, D.P., Berendsen, H.J.C., 1996. Molecular dynamics simulations of a fully hydrated dipalmitoylphosphatidylcholine bilayer with different macroscopical boundary conditions and parameters. J. Chem. Phys. 105, 4871–4880.

Tristram-Nagle, S., Petrache, H.I., Nagle, J.F., 1998. Structure and interactions of fully hydrated dioleoylphosphatidylcholine bilayers. Biophys. J. 75, 917–925.

Vainio, S., Jansen, M., Koivusalo, M., Róg, T., Karttunen, M., Vattulainen, I., Ikonen, E., 2006. Significance of sterol structural

specificity: desmosterol cannot replace cholesterol in lipid rafts. J. Biol. Chem. 281, 1121–1135.

van den Brink-van der Laan, E., Killian, J.A., de Kruijff, B., 2004a. Nonbilayer lipids affect peripheral and integral membrane proteins via changes in the lateral pressure profile. Biochim. Biophys. Acta 1666, 275–288.

van den Brink-van der Laan, E., Chupin, V., Killian, J.A., de Kruijff, B., 2004b. Stability of KcsA tetramer depends on membrane lateral pressure. Biochemistry 43, 5937–5942.

Vist, M.R., Davis, J.H., 1990. Phase equilibria of cholesterol/dipalmitoylphosphatidylcholine mixtures: 2H nuclear magnetic resonance and differential scanning calorimetry. Biochemistry 29, 451–464.

Warschawski, D.E., Devaux, P.F., 2005. Order parameters of unsaturated phospholipids in membranes and the effect of cholesterol: A ^{1}H–^{13}C solid-state NMR study at natural abundance. Eur. Biophys. J. 34, 987–996.

White, S.H., 2004. The progress of membrane protein structure determination. Protein Sci. 13, 1948–1949.

Wiedmann, T.S., Pates, R.D., Beach, J.M., Salmon, A., Brown, M.F., 1988. Lipid–protein interactions mediate the photochemical function of rhodopsin. Biochemistry 27, 6469–6474.

Wiggins, P., Phillips, R., 2005. Membrane-protein interactions in mechanosensitive channels. Biophys. J. 88, 880–902.

Xu, X., Bittman, R., Duportail, G., Heissler, D., Vilcheze, C., London, E., 2001. Effect of the structure of natural lipids and sphingolipids on the formation of ordered sphingolipid/sterol domains (rafts). J. Biol. Chem. 276, 33540–33546.

III

Publication III

Niemelä, P. S., Ollila, S., Hyvönen, M. T., Karttunen, M., and Vattulainen, I., Assessing the nature of lipid raft membranes, PLoS Computational Biology 3, 304-312 (2007).

Assessing the Nature of Lipid Raft Membranes

Perttu S. Niemelä[1,2*], Samuli Ollila[1,2], Marja T. Hyvönen[1,2,3], Mikko Karttunen[4], Ilpo Vattulainen[1,5,6,7]

1 Laboratory of Physics, Helsinki University of Technology, Helsinki, Finland, **2** Helsinki Institute of Physics, Helsinki University of Technology, Helsinki, Finland, **3** Wihuri Research Institute, Helsinki, Finland, **4** Department of Applied Mathematics, The University of Western Ontario, London, Ontario, Canada, **5** Memphys Center for Biomembrane Physics, University of Southern Denmark, Odense, Denmark, **6** Physics Department, University of Southern Denmark, Odense, Denmark, **7** Institute of Physics, Tampere University of Technology, Tampere, Finland

The paradigm of biological membranes has recently gone through a major update. Instead of being fluid and homogeneous, recent studies suggest that membranes are characterized by transient domains with varying fluidity. In particular, a number of experimental studies have revealed the existence of highly ordered lateral domains rich in sphingomyelin and cholesterol (CHOL). These domains, called functional lipid rafts, have been suggested to take part in a variety of dynamic cellular processes such as membrane trafficking, signal transduction, and regulation of the activity of membrane proteins. However, despite the proposed importance of these domains, their properties, and even the precise nature of the lipid phases, have remained open issues mainly because the associated short time and length scales have posed a major challenge to experiments. In this work, we employ extensive atom-scale simulations to elucidate the properties of ternary raft mixtures with CHOL, palmitoylsphingomyelin (PSM), and palmitoyloleoylphosphatidylcholine. We simulate two bilayers of 1,024 lipids for 100 ns in the liquid-ordered phase and one system of the same size in the liquid-disordered phase. The studies provide evidence that the presence of PSM and CHOL in raft-like membranes leads to strongly packed and rigid bilayers. We also find that the simulated raft bilayers are characterized by nanoscale lateral heterogeneity, though the slow lateral diffusion renders the interpretation of the observed lateral heterogeneity more difficult. The findings reveal aspects of the role of favored (specific) lipid–lipid interactions within rafts and clarify the prominent role of CHOL in altering the properties of the membrane locally in its neighborhood. Also, we show that the presence of PSM and CHOL in rafts leads to intriguing lateral pressure profiles that are distinctly different from corresponding profiles in nonraft-like membranes. The results propose that the functioning of certain classes of membrane proteins is regulated by changes in the lateral pressure profile, which can be altered by a change in lipid content.

Citation: Niemelä PS, Ollila S, Hyvönen MT, Karttunen M, Vattulainen I (2007) Assessing the nature of lipid raft membranes. PLoS Comput Biol 3(2): e34. doi:10.1371/journal.pcbi.0030034

Introduction

The understanding of lipid membrane structures and their role in cellular functions has developed significantly since the introduction of the classical fluid-mosaic model by Singer and Nicolson [1]. The fluid-mosaic model predicted that cellular membranes are fluid and characterized by random distribution of molecular components in the membrane, resulting in lateral and rotational freedom. The more recent picture is considerably more elaborate, however. A large number of experimental results converge toward the idea that lateral domains enriched in sphingomyelin (SM) and cholesterol (CHOL) exist in biological membranes. These nanosized domains, called functional lipid rafts, have been suggested to take part in various dynamic cellular processes such as membrane trafficking, signal transduction, and regulation of the activity of membrane proteins [2–4]. The existence of stable lipid rafts in biological membranes is under intense scrutiny, and their existence is actually under debate since the lipid rafts, if they do exist, are probably too small to be resolved by techniques such as fluorescence microscopy [5]. Direct evidence of rafts in vivo is mainly based on monitoring the motions of membrane proteins [6] or on differential partitioning of fluorescent probes in membrane environments [7]. It is, however, difficult to perform experiments using living cells, which complicates measurements of physical quantities of the rafts, such as the exact lipid composition, characteristic size, and lifetime [8,9]. In model membranes, the coexistence of domains in the liquid ordered (l_o) and the liquid disordered (l_d) phase is widely accepted [9,10]. For example, the l_d phase may be formed by an unsaturated phosphatidylcholine (PC), while the formation of the l_o phase is promoted by a mixture of SM and CHOL. As for rafts, the current understanding of lipid rafts in biological membranes suggests a granular structure of nanometer-scale domains of various compositions [9,11,12] rather than a large-scale phase separation.

The exact nature of the underlying interactions that lead to lipid immiscibilities in membranes is under debate [13,14]. CHOL is particularly important as it has been shown to increase the conformational order of acyl chains and reduce the bilayer area, hence significantly increasing the packing density of the lipids [15–17]. CHOL is particularly effective in

Editor: Amy Rowat, Harvard University, United States of America

Received July 14, 2006; **Accepted** January 5, 2007; **Published** February 23, 2007

A previous version of this article appeared as an Early Online Release on January 5, 2007 (doi:10.1371/journal.pcbi.0030034.eor).

Abbreviations: A, average area per lipid; CHOL, cholesterol; d, bilayer thickness; *D*, lateral diffusion coefficient; K_A, area compressibility modulus; k_BT, thermal energy scale (k_B is the Boltzmann constant, T is the absolute temperature); k_c, bending rigidity; l_d, liquid disordered phase; l_o, liquid ordered phase; PC, phosphatidylcholine; POPC, palmitoyloleoylphosphatidylcholine; PSM, palmitoylsphingomyelin; S_{CD}, deuterium order parameter values; SM, sphingomyelin

* To whom correspondence should be addressed. E-mail: psn@fyslab.hut.fi

Author Summary

Biological membranes are complex 2-D assemblies of various lipid species and membrane proteins. For long, it was thought that the main role of lipid membranes is to provide a homogeneous, liquid-like platform for membrane proteins to carry out their functions as they diffuse freely in the membrane plane. Recently, that view has changed. It has become evident that several lipid environments with different physical properties may coexist, and that the properties of the different lipid domains may play an active role in regulating the conformational state and dynamic sorting of membrane proteins. We have carried out atom-scale computer simulations for three-component lipid bilayers, so-called lipid rafts, rich in cholesterol and sphingolipids. They show that arising from the local interactions between the lipid species, the elastic and dynamic properties of the membranes depend strongly on the lipid composition. The changes in elastic properties are suggested to alter the functional states of various membrane proteins. Changes in lipid composition are also shown to alter the distribution of local pressure inside the membrane. This is likely to affect proteins that undergo large anisotropic conformational changes between the functional states, such as the ion channel MscL, used as an example here. A great number of important physiological phenomena, such as transmitting neural impulses or trafficking molecules in and out of the cell, involve activation of membrane proteins, so it is relevant to understand all factors affecting them. Our findings support the idea that general physical properties of the lipid environment are capable of regulating membrane proteins.

reducing the void space within the acyl chain region of the lipids [15], which is related to suppressed area compressibility and increased bending rigidity of the membrane with increasing CHOL concentrations. However, the lateral diffusion rates are not expected to slow down by more than a factor of 2–3 when the l_d phase is compared with CHOL-induced l_o phase [6,18]. Also, CHOL has recently been reported to significantly alter the lateral pressure profile of membranes [19]. This is important, as changes in the lateral pressure profiles have been suggested to be related to changes in membrane protein structure and activity [20].

Considering that the smallest estimates for the sizes of rafts fall in the range of nanometers [21,22], they make an accessible subject for computational studies. Though, in spite of the considerable importance of rafts, it is somewhat surprising that only a few atom-scale simulations have dealt with ternary mixtures of CHOL, SM, and PC [23,24], concentrating mainly on small-scale structural properties and local interactions between the lipids. In particular, there are no previous atom-level computational studies of rafts aiming to characterize the nature of their structural and dynamical features. For example, the nanometer scale structure within raft domains and its interplay with CHOL-induced effects are not understood. Further, the resulting large-scale properties, such as membrane elasticity in ternary raft-like lipid mixtures, are not understood either. Finally, and perhaps most importantly, the lateral pressure profiles associated with rafts are completely unknown. The concept of the lateral pressure profile across the lipid membrane is exceptionally significant, since it describes the pressure exerted on molecules embedded in a membrane. Cantor has proposed that incorporation of molecules into membrane and changes in lipid content would alter the lateral pressure profile across a membrane, and hence changes in the pressure profile would induce changes in membrane protein structure [20,25]. Experimental studies of this issue are remarkably difficult, however: currently there is only one study that employed fluorescent probes to gauge the overall shape of the lateral pressure profile [26]. Evidently, detailed atomistic simulations are called for.

The state-of-the-art extent of the simulations conducted in this work, 15–20 nm in lateral dimensions and 100 ns in time, enables a reliable quantitative analysis of the properties of raft-like membranes not accomplished before. We employ large-scale atom level simulations for three mixtures of palmitoyloleoylphosphatidylcholine (POPC), PSM, and CHOL. The molar fractions are POPC:PSM:CHOL = 1:1:1, 2:1:1, and 62:1:1 for systems that we call S_A, S_B, and S_C, respectively (see Figure 1). Based on a recent experimental phase diagram [27], these mixtures are expected to display the coexistent l_o and l_d phase domains (S_A and S_B) or a single l_d phase (S_C). Here, we illustrate the distinct nature of raft-like domains in three parts. First, we consider the elastic, thermodynamic, and dynamic properties of rafts that turn out to be very different from those of nonraft-like membranes. Second, we provide evidence that the presence of PSM and CHOL in raft-like membranes leads to strongly packed and rigid bilayers, characterized by significant nanoscale lateral heterogeneity within the raft domains. These findings express the prominent role of favored lipid–lipid interactions within rafts and highlight the significant role of CHOL in promoting the formation of rafts. Third, we provide compelling evidence that the lateral pressure profiles can be altered by a change in lipid content. In particular, we show how the presence of PSM and CHOL leads to intriguing lateral pressure profiles that are distinctly different from corresponding lateral pressure profiles in nonraft-like membranes, proposing that lipid membranes may regulate the functioning of certain classes of membrane proteins such as mechanosensitive channels through changes in lipid composition, and hence the lateral pressure profile.

Results

Elastic, Thermodynamic, and Dynamic Properties

Selected properties of the simulated membranes are summarized in Table 1. For system S_C, the average area per lipid, A, and the bilayer thickness, d, are in agreement with previous findings on pure POPC bilayers [28,29], indicating negligible effects of PSM and CHOL on the bilayer dimensions. Also, the area compressibility modulus, K_A, and the bending rigidity, k_c, are in line with previous studies of pure PC bilayers, reporting $K_A = 140–300 \times 10^{-3}$ N/m and $k_c = 4–9 \times 10^{-20}$ J [30–32]. The lateral diffusion coefficient, D, for POPC in system S_C is about 50% lower than the value of 1.4×10^{-7} cm^2/s measured for pure POPC bilayer at 313 K [33]. A similar trend was found in comparison of our previous simulations on pure SM and PC bilayers [34] with this particular study [33]. This suggests that bilayer S_C is close to the liquid disordered state of a POPC bilayer. This is also supported by the finding that small CHOL [33] or SM [35] concentrations have minor effects on D values of PC above melting temperatures.

The condensing effect of CHOL becomes evident when comparing the values of A and d between systems S_A to S_C. As

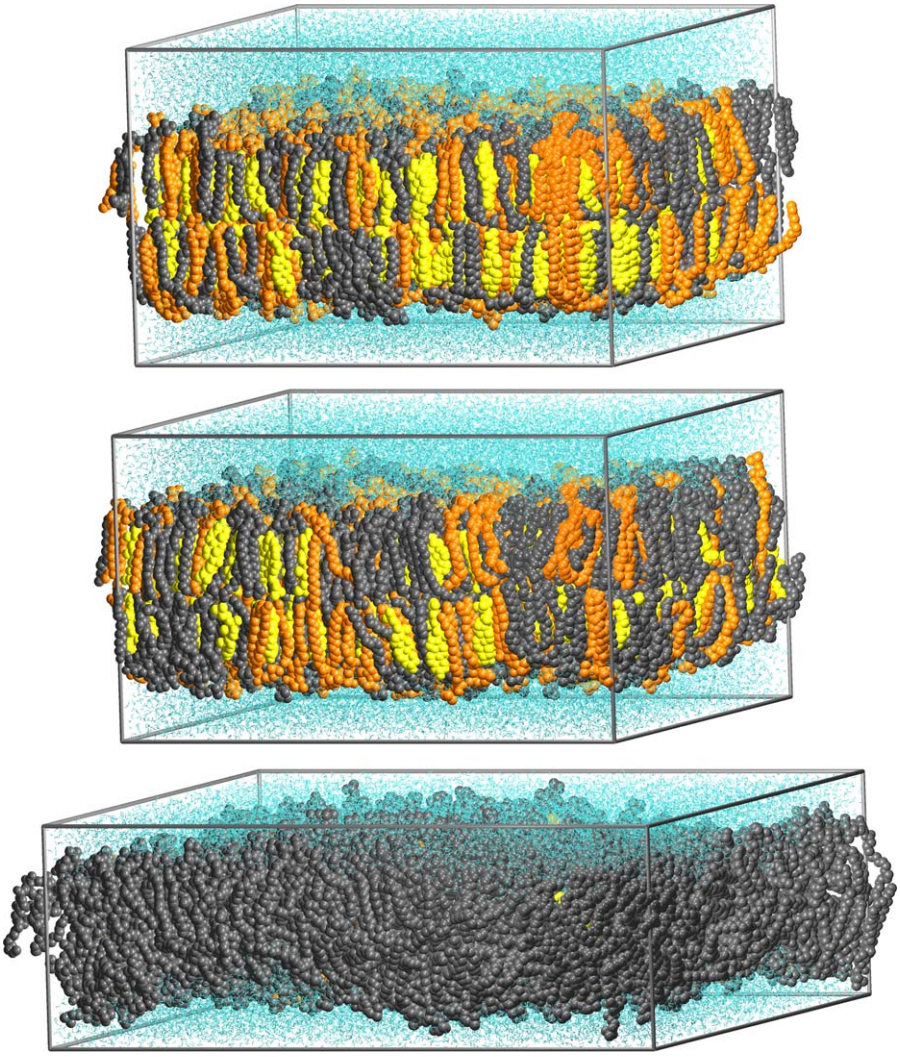

Figure 1. Snapshots at the End of Simulations for Systems S_A (Top), S_B (Middle), and S_C (Bottom)
POPC molecules are shown in gray, PSM in orange, CHOL in yellow, and water in cyan.
doi:10.1371/journal.pcbi.0030034.g001

suggested in several previous works, CHOL's tendency to increase the order of neighboring acyl chains leads to decreased area per lipid and increased bilayer thickness upon increasing CHOL concentration [36–38]. Comparison with previous studies shows that the values for A in Table 1 for S_A and S_B are 0.1–0.4 nm^2 lower than expected for binary PC–CHOL systems with similar CHOL concentrations [15,16]. CHOL's strong tendency to reduce fluctuations and increase the rigidity of membranes is best revealed by the K_A values in Table 1. Previous reports have predicted maximally 5-fold to 7-fold increases in the K_A values upon CHOL addition into PC bilayers [16,39]. The presently found unexpectedly large K_A and small A as compared with PC–CHOL systems suggests an additional effect of PSM to decrease area fluctuations, possibly related to the tendency of SM to form intermolecular hydrogen bonds [34,40]. This idea is further supported by an experiment reporting a much higher value of K_A ($1{,}718 \times 10^{-3}$ N/m) for a SM–CHOL bilayer than the value for a PC–CHOL bilayer ($K_A = 781 \times 10^{-3}$ N/m), both with 50 mol% CHOL [41]. Our values for the bending rigidity, k_c, are roughly in line with experimental results for PC–CHOL mixtures, which have shown a 120%–170% increase in the k_c value upon increasing CHOL fraction from 0 to 30–50 mol% [31,42]. As the experimental values vary and computational reports on CHOL's effect on k_c values in PC membranes are lacking, a more quantitative evaluation on PSM's effect in this case is difficult. However, its tendency to increase K_A would suggest a role also on bending rigidity.

The fact that our values for the bilayer thickness agree with an AFM study, reporting a difference of 0.6–0.9 nm between l_d and l_o phases, is an indication that our model systems are in line with the experimental l_o/l_d phases [43]. However, when comparing the diffusion coefficients between systems S_A to S_C, we find that systems S_A and S_B are relatively much more slowed down than predicted from the changes of pure POPC bilayer upon addition of 25–30 mol% CHOL [33]. This further supports the idea that SM (together with CHOL) has an additional role in rigidifying the bilayer and consequently slowing down diffusion. For comparison, a recent pulsed-field gradient NMR study [44] reported two populations of D values in DOPC–SM–CHOL mixtures with 10–30 mol% CHOL at 300 K, one corresponding to l_d phase ($D \approx 1 \times$

Table 1. Average Structural and Thermodynamic Properties Calculated from the Simulations of Systems S_A, S_B, and S_C

System	S_A	S_B	S_C
POPC:PSM:CHOL	1:1:1	2:1:1	62:1:1
A [nm^2]	0.41 ± 0.01	0.44 ± 0.01	0.66 ± 0.01
d [nm]	4.40 ± 0.05	4.29 ± 0.05	3.53 ± 0.05
K_A [10^{-3} N/m]	2,700 ± 700	1,000 ± 400	200 ± 100
k_c [10^{-20} J]	10 ± 2	7 ± 2	6 ± 2
D_{popc} [10^{-7} cm^2/s]	0.037 ± 0.002	0.08 ± 0.02	0.67 ± 0.06
D_{psm} [10^{-7} cm^2/s]	0.036 ± 0.002	0.07 ± 0.02	0.8 ± 0.2
D_{chol} [10^{-7} cm^2/s]	0.038 ± 0.002	0.08 ± 0.02	0.5 ± 0.2

A, average area per lipid; *d*, bilayer thickness; K_A, area compressibility modulus; k_c, bending rigidity modulus; *D*, lateral diffusion coefficients.

doi:10.1371/journal.pcbi.0030034.t001

10^{-7} cm^2/s) and the other to l_o phase ($D \approx 1 \times 10^{-8}$ cm^2/s). As the exact lipid composition within the proposed domains is unknown, our simulated D values for systems S_A and S_B are in good agreement with the proposed l_o phase. This is interesting, since the l_o phase is usually characterized as having similar diffusion rates with the l_d phase. Recent evidence on large variations in the properties of a single l_o phase [45] also supports the idea that bilayers S_A and S_B do display the l_o phase. Clearly, diffusion within raft domains is strongly suppressed due to the presence of PSM and CHOL.

The material properties of lipid bilayers have been suggested to play a major role in regulating the activity and partitioning of membrane proteins. First, the thickness difference of raft and nonraft membranes may be relevant due to the effects of hydrophobic matching [46,47]. For example, the free energy of opening of a bacterial stretch-activated channel has been observed to change from 4 to 20 k_BT when the acyl chain length of the surrounding PC-lipids changes from 16 to 20 carbons [48]. Another example is the transmembrane protein OmpA, whose free energy of unfolding was reported to change by about 5 k_BT per nm when the hydrophobic thickness of the surrounding saturated PC-membrane was varied [49]. Using this value as a simplistic estimate for the effect of hydrophobic thickness, one gets a difference of about 4 k_BT in the free energy of unfolding when this particular protein would be transferred from nonraft to raft membrane. As the higher bending rigidity of the raft membrane probably decreases the ability of the membrane to adapt its thickness to match the hydrophobic thickness of the protein, the actual value should be larger than the above estimate. The role of membrane elasticity in protein functionality is further emphasized by the fact that, based on recent studies, it costs much more energy to deform a membrane by changing its area per lipid than by bending or chain tilting [50]. It has been suggested that the free energy to create a protein-shaped cavity in a bilayer is proportional to K_A [51], and evidence exists that the binding free energy of certain amphipathic peptides indeed depends linearly on K_A [52]. Our data suggests a 5-fold to 14-fold difference in the values of K_A between raft and nonraft membranes (see Table 1), which practically means a free energy cost of about 4–8 k_BT when a membrane protein (Mellitin) is transferred from a nonraft to a raft environment [52]. Summarizing, the elasticity of raft-like membranes is substantially different from that of nonraft membranes, and this likely influences membrane protein functionality.

Lateral Heterogeneity

The above results highlight the different bulk properties of raft-like domains with respect to more disordered bilayers. However, as becomes evident below, raft domains are also characterized by strong spatial and temporal variations. Figure 2 reveals lateral heterogeneity in the calculated deuterium-order parameter values (S_{CD}) when averaged over 10 ns. The nature of chain ordering varies in different systems. System S_A exhibits the highest overall order (average $S_{CD} = -0.41$) that is almost uniformly distributed over the bilayer plane and broken only by a few small low-order areas and empty points due to poor sampling. System S_B is slightly less ordered ($S_{CD} = -0.36$) and contains domains of a few nanometers in size, differing significantly in their S_{CD} values. The overall ordering in S_C is much weaker ($S_{CD} = -0.18$) than in the two other systems, but even S_C displays lateral heterogeneity, though the domains appear larger, smoother, and with smaller variations in the S_{CD} values. The average S_{CD} values are in line with corresponding experimental order parameter profiles of fluid POPC [53,54] and DPPC–CHOL mixtures with similar CHOL concentrations [45,55].

In Figure 2, the more ordered regions in S_{CD} plots are clearly correlated with a higher density of CHOL. This is in line with a previous study showing CHOL's ability to order the neighboring acyl chains within a radius of few nanometers [56]. The σ_{chain} plots in Figure 2 reveal high localization of the chains in S_A, whereas in S_B some of the regions are smeared out. The S_C plot is much more homogeneous, indicating higher overall mobility and more isotropic distribution of the chains. In S_C, the small concentration of CHOL does not seem sufficient to account for the observed large-scale lateral heterogeneity in chain-order parameters. Instead, we find that the S_{CD} value is clearly correlated with bilayer thickness. This is particularly supported by the fact that the amplitudes of the large-scale peristaltic wave modes are significantly larger for system S_C than for the other systems (see Figure S6). Even though the autocorrelation functions for most of the largest undulations and peristaltic modes decay roughly within a few nanoseconds (unpublished data), some modes display much longer decay times. In particular for system S_C, this may be related to the heterogeneity induced by the few CHOL and SM molecules that are embedded in the bilayer.

To judge our findings for lateral heterogeneity, it is worthwhile to stress the slow dynamics in the bilayer plane: despite the extensive time scale simulated, the lateral diffusion coefficients indicate that the molecules move in the plane of the membrane approximately over only their own size within the simulated time scale. Hence, it is evident that the simulation time is not long enough to adequately relax the large-scale structure of the initial configuration and lead to complete mixing of the lipids. The nanoscale heterogeneity observed in this work could thus be debated. However, there is reason to emphasize that while systems S_A and S_B were started from different initial configurations, they lead to similar conclusions. Further, the small-scale movements of the molecules relative to each other can be characterized; see the 2-D radial distribution functions in Figure 3. The unfavorable close contacts of CHOL–CHOL

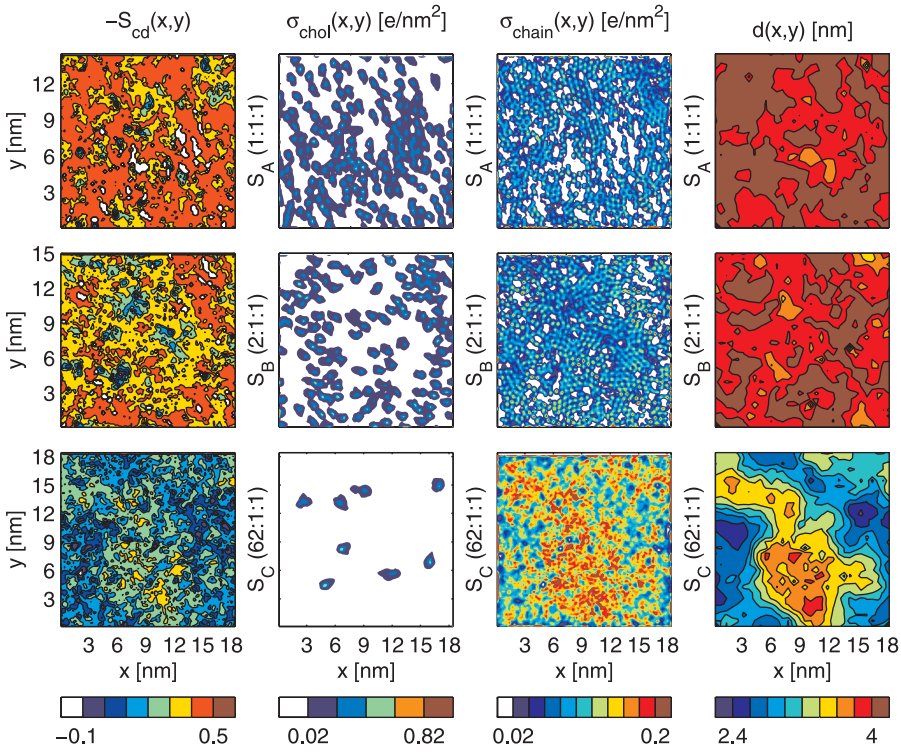

Figure 2. Snapshots Averaged over the Last 10 ns from the End of Each Simulation

The deuterium order parameters, S_{CD}, of selected carbons (C5–C7) of POPC and PSM chains were binned in the xy-plane (column 1, from left). The in-plane electron densities, σ, have been plotted separately for CHOL (column 2) and the selected chain carbons (column 3). The average bilayer thickness, *d*, was obtained from the grid of the undulation analysis (column 4). Systems S_A to S_C are represented on rows from top to bottom, respectively. Only the bottom leaflet has been used for columns 1–3, whereas both leaflets were used for column 4. The equivalent plots for the top leaflet have been presented in Figure S2.

doi:10.1371/journal.pcbi.0030034.g002

pairs are revealed by the lowering of the nearest neighbor peak in time. Simultaneously, the secondary peak at 1.0 nm increases, indicating small-scale reorganization of CHOL molecules. Significant changes in time can also be seen in the other plots of Figure 3, revealing the tendency of closer contacts between CHOL–POPC center of mass pairs with respect to PSM–CHOL pairs. In all, this provides further support for lateral reorganization and heterogeneity. The details of the lipid–lipid interactions are related to the widely speculated specific interaction between SM and CHOL, which is discussed elsewhere [57,58].

Lateral Pressure Profiles

Structure and dynamics of membrane proteins are likely to be influenced by the lateral pressure profile, which has been proposed as a mechanism for, e.g., general anesthesia [20,59]. To elucidate this issue, we computed the lateral pressure profiles of various lipid membrane systems (see Figure 4). For a discussion of the coupling of the peaks in the lateral pressure profile with the molecular groups and different interaction types, see previous related simulation studies [19,60–63]. Here, we focus on a more generic issue, that is, the joint effect of CHOL and PSM on the pressure profile.

The pressure profiles across the membranes of S_A and S_B, shown in Figure 4A, indicate a striking difference compared with profiles in nonraft membranes (see Figure 4B): raft bilayers display qualitatively different behavior with a greater number of peaks as compared with single component POPC and PSM bilayers in l_d phase. Rather, raft systems display a qualitative similarity to the DPPC–CHOL system, shown in Figure 4B. These observations are in line with previous simulation studies, if reports on other single component l_d bilayers [60–62] are compared with binary PC–CHOL systems [19,63]. A remarkable difference found here is the significant increase of positive (repulsive) pressure at the middle of raft bilayers compared with pure POPC, the effect being particularly large in the case of raft-mixture S_A.

Notably, the peak heights in the lateral pressure profile are of the order of 1,000 bar. Thus, molecules such as integral membrane proteins are under the influence of huge local pressures that likely affect their conformational state. Particularly, proteins whose cross-sectional area undergoes significant anisotropic changes when shifting from active to inactive state are likely to be governed or regulated by the pressure profile [20,64]. To further quantify this idea, we estimated the lateral pressure profile–induced component of the energy between open and closed conformations of a channel protein MscL (see Methods). For this quantity, we get $\Delta W = (11 \pm 2)\ k_BT$ and $(4 \pm 1)\ k_BT$ for systems S_A and S_B, respectively. These are significantly higher than the values found for the pure POPC bilayer $(1.9 \pm 0.2)\ k_BT$, the pure PSM bilayer $(1.0 \pm 0.6)\ k_BT$, or the binary DPPC–CHOL bilayer $(1.0 \pm 0.4)\ k_BT$. The above result for a POPC bilayer is in agreement with the previous calculation by Gullingsrud and Schulten [62], who found $1.7\ k_BT$ for POPC. The positive values of ΔW indicate that the lateral pressure profiles of these bilayers lower the open state energy of MscL relative to the closed state; that is, they are in favor of the open state.

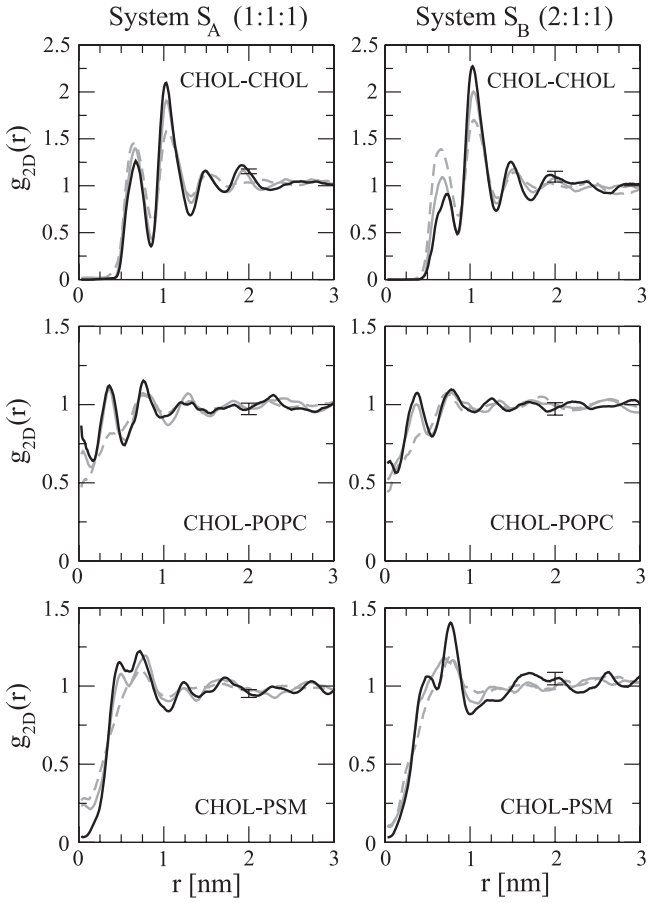

Figure 3. 2-D Radial Distribution Functions between the Molecular Center of Mass Positions in S_A and S_B

The figures show the time evolution in the system at three different time intervals: 0–10 ns (gray, dashed), 30–40 ns (gray), and 90–100 ns (black). The error bars for the black curve indicate the average difference of the two monolayers.

doi:10.1371/journal.pcbi.0030034.g003

Especially interesting are the large values found for the raft systems, which suggest that the lateral pressure profiles characteristic of raft-like environments would facilitate the opening of MscL. For comparison, it has been estimated that the free energy difference associated with the opening of MscL is about 20–50 k_BT [62,65]. The contribution due to the pressure profile in a raft domain could therefore be significant. In general terms, it is clear from the above estimates that the equilibrium probability of MscL to be in the open state must be significantly altered by the pressure profile of the lipid environment. Additionally, we wish to underline that the values for ΔW have been estimated for different bilayers that are all under identical surface tension conditions ($\gamma = 0$) and are thus not related to the usual picture of the effect of overall stress on mechanosensitive channels.

Discussion

In this work, we have elucidated properties of lipid raft mixtures through atom-scale simulations and compared them with properties of a bilayer in liquid disordered phase. We found that the presence of PSM and CHOL in S_A and S_B not only significantly enhanced the lateral packing of lipids and increased the acyl chain order, but also reduced the lateral

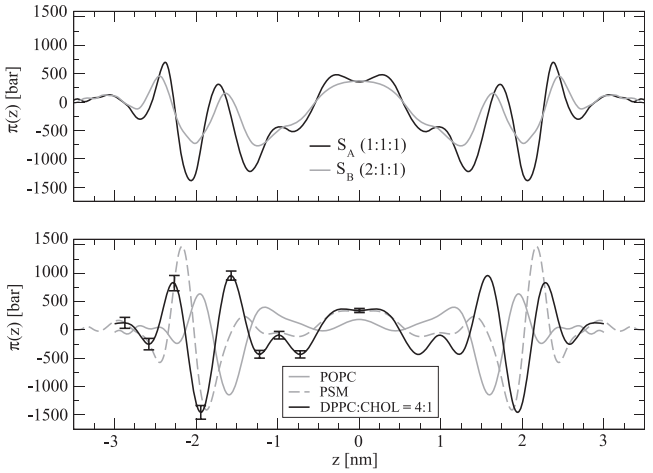

Figure 4. Lateral Pressure Profiles of Systems S_A and S_B (Top) and of Previously Simulated Pure POPC/PSM Systems and a Binary DPPC–CHOL System (Bottom)

The center of the membrane is at $z = 0$. The graphs have been averaged to be symmetric on both sides of the center and smoothed by adaptive high-order spline fitting [90]. Error bars are statistical errors for each slab. The errors have been shown for only one of the monolayers of the DPPC–CHOL system because they are equal for both monolayers and also smaller or equal for the other systems.

doi:10.1371/journal.pcbi.0030034.g004

diffusion rates by more than an order of magnitude when compared with the l_d phase. This observation is contradictory to the traditional definition of the l_o phase, but is in agreement with recent reports on varying properties of this particular phase [45,54]. It is interesting to note that the difference in the lipid dynamics of the different phases may in itself have a contribution to the dynamical partitioning of membrane proteins [5], as they spend more time in the ordered domains due to slower diffusion and allow more time for cross-linking between proteins to occur.

The elasticity of the raft mixtures was found to be reduced significantly when compared with S_C. The fact that this reduction was greater than expected from previous reports on binary PC–CHOL mixtures, suggests that SM has a further rigidifying effect on raft mixtures. The 5-fold to 14-fold increase in K_A suggests significant implications on the partitioning of membrane proteins. First, the free energy of creating a cavity to the membrane, and thus the solvation free energy of a protein into a membrane, is directly proportional to K_A, which leads to unfavored partitioning of certain proteins into raft-like membranes. On the basis of a recent experimental report [52], we estimated that the transfer free energy of Mellitin from nonraft to raft membrane would be about 4–8 k_BT. Second, the difference in thickness of about 0.8–0.9 nm between raft and nonraft membranes suggests a contribution to the transfer free energy of proteins due to changed hydrophobic matching. This effect is practically always present and the reported strength of the effect, about 5 k_BT per nm [49], makes it comparable to the effect of the K_A.

The lateral heterogeneity in the simulated membranes was found to be related to either the tendency of CHOL to order neighboring acyl chains or to the relatively slow peristaltic modes of the bilayer. The emergence of these heterogeneities may be related to the idea of small granular arrangement of nanodomains in biological membranes [9,12]. Considering the perhaps surprisingly slow diffusion rates observed for the

l_o phase of the ternary mixtures in this study, it suggests an absolute minimum of about 10–100 ns for the lifetimes of the domains. Also, the analysis of the heterogeneity provided more support for the idea that CHOL changes the lipid environment in its local neighborhood, e.g., by increasing the order of the acyl chains.

Analysis of the raft-like membranes S_A and S_B revealed large differences in lateral pressure profiles when compared with bilayers in l_d phase, but also changes of significant magnitude in the local pressure were found in comparison with PC–CHOL systems. All membrane proteins, which undergo anisotropic structural changes between functional states, are likely to be affected by the lateral pressure profile. A good example would be proteins that tilt their helices when opening a channel, such as the MscL [66]. We found that the free energy difference between the open and closed states of the MscL channel changed from 1.0 k_BT to 4–11 k_BT when single component bilayers in l_d phase were compared with raft mixtures. This result, together with previous reports on pressure profiles of similar systems [19,63], provides strong evidence for the idea that the lipid environment plays an important role in regulating the activity of certain membrane proteins through changes in lateral pressure profile. Though only a few experimental studies have been done to assess local pressures within the bilayer [26,67], evidence exists that the activity of a number of membrane proteins is dependent on the lipid composition and thus very probably on the lateral pressure profile [67,68]. For example, the free energy of binding of alamethicin has been reported to be a simple function of monolayer spontaneous curvature [69], which is most probably related to changes in local pressures.

The role of the lipid environment has been discussed in relation to a variety of membrane proteins, from mechanosensitive channels such as MscL [48,62,70] to other important channels such as rhodopsin [71], KcsA [67], P-glycoprotein [72,73], the insulin receptor [17], and others whose activity has been shown to depend on the membrane composition [67]. It has been shown that different lipids have different binding affinities on the surface of membrane proteins [74] and that the specific lipid-protein interactions probably play a role in regulating the activity and/or partitioning of certain proteins such as the yeast cytochrome bc_1 complex [75]. However, various evidence exists that generic interaction mechanisms in terms of for example elastic properties of the membrane are also important for a number of membrane proteins [47]. For example, different sterols have been shown to alter the elastic properties of membranes in a similar manner, if only applied in different concentrations [76]. Finally, it is exciting to note that the present results also provide support for a recent suggestion that the (unknown) mechanism of general anesthesia is related to changes in the lateral pressure profile due to incorporation of anesthetics, such as alcohols, into the membrane [20,64,77].

From now on, the quest is to understand the (concerted) effect of different lipid species on the lateral pressure profiles and the interplay between lipid environment and protein activity. The lateral pressure profile is an important quantity, as many membrane elastic coefficients (such as bending modulus, spontaneous curvature, and the saddle splay modulus) can be directly extracted from it [78]. In the future, it would be highly useful to see computational works on lipid bilayers that gather enough statistics to evaluate the relationship between these quantities and to increase our understanding of their relationship. Also, it would be highly interesting to develop experimental techniques to measure the pressure profiles and to relate these to the already existing simulation data of different membrane compositions.

Materials and Methods

Starting coordinates were obtained by expanding a previously equilibrated POPC bilayer [28] to 1,024 lipids. Two ternary mixtures were created by replacing random POPC molecules by PSM and CHOL to result in POPC:PSM:CHOL = 1:1:1 or 2:1:1 molar ratios (systems S_A and S_B, respectively), whereas for the third system (S_C) we replaced 32 selected POPC molecules to result in a POPC matrix with eight CHOL-PSM dimers and 16 monomers that are as far as possible from each other. The configuration in S_C was created to study the local interactions between PSM and CHOL in a POPC matrix, which will be discussed elsewhere [58]. The force-field parameters for POPC [79], PSM [34], and CHOL [80] were obtained from previous works. Each of the three bilayers were fully hydrated with about 28 SPC (simple point charge) water molecules/lipid [81], resulting in ~140,000 atoms per system (see Figure 1). Using GROMACS (http://www.gromacs.org) [82] for integrating the equations of motion with a 2-fs time step, each system was initially equilibrated by the Langevin thermostat in NVT-ensemble (50 ps) and then in NpT-ensemble (500 ps). The first 5 ns of the actual simulations were run in NpT-ensemble ($T = 310$ K, $p = 1$ atm) using the Berendsen thermostat and barostat [83], after which we switched to the Nosé-Hoover thermostat and the Parrinello–Rahman barostat to produce the correct ensemble. The pressure coupling was applied in a semi-isotropic way to result in zero surface tension. The long-range electrostatic interactions were accounted for by the reaction-field method (with $r_c = 2.0$ nm) and a 1.0-nm cutoff was used for the Lennard–Jones interactions. Reaction-field has been shown to be a reliable and well-scalable method for simulating noncharged lipid bilayers [84]. The simulation time was 100 ns for S_A and S_B, but 50 ns for system S_C, which together took about ten cpu-years on a parallel machine. For the analysis, we have included the last 40 ns of each simulation trajectory whenever not indicated otherwise.

The equilibration of the bilayer structure was monitored by the area per lipid (see Figure S1). The magnitude of area fluctuations were used to estimate the area compressibility of each bilayer [85]. The average bilayer thickness was estimated from the peak-to-peak distance of the electron density plot of all atoms across the simulation box. To characterize undulatory and peristaltic motions, we followed the procedure by Lindahl and Edholm [30], in which a grid was fitted to selected atoms in the POPC and PSM backbone (glycerol C2 in POPC and the corresponding carbon in PSM). The grids for the two monolayers were then averaged for undulatory analysis whereas their difference was used for describing the peristaltic motions, and in both cases 2-D FFT was applied to the grid points. k_c was estimated by summing over the undulatory spectral modes and utilizing the formula $<u^2_{und}> \approx k_BTA/(8.3\pi^3 k_c)$. Consistent results for k_c were found through a fit to the function $u^2_{und}(k) \sim k^{-4}$.

The deuterium (NMR)–order parameter S_{CD} values were calculated from the diagonal elements of the molecular order tensor (see [84]) at selected carbon locations of the PSM and POPC chains. To characterize the lateral heterogeneity in the system, carbons 5–7 were chosen from each acyl chain (together with the structurally correspondent carbons from the sphingosine chain), and the instantaneous S_{CD} values were binned on a grid on the bilayer plane. Similarly, the average in-plane electron densities were calculated by binning the number of electrons in the selected molecules or atoms. For the 2-D radial distribution functions, $g_{2D}(r)$, we used the projected center of mass positions of the lipid molecules. The centers of mass were also used to obtain the lateral diffusion coefficients (for details see [15]).

Finally, lateral pressure profiles were determined using an approach similar to the ones presented and validated by several authors [19,60–62], more details of our method in [86]. The lateral pressure was calculated using the Irving–Kirkwood contour and dividing the systems in ~0.1 nm thick slabs (100 slabs). Pairwise forces were calculated from the force field description and MD trajectory. A 2.0-nm truncation was used for electrostatic interactions. Constrained forces arising from SETTLE and LINCS were calculated from the general equation by Hess et al. [87]. As undulations in system S_C render the lateral pressure calculation more difficult, we chose three previous simulations on single-component lipid systems,

POPC [86], PSM [34], and a binary 1:4 DPPC–CHOL [17] for reference. For each system, the pressure profile was calculated the same way. To estimate the effect of pressure profile on membrane proteins, we followed the approach introduced by Cantor [88] and later applied to molecular simulation data of single-component bilayers by Gullingsrud et al. [62]. As a model we use the mechanosensitive ion channel MscL, whose conformation has been found to change anisotropically between cylindrical (open) and cone (closed) shapes [89]. Here we calculate the work, ΔW, done against the lateral pressure profile to alter the shape of the membrane cavity occupied by the protein as it changes conformation from the closed to an open state. Then ΔW can be written as:

$$\Delta W = \int p(z)\,\Delta A(z)\,dz, \qquad (1)$$

where $\Delta A(z)$ is the change in the cross-sectional area of the protein and $p(z)$ is the pressure profile. Here, we use an approach identical to that used in [62], and identical values for $\Delta A(z)$ for MscL as used in [62], in which the area is kept unchanged in the middle of the membrane between the two states. Error bars for ΔW have been calculated using results for different monolayers. It is, however, important to realize that ΔW depends on the second moment of the lateral pressure profile [62] and thus is susceptible to small changes of lateral pressure far from the bilayer center. Therefore, extra caution must be followed when interpreting these results. Also, in this approach the influence of inserting a protein into the membrane on the lateral pressure profile is not taken into account.

Supporting Information

Figure S1. The Area per Lipid versus Simulation Time

Found at doi:10.1371/journal.pcbi.0030034.sg001 (509 KB EPS).

Figure S2. Averaged Snapshots from the Last 10 ns of Each Simulation

The data is represented as in Figure 2 of the main article, but plotted for the top monolayer (columns 1–3) instead of the bottom monolayer.

Found at doi:10.1371/journal.pcbi.0030034.sg002 (212 KB EPS).

Figure S3. Snapshots (1-ns Averages) Revealing the In-Plane Electron Density of CHOL at 10-ns Time Intervals

Columns A1–C1 are the bottom monolayer and columns A2–C2 the top monolayer in systems S_A to S_C, respectively.

Found at doi:10.1371/journal.pcbi.0030034.sg003 (1.2 MB EPS).

Figure S4. Snapshots (1-ns Averages) Revealing the Undulation and Peristaltic Motions at 10-ns Time Intervals

Columns A1–C1 are the average bilayer height ($z(x,y)$, the mean height of the two monolayers), whereas columns A2–C2 are the bilayer thickness ($d(x,y)$, the difference in height of the two monolayers) in systems S_A to S_C, respectively. For calculating $z(x,y)$ and $d(x,y)$, we used the grid method discussed in the Methods section.

Found at doi:10.1371/journal.pcbi.0030034.sg004 (725 KB EPS).

Figure S5. Undulatory Spectral Intensity per Wave Mode versus Wave Vector Magnitude for Systems S_A to S_C

The legend shows k_c values calculated by two different methods, the summing method utilizing Equation 4 and fitting Equation 3 in [30].

Found at doi:10.1371/journal.pcbi.0030034.sg005 (183 KB EPS).

Figure S6. Peristaltic Spectral Intensity per Wave Mode versus Wave Vector Magnitude for Systems S_A to S_C

Found at doi:10.1371/journal.pcbi.0030034.sg006 (97 KB EPS).

Acknowledgments

We thank Dr. Tomasz Róg for providing the simulation trajectory of the DPPC–CHOL system and Jussi Aittoniemi for help in running the raft simulations.

Author contributions. PSN, MTH, MK, and IV conceived and designed the experiments. PSN performed the experiments and analyzed the data, except for the lateral pressure profiles computed by SO. PSN wrote the paper together with the other authors.

Funding. This work has, in part, been supported by the Academy of Finland (PSN, MTH, MK, and IV), the Academy of Finland Center of Excellence Program (SO, PSN, and IV), the Jenny and Antti Wihuri Foundation (MTH), the Finnish Academy of Science and Letters (PSN), the Emil Aaltonen Foundation (MK), and the Natural Sciences and Engineering Council (NSERC) of Canada (MK). We acknowledge the Finnish IT Center for Science and the HorseShoe (DCSC) supercluster computing facility at the University of Southern Denmark for computer resources.

Competing interests. The authors have declared that no competing interests exist.

References

1. Singer SJ, Nicolson GL (1972) The fluid mosaic model of the structure of cell membranes. Science 175: 720–731.
2. Simons K, Ikonen E (1997) Functional rafts in cell membranes. Nature 387: 569–572.
3. Edidin M (2003) The state of lipid rafts: From model membranes to cells. Annu Rev Biophys Biomol Struct 32: 257–283.
4. Pike LJ (2004) Lipid rafts: Heterogeneity on the high seas. Biochem J 378: 281–292.
5. Hancock JF (2006) Lipid rafts: Continuous only from simplistic standpoints. Nat Rev Mol Cell Biol 7: 456–462.
6. Simons K, Vaz WLC (2004) Model system, lipid rafts, and cell membranes. Annu Rev Biophys Biomol Struct 33: 269–295.
7. Gaus K, Gratton E, Kable EPW, Jones AS, Gelissen I, et al. (2003) Visualizing lipid structure and raft domains in living cells with two-photon microscopy. Proc Natl Acad Sci U S A 100: 15554–15559.
8. Brown RE (1998) Sphingolipid organization in biomembranes: What physical studies of model membranes reveal. J Cell Sci 111: 1–9.
9. London E (2005) How principles of domain formation in model membranes may explain ambiguities concerning lipid raft formation in cells. Biochim Biophys Acta 1746: 203–220.
10. Almeida PFF, Pokorny A, Hinderliter A (2005) Thermodynamics of membrane domains. Biochim Biophys Acta 1720: 1–13.
11. Shaikh SR, Edidin MA (2006) Membranes are not just rafts. Chem Phys Lipids 144: 1–3.
12. Hevonoja T, Pentikäinen MO, Hyvönen MT, Kovanen PT, Ala-Korpela M (2000) Structure of low density lipoprotein (LDL) particles: Basis for understanding molecular changes in modified LDL. Biochim Biophys Acta 1488: 189–210.
13. Ramstedt B, Slotte JP (2002) Membrane properties of sphingomyelins. FEBS Lett 531: 33–37.
14. Holopainen JM, Metso AJ, Mattila JP, Jutila A, Kinnunen PKJ (2004) Evidence for the lack of a specific interaction between cholesterol and sphingomyelin. Biophys J 86: 1510–1520.
15. Falck E, Patra M, Karttunen M, Hyvönen MT, Vattulainen I (2004) Lessons of slicing membranes: Interplay of packing, free area, and lateral diffusion in phospholipid/cholesterol bilayers. Biophys J 87: 1076–1091.
16. Hofsäss C, Lindahl E, Edholm O (2003) Molecular dynamics simulations of phospholipid bilayers with cholesterol. Biophys J 84: 2192–2206.
17. Vainio S, Jansen M, Koivusalo M, Róg T, Karttunen M, et al. (2006) Significance of sterol structural specificity. Desmosterol cannot replace cholesterol in lipid rafts. J Biol Chem 281: 348–355.
18. Kupiainen M, Falck E, Ollila S, Niemelä P, Gurtovenko AA, et al. (2005) Free volume properties of sphingomyelin, DMPC, DPPC, and PLPC bilayers. J Comput Theor Nanosci 2: 401–413.
19. Patra M (2005) Lateral pressure profiles in cholesterol–dppc bilayers. Eur Biophys J 35: 79–88.
20. Cantor RS (1997) The lateral pressure profile in membranes: A physical mechanism of general anesthesia. Biochemistry 36: 2339–2344.
21. Varma R, Mayor S (1998) GPI-anchored proteins are organized in submicron domains at the cell surface. Nature 394: 798–801.
22. Plowman SJ, Muncke C, Parton RG, Hancock JF (2005) H-ras, K-ras, and inner plasma membrane raft proteins operate in nanoclusters with differential dependence on the actin cytoskeleton. Proc Natl Acad Sci U S A 102: 15500–15505.
23. Pandit SA, Jakobsson E, Scott HL (2004) Simulation of the early stages of nano-domain formation in mixed bilayers of sphingomyelin, cholesterol, and dioleylphosphatidylcholine. Biophys J 87: 3312–3322.
24. Pandit SA, Vasudevan S, Chiu SW, Mashl RJ, Jakobsson E, et al. (2004) Sphingomyelin–cholesterol domains in phospholipid membranes: Atomistic simulation. Biophys J 87: 1092–1100.
25. Cantor RS (1997) Lateral pressures in cell membranes: A mechanism for modulation of protein function. J Phys Chem B 101: 1723–1725.
26. Templer RH, Castle SJ, Curran AR, Rumbles G, Klug DR (1998) Sensing isothermal changes in the lateral pressure in model membranes using dipyrenyl phosphatidylcholine. Faraday Discuss 111: 41–53.
27. de Almeida RFM, Fedorov A, Prieto M (2003) Sphingomyelin/phosphatidylcholine/cholesterol phase diagram: Boundaries and composition of lipid rafts. Biophys J 85: 2406–2416.
28. Patra M, Salonen E, Terama E, Vattulainen I, Faller R, et al. (2006) Under

the influence of alcohol: The effect of ethanol and methanol on lipid bilayers. Biophys J 90: 1121–1135.
29. Kucerka N, Tristram-Nagle S, Nagle JF (2005) Structure of fully hydrated fluid phase lipid bilayers with monounsaturated chains. J Membrane Biol 208: 193–202.
30. Lindahl E, Edholm O (2000) Mesoscopic undulations and thickness fluctuations in lipid bilayers from molecular dynamics simulations. Biophys J 79: 426–433.
31. Evans E, Rawicz W (1990) Entropy driven tension and bending elasticity in condensed-fluid membranes. Phys Rev Lett 64: 2094–2097.
32. Rawicz W, Olbrich KC, McIntosh T, Needham D, Evans E (2000) Effect of chain length and unsaturation on elasticity of lipid bilayers. Biophys J 79: 328–339.
33. Filippov A, Orädd G, Lindblom G (2003) The effect of cholesterol on the lateral diffusion of phospholipids in oriented bilayers. Biophys J 84: 3079–3086.
34. Niemelä P, Hyvönen MT, Vattulainen I (2004) Structure and dynamics of sphingomyelin bilayer: Insight gained through systematic comparison to phosphatidylcholine. Biophys J 87: 2976–2989.
35. Filippov A, Orädd G, Lindblom G (2004) Lipid lateral diffusion in ordered and disordered phases in raft mixtures. Biophys J 86: 891–896.
36. McIntosh TJ (1978) The effect of cholesterol on the structure of phosphatidylcholine bilayers. Biochim Biophys Acta 513: 43–58.
37. Sankaram MB, Thompson TE (1990) Modulation of phospholipid acyl chain order by cholesterol. A solid-state 2H nuclear magnetic resonance study. Biochemistry 29: 10676–10684.
38. Smaby JM, Momsen M, Kulkarni VS, Brown RE (1996) Cholesterol-induced interfacial area condensations of galactosylceramides sphingomyelins with identical acyl chains. Biochemistry 35: 5696–5704.
39. Needham D, McIntosh TJ, Evans E (1988) Thermomechanical and transition properties of dimyristoylphosphatidylcholine/cholesterol bilayers. Biochemistry 27: 4668–4673.
40. Niemelä P, Hyvönen MT, Vattulainen I (2006) Influence of chain length and unsaturation on sphingomyelin bilayers. Biophys J 90: 851–863.
41. Needham D, Nunn RS (1990) Elastic deformation and failure of lipid bilayer membranes containing cholesterol. Biophys J 58: 997–1009.
42. Henriksen J, Rowat AC, Ipsen JH (2004) Vesicle fluctuation analysis of the effect of sterols on membrane bending rigidity. Eur Biophys J 33: 732–741.
43. Rinia HA, Snel MME, van der Eerden JPJM, de Kruijff B (2001) Visualizing detergent resistant domains in model membranes with atomic force microscopy. FEBS Lett 501: 92–96.
44. Filippov A, Orädd G, Lindblom G (2006) Sphingomyelin structure influences the lateral diffusion and raft formation in lipid bilayers. Biophys J 90: 2086–2092.
45. Clarke JA, Heron AJ, Seddon JM, Law RW (2006) The diversity of the liquid ordered (l_o) phase of phosphatidylcholine/cholesterol membranes: A variable temperature multinuclear solid-state nmr and X-ray diffraction study. Biophys J 90: 2383–2393.
46. Jensen MO, Mouritsen OG (2004) Lipids do influence protein function—The hydrophobic matching hypothesis revisited. Biochim Biophys Acta 1666: 205–226.
47. McIntosh TJ, Simon SA (2006) Roles of bilayer material properties in function and distribution of membrane properties. Annu Rev Biophys Biomol Struct 35: 177–198.
48. Perozo E, Kloda A, Cortes DM, Martinac B (2002) Physical principles underlying the transduction of bilayer deformation forces during mechanosensitive channel gating. Nature Struct Biol 9: 696–703.
49. Hong H, Tamm LK (2004) Elastic coupling of integral membrane protein stability to lipid bilayer forces. Proc Natl Acad Sci U S A 101: 4065–4070.
50. Kuzmin PI, Akimov SA, Chizmadzhev YA, Zmmerberg J, Cohen FS (2005) Line tension and interaction energies of membrane rafts calculated from lipid splay and tilt. Biophys J 88: 1120–1133.
51. Zhelev DV (1998) Material property characteristics for lipid bilayers containing lysolipid. Biophys J 75: 321–330.
52. Allende D, McIntosh TJ (2003) Mellitin-induced bilayer leakage depends on lipid material properties: Evidence for toroidal pores. Biophys J 88: 1828–1837.
53. Seelig J, Waespe-Sarcevic N (1978) Molecular order in cis and trans unsaturated phospholipid bilayers. Biochemistry 17: 3310–3315.
54. Mehnert T, Jacob K, Bittman R, Beyer K (2006) Structure and lipid interaction of N-palmitoylsphingomyelin in bilayer membranes as revealed by 2H-NMR spectroscopy. Biophys J 90: 939–946.
55. Guo W, Kurze V, Huber T, Afdhal NH, Beyer K, et al. (2002) A solid-state NMR study of phospholipid–cholesterol interactions: Sphingomyelin–cholesterol binary systems. Biophys J 83: 1465–1478.
56. Pitman MC, Suits F, MacKerell AD Jr, Feller SE (2004) Molecular-level organization of saturated and polyunsaturated fatty acids in a phosphatidylcholine bilayer containing cholesterol. Biochemistry 43: 15318–15328.
57. Róg T, Pasenkiewicz-Gierula M (2006) Cholesterol–sphingomyelin interactions: A molecular dynamics simulation study. Biophys J 91: 3756–3767.
58. Aittoniemi J, Niemelä PS, Hyvonen MT, Karttunen M, Vattulainen I (2007) Insight into the putative specific interactions between cholesterol, sphingomyelin and palmitoyl–oleoyl phosphatidylcholine. Biophys J 92: 1125–1127.
59. Eckenhoff RG (2001) Promiscuous ligands and attractive cavities. How do the inhaled anesthetics work? Mol Interv 1: 258–268.
60. Lindahl E, Edholm O (2000) Spatial and energetic–entropic decomposition of surface tension in lipid bilayers from molecular dynamics simulations. J Chem Phys 113: 3882–3893.
61. Sonne J, Hansen FY, Peters GH (2005) Methodological problems in pressure profile calculations for lipid bilayers. J Chem Phys 122: 124903.
62. Gullingsrud J, Schulten K (2004) Lipid bilayer pressure profiles and mechanosensitive channel gating. Biophys J 86: 3496–3509.
63. Carrillo-Tripp M, Feller SE (2005) Evidence for a mechanism by which ω-3 polyunsaturated lipids may affect membrane protein function. Biochemistry 44: 10164–10169.
64. Cantor RS (1998) The lateral pressure profile in membranes: A physical mechanism of general anesthesia. Toxicol Lett 100–101: 451–458.
65. Sukhraev SI, Sigurdson WJ, Kung C, Sachs F (1999) Energetic and spatial parameters for gating of the bacterial large conductance mechanosensitive channel, MscL. J Gen Physiol 113: 525–593.
66. Doyle DA (2004) Structural changes during ion channel gating. Trends Neurosci 27: 298–302.
67. van den Brink–van der Laan E, Killian JA, de Kruijff B (2004) Nonbilayer lipids affect peripheral and integral membrane proteins via changes in the lateral pressure profile. *Biochim Biophys Acta* 1666: 275–288.
68. Bezrukov SM (2000) Functional consequences of lipid packing stress. Curr Opin Coll Int Sci 5: 237–243.
69. Lewis JR, Cafiso DS (1999) Correlation of the free energy of a channel-forming voltage-gated peptide and the spontaneous curvature of bilayer lipids. Biochemistry 38: 5932–5938.
70. Meyer GR, Gullingsrud J, Schulten K, Martinac B (2006) Molecular dynamics study of MscL interactions with a curved lipid bilayer. Biophys J 91: 1630–1637.
71. Botelho AV, Gibson NJ, Thurmond RL, Wang Y, Brown MF (2002) Conformational energetics of rhodopsin modulated by nonlamellar-forming lipids. Biochemistry 41: 6354–6368.
72. Troost J, Lindenmaier H, Haefeli WE, Weiss J (2004) Modulation of cellular cholesterol alters p-glycoprotein activity in multidrug-resistant cells. Mol Pharmacol 66: 1332–1339.
73. Kamau SW, Krämer SD, Günthert M, Wunderli-Allenspach H (2005) Effect of the modulation of the membrane lipid composition on the localization and function of p-glycoprotein in MDR1-MDCK cells. In Vitro Cell Dev Biol Anim 41: 207–216.
74. Powl AM, Carney J, Maurius P, East JM, Lee AG (2005) Lipid interactions with bacterial channels: Fluorescence studies. Biochem Soc Trans 33: 905–909.
75. Palsdottir H, Hunte C (2004) Lipids in membrane protein structures. Biochim Biophys Acta 1666: 2–18.
76. Henriksen J, Rowat AC, Brief E, Hsueh YW, Thewalt JL, et al. (2006) Universal behavior of membranes with sterols. Biophys J 90: 1639–1649.
77. van den Brink–van der Laan E, Chupin V, Killian JA, de Kruijff B (2004) Small alcohols destabilize the KcsA tetramer via their effect on the membrane lateral pressure. *Biochemistry* 43: 5937–5942.
78. Safran S (1994) Frontiers in physics. Volume 90. Statistical thermodynamics of surfaces, interfaces, and membranes. New York: Addison-Wesley. 498 p.
79. Tieleman DP, Berendsen HJC (1998) A molecular dynamics study of the pores formed by *Escherichia coli* OmpF porin in a fully hydrated palmitoyloleoylphosphatidylcholine bilayer. Biophys J 74: 2786–2801.
80. Höltje M, Förster T, Brandt B, Engels T, von Rybinski W, et al. (2001) Molecular dynamics simulations of stratum corneum lipid models: Fatty acids and cholesterol. Biochim Biophys Acta 1511: 156–167.
81. Berendsen HJC, Postma JPM, van Gunsteren WF, Hermans J (1981) Interaction models for water in relation to protein hydration. In: Pullman B, editor. Intermolecular forces. Dordrecht: Reidel. pp. 331–342.
82. Lindahl E, Hess B, van der Spoel D (2001) Gromacs 3.0: A package for molecular simulation and trajectory analysis. J Mol Mod 7: 306–317.
83. Berendsen HJC, Postma JPM, van Gunsteren WF, DiNola A, Haak JR (1984) Molecular dynamics with coupling to an external bath. J Chem Phys 81: 3684–3690.
84. Patra M, Karttunen M, Hyvönen MT, Falck E, Vattulainen I (2004) Lipid bilayers driven to a wrong lane in molecular dynamics simulations by subtle changes in long-range electrostatic interactions. J Phys Chem B 108: 4485–4494.
85. Feller SE, Pastor RW (1999) Constant surface tension simulations of lipid bilayers: The sensitivity of surface areas and compressibilities. J Chem Phys 111: 1281–1287.
86. Ollila S (2006) Lateral pressure profile calculations of lipid membranes from atomic scale molecular dynamics simulations. [Master's thesis]. Helsinki: Helsinki University of Technology.
87. Hess B, Bekker H, Berendsen HJC, Fraaije JGEM (1997) LINCS: A linear constraint solver for molecular simulations. J Comput Chem 18: 1463–1472.
88. Cantor RS (1999) The influence of membrane lateral pressure on simple geometric models of protein conformational equilibra. Chem Phys Lipids 101: 45–56.
89. Sukharev S, Durell SR, Guy HR (2001) Structural models of the MscL gating mechanism. Biophys J 81: 917–936.
90. Thijsse BJ, Hollanders MA, Hendrikse J (1998) A practical algorithm for least-squares spline approximation of data containing noise. Comp Phys 12: 393–399.

IV

Publication IV

Terama, E., Ollila, O. H. S., Salonen, E., Rowat, A., Trandum, C., Westh, P., Patra, M., Karttunen, M., and Vattulainen, I., Influence of ethanol on lipid membranes: rrom lateral pressure profiles to dynamics and partitioning, Journal of Physical Chemistry B 112, 4131-4139 (2008).

Influence of Ethanol on Lipid Membranes: From Lateral Pressure Profiles to Dynamics and Partitioning

Emma Terama,[†] O. H. Samuli Ollila,[‡] Emppu Salonen,[§] Amy C. Rowat,[||] Christa Trandum,[⊥,#] Peter Westh,[⊥,#] Michael Patra,[▽] Mikko Karttunen,[¶] and Ilpo Vattulainen*[,‡,§,#]

International Institute for Applied Systems Analysis, Schlossplatz 1, A-2361 Laxenburg, Austria, Institute of Physics, Tampere University of Technology, P. O. Box 692, FI−33101 Tampere, Finland, Laboratory of Physics and Helsinki Institute of Physics, Helsinki University of Technology, P. O. Box 1100, FI-02015 HUT, Finland, Department of Physics/DEAS, Harvard University, McKay Laboratory, 40 Oxford Street, Cambridge, Massachusetts 02138, Department of Life Science and Chemistry, Roskilde University, P. O. Box 260, DK−4000 Roskilde, Denmark, MEMPHYS−Center for Biomembrane Physics, Physics Department, University of Southern Denmark, Campusvej 55, DK−5230 Odense M, Denmark, Physical Chemistry I, Lund University, Sweden, and Department of Applied Mathematics, The University of Western Ontario, London, Ontario, Canada

Received: June 29, 2007; In Final Form: January 11, 2008

We have combined experiments with atomic-scale molecular dynamics simulations to consider the influence of ethanol on a variety of lipid membrane properties. We first employed isothermal titration calorimetry together with the solvent-null method to study the partitioning of ethanol molecules into saturated and unsaturated membrane systems. The results show that ethanol partitioning is considerably more favorable in unsaturated bilayers, which are characterized by their more disordered nature compared to their saturated counterparts. Simulation studies at varying ethanol concentrations propose that the partitioning of ethanol depends on its concentration, implying that the partitioning is a nonideal process. To gain further insight into the permeation of alcohols and their influence on lipid dynamics, we also employed molecular dynamics simulations to quantify kinetic events associated with the permeation of alcohols across a membrane, and to characterize the rotational and lateral diffusion of lipids and alcohols in these systems. The simulation results are in agreement with available experimental data and further show that alcohols have a small but nonvanishing effect on the dynamics of lipids in a membrane. The influence of ethanol on the lateral pressure profile of a lipid bilayer is found to be prominent: ethanol reduces the tension at the membrane−water interface and reduces the peaks in the lateral pressure profile close to the membrane−water interface. The changes in the lateral pressure profile are several hundred atmospheres. This supports the hypothesis that anesthetics may act by changing the lateral pressure profile exerted on proteins embedded in membranes.

I. Introduction

The influence of alcohols and small solutes on the properties of lipid membranes has been studied extensively during the past few decades. As alcohols are anesthetics, this work has in part been motivated by the desire to understand the molecular-level mechanism of general anesthesia. One possible model is that anesthetic molecules bind specifically to proteins. By this direct mechanism, anesthetics, such as ethanol, may influence the binding of ions to the proteins acting as ions channels, shifting protein conformational equilibria. On the other hand, there are also studies that support the existence of an indirect mechanism[1] in which a change in membrane properties, induced nonspecifically by anesthetic molecules incorporated into the membranes, changes the structure and hence activity of membrane proteins.

Cantor has proposed that the indirect mechanism would involve anesthetic molecules partitioning into the membrane, thus altering the lateral pressure profile. Changes in the local pressure across a membrane would induce changes in membrane protein conformation.[2,3] Recent simulation studies have shown that minor changes in lipid composition can lead to significant changes in the lateral pressure profile.[4−10] Since alcohols induce changes in membrane properties, effects on the pressure profile can also be awaited.

On the basis of earlier studies, it is evident that anesthesia-producing molecules have influence on lipid membrane structure. Alcohols in lipid bilayers have been studied by a variety of different experimental methods, such as NMR,[11−16] X-ray,[17] micropipette techniques,[18,19] and volumetric analyses.[20,21] By ^{2}H NMR, ethanol has been observed to have a disordering effect on lipids.[11] The observed similarities in ethanol and water interaction with lipids further suggest strong influence of hydrogen bonding.[11] A separate NOESY study identified hydrogen bond formation as the main source of hydrophilic interaction between ethanol and palmitoyloleoylphosphatidyl-

* Author to whom correspondence may be addressed. E-mail: ilpo.vattulainen@csc.fi.
[†] International Institute for Applied Systems Analysis.
[‡] Tampere University of Technology.
[§] Helsinki University of Technology.
[||] Harvard University.
[⊥] Roskilde University.
[#] University of Southern Denmark.
[▽] Lund University.
[¶] The University of Western Ontario.

10.1021/jp0750811 CCC: $40.75
Published on Web 03/15/2008

choline (POPC) bilayers.[13] Along the same lines, Holte and Gawrisch state that ethanol resides with the highest probability at the membrane−water interface near the lipid glycerol backbone and upper methylene portions.[14] Results of similar nature have been observed in studies of other anesthetic molecules, supporting the preference of anesthetics to partition close to the membrane−water interface.[22,23] Results of Klemm and Williams also indicate that alcohol alters the organization of water, and that, with respect to lipids, ethanol interacts near the carbonyl domain.[16] In differential scanning calorimetry and X-ray studies, it has likewise been shown that, above the main phase transition temperature of the lipids, ethanol produces structural changes in bilayers.[17] In addition, alcohol partitioning into lipid/water phases has been characterized by Cantor in a more approximate theoretical study.[24] His model studies predict that increasing lipid chain cis-unsaturation increases the bilayer−water partition coefficient of short-chain alkanols.

Computational approaches are few and mainly based on atom-scale molecular dynamics methods.[13,25−28] Feller et al. found a disordering effect in a membrane due to ethanol.[13] Patra et al. found a similar effect, but add that the influence of ethanol on the ordering of dipalmitoylphosphatidylcholine (DPPC) and POPC hydrocarbon chains depends on ethanol concentration.[26] They observed a slight increase in acyl chain order at small ethanol concentrations, a maximum at intermediate concentrations, and a reduction in order for a large fraction of ethanol. The observed nonlinear ordering of lipid hydrocarbon chains is in line with recent experiments that have indicated nonlinear coupling between ethanol mole fraction and ethanol density at a soft interface.[29] In a recent study, Dickey and Faller have elaborated on the hydrogen-bonding properties of a variety of alcohols.[27] As for coarse-grained simulations, the studies by Dickey et al.[30] have suggested that increasing amounts of butanol lead to an increasing area per lipid in a membrane, in qualitative agreement with related experiments.[18] They have further provided support for increasing interdigitation at high alcohol concentrations, a finding that has also been observed in the coarse-grained simulations of Kranenburg et al.[31] Recent coarse-grained simulations have additionally proposed that alcohols may reduce lateral membrane pressures.[32] Overall, these studies have complemented experimental efforts considerably, and provide insight into the structural features of systems where membranes are interacting with different alcohols.

While the structures of ethanol−membrane systems are rather well-known, the kinetics and dynamics of ethanol−membrane interactions are considerably less well understood. Nevertheless, investigating the partitioning of alcohols into membranes and the dynamics of alcohols within membranes is important in order to understand their interaction with lipids and consequences for anesthetic action. Yet even the basic processes such as the migration mechanism of ethanol permeation through a membrane are not known. This can be attributed to the lack of atomic-scale simulation data for dynamic properties. The only exception we are aware of is the work by Chanda et al., who focused on the dynamics of hydrogen bonding in the hydration layer of lipid head groups.[33] Essentially all other studies to date have been based on experiments focusing on the partitioning, permeation, and permeability coefficients of alcohols.[18,24,34−39] Summarizing, a complete picture of the dynamics, in particular the dependence of partitioning and permeation on membrane composition, has largely remained open.

Here we use both experiments and simulations to elucidate the influence of ethanol on a variety of membrane properties related to the action of ethanol as an anesthetic. We introduce dynamical analysis of both lipid molecules in membrane structures as well as ethanol molecules penetrating the bilayer, complementing our previous study,[26] which focused on structural properties. Experimental observations yield partition coefficients of ethanol in saturated and unsaturated bilayers. Through atomistic computer simulations, we observe the permeation path of ethanol in DPPC and palmitoyl-docosahexaenoyl-phosphatidylcholine (PDPC) bilayers and discuss the partitioning with respect to the experimental results. A second and most intriguing finding of the computer simulation study is the influence of ethanol on the lateral pressure profile of a membrane. We observe that ethanol reduces the peaks of the pressure profile and hence the interfacial tension at the membrane−water interface considerably. The changes are on the order of several hundred atmospheres. The consequent effects on the elastic properties of a membrane provide support for the hypothesis[2,3] that anesthetics change the activity of proteins by altering membrane properties.

II. Experimental Methods

Sample Preparation. All lipids (DMPC, DPPC, and DOPC) were obtained from Avanti Polar Lipids (Birmingham, AL) in powder form and were used without further purification. Anhydrous ethanol (purity >99.9%) was purchased from Merck (Darmstadt, Germany). Six aqueous solutions of varying ethanol concentrations between 3.0 and 15.0 mg/g MilliQ water (Millipore, Bedford, MA) were prepared. MilliQ water was added to the powder form of lipid to yield a 100 mM dispersion. The dispersion was placed in a 40 °C water bath (50 °C for DPPC) for 60 min and was intermittently vortexed to promote dissolution. The dispersion was then extruded (Lipex Biomembranes, Vancouver, BC) 10 times repeatedly through two stacked polycarbonate filters of 100 nm pore size at 40 °C (50 °C for DPPC) to produce unilamellar vesicles of 0.1 μm diameter.[40,41] Ethanol was added to the lipid dispersion at a concentration of between 3.0 and 25.0 mg ethanol/g lipid suspension. Lipid concentrations were confirmed gravimetrically by drying 100 μL aliquots of the sample. In this way, we determined that water occupied 94% by mass of the lipid−water suspension and determined the concentration of the lipid−water−ethanol suspension in terms of milligrams of ethanol per gram of water.

Isothermal Titration Calorimetry (ITC). Interactions between membranes and ethanol were investigated by determining the enthalpy change associated with the transfer of lipid vesicles from a lipid−water−ethanol suspension into an ethanol−water solution using high sensitivity ITC (MSC−ITC, MicroCal, Northampton, MA). The lipid−water−ethanol suspension was titrated in injection volumes of 8 μL (with the first injection volume at 2 μL) into the ethanol−water solution at a temperature of 35 °C (DMPC and DOPC) or 50 °C (DPPC). The solution was stirred at a constant rate of 265 rpm and the reference power was 15 μcal/s. This procedure was repeated for ethanol solutions of varying concentrations.

Analysis by the Solvent-Null Method. Ethanol−membrane partition coefficients were determined using the solvent-null method originally described by Zhang and Rowe.[42] In brief, ethanol is assumed to exist in either bound or free state. The addition of lipid−water−ethanol suspension (from the syringe) to the ethanol−water solution (in the cell) generates an enthalpic response that depends on the concentration of ethanol in solution. For example, when the ethanol concentration in the cell is greater than the free concentration of the alcohol in the lipid−water−ethanol suspension, mixing generates an endothermic response ($\Delta H > 0$) as alcohol partitions into the

membrane (heat is absorbed upon solute dehydration and membrane association). On the other hand, if the ethanol concentration in the alcohol−water solution is less than the free concentration in the lipid−water−alcohol suspension, mixing results in an exothermic response ($\Delta H < 0$) as a result of the heat of dilution accompanying the transfer of ethanol from membrane to bulk water. At the point where there is no heat exchange ($\Delta H = 0$), the concentration of ethanol in the sample cell equals the concentration of free ethanol in the lipid−water−ethanol suspension and there is no net exchange of ethanol in or out of the membrane. Determining the ethanol concentration at this null point yields a measure of the free ethanol concentration in the lipid−water−ethanol suspension. Subtracting the free concentration of ethanol from the total concentration of ethanol provides a measure of how much ethanol is partitioned in the membrane: $n_{\mathrm{eth}}^{\mathrm{lipid}} = n_{\mathrm{eth}}^{\mathrm{total}} - n_{\mathrm{eth}}^{\mathrm{free}}$. The partition coefficient, K_{p}, can then be determined:

$$K_{\mathrm{p}} = \frac{X_{\mathrm{eth}}^{\mathrm{lipid}}}{X_{\mathrm{eth}}^{\mathrm{aq}}} = \frac{(n_{\mathrm{eth}}^{\mathrm{lipid}})/(n_{\mathrm{eth}}^{\mathrm{lipid}} + n_{\mathrm{lipid}})}{(n_{\mathrm{eth}}^{\mathrm{aq}})/(n_{\mathrm{eth}}^{\mathrm{aq}} + n_{\mathrm{aq}})} \quad (1)$$

where $X_{\mathrm{eth}}^{\mathrm{lipid}}$ is the molar fraction of ethanol in lipids (bound), and $X_{\mathrm{eth}}^{\mathrm{aq}}$ is the molar fraction of ethanol in the aqueous solution (free). Here, K_{p} is the equilibrium constant (partition coefficient) that characterizes the distribution of ethanol between the aqueous and membrane phases.

III. Computational Methods

System Preparation. The simulated systems consisted of a fully hydrated system of 128 molecules, either PDPC or DPPC, and 90 ethanols. PDPC contains a polyunsaturated omega-3 fatty acid, which, together with the saturated DPPC, allows us to investigate the dependence of unsaturation on alcohol−membrane interactions. A combination of these two systems resulted in two simulations with a duration of 50 ns each. The starting configuration of the DPPC model system was based on a previous 100 ns simulation.[26] For PDPC, we used a 50 ns simulation[10] whose end configuration was chosen as the starting configuration for the present study. The 90 alcohol molecules were added randomly to the space around the bilayer after which the remaining space was filled with 8958 (DPPC) or 8951 (PDPC) water molecules. For comparison, pure one-component bilayers of 128 lipids were studied in the absence of alcohols with hydration of 3655 water molecules. Additionally, we studied the alcohol concentration dependence through simulations of a DPPC−ethanol bilayer by varying the number of ethanol molecules from 45 to 900. Other relevant simulation details were as reported in ref 26.

Simulation Method. All simulations were atomistic molecular dynamics simulations using the GROMACS package.[43] The lipid bilayer was formed in the $x-y$ plane, and long-range electrostatic interactions of the charged groups were handled by the particle mesh Ewald (PME) method.[44−46] The system was simulated at 323 K, well above the main phase transition temperature T_{m}, which is highest for DPPC at 315 K. Simulations were conducted in the NpT ensemble by the Berendsen thermostat and the Berendsen barostat[47] using coupling time constants of 0.1 and 1 ps, in respective order. Further simulations were also conducted using the Parrinello−Rahman barostat and Nose−Hoover thermostat; no essential differences were observed. Force field parameters for bonded interactions were taken from ref 48, available online at http://moose.bio.ucalgary.ca/. Partial charges were from Tieleman and Berendsen,[49] also available online. For PDPC, the only difference with respect to DPPC is the polyunsaturated *sn*-2 chain, for which we used the description discussed and validated elsewhere.[10] For solvent particles, we used the simple point charge (SPC) model.[50] The ethanol force field was the one by Lindahl et al.[43] Further simulation details can be found in the work of Patra et al.[26] where the properties of static quantities of the simulated systems are discussed in detail.

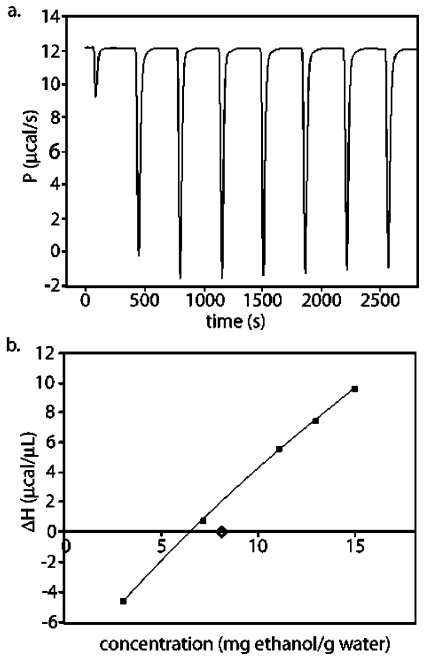

Figure 1. Plot of the enthalpy of injection determined by ITC versus ethanol concentration at 35 °C. Here DOPC−water−ethanol suspension with an ethanol concentration of 7.66 mg/g water is titrated into aqueous ethanol solutions varying between 3.0 and 15.0 mg/mL in concentration. The point at which there is no net heat exchange upon mixing is determined by interpolation. The difference between this "null" point and the amount of ethanol in the lipid−water−ethanol suspension (denoted by a diamond on the *x*-axis) yields an estimate of the partition coefficient, K_{p}.

Data Analysis. Of the 50 ns simulation time, only the last 30−40 ns were used for analysis. This ensured that all systems had equilibrated fully (see ref 26), and the alcohol molecules had acquired an equilibrium distribution in the system according to their natural partitioning. The lateral pressure profile was calculated by using the Irving−Kirkwood contour, following ref 10 (see also refs 5−7). This contour does not allow the use of PME for long-range interactions. Consequently, we calculated the pressure profiles by a post-analysis where Coulomb interactions were truncated at 2.0 nm. Recently, Sonne et al. have confirmed that, for a truncation distance larger than 1.8 nm, this approach yields results consistent with those found by PME together with the Harasima contour.[5]

IV. Results and Discussion

A. Partition Coefficients: Influence of Unsaturation. The enthalpy change upon titration of water−lipid−ethanol suspension into aqueous ethanol solution of defined alcohol concentration is measured using ITC. Raw data is obtained in the form of an enthalpogram, where the integrated area beneath each peak is the enthalpy of the injection (ΔH) that is determined to within $\sim 2 \times 10^{-6}$ J s(ee Figure 1A). This procedure is repeated for a series of aqueous ethanol solutions varying in alcohol concentration (3.0−15.0 mg/L), and a plot of ΔH versus ethanol

concentration can then be generated. Figure 1B displays such a plot for a DOPC−ethanol−water suspension with an ethanol concentration of 7.66 mg/g water. Using the solvent-null method as described above, the concentration of free ethanol was determined for each lipid species, and values for the partition coefficient, K_p, were calculated. Partition coefficients are found to depend strongly upon lipid composition. K_p for DMPC−ethanol at 35 °C was found to be 15 ± 2, and a similar value for DPPC was found at 50 °C (14 ± 4). These values for DMPC are in reasonable accord with literature data: $K_p = 19$ for DMPC at 35 °C,[51] and $K_p = 28$ at 28 °C.[52,53] For DOPC, much stronger partitioning was observed, and K_p was 71 ± 10 at 35 °C.

It is evident that ethanol partitions into a bilayer of unsaturated lipids considerably more strongly than into a membrane of saturated lipids. This result is in agreement with theoretical predictions by Cantor.[24] As the only essential difference between DMPC and DPPC compared to DOPC lies in the hydrocarbon region where DOPC has two double bonds (unlike DMPC and DPPC, which have none), this indicates that the partitioning of ethanol depends on the level of unsaturation in phosphatidylcholine (PC) bilayers. As ethanol is known to partition into the interfacial region of the bilayer,[14,26] this difference in K_p can be attributed to modifications in the packing of saturated versus unsaturated lipids due to the presence of the cis-double bond at the 9−10 position in DOPC. An increase in ethanol partitioning is hence likely attributed to an increase in interfacial volume or area of the unsaturated bilayer. The concept of surface density and its relationship to the partitioning of small molecules has previously been theoretically discussed and experimentally confirmed by Dill and co-workers.[54,55] Furthermore, unsaturated lipids have a larger area per lipid that results from less ordered acyl chains.[18,30] Together with experimental evidence showing that ethanol partitions with the highest probability in the interfacial region,[14,56] it is logical that more ethanol would partition into unsaturated lipid membranes with increased interfacial area. Membranes composed of unsaturated lipids also show increased molecular volume compared to saturated lipids.[53,57,58] A consequence of this altered lipid packing may be a lower entropic cost of inserting a small cosurfactant at the membrane−aqueous interface. In addition, the average axial location of ethanol in the bilayer may shift, resulting in greater numbers of ethanol molecules that can access the center of the lipid bilayer. This may further increase the amount of ethanol that can partition into the bilayer.

B. Partition Coefficients: Computational Results. The study of partition coefficients is experimentally feasible through various techniques.[59] The motivation of the analysis lies in obtaining information on the partitioning of given molecules under steady-state conditions. Computationally, the extraction of quantitative values for the partitioning of molecules in lipid membranes is very challenging. This is largely due to the small size of the simulated system, which is not comparable to experimental conditions. In principle, one should simulate comparatively large unilamellar lipid bilayers under full hydration, including the investigated solute, in order to obtain data that can be quantitatively compared to experiments. In practice, lipid bilayers are simulated with periodic boundary conditions, implying that the bilayer is comparable to a large multilamellar vesicle. Under these conditions, the solvent bulk phase is not included in the simulated system, and there is no exchange of solute molecules from the bulk reservoir to the region in the vicinity of the membrane. Obviously, in such simulations, the concentration of alcohol in the aqueous phase is ill-defined.

Considering these limitations, there is ample reason to proceed with care when partitioning coefficients extracted from simulations are compared with experimental results. A more dependable approach we have taken is to focus on the qualitative trends and elucidate the behavior of partition coefficients as the alcohol concentration is varied over a wide range.

To calculate K_p, see eq 1, one has to define which ethanols are in solution and which ones are inside the bilayer. There is no obvious way of doing this. We use the mass density profiles of water and ethanol in the direction normal to the bilayer (see ref 26) and find regions with almost constant values away from the membrane boundary. We take this region as the pure solvent phase and the corresponding alcohols as "free" ethanols; the remaining alcohol molecules are "bound" to lipids. This choice likely exaggerates the partition coefficient but, on the other hand, accounts for those ethanol molecules that are partly influenced by the membrane although not completely partitioned into it.

On average, the amount of alcohol molecules partitioned in the lipid phase is found to be 85.6 ± 2.5 for DPPC−EtOH, and larger for PDPC−EtOH. The estimated error of ±2.5 results from the arbitrary choice of boundaries for the free vs bound ethanol molecules. Out of the 90 ethanol molecules in the system, this result corresponds to almost complete partitioning. The trend is thus the same as witnessed in the experimental analysis, where partitioning was found to increase with increasing unsaturation.

The K_p values computed from simulations are larger than those found through experiments. Considering the limitations of simulations discussed above, and the fact that force fields for alcohols used in simulations are under further development, this is not surprising. Further, the concentration dependence of K_p (see next section) renders comparison of simulation and experimental results very difficult. Nonetheless, as the objective is to gain insight into the qualitative trends rather than full quantitative agreement, the simulations do measure up to one's standards.

With higher ethanol concentrations, the extent of partitioning into the membrane rapidly declined (see below).

C. Partition Coefficients: Ethanol Concentration Dependence. We next focused on the DPPC bilayer and examined the influence of ethanol concentration on partitioning. The results in Figure 2 show that the partitioning coefficient of ethanol depends rather substantially on its concentration. The line is fitted such as to aid the eye in interpreting the rather minute data points with their incorporated error bars. For increasing ethanol concentration, the partition coefficient decreases monotonically. The partition coefficient is reduced significantly at relatively low ethanol concentrations, and levels off at a near-exponential decrease to a plateau value at higher concentrations.

The above findings suggest that the partitioning of ethanol depends on its concentration also. This behavior is known as *nonideal* partitioning, and has been observed in experiments.[60] Despite its importance for quantitative comparison of different partitioning studies, this behavior has been given rather little attention. From these results it is clear that, even at low solute concentrations, results for partitioning can vary greatly from one study to the other, as the concentration dependence in the case of ethanol shows. At much greater than physiological concentrations, the partitioning is easier to control. These findings underline the difficulties of comparing different studies for the effects of alcohols and stress the need to complement any study by reference alcohol concentrations that would enable comparison. From a simulations point of view, adding more solute to the system means more demand for solvation of the

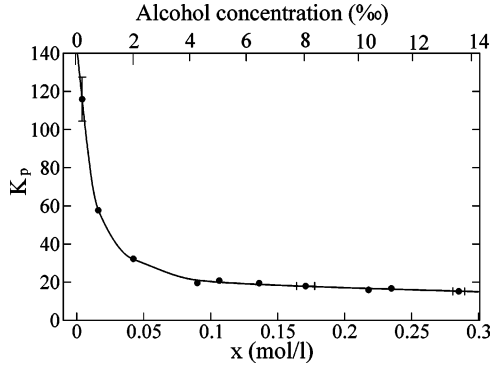

Figure 2. Ethanol concentration dependence of the partitioning coefficient of ethanol in a DPPC bilayer. The lower *x*-axis describes the concentration of ethanols in the water phase, not including ethanol molecules adsorbed on the membrane. The error bars in the *x*-direction are therefore due to ethanol number fluctuations in the water phase as ethanols occasionally enter and leave the membrane. For the small system simulated in this work, this description is appropriate to highlight the concentration dependence. For reason of completeness, the upper *x*-axis in turn illustrates the molar concentration of all ethanol molecules in a system. This gives a measure for corresponding physiological plasma concentrations of ethanol, which usually are less than ~1%. However, in processes such as fermentation, ethanol concentrations are much higher, up to 15%. The solid curve is only a guide to the eye. The number of alcohols in the system varied from 45 (the first data point) to 900 (the last data point).

molecules. This in turn is costly in terms of computational resources. We have, however, started working on more explicit concentration dependence studies after this striking result was obtained. It would be interesting to clarify how the concentration dependence of the partitioning coefficient and the degree of lipid unsaturation are correlated.

D. Bilayer Permeation. *1. Permeation Rates and Crossing Times.* In order to characterize the permeation of ethanol through a membrane, we identify three regions in a bilayer where the partitioned alcohol molecules may reside. As described in detail in our earlier paper[26] and observed by NMR,[14] most of the ethanol molecules bound in a bilayer localize in the *accumulation layer* below the lipid headgroups. This localization results from the amphiphilic nature of the ethanol molecules, favoring the embedding of their hydrophobic tails in the lipid acyl chain region, while retaining the polar hydroxyl groups at the water−lipid interface. Furthermore, specific localization of ethanol molecules results from hydrogen bonding with the lipid ester and phosphate group oxygens. For example, in the case of PDPC, analysis of hydrogen bonding (see ref 26 for details) shows that each ethanol molecule forms, on average, 0.91 hydrogen bonds with the lipids. Out of these hydrogen bonds, approximately 62% are formed with the *sn*-2 tail ester group oxygens (carbonyl and ester bond oxygens), and 19% are formed with the phosphate group. In essence, the positions in the bilayer where hydrogen bonding with the lipid oxygens are possible can be thought of as a set of discrete binding sites for the ethanol molecules.

Below the accumulation layer is the hydrophobic chain region, where the ethanol molecules can make brief excursions.[26] Further, at the center of the bilayer is the methyl trough, where the lipid chain density in general exhibits clear minima.

In the following, the process of a single ethanol molecule drifting from the accumulation layer to the hydrophobic chain region, past the methyl trough, and finally reaching the accumulation layer on the opposite bilayer leaflet is termed a *crossing event*. A detailed analysis of the alcohol trajectories showed that, in many cases, the ethanol molecules can diffuse all the way to the methyl trough region, but are subsequently reflected back. In addition, processes where the ethanols traversed past the methyl trough but were then reflected back to their leaflet of origin were also common.[26] Thus, the successful crossing events analyzed below constitute only a small part of all the ethanol movement in the direction of the bilayer normal.

TABLE 1: Mean, Minimum, and Maximum Times for Bilayer Crossing Events by Ethanol

bilayer	$\langle\tau_{cross}\rangle$ (ps)	τ_{cross}^{min} (ps)	τ_{cross}^{max} (ps)
DPPC	325 ± 50	60	1760
PDPC	380 ± 60	80	1080

For PDPC, there were a total of 22 crossing events during the 37.5 ns that was used in the analysis. With 90 ethanol molecules bound in the membrane, the characteristic crossing rate per molecule is

$$P_{trans} = \frac{22}{37.5\ \text{ns} \times 90} \approx 6.5 \times 10^{-3}\ \text{ns}^{-1}$$

Conversely, the inverse of the crossing rate gives a characteristic crossing time of ~150 ns (the statistical error here is approximately 20%). As reported previously,[26] characteristic crossing time of EtOH in DPPC was ~130 ns. Considering ~20% error, we conclude that, on the basis of the present data and those of ref 26, there were no statistically significant differences between the ethanol crossing rates of DPPC, PDPC, and POPC bilayers. While we cannot estimate ethanol permeability coefficients on the basis of these crossing rates, the obtained values corroborate experimental estimates:[18] the characteristic crossing times for ethanol are very small compared to the time for ethanol concentration equilibration between two volumes separated by a phospholipid bilayer. This equilibration is mainly governed by the adsorption and desorption of ethanol at the water−lipid interface.[18]

The time associated with the bilayer crossing process, τ_{cross}, was estimated from the ethanol molecule trajectories as follows: the starting point for a crossing event was the instant in time when the center of mass (CM) of the molecule diffused to a certain distance from the bilayer center, and did not return again to this level during the rest of the crossing process. These threshold distances were chosen as 0.9 and 1.0 nm for DPPC and PDPC membranes, respectively, based on the typical molecule CM *z*-coordinate fluctuations in the accumulation layer. When the molecule drifted further than the chosen threshold distance in the opposite bilayer leaflet, and subsequently remained in the respective accumulation layer, the crossing process was considered to be terminated. While clearly operational, this is still a natural way of determining the specific values of τ_{cross} based on the molecular trajectories. The choices of the starting and ending points for the crossing events ensure that the values of τ_{cross} obtained are accurate to within a few tens of picoseconds, given that the resolution of the molecular trajectories in time was 10 ps.

The small number of bilayer crossing events prevents us from presenting comprehensive distributions of τ_{cross}. Thus, in Table 1 we present only the mean, minimum, and maximum values of τ_{cross} for both DPPC and PDPC membranes.

2. Ethanol Orientation during Crossing. Previous simulations and experiments have shown that the most probable position for an ethanol molecule in a lipid bilayer is right below the lipid head groups.[14,26] This position is maintained by transient hydrogen bonds (with a lifetime of ~1 ns) between the ethanol

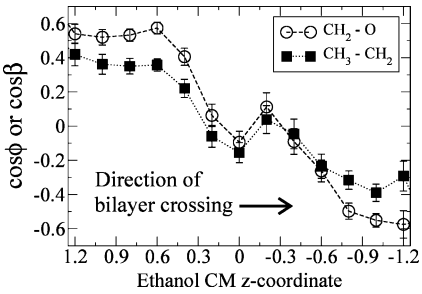

Figure 3. Ethanol orientation described by I_ϕ and I_β (see text) when ethanol crosses a DPPC membrane.

hydroxyl group and lipid tail ester oxygens. In order for EtOH to traverse the membrane, ethanol molecules need to break their hydrogen bonds and penetrate past the hydrophobic chain region of the bilayer. Upon reaching the methyl trough, the alcohols can either drift back to the original accumulation layer or cross to the other one in the opposite leaflet.

For the shorter-chain alcohol methanol, free-energy calculations have shown a major free-energy barrier at the membrane center.[38] This was also corroborated by our simulations[26] where no methanol molecules were observed to cross DPPC and POPC bilayers within the time scale studied. However, for ethanol, the crossing process is facilitated by the additional methylene group in its structure. According to our simulations, an ethanol molecule permeating a bilayer is steered through the hydrophobic region with the help of its CH_3-CH_2 tail, whereas the polar OH group is pointed toward the water−lipid interface of the leaflet in question. This is illustrated in Figure 3 where we plot the average orientation of the ethanol molecules with respect to the membrane normal. The data for crossing events from the lower leaflet to the upper one were mirrored in reference to the midplane of the bilayer for more comprehensive statistics. This way, *all* the crossing events in the analysis occur from the upper leaflet to the lower one. The ethanol orientation is defined through $I_\phi = \langle \cos \phi \rangle$ and $I_\beta = \langle \cos \beta \rangle$, where ϕ (β) is the angle between the H_2C-O bond (H_3C-CH_2 bond) and the z−axis. At the midplane of the bilayer, the ethanol molecules flip in order to electrostatically facilitate the transport to the opposing leaflet.

E. Diffusion. *1. Ethanol and Lipid Diffusion in Membrane Plane*. Studies of lateral diffusion of ethanol can give insight into the migration time scales of ethanol motion within the bilayer. These results are complemented by studies of actual diffusion events, either as single-molecule motion or in terms of collective diffusion mechanisms involving both alcohols and lipids. Taken together, these analyses provide a better understanding of possible mechanisms of alcohol interactions as well as their implications for membrane dynamics.

The lateral diffusion coefficient is defined as

$$D_T = \lim_{t\to\infty} \frac{1}{2dt} \langle [\vec{r}(t)]^2 \rangle \qquad (2)$$

where $d = 2$ is the dimension of the system, and $\langle [\vec{r}(t)]^2 \rangle$ is the mean squared displacement of the CM of the molecules. For lipids, the calculation is performed with respect to the CM of the leaflet in which a molecule under study is located (see ref 61 for details). In the case of ethanol, the relative motion of the two leaflets is of less concern due to transitions from one leaflet to another. For the same reason, we analyze here the migration mechanisms of ethanols instead of their lateral diffusion coefficient, which is less well-defined due to rather frequent crossing attempts.

TABLE 2: Lateral Diffusion Coefficients of Lipids in Pure Membranes and under the Influence of Ethanol[a]

	pure	ethanol
DPPC	13.3 ± 1 (11.8 ± 0.5)	17.0 ± 3 (11.4 ± 2)
PDPC	20.1 ± 2 (20.1 ± 2)	28.1 ± 4 (18.0 ± 3)

[a]Results are given for data collected between 2 and 3 ns and 5−10 ns (in parentheses). Units are 10^{-8} cm^2/s.

The lateral diffusion coefficient for a pure DPPC bilayer, approximately 1×10^{-7} cm^2/s, is in agreement with experimental evidence with diffusion coefficients ranging from 1.0×10^{-7} cm^2/s to 1.5×10^{-7} cm^2/s (see ref 62 and references therein).

The lateral diffusion coefficients acquired for the lipids in the presence of ethanol are shown in Table 2, which also includes a comparison to the results in pure lipid bilayers. The diffusion coefficients were determined from the mean squared displacement over a time interval of 2−3 (5−10) ns. In this manner, we first considered the short-time diffusion that is in part related to the motion in a "cage", influenced by its free volume distribution. The latter time scale is more closely related to the diffusive behavior in the hydrodynamic long-time limit. Strictly speaking, only the long-time diffusion is well defined (see the definition in eq 2), but, as some experimental techniques such as quasi-elastic neutron scattering measure dynamics over time scales on the order of 1 ns, we have considered the two time scales separately.

We find that the lateral diffusion of DPPC is only weakly affected by the influence of ethanol. This finding is in agreement with recent simulation results.[27] A more careful consideration shows that at short times the lateral diffusion of DPPC is somewhat affected by ethanol, but at longer times the difference essentially vanishes. For PDPC the trend is the same as that for DPPC: on a short diffusion time scale, the presence of ethanol contributes to faster lipid diffusion. However, the effects of ethanol wear off fast, and already, considering the 5−10 ns regime, the diffusion coefficient values for the lipids are comparable to those of pure lipid cases. Thus there seems to be no major effect on lateral diffusion coefficients that can be attributed to the presence of ethanol.

2. Rotational Diffusion of Lipid Molecules. Next we investigated the effect of ethanol on the rotational dynamics of lipid molecules. Earlier studies of the effect of ethanol on the rotational dynamics of lipid−protein systems using electron paramagnetic resonance (EPR)[63−65] show that ethanol increases the rotational dynamics of the spin-labeled lecithins in a pure bilayer[63] and strongly immobilizes the protein side chains.[64] However, the effect of spin labeling on the rotational dynamics has remained an open issue.

Here we describe the dynamics of lipid molecules using the second rank reorientational autocorrelation function

$$C_2(t) = \frac{1}{2} \langle 3[\vec{\mu}(t)\cdot\vec{\mu}(0)]^2 - 1 \rangle \qquad (3)$$

where $\vec{\mu}(t)$ is a unit vector that defines the chosen rotational mode. We consider here the autocorrelation functions of various vectors describing different parts of the lipid molecules: the glycerol region through the vector from the *sn*-1 to the *sn*-3 carbon (Cg1−Cg3), the head group region through the P−N vector, and the slowest mode of the molecule through the vector from the first carbon of the *sn*-1 chain to the first carbon of the *sn*-2 chain (C1(*sn*-1)−C1(*sn*-2)).

The rotational correlation functions for the different systems are presented in Figure 4. Our results show that the correlation

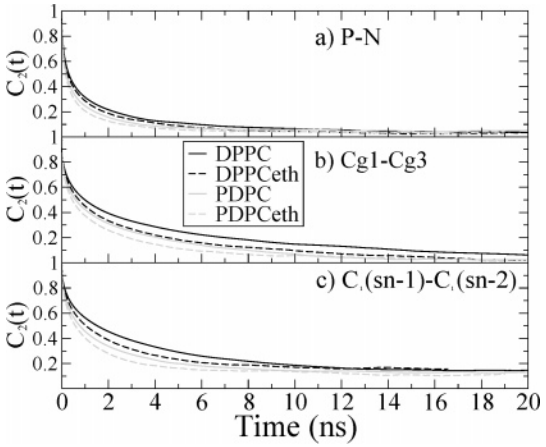

Figure 4. Rotational autocorrelation functions for (a) headgroup (P−N vector), (b) glycerol group (Cg1−Cg3 vector), and (c) the C1(*sn*-1)−*C*2(*sn*-2) vector.

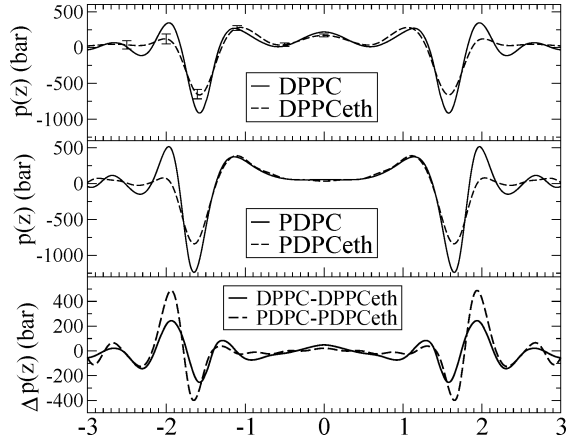

Figure 5. Lateral pressure profiles, $p(z)$, across a membrane for pure DPPC and PDPC bilayers, and the influence of 90 ethanol molecules. The membrane center is at $z = 0$ along the membrane normal direction. The lowest panel shows the difference due to ethanol. The profiles have been made symmetric with respect to $z = 0$. The minor oscillations at the tails of the profile in the water phase are due to statistical fluctuations.

times systemically decrease with added ethanol or increased number of double bonds. The enhanced dynamics resulting from double bonds has been reported elsewhere,[10] thus we concentrate here only on the influence of ethanol. The decrease of correlation times due to ethanol is larger for the Cg1−Cg3 and the C1(*sn*-1)−C2(*sn*-2) vectors than for the P−N vector. On the other hand, the dynamics of individual carbons in the acyl chains was not affected (data not shown). This finding is in agreement with recent simulations.[66] The enhanced dynamics due to ethanol is in agreement with EPR measurements[63] and recent simulations.[27]

There are two obvious explanations for the enhanced dynamics of the lipids due to ethanol. First, ethanol increases the area per molecule, thereby facilitating the rotations of lipid molecules. Second, as ethanol forms hydrogen bonds with lipid molecules and hence perturbs the interactions between water and lipids, this may speed up the dynamics of lipids.[33]

F. Lateral Pressure Profiles under the Influence of Ethanol. Small alcohols such as methanol and ethanol have been found to destabilize KcsA, a commonly studied potassium channel.[1] It has been suggested in ref 1 that the ability of small alcohols to dissociate the tetramer unit in KcsA and, more generally, to function as anesthetics depends on their effect on the lateral pressure profile; direct evidence for this mechanism has been lacking, though.

In Figure 5 we show the lateral pressure profiles for pure DPPC and PDPC bilayers together with the results for EtOH−DPPC and EtOH−PDPC systems. The profiles for pure DPPC and PDPC are consistent with previous atomistic simulation studies.[4,5,10] The difference due to ethanol is striking. The pure bilayers exhibit a prominent positive peak at the membrane−water interface ($z \approx 2$ nm); this is usually interpreted as a repulsive contribution due to electrostatic and steric interactions, as well as hydration repulsion, that tend to expand the bilayer. However, this peak is markedly diminished in both DPPC and PDPC systems because of the addition of ethanol. Closer to the membrane interior around ester oxygens ($z \approx 1.6$ nm), there is a pronounced negative peak characterizing an attractive contribution due to the interfacial energy between water and the hydrocarbon chain region; this contracts the bilayer. In this case, too, ethanol suppresses the negative peak in both DPPC and PDPC systems. The extent of suppression is approximately as large as in the main peak in the head group region. The changes due to ethanol are clearly localized to the region under the lipid head groups, where ethanol is located. In the membrane center, the changes in the lateral pressure profile due to ethanol are minor: the positive stress is reduced slightly, but, overall, the effect is weak.

The reduction in the negative peak of the lateral pressure profile is consistent with recent coarse-grained simulations[32] and micropipette aspiration studies,[19] and further with an increased area per lipid,[26] which has also been found in experiments.[18] A natural explanation for the reduction of the peak is the decrease in surface tension due to ethanol between the water and hydrocarbon regions. The decrease in surface tension is possible because ethanol located at the boundary between the hydrophobic and hydrophilic regions reduces the hydrophobic effect at this interface. The reduction of the peak in the head group region can be explained by ethanol screening electrostatic interactions between the head groups, an effect that is complemented by an increase in area per molecule due to ethanol.

By comparing the effect of ethanol between DPPC and PDPC systems, we can see that the effect is clearly larger for PDPC. This is particularly interesting, because the amount of ethanol is the same in the two systems. Also, the differences between DPPC and PDPC in partitioning and other properties are relatively minor compared to the induced difference in lateral pressure profiles. This difference can be understood by comparing the order parameters between DPPC and PDPC systems. In the present case, the incorporated ethanol in DPPC increases the order of both saturated hydrocarbon chains (data not shown). In principle, this ordering would increase surface tension, which, however, is not the case. As the average area per lipid increases and the surface tension actually decreases, we conclude that the reduction in the hydrophobic effect dominates over changes in ordering effects. Meanwhile, in PDPC, only the order of the saturated chain increases because of ethanol, while the order of the unsaturated chain remains unchanged (data not shown). Consequently, the ethanol-induced decrease in surface tension is larger in the unsaturated bilayer.

As for the specific details in the profiles, the difference in peak heights in the head group region is likely due to differences in the ordering of head groups and waters in that region. Also the mass distribution of ethanols is slightly moved closer to the head group region in the unsaturated case, which may increase the screening effect.

As for the destabilization of KcsA, it has been proposed that it could occur because ethanol decreases the positive lateral

pressure in the acyl chain region of the membrane interior.[1] Our data provides an alternate mechanism: ethanol partitions into the lipid head group region, thus replacing water and affecting the interfacial contributions in the lateral pressure profile, and in this way destabilizes the tetramer complex of KcsA.

Our results demonstrate that cellular membranes are characterized by large lateral stresses that vary through depth of the membrane. Incorporation of ethanol alters the lateral pressure profile considerably. Similar changes resulting from other anesthetic substances are expected. As integral membrane proteins perform work against the lateral pressure when undergoing structural transitions upon activation, changes in the lateral pressure may consequently alter membrane protein function. Proteins that change their shape, such as the light-sensitive integral protein rhodopsin, are hence expected to be affected by the lateral pressure in a membrane. Recent work[7,8] on one of the mechanosensitive channels supports this view. More generally, proteins such as ion channels involved in general anesthesia are also likely candidates for being affected by the lateral pressure profile.[3] If channel opening increases the cross-sectional area of the protein nonuniformly across the membrane, then ethanol-induced changes in lateral pressure may shift the protein conformational equilibrium to favor either the open or closed state, depending on the changes in the lateral pressure profile. Furthermore, a resulting change in the lateral pressure profile implies changes in elastic properties of a bilayer, as various elastic coefficients such as the curvature modulus and the compressibility can be determined from the lateral pressure profile.[67] Obviously, understanding the coupling between microscopic interactions, local stresses within a membrane, and the continuum level properties is essential to gain a complete view of how soft biological membranes mediate and control protein functions.

V. Concluding Remarks

The aim of this study was twofold. First, our objective was to compare the partitioning of ethanol molecules into lipid bilayers consisting of one lipid but different degrees of lipid saturation, and to investigate the details of partitioning dynamics. Second, we wanted to characterize the influence of ethanol on the lateral pressure profile of a lipid membrane.

We used calorimetric experiments as well as atom-scale molecular dynamics simulations to show that lipid unsaturation markedly affects ethanol−membrane interactions. The partitioning of ethanol is strongly enhanced by unsaturation, which is likely due to the more open nature of the membrane−water interface in unsaturated lipid bilayers, characterized by an increasing area per lipid for increasing unsaturation. The analysis of the partitioning process from the simulations suggested a pronounced nonideality (i.e., concentration dependence of the apparent K_p) at the lowest alcohol concentrations. Because of technical difficulties, this range (∼1 mg/mL**)** is poorly investigated in experimental trials, but the current results suggest that further work at low concentrations is well motivated both for the fundamental understanding of ethanol−PC interactions and from the point of view of the biological effects of ethanol. The atom-scale simulations further complemented this view by providing insight into the permeation mechanisms of ethanol through a bilayer: the crossing times of ethanols were found to be almost identical in saturated and polyunsaturated environments. Further studies of dynamic quantities support the view that the dynamics of both alcohols and lipids in polyunsaturated lipid bilayers is faster compared to the their saturated counterparts; however, the differences are not substantial.

Perhaps the most interesting topic deals with the influence of ethanol on the lateral pressure profile of a lipid membrane. The present results provide compelling evidence that ethanol, which prefers to be located at the membrane−water interface region, markedly alters the pressure profile for both saturated, and even more so, for unsaturated lipid membranes. These changes are particularly pronounced in the interfacial region where both the repulsive and the attractive peaks of the lateral pressure profile are decreased substantially. The observed strong decrease in the surface tension is consistent with recent coarse-grained modeling results.[32] When these findings are combined with recent results for lateral pressure profiles in one-[4,5,7,10] and two-component[6,9] lipid bilayers, and with many-component lipid raft membranes,[8] we may conclude that the lateral pressure profiles do depend on the membrane composition, and the dependence is actually profoundly strong. Recent simulation results[68] have further shown that the lateral pressure profile is affected by the presence of a membrane protein. What remains to be done is to show the explicit coupling between the lateral pressure profile and membrane protein activation as the composition of the membrane is varied. Work in this direction is in progress.

Acknowledgment. Funding from the Academy of Finland, NSERC of Canada, and the Danish National Research Foundation is gratefully acknowledged. The simulations were performed at the Finnish IT Center for Science, the HorseShoe (DCSC) supercluster at the University of Southern Denmark, and the SharcNet grid computing facility (www.sharcnet.ca).

References and Notes

(1) van den Brink-van der Laan, E.; Chupin, V.; Killian, J. A.; de Kruijff, B. *Biochemistry* **2004**, *43*, 5937−5942.
(2) Cantor, R. S. *J. Phys. Chem.* **1997**, *101*, 1723−1725.
(3) Cantor, R. S. *Biochemistry* **1997**, *36*, 2339−2344.
(4) Lindahl, E.; Edholm, O. *J. Chem. Phys.* **2000**, *113*, 3882−3893.
(5) Sonne, J.; Hansen, F. Y.; Peters, G. H. *J. Chem. Phys.* **2005**, 122, 124903.
(6) Patra, M. *Eur. Biophys. J.* **2005**, *135*, 79−88.
(7) Gullingsrud, J.; Schulten, K. *Biophys. J.* **2004**, *86*, 3496−3509.
(8) Niemelä, P.; Ollila, S.; Hyvönen, M. T.; Karttunen, M.; Vattulainen, I. *PLoS Comput. Biol.* **2007**, *3*, 304−312.
(9) Ollila, S.; Róg, T.; Karttunen, M.; Vattulainen, I. *J. Struct. Biol.* **2007**, *159*, 311−323.
(10) Ollila, S.; Hyvönen, M. T.; Vattulainen, I. *J. Phys. Chem. B* **2007**, *111*, 3139−3150.
(11) Barry, J. A.; Gawrisch, K. *Biochemistry* **1995**, *34*, 8852−8860.
(12) Barry, J. A.; Gawrisch, K. *Biochemistry* **1994**, *33*, 8082−8088.
(13) Feller, S. E.; Brown, C. A.; Nizza, D. T.; Gawrisch, K. *Biophys. J.* **2002**, *82*, 1396−1404.
(14) Holte, L. L.; Gawrisch, K. *Biochemistry* **1997**, *36*, 4669−4674.
(15) Klemm, W. R. *Alcohol* **1998**, *15*, 249−267.
(16) Klemm, W. R.; Williams, H. J. *Alcohol* **1996**, *13*, 133−138.
(17) Wachtel, E.; Borochov, N.; Bach, D.; Miller, I. R. *Chem. Phys. Lipids* **1998**, *92*, 127−137.
(18) Ly, H. V.; Longo, M. L. *Biophys. J.* **2004**, *87*, 1013−1033.
(19) Ly, H. V.; Block, D. E.; Longo, M. L. *Langmuir* **2002**, *18*, 8988−8995.
(20) Aagaard, T. H.; Kristensen, M. N.; Westh, P. *Biophys. Chem.* **2006**, *119*, 61−68.
(21) Westh, P.; Trandum, C. *J. Phys. Chem. B* **2000**, *104*, 11334−11341.
(22) Xu, Y.; Tang, P. *Biochim. Biophys. Acta* **1997**, *1323*, 154−162.
(23) Pasenkiewicz-Gierula, M.; Róg, T.; Grochowski, J.; Serda, P.; Czarnecki, R.; Librowski, T.; Lochyński, S. *Biophys. J.* **2003**, *85*, 1248−1258.
(24) Cantor, R. S. *J. Phys. Chem. B* **2001**, *105*, 7550−7553.
(25) Lee, B. W.; Faller, R.; Sum, A. K.; Vattulainen, I.; Patra, M.; Karttunen, M. *Fluid Phase Equilib.* **2004**, *225*, 63−68.
(26) Patra, M.; Salonen, E.; Terama, E.; Vattulainen, I.; Faller, R.; Lee, B. W.; Holopainen, J.; Karttunen, M. *Biophys. J.* **2006**, *90*, 1121−1135.
(27) Dickey, A. N.; Faller, R. *Biophys. J.* **2007**, *92*, 2366−2376.
(28) Griepernau, B.; Leis, S.; Schneider, M. F.; Sikor, M.; Steppich, D.; Bockmann, R. A. *Biochim. Biophys. Acta* **2007**, *1768*, 2899−2913.

(29) Aratono, M.; Toyomasu, T.; Villeneuve, M.; Uchizono, Y.; Takiue, T.; Motomoura, K.; Ikeda, N. *J. Colloid Interface Sci*. **1999**, *191*, 146−153.
(30) Dickey, A. N.; Faller, R. *J. Polym. Sci., Part B: Polym. Phys.* **2005**, *43*, 1025−1032.
(31) Kranenburg, M.; Vlaar, M.; Smit, B. *Biophys. J.* **2004**, *87*, 1596−1605.
(32) Frischknecht, A. L.; Frink, L. J. D. *Biophys. J.* **2006**, *91*, 4081−4090.
(33) Chanda, J.; Chakraborty, S.; Bandyopadhyay, S. *J. Phys. Chem. B* **2006**, *110*, 3791−3797.
(34) Brahm, J. *J. Gen. Physiol*. **1983**, *81*, 283−304.
(35) Rowe, E. S. *Biochim. Biophys. Acta* **1985**, *813*, 321−330.
(36) Rowe, E. S. *Biochemistry* **1983**, *22*, 3299−3305.
(37) Westh, P.; Trandum, C.; Koga, Y. *Biophys. Chem.* **2001**, *89*, 53−63.
(38) Bemporad, D.; Essex, J. W.; Luttmann, C. *J. Phys. Chem. B* **2004**, *108*, 4875−4884.
(39) Cantor, R. S. *Biophys. J.* **2001**, *80*, 2284−2297.
(40) Hope, M. J.; Bally, M. B.; Mayer, L. D.; Janoff, A. S.; Cullis, P. R. *Chem. Phys. Lipids* **1986**, *40*, 89−107.
(41) MacDonald, R. C.; MacDonald, R. I.; Menco, B. P. M.; Takeshita, K.; Subbarao, N. K.; Hu, L. *Biochim. Biophys. Acta* **1991**, *1061*, 297−303.
(42) Zhang, F.; Rowe, E. S. *Biochemistry* **1992**, *31*, 2005−2011.
(43) Lindahl, E.; Hess, B.; van der Spoel, D. *J. Mol. Model.* **2001**, *7*, 306−317.
(44) Essman, U.; Perera, L.; Berkowitz, M. L.; T. Darden, H. L.; Pedersen, L. G. *J. Chem. Phys.* **1995**, *103*, 8577−8592.
(45) Patra, M.; Karttunen, M.; Hyvnen, M. T.; Falck, E.; Lindqvist, P.; Vattulainen, I. *Biophys. J.* **2003**, *84*, 3636−3645.
(46) Patra, M.; Karttunen, M.; Hyvnen, M. T.; Falck, E.; Vattulainen, I. *J. Phys. Chem. B* **2004**, *108*, 4485−4494.
(47) Berendsen, H. J. C.; Postma, J. P. M.; van Gunsteren, W. F.; DiNola, A.; Haak, J. R. *J. Chem. Phys.* **1984**, *81*, 3684−3690.
(48) Berger, O.; Edholm, O.; Jahnig, F. *Biophys. J.* **1997**, *72*, 2002−2013.
(49) Tieleman, D. P.; Berendsen, H. J. C. *J. Chem. Phys.* **1996**, *105*, 4871−4880.
(50) Berendsen, H. J. C.; Postma, J. P. M.; van Gunsteren, W. F.; Hermans, J. In *Intermolecular Forces*; Pullman, B. Ed.; Reidel: Dordrecht, The Netherlands, 1981; pp 331−342.
(51) Katz, Y.; Diamond, J. M. *J. Membr. Biol.* **1974**, *17*, 101−120.
(52) Trandum, C.; Westh, P.; Jørgensen, K.; Mouritsen, O. G. *Biophys. J.* **2000**, *78*, 2486−2492.
(53) Trandum, C.; Westh, P.; Jørgensen, K.; Mouritsen, O. G. *Biochim. Biophys. Acta* **1999**, *1420*, 179−188.
(54) Dill, K. A.; Naghizadeh, J.; Marqusee, J. A. *Annu. Rev. Phys. Chem.* **1988**, *39*, 425−461.
(55) DeYoung, L. R.; Dill, K. A. *Biochemistry* **1988**, *27*, 5281−5289.
(56) Rottenberg, H. *Biochemistry* **1992**, *31*, 9473−9481.
(57) Tristram-Nagle, S.; Petrache, H. I.; Nagle, J. F. *Biophys. J.* **1998**, *75*, 917−925.
(58) Wiener, M. C.; White, S. H. *Biophys. J.* **1992**, *61*, 434−447.
(59) Santos, N. C.; Prieto, M.; Castanho, M. A. R. B. *Biochim. Biophys. Acta* **2003**, *1612*, 123−135.
(60) Sarasua, M. M.; Faught, K. R.; Steedman, S. L.; Gordin, M. D.; Washington, M. K. *Alcohol.: Clin. Exp. Res.* **1989**, *13*, 698−705.
(61) Falck, E.; Patra, M.; Karttunen, M.; Hyvönen, M. T.; Vattulainen, I. *Biophys. J.* **2004**, *87*, 1076−1091.
(62) Falck, E.; Patra, M.; Karttunen, M.; Hyvönen, M. T.; Vattulainen, I. *Biophys. J.* **2005**, *89*, 745−752.
(63) Dalton, L. A.; Miller, K. W. *Biophys. J.* **1993**, *65*, 1620−1631.
(64) Abadji, V.; Raines, D. E.; Dalton, L. A.; Miller, K. W. *Biochim. Biophys. Acta* **1994**, *1194*, 25−34.
(65) Seto, T.; Firestone, L. L. *Biochim. Biophys. Acta* **2000**, *1509*, 111−122.
(66) Chanda, J.; Bandyopadhyay, S. *Langmuir* **2006**, *22*, 3775−3781.
(67) Szleifer, I.; Kramer, D.; Ben-Shaul, A.; Gelbart, W. M.; Safran, S. A. *J. Chem. Phys.* **1990**, *92*, 6800−6817.
(68) Gullingsrud, J.; Babakhani, A.; McCammon, J. A. *Mol. Simul.* **2006**, *32*, 831−838.

V

Publication V

Ollila, O. H. S., Risselada, J., Louhivuori, M., Lindahl, E., Vattulainen, I., and Marrink, S. J., 3D Pressure field in lipid membranes and membrane-protein complexes, Physical Review Letters 102, 078101 (2009).

3D Pressure Field in Lipid Membranes and Membrane-Protein Complexes

O. H. Samuli Ollila,[1] H. Jelger Risselada,[2] Martti Louhivuori,[2] Erik Lindahl,[3] Ilpo Vattulainen,[1,4,5] and Siewert J. Marrink[2]

[1]*Department of Physics, Tampere University of Technology, P.O. Box 692, FI–33101 Tampere, Finland*
[2]*Department of Biophysical Chemistry, University of Groningen, Nijenborgh 4, 9747 AG Groningen, The Netherlands*
[3]*Department of Biochemistry and Biophysics, Stockholm University, SE-10691, Sweden*
[4]*Department of Applied Physics, Helsinki University of Technology, P.O. Box 1100, FI–02015 HUT, Finland*
[5]*MEMPHYS–Center for Biomembrane Physics, Physics Department, University of Southern Denmark, Campusvej 55, DK-5230 Odense M, Denmark*

(Received 19 September 2008; published 19 February 2009)

We calculate full 3D pressure fields for inhomogeneous nanoscale systems using molecular dynamics simulation data. The fields represent systems with increasing level of complexity, ranging from semivesicles and vesicles to membranes characterized by coexistence of two phases, including also a protein-membrane complex. We show that the 3D pressure field is distinctly different for curved and planar bilayers, the pressure field depends strongly on the phase of the membrane, and that an integral protein modulates the tension and elastic properties of the membrane.

DOI: 10.1103/PhysRevLett.102.078101 PACS numbers: 87.16.D−, 87.16.A−, 87.15.A−

Introduction.—The lateral pressure profile, or stress profile, across a cell membrane results from the inhomogeneous nature of the interactions within a membrane. As water, head groups, and acyl chains contribute through different forces, one finds the emergence of a nonuniform pressure profile inside a lipid bilayer. The profile has been proposed to be coupled to membrane-protein structure and functionality in a manner where changes in the pressure profile affect protein activation [1,2] and/or association [3]. The moments of the pressure profile can be connected, e.g., to the mean and Gaussian bending elasticity [4].

While experimental studies of lateral pressure profiles are rare and indirect [5,6], several computational studies have shed light on pressure profiles of planar lipid bilayers [7–10]. In these studies, a bilayer is divided into slabs perpendicular to the membrane normal, and pressure is calculated in each slab. However, this approach does not work for vesicles, membranes with proteins, or heterogeneous bilayers, because in these physiologically relevant cases the pressure profile can not be characterized by the normal coordinate as in a planar bilayer; there is a 3D field instead of a profile. Yet it has been shown that the work exerted by the pressure profile when a protein conformational change takes place is significant, of the order of $10k_BT$ [11,12], and that the lateral pressure profile averaged over the whole membrane is modified by the inclusion of a membrane protein [13]. Indeed, understanding the full 3D coupling for stress arising from protein-lipid interactions is of profound importance and calls for elucidation.

Here, we calculate the full 3D pressure field for a number of systems with varying degree of complexity using molecular dynamics simulations. We define the 3D pressure tensor and derive expressions for planar and spherical symmetry. We apply the new methodology to three cases: lipid vesicles, a membrane with an embedded protein, and a bilayer with liquid-gel phase coexistence. The membrane embedded protein, MscL, is of particular interest as it is mechanosensitive, i.e., it gates in response to membrane tension [14,15].

Theoretical background.—The pressure for an inhomogenous system is represented as a tensor $\mathbf{P}(\mathbf{r})$ that depends on the location $\mathbf{r}$. For a system consisting of pointwise particles with n-body potentials U^n the local pressure can be defined as a sum of kinetic and configurational contribution [8,10,16,17]:

$$p^{\alpha\beta}(\mathbf{r}) = \sum_i m_i v_i^\alpha v_i^\beta \delta(\mathbf{r}-\mathbf{r}_i) - \sum_n \frac{1}{n} \sum_{\langle j\rangle} \sum_{\langle k,l\rangle} (\nabla_{j_k}^\alpha U^n - \nabla_{j_l}^\alpha U^n) \oint_{C_{j_l j_k}} dl^\beta \delta(\mathbf{r}-\boldsymbol{l}), \tag{1}$$

where $C_{j_l j_k}$ is a contour from the particle j_l to the particle j_k, $\langle j\rangle$ stands for summation over all n clusters in the system, $\langle k, l\rangle$ describes summation over all pairs of particles within a given n cluster, and m_i, v_i, and $\mathbf{r}_i$ refer to the mass, velocity, and location of atom i, respectively, and α and β refer to the components. Equation (1) gives a continuous pressure field. To find the pressure tensor $\mathbf{P}_V$ for a volume element V, we have to take an average over the volume element $\mathbf{P}_V = \int_V \mathbf{P}(\mathbf{r}) d\mathbf{r}/V$. Together with Eq. (1) one finds the pressure tensor for volume V

$$p_V^{\alpha\beta} = \frac{1}{V} \sum_{i\in V} m_i v_i^\alpha v_i^\beta + \sum_n \frac{1}{nV} \sum_{\langle j\rangle} \sum_{\langle k,l\rangle} (\nabla_{j_k}^\alpha U^n - \nabla_{j_l}^\alpha U^n) \frac{r_{j_l j_k}^\beta}{N} \times \sum_{\lambda=0}^{N} f_V(\mathbf{r}_{j_l} + \frac{\lambda}{N}\mathbf{r}_{j_l j_k}), \tag{2}$$

where $f_V(\mathbf{r}) = 1$, if $\mathbf{r} \in V$, and zero otherwise. Each vec-

tor $\mathbf{r}_{j_l j_k} = \mathbf{r}_{j_k} - \mathbf{r}_{j_l}$ is divided into N parts and the contribution of a given part λ is added only if the contour goes through V, i.e., if $f_V = 1$. For the contour we use the Irving-Kirkwood (IK) contour [18], see the supplementary material (SM) [19]. We call $\mathbf{P}_V(\mathbf{r})$ as pressure field.

For a system with planar symmetry the local pressure can be divided into planar p_L and normal components p_{zz} via $\mathbf{P}(z) = (\mathbf{e_x e_x} + \mathbf{e_y e_y})p_L(z) + \mathbf{e_z e_z} p_{zz}(z)$, where the coordinate z is along the membrane normal. It follows from planar symmetry that $p_L(z) = p_{xx}(z) = p_{yy}(z)$ depends only on z. Furthermore, the surface tension of a layer between z_1 and z_2 is given by [20] $\gamma = -\int_{z_1}^{z_2} dz \pi(z)$. Traditionally, the integrand of this equation $\pi(z) = p_L(z) - p_{zz}(z)$ is referred to as the lateral pressure profile. The first moment of $\pi(z)$ gives an example of a connection to elastic properties of a layer between z_1 and z_2 [4] via $c_0\kappa = \int_{z_1}^{z_2} dz(z - z_0)\pi(z)$, where c_0 denotes the spontaneous curvature with respect to a pivotal plane z_0, and κ the bending modulus.

For a system with spherical symmetry, e.g., a vesicle, we divide the pressure tensor into tangential p_T and radial p_{rr} components $\mathbf{P}(\mathbf{r}) = (\mathbf{e}_\theta \mathbf{e}_\theta + \mathbf{e}_\phi \mathbf{e}_\phi)p_T(r) + \mathbf{e_r e_r} p_{rr}(r)$, where r is the distance from the origin of the coordinate system. From spherical symmetry, it follows that $p_T(r) = p_{\theta\theta}(r) = p_{\phi\phi}(r)$ depend only on r. A spherical surface with radius R has a surface tension [20]

$$\sigma = -(1/R^2) \int_0^\infty dr r^2 [p_T(r) - p_{rr}(r)]. \qquad (3)$$

The pressure tensor for a system with cylindrical or approximately cylindrical symmetry, e.g., a membrane protein, is discussed in the SM [19]. The pressure tensor becomes diagonal when the coordinate system aligns with the physical surface.

Implementation.—We discretize Eq. (1) into cubes, typically with a linear dimension of 0.1–0.4 nm, allowing us to calculate the average pressure over arbitrary volume elements. The local pressure tensor is calculated for each cube using Eq. (2). The vector between two particles is divided into $N = 100$ segments in Eq. (2). Though increasing N increases computational cost, the segments must be smaller than the cube size.

For a system with spherical symmetry, the pressure tensor is transformed in each cube from Cartesian coordinates $\mathbf{P}(x, y, z)$ to spherical ones $\mathbf{P}'(r, \theta, \phi)$ by applying a transformation matrix $\mathbf{T}$, i.e., $\mathbf{P}' = \mathbf{T}\mathbf{P}\mathbf{T}^T$ [21]. The average of the pressure tensor is calculated over spherical shells $\mathbf{P}'(r) = \langle \mathbf{P}'(r, \theta, \phi) \rangle_{\theta,\phi}$ to get $p_T(r)$ and $p_{rr}(r)$. A similar approach for cylindrical symmetry is described in the SM [19]. Here we refer to these averages as pressure profiles.

For the sake of validation, we also determined the pressure profile in a vesicular system using a novel mean-field boundary potential method [22]. The advantage of this method is the freedom from ambiguity in the virial definition, Eq. (1). See the SM for details [19].

Simulated systems.—The GROMACS package [23] was used for simulations. The coarse grained (CG) MARTINI force field and attached simulation protocol [24–26] were used to model the systems. The temperature was set to 323 K except in the phase coexistence simulation it was 273 K. Time scales are given in CG units. In addition to a DPPC semivesicle, we studied a spherical DOPC vesicle with different amounts of water inside to create two systems with different internal pressures. A tension-free planar DOPC bilayer was modeled for comparison. Further, we modeled a two-phase DPPC bilayer at a constant area per lipid of 0.52 nm^2. The constant area creates a surface tension of 69 mN/m and forces the membrane into a gel-liquid phase coexistence. Finally, a mechanosensitive channel Tb-MscL (PDB: 2oar) was simulated in a DOPC bilayer following [15]. A tension of 39 mN/m was applied to keep MscL in the open state. More details are in [19].

Results.—We first compare the results obtained with the new method to the results obtained independently with the mean-field boundary approach. The comparison is made for a semivesicle adsorbed on a boundary plane. Figure 1 depicts the tangential component $p_T(r)$ for the semivesicle as a function of r calculated using both methods. We see that the virial, Eq. (2), together with the IK contour gives similar results as the force per area calculated from the boundary. In the virial calculation the semivesicle is assumed to be spherically symmetric. This is not exactly true in our case, which leads to the small deviations between the two cases. The results justify the use of the IK contour to calculate local virials in three dimensions.

Because of its curved geometry, a vesicular membrane has distinct properties compared to a lamellar membrane, most noticeable with small radius of curvature. The effect of curvature on the pressure profile across the membrane has not been addressed before. The 3D virial decomposition method allows such an analysis. In Fig. 2(a) the results of this analysis, assuming spherical symmetry for the vesicle, are shown. The pressure is set to zero outside the vesicle, yielding the pressure difference $\Delta\mathbf{P} = \mathbf{P}(r) - \mathbf{P}_{\text{out}}$. The pressure profile for a planar, tensionless DOPC

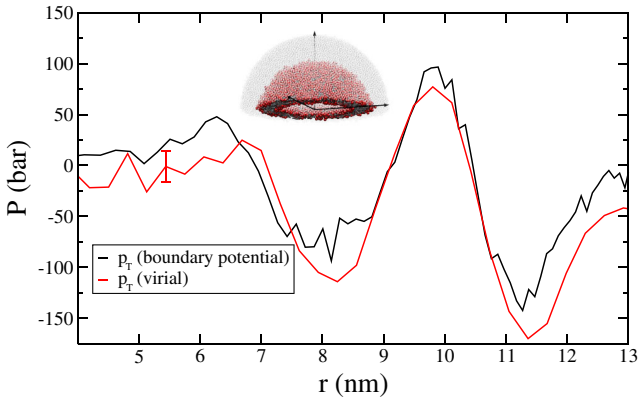

FIG. 1 (color online). The $p_T(r)$ for the DPPC semivesicle as a function of r calculated using mean-field and virial methods.

bilayer is shown for comparison, shifted horizontally such that the negative peaks of the inner monolayer coincide. Most striking differences are the magnitudes of the peaks and the asymmetry in the pressure profile of a vesicle. The asymmetry results from different packing properties [27]: in the inner monolayer the headgroup peak is more pronounced due to the negative curvature and tighter packing of the headgroups, and *vice versa* for the outer monolayer. The broader peaks reflect a less clear boundary between hydrophilic and hydrophobic regions in a vesicle. The results highlight the role of curvature and imply that the pressure profile, and the associated elastic behavior are distinctly different for small vesicles compared to large unilamellar liposomes.

Pressure profiles between vesicles with different internal pressures are compared in Fig. 2(b). The pressure difference is obvious from different bulk values inside the vesicles. Furthermore, the increasing pressure inside a vesicle increases the vesicle size and induces tension into the bilayer quantified by Eq. (3). We approximate the limits of σ considering a minimal and maximal radius R given by the intersections of water and hydrocarbon densities for each monolayer (see Fig. 2). We find $\sigma \approx -(1\text{–}6)$ mN/m and $\sigma \approx (45\text{–}91)$ mN/m for the smaller and larger vesicle, respectively. Comparing these tensions to the experimentally determined gating tension of MscL [28] that is $\sim(10\text{–}20)$ mN/m suggests that if incorporated into these vesicles, the channel would be closed in the smaller one and open in the swollen one.

Next, we analyze the stress profile of a DOPC bilayer with an open MscL channel embedded. We assume cylindrical symmetry and take the average over angles, see the SM [19]. Figure 3(a) presents $\pi(z, r)$ as a function of z (normal coordinate of the bilayer) and r (distance from the center of MscL in cylindrical coordinates). Figure 3(b) shows the surface tension γ for the monolayers and the bilayer. The total tension of the system is (38 ± 1) mN/m as set by the barostat to keep the MscL channel in an open state. However, the tension varies strongly with the lateral position. In the protein region ($r < 4$ nm) the average tension is 33 ± 1 mN/m whereas in the bilayer region ($r > 4$ nm) it is 43 ± 1. This perturbing effect of the protein is maintained across the entire membrane patch. A slowly decaying stress field around the protein is not observed.

Another conclusion drawn from Fig. 3(b) is that the monolayers behave differently. The average tensions for the lower and upper leaflets, protein region included, are (14 ± 1) mN/m and (23 ± 1) mN/m, respectively. The higher tension in the upper leaflet implies that it tends to decrease the area more than the lower one. As a consequence, emergence of spontaneous curvature in the bilayer is anticipated. To quantify this, we calculate the first moment of the pressure profile, see Fig. 3(c). The average over the bilayer region ($r > 4$ nm) gives $\kappa c_0 = (-43 \pm 6) \times 10^{-13}$ J/m for the bilayer, while the average over the whole system yields $\kappa c_0 = (-151 \pm 6) \times 10^{-13}$ J/m. Experimental values for κ for different lipid bilayers vary between $(0.1 - 6) \times 10^{-19}$ J [29]. The effect of an embedded protein on κ is unknown, but a recent simulation study suggests that the area compressibility modulus is

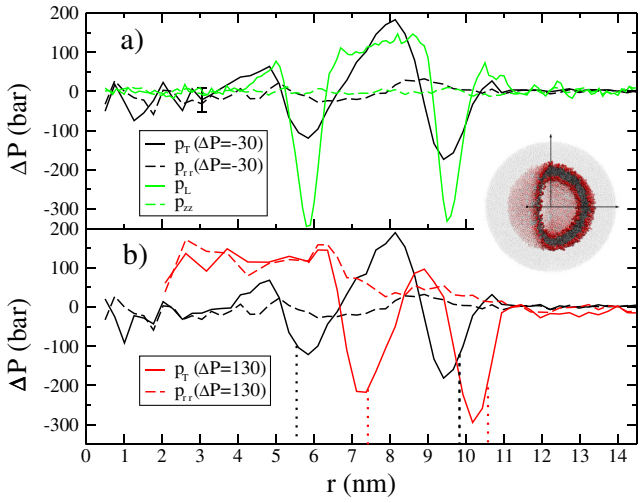

FIG. 2 (color online). Pressure profiles for DOPC bilayers and vesicles. (a) For the bilayer, the solid line and dashed green line stand for p_L and p_{zz}, respectively. For the vesicle, the solid line and dashed black line correspond to p_T and p_{rr} with $\Delta P \approx -30$ bar, in respective order. (b) Results for the vesicle with $\Delta P \approx 130$ bar. Solid line and dashed red line correspond to p_T and p_{rr}, respectively. Black lines are as in panel (a). Vertical dotted lines show the location of intersections between acyl chain and water density.

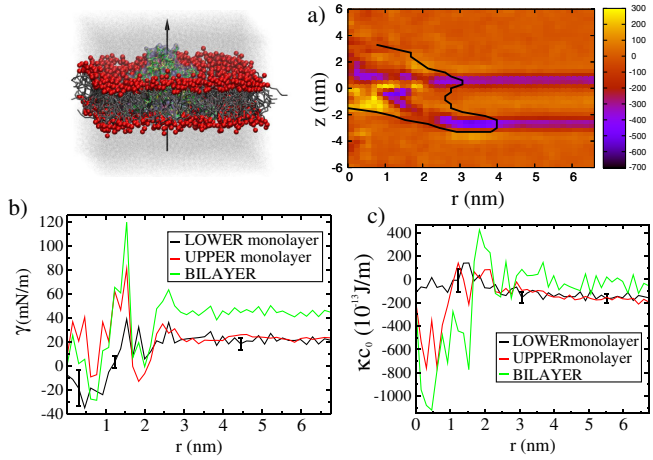

FIG. 3 (color online). Pressure profile of a membrane-protein system. (a) Horizontal axis is the distance from protein center, vertical axis is the normal component of the bilayer (protein center at $z = 0$). The lower and upper leaflets are characterized by $z \in [-4, -1)$ nm and $z \in [-1, 2]$ nm, respectively, and color represents the local pressure (in units of bar). The approximate boundary of the protein region is presented with a full black line (see the SM [19]). (b) Surface tension γ as a function of distance from the protein center r. (c) Product κc_0 vs r. Pivotal planes are located in $z_0 = -2$ nm and $z_0 = 0$ nm, for lower and upper [see order in panel (a) leaflets], respectively.

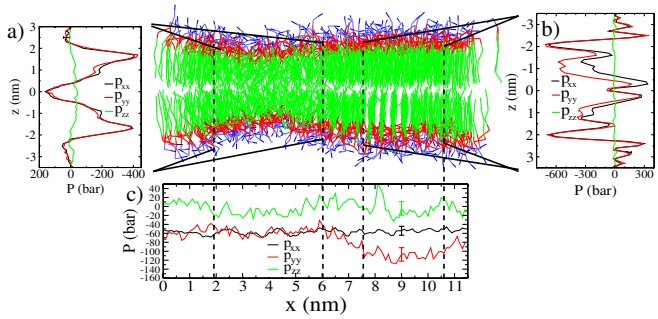

FIG. 4 (color online). Pressure tensor components in (a) liquid and (b) gel phases. (c) Pressure as a function of normal to the phase boundary $\mathbf{P}(x)$ (see text). The pure liquid phase is located between $x = 2$–6 nm and the pure gel between 7.5–10.5 nm.

increased 22% due to inclusion of MscL [30]. Similar behavior can be expected for κ. Using experimental values for κ, we approximate spontaneous curvatures for the whole system and the bilayer region, $c_0 = (-0.025) - (-1.5)\ (\mathrm{nm})^{-1}$ and $c_0 = (-0.0072) - (-0.43)\ (\mathrm{nm})^{-1}$, respectively.

Taken together, our results suggest that inclusion of MscL in a symmetric bilayer causes additional stress in the membrane and introduces a significant spontaneous curvature. In real membranes the spontaneous curvature would either lead to a curved membrane surface, and/or redistribution of lipids between the two leaflets. Here, these are not observed since the time scale of lipid flips-flops is inaccessible and the periodic boundary conditions prevent curving of the membrane.

Finally, we consider a DPPC bilayer in a state of gel-liquid phase coexistence, serving as an example for phase separated membranes. Figure 4 illustrates the liquid and gel domains separated by a $\sim$1.5 nm thick transition region. The lateral pressure profiles are shown in Figs. 4(a) and 4(b), for the liquid and gel phase, respectively. Planar symmetry is assumed for the gel and liquid parts separately. The pressure profile for the liquid phase is similar to that of a homogeneous fluid bilayer as shown in Fig. 2(a). In contrast, in the gel phase it is strikingly different, and is closely reminiscent of the profiles found for bilayers with large amounts of cholesterol [11]. Clearly, the pronounced ordering of the acyl chains in a bilayer gives rise to the complex peaked structure of the pressure profile, complemented by its anisotropic nature in the gel phase.

The pressure field averaged over y and z coordinates $\mathbf{P}(x) = \langle \mathbf{P}(x, y, z) \rangle_{yz}$ is presented in Fig. 4(c). Both lateral components are negative, as the bilayer is under stress, inducing gel-liquid coexistence. Whereas $p_{xx}(x)$ and $p_{zz}(x)$ are basically constant, $p_{yy}(x)$ is smaller in the gel than in the liquid phase. This is due to the phase boundary lying along the y direction, with an associated line tension.

Concluding remarks.—We have shown the prominent role of 3D stress profiles inside membranes and membrane-protein complexes. The pressure field is distinctly nonuniform both across the membranes and also in the membrane plane. This is most evident at interfaces that bridge membrane domains in different phases, and in membranes rich in proteins where the pressure field and the resulting membrane elasticity vary strongly in space. The present results provide a novel view of the general interplay between membranes and proteins.

We acknowledge H. J. C. Berendsen for fruitful discussions. We thank the Finnish Cultural Foundation, Academy of Finland, Swedish Research Council, Foundation for Strategic Research, the Marie Curie research program, and the Netherlands Organisation for Scientific Research (NWO) for financial support.

[1] R. S. Cantor, J. Phys. Chem. B **101**, 1723 (1997).
[2] M. F. Brown, Chem. Phys. Lipids **73**, 159 (1994).
[3] A. V. Botelho *et al.*, Biophys. J. **91**, 4464 (2006).
[4] S. A. Safran, *Statistical Thermodynamics of Surfaces, Interfaces, and Membranes* (Addison-Wesley, Reading, MA, 1994).
[5] R. H. Templer *et al.*, Faraday Discuss. **111**, 41 (1999).
[6] T. Kamo *et al.*, J. Phys. Chem. B **110**, 24987 (2006).
[7] J. Sonne *et al.*, J. Chem. Phys. **122**, 124903 (2005).
[8] E. Lindahl and O. Edholm, J. Chem. Phys. **113**, 3882 (2000).
[9] J. Gullingsrud and K. Schulten, Biophys. J. **86**, 3496 (2004).
[10] S. Ollila *et al.*, J. Phys. Chem. B **111**, 3139 (2007).
[11] O. H. S. Ollila *et al.*, J. Struct. Biol. **159**, 311 (2007).
[12] P. S. Niemelä *et al.*, PLoS Comput. Biol. **3**, 304 (2007).
[13] J. Gullingsrud *et al.*, Mol. Simul. **32**, 831 (2006).
[14] S. Sukharev *et al.*, Nature (London) **409**, 720 (2001).
[15] S. Yefimov *et al.*, Biophys. J. **94**, 2994 (2008).
[16] P. Schofield and J. R. Henderson, Proc. R. Soc. A **379**, 231 (1982).
[17] R. Goetz and R. Lipowsky, J. Chem. Phys. **108**, 7397 (1998).
[18] J. H. Irving and J. G. Kirkwood, J. Chem. Phys. **18**, 817 (1950).
[19] See EPAPS Document No. E-PRLTAO-102-030909 for technical details. For more information on EPAPS, see http://www.aip.org/pubservs/epaps.html.
[20] J. S. Rowlinson and B. Widom, *Molecular Theory of Capillarity* (Clarendon Press, Oxford, 1982).
[21] G. B. Arfken and H. J. Weber, *Mathematical Methods for Physicists* (Academic Press, New York, 1995).
[22] H. J. Risselada *et al.*, J. Phys. Chem. B **112**, 7438 (2008).
[23] D. van der Spoel *et al.*, J. Comput. Chem. **26**, 1701 (2005).
[24] S. J. Marrink *et al.*, J. Phys. Chem. B **108**, 750 (2004).
[25] S. J. Marrink *et al.*, J. Phys. Chem. B **111**, 7812 (2007).
[26] L. Monticelli *et al.*, J. Chem. Theory Comput. **4**, 819 (2008).
[27] S. J. Marrink and A. E. Mark, J. Am. Chem. Soc. **125**, 15 233 (2003).
[28] P. Moe and P. Blount, Biochemistry **44**, 12 239 (2005).
[29] D. Marsh, Chem. Phys. Lipids **144**, 146 (2006).
[30] J. Jeon and G. A. Voth, Biophys. J. **94**, 3497 (2008).

SUPPLEMENTARY MATERIAL: 3D Pressure Field in Lipid Membranes and Membrane-Protein Complexes

O. H. Samuli Ollila,[1] H. Jelger Risselada,[2] Martti Louhivuori,[2]
Erik Lindahl,[3] Ilpo Vattulainen,[1,4,5] and Siewert-Jan Marrink[2]

[1] *Department of Physics, Tampere University of Technology, P. O. Box 692, FI–33101 Tampere, Finland*

[2] *Department of Biophysical Chemistry, University of Groningen, Nijenborgh 4, 9747 AG Groningen, the Netherlands*

[3] *Department of Biochemistry and Biophysics, Stockholm University, SE-10691, Sweden*

[4] *Department of Applied Physics, Helsinki University of Technology, P. O. Box 1100, FI–02015 HUT, Finland*

[5] *MEMPHYS – Center for Biomembrane Physics, Physics Department, University of Southern Denmark*

CHOICE OF THE CONTOUR BETWEEN TWO PARTICLES

As discussed by many authors, the choice of the contour in Eq. (1) is ambiguous. The original choice, the so-called Irving-Kirkwood contour, is a straight line from particle j_l to j_k (1). Another suggested contour, the so-called Harasima contour, goes along coordinate axes (2). Schofield et al. (3) showed that the choice of the contour is arbitrary. For planar bilayers, the contours yield consistent results (4), while in spherical systems the Harasima contour has been proposed to give non-physical results (5). Also theoretical arguments have been proposed in favor of the Irwing-Kirkwood contour (6), which is used in this work. Macroscopic observables such as the integral over the pressure profile, i.e. the interfacial tension, have been shown to be independent of the choice of the contour.

PRESSURE TENSOR IN CYLINDRICAL SYMMETRY

For a system with cylindrical symmetry, e.g. a membrane protein, we divide the pressure tensor into normal p_{zz}, angular $p_{\theta\theta}$ and radial p_{rr} components in cylindrical coordinates

$$\mathbf{P}(\mathbf{r}) = \mathbf{e}_\theta \mathbf{e}_\theta p_{\theta\theta}(r,z) + \mathbf{e_r} \mathbf{e_r} p_{rr}(r,z) + \mathbf{e_z} \mathbf{e_z} p_{zz}(r,z). \tag{S1}$$

Main difference between this and other coordinate systems discussed is that the tensor depends now on two variables r and z instead of one, and none of the components are equal due to the symmetry.

COORDINATE TRANSFORMATION OF THE PRESSURE TENSOR

The transformation matrix for the spherical symmetry case is (7)

$$\mathbf{T} = \begin{pmatrix} \sin\theta\cos\phi & \sin\theta\sin\phi & \cos\theta \\ \cos\theta\cos\phi & \cos\theta\sin\phi & -\sin\theta \\ -\sin\phi & \cos\phi & 0 \end{pmatrix}. \tag{S2}$$

In a spherically symmetric system the angle components are the same, i.e. $p'_{\theta\theta}(r) = p'_{\phi\phi}(r)$. Since the trace of a tensor is not changed in coordinate transformations, we have

$$p'_{\theta\theta}(r) = p'_{\phi\phi}(r) = \frac{1}{2}(\mathrm{Tr}[P(r)] - p'_{rr}). \tag{S3}$$

Thus, in principle, it is sufficient to transform only the radial component using the transformation matrix and then use Eq. (S3) to obtain the angular component. This gives the same result as usage of the transformation matrix for all components.

The transformation for the cylindrical symmetry can be done in the same way but the transformation matrix is different (7)

$$\mathbf{T}_{cyl} = \begin{pmatrix} \cos\theta & \sin\theta & 0 \\ -\sin\theta & \cos\theta & 0 \\ 0 & 0 & 1 \end{pmatrix}. \tag{S4}$$

AVERAGE OVER CYLINDRICAL SYMMETRY

In a cylindrically symmetric case we take an average over angle using the same idea as we did in the spherical and planar cases. The difference is that here we can average only over one coordinate instead of two in previous cases. To get $p_{zz}(r, z)$, $p_{\theta\theta}(r, z)$, and $p_{rr}(r, z)$ in Eq. (S1), we take the average over angle θ

$$\mathbf{P}(r, z) = \langle \mathbf{P}(r, \theta, z) \rangle_\theta. \tag{S5}$$

VALIDITY OF LAPLACE EQUATION FOR LIPID VESICLES

For an approximately spherical object, e.g. a lipid vesicle, the sphere radius R is easy to define if it is much larger than the thickness of the surface. If that is the case, then the Laplace equation

$$\sigma = \frac{R\Delta P}{2} \tag{S6}$$

can also be used to calculate the surface tension. The pressure difference between bulk inside and bulk outside ΔP is scalar because diagonal components of the pressure tensor are equivalent in bulk.

For very small membrane vesicles, this is not the case, and the calculation of the surface tension becomes problematic (8).

COMPARISON OF THE VIRIAL METHOD AND THE BOUNDARY POTENTIAL APPROACH

In order to justify the results from the direct virial calculations presented, we also determined the pressure profile in a vesicular system using a novel mean-field boundary potential method (9).

The boundary potential approach, developed to simulate vesicles at low computational cost, replaces excess solvent either inside and/or outside the vesicle. The pressure is obtained directly from the force per unit area which is exerted by the particles against the boundary. To study the pressure profile of a vesicle using this method, we simulated a semi-vesicle (see Fig. 1), i.e. a half vesicle adsorbed on a planar boundary. By dividing the boundary into circular slabs, the pressure acting on each slab can be calculated, yielding the tangential pressure profile $p_T(r)$ as a function of distance from the center. The advantage of this method is that it is free from ambiguity in the definition of the virial, i.e., Eq. (1). However, as the pressure is calculated at the surface of the boundary, only the tangential component is available.

We have used this approach to compare $p_T(r)$ calculated using the virial method and the boundary potential approach.

SIMULATION DETAILS

All the simulations were performed with the GROMACS molecular dynamics software (10) using the MARTINI coarse-grained model (11, 12). A 20 fs time step was used in all simulations. Temperature was coupled using the Berendsen thermostat with $\tau_T = 1.0\text{ps}^{-1}$. (13) The pressure in the system was coupled with either the Berendsen barostat (13), with coupling constant $\tau_P = 1.0\text{ps}^{-1}$ and compressibility $5 \times 10^{-5}\text{bar}^{-1}$, in the case of planar bilayers, or the Langevin piston method (see next section) with a friction coefficient of 60 ps^{-1} and a mass of 500 u in the case of the vesicular systems. The configurations were saved every 40-100 ps during simulation. All time scales given in the article and in this SM are in

simulation units and can be transformed to real units using a factor of four (11, 12).

Vesicle and Semi-vesicle

MFFA method - The vesicular systems were simulated using the MFFA (Mean Field Force Approximation) boundary method (9). Here, instead of using periodic boundary methods, boundary potentials with a predefined geometrical shape (e.g spherical, cylindrical and planar) are used to embed the system. The nature of these potentials is to reduce the surface tension which would otherwise occur in a system having a finite size. In vesicular systems, the usage of spherical boundaries makes it possible to reduce the surrounding solvent which enhances computational efficiency.

Langevin Piston - The coupling of pressure in vesicular systems is not trivial. Ideally, the surrounding solvent of the vesicle is under constant atmospheric pressure while the pressure of the solvent inside can be much higher due to osmotic conditions. In this case, coupling of the pressures which are derived from the internal virial of the total system is incorrect. Therefore, in this work the vesicular systems were coupled to an external pressure bath using the Langevin piston (14) method applied to non-periodic systems (15). Here, the position of the outer spherical boundary was coupled to the equations of motion using a Langevin integration scheme. The resultant force on the boundary piston is a result of both the force coming from the external pressure bath and the total force of the boundary on the particles in the system. In this case pressure is obtained as the force per unit boundary area. The method can be used when a pressure gradient is present, because this definition of pressure is local.

Vesicle - The spherical vesicle was formed spontaneously from 2217 DOPC lipids and filled twice with different amounts of water to create two systems with different internal pressures. The pressure differences between the inside and the outside of the vesicles were not known prior to the simulations. Temperature was coupled to 323 K and the pressure on the spherical boundary that enveloped the system was coupled to 1 bar using a Langevin piston.

The spontaneously formed lipid vesicle filled and surrounded with water equilibrated at a pressure of 1 bar was used as the starting configuration for the vesicle with small internal pressure. In total 130120 water beads were used, creating an approximately 5 nm thick

water layer around the vesicle. The system was simulated for 20 ns.

The starting configuration for the vesicle with large internal pressure was created by growing a cavity inside the vesicle and filling that with 8183 water beads. The cavity was slowly formed during a 21 ns simulation using an additional, slowly expanding mean-field boundary potential in the center of the vesicle. After the cavity was filled with water the additional internal boundary potential was removed. The system was simulated for 30 ns.

Semi-vesicle - The semi-vesicle system consisted of 1356 DPPC lipids and 41 675 water beads (see Fig. 1). It was simulated for 80 ns in a boundary potential (9) having the form of a hemi-sphere. Temperature was coupled to 323 K and the pressure on the boundary was coupled to 1 bar using a Langevin piston.

The semi vesicle was obtained from a complete DPPC vesicle formed by spontaneous aggregation of 2528 lipids under spherical boundary conditions. As the center of this vesicle was also nearly at the center of the simulation sphere, 'half' of the spherical system was cut through the geometrical center along the Z-axis. This yielded a 'semi-vesicle' consisting of 1356 DPPC lipids and 41675 water beads, with an approximately 3 nm thick water layer around the vesicle. Afterwards, a planar boundary potential was placed at the position of the cut. The interaction of the boundary with a particle was only dependent of the distance between the boundary and the particle along the Z-axis. The same boundary potential was used for both the membrane and the CG water. Although the potential was in fact parametrized for the CG water, it yielded a stable membrane connection with the boundary interface with only some increased ordering of the lipid chains located at the boundary as a result.

MscL in DOPC membrane

Mechanosensitive membrane protein MscL (PDB: 2oar) was simulated embedded in a DOPC lipid bilayer. MscL consists of 5 alpha-helical subunits each containing two transmembrane helices and a cytoplasmic cap-region. The bilayer consisted of 383 lipids and was solvated in 13966 water beads.

The starting configuration was formed by equilibrating a DOPC lipid bilayer, inserting the crystal structure of MscL approximately to the correct position relative to the bilayer, removing overlapping lipids and water and running an equilibration simulation until the

system had stabilised. A lateral pressure of -30 bar was then imposed on the system creating a tension of -39 mN/m, which is large enough to keep MscL in the open state, and a simulation of 700 ns was performed using 20 fs time steps.

A tension-free DOPC bilayer, consisting of 512 lipids and 15009 water beads was also modeled for comparison.

DPPC membrane with phase coexistence

A DPPC bilayer consisting of 512 lipids and 6000 water beads was equilibrated at 323 K and a pressure of 1 bar for 10 ns. This equilibrated bilayer was cooled to 273 K until the area per lipid was 0.52 nm^2. After this point the simulation was continued under a constant area constraint for 120 ns (x,y-dimensions). The dimension normal to the membrane (z-dimension) remained coupled to 1 bar. The constant area creates a surface tension of 69 mN/m and forces the membrane into a state of gel-liquid phase coexistence.

STABILITY CONDITION IN SPHERICAL SYSTEMS

From spherical symmetry and the condition for mechanical equilibrium $\nabla \cdot \mathbf{P} = 0$, it follows that $p_T(r) = p_{\theta\theta}(r) = p_{\phi\phi}(r)$ depend only on r and that the pressure difference between $r = 0$ and $r = \infty$ is (16)

$$\Delta P = -2 \int_0^\infty \mathrm{d}r \frac{1}{r}[p_T(r) - p_{rr}(r)]. \tag{S7}$$

A useful cross-check for the calculated pressure fields of the vesicles is the fulfilment of this stability condition for spherical systems. To check this, we calculate the pressure difference between the inside and the outside in two ways: as a difference between bulk values inside and outside the vesicle, and using the integral on the right-hand side of Eq. (S7). The first approach results in $\Delta P \approx (128 \pm 10)$ bar and $\Delta P \approx (-18 \pm 10)$ bar for the two systems with large and smaller amounts of water inside the vesicle, respectively. The second approach yields $\Delta P \approx (123 \pm 10)$ bar and $\Delta P \approx (-22 \pm 10)$ bar, in respective order. The results show that the computed pressure fields fulfil the stability condition.

MEMBRANE PROTEIN AVERAGES AND PROTEIN BOUNDARY

To simplify analysis we approximated MscL as cylindrically symmetric. Of course this is only a rough estimate, because MscL is actually five fold symmetric. However, taking angle dependency into account would complicate the analysis substantially, thus as a first approximation we assume cylindrical symmetry to hold. In future studies angle dependency will also be included. In the gif animation, movie.gif, is presented the full 3D tension field, $\pi(z,r) = p_L(z,r) - p_N$, for the MscL system by taking cross-sections through the system.

To approximate the boundary of the protein, the system is first divided into the same grid of small cubes as in pressure calculations and the cumulative density in each cube is calculated. Then the density field is averaged over angle in the same way as the pressure field. The boundary is defined to be where the cumulative density is 10-20 % of the maximum.

In Fig 3 a) of the article, the lateral pressure profile $\pi(z,r) = p_L(z,r) - p_N$ is presented. It would be also possible to present other profiles calculated from the pressure components. The lateral pressure profile is chosen because it can be connected to elastic properties of the bilayer.

CALCULATION OF ERROR BARS

In principle, the pressure field of bulk water in the fluid phase is constant and the tension is zero. However, in simulations, values for bulk water are fluctuating around constant values due to statistical fluctuations. The size of these fluctuations in the bulk water region are determined for each system and the error bars shown for pressure and tension are the maximum fluctuations from the average value in bulk water.

1. J. H. Irving and J. G. Kirkwood, J. Chem. Phys. **18**, 817 (1950).
2. A. Harasima, Adv. Chem. Phys. **1**, 203 (1958).
3. P. Schofield and J. R. Henderson, Proc. R. Soc. London, Ser. A **379**, 231 (1982).
4. J. Sonne, F. Y. Hansen, and G. H. Peters, J. Chem. Phys. **122**, 124903 (2005).
5. B. Hafskjold and T. Ikeshoji, Phys. Rev. E **66**, 011203 (2002).
6. L. Mistura, Int. J. Thermophys. **8**, 397 (1987).

7. G. B. Arfken and H. J. Weber, *Mathematical Methods for Physicist* (Academic Press, 1995).
8. S. H. White, Proc. Natl. Acad. Sci. USA **77**, 4048 (1980).
9. H. J. Risselada, A. E. Mark, and S. J. Marrink, J. Phys. Chem. B. **112**, 7438 (2008).
10. D. van der Spoel, E. Lindahl, B. Hess, G. Groenhof, A. E. Mark, and H. J. C. Berendsen, J. Comp. Chem. **26**, 1701 (2005).
11. S. J. Marrink, H. J. Risselada, S. Yefimov, D. P. Tieleman, and A. H. de Vries, J. Phys. Chem. B **111**, 7812 (2007).
12. L. Monticelli, S. K. Kandasamy, X. Periole, R. G. Larson, D. P. Tieleman, and S.-J. Marrink, J. Chem. Theor. Comp. **4**, 819 (2008).
13. H. J. C. Berendsen, J. P. M. Postma, W. F. van Gunsteren, A. DiNola, and J. R. Haak, J. Chem. Phys. **81**, 3684 (1984).
14. S. E. Feller, Y. Zang, R. W. Pastor, and B. R. Brooks, J. Chem. Phys. **103**, 4613 (1995).
15. H. Heller, M. Schaefer, and K. Schulten, J. Phys. Chem. **97**, 8343 (1993).
16. J. S. Rowlinson and B. Widom, Molecular Theory of Capillarity (Clarendon press, Oxford, 1982).

VI

Publication VI

Ollila, O. H. S., Louhivuori, M., Marrink, S. J., and Vattulainen, I.,Protein shape change has a major effect on the gating energy of a mechanosensitive channel, submitted (2010)

Protein shape change has a major effect on the gating energy of a mechanosensitive channel

O. H. Samuli Ollila
Department of Physics, Tampere University of Technology, P. O. Box 692, FI–33101 Tampere, Finland

Martti Louhivuori and Siewert J. Marrink
Groningen Biomolecular Sciences and Biotechnology Institute & Zernike Institute for Advanced Materials, University of Groningen, Nijenborgh 4, 9747 AG Groningen, the Netherlands

Ilpo Vattulainen
Department of Physics, Tampere University of Technology, P. O. Box 692, FI–33101 Tampere, Finland
Department of Applied Physics, Aalto University School of Science and Technology, P. O. Box 1100, FI–02015 HUT, Finland and
Memphys – Center for Biomembrane Physics, Physics Department,
University of Southern Denmark, Campusvej 55, DK–5230 Odense M, Denmark

Increasing experimental evidence shows that the membrane protein functionality depends on the content of the cell membrane. However, origin of this dependence is not fully understood yet. While some cases can be explained by specific interactions between lipids and proteins, often the generic mechanical properties of lipid bilayers play a significant role too. Previously it has been demonstrated using elastic models or the lateral pressure profile that the mechanical properties of lipid bilayer can have even $10k_{\mathrm{B}}T$ contribution on activation energy. In this work we extend the lateral pressure profile approach to more realistic system containing a mechanosensitivive channel (MscL). We use molecular dynamics and the MARTINI force field to simulate open and closed states of mechanosensitive channel embedded in a DOPC bilayer. Then we present a procedure to calculate the mechanical energy change in the channel gating using 3D pressure distribution calculated from molecular dynamics simulations. We also divide the energy to the area dilation and the shape contribution. According to our results the lateral pressure profile of a lipid bilayer together with the shape change in gating can induce even $30k_{\mathrm{B}}T$ contribution on gating energy of the MscL. This contribution arises from the interfacial tension between hydrophopic and hydrophilic phases in a lipid bilayer.

I. INTRODUCTION

It is known that the functionality of many membrane proteins is sensitive to the lipid environment [1]. Mechanosensitive channels and rhodopsin are classical examples of such proteins [2, 3]. However, while some of these cases can be explained by specific interactions between lipids and proteins, often the generic mechanical properties of lipid bilayers play a significant role too [1, 4]. In the same spirit it has been suggested [5, 6] that anesthetics may work by modifying the mechanical properties of cell membranes.

The effect of mechanical properties of membranes on embedded proteins has been studied using the elastic deformation model [4, 7–12]. In such a model, lipid bilayer deformation energies are usually divided into four components: thickness deformations due to hydrophobic mismatch, area dilation, midplane bending, and curvature frustration. An alternative way to analyze the mechanical energy is to use the so-called lateral pressure profile [13–16], which depicts the non-uniform pressure distribution in a lipid bilayer to arise from the inhomogenous nature of lipid bilayers [17, 18]. The main idea in this approach is that, when a protein goes through a transition where its cross-sectional area profile across the membrane is changed, work has to be done against the pressure profile of the bilayer. For small area changes this work can be written as a function of elastic coefficients, and it can be shown that the elastic deformation model is then just a lower order approximation of the pressure profile model [9, 14, 16].

In the elastic model the deformation energy is related to the membrane's elastic coefficients, which are measurable quantities. Using known elastic coefficients and a simple approximation for the cross-sectional area change, deformation energies have been estimated to be $\sim$10$\mathrm{k_B}$T [9, 10]. Similar estimates have been made using lateral pressure profiles calculated from molecular dynamics (MD) simulations, and the results have been observed to vary between 1–10 $k_{\mathrm{B}}T$. [19–22]. Yet, it has been previously noted [20] that the resulting energy is very sensitive to inaccuracies in the cross-sectional area of membrane proteins. In practice there are no membrane proteins for which the structure of both the closed and the open state are known with sufficient accuracy. For this reason, previous studies have been forced to use simple approximations for protein shape and thus the results have only hinted at the possibility of the protein shape change having a significant contribution to the transformation energy.

The open-close transition of one particular membrane protein, the mechanosensitive channel of large conductance (MscL) is, however, amenable through coarse-grained MD simulations [23]. In this work, we calculate the energy cost of the shape change associated with the activation of this channel, based on the changes in cross-sectional area and lateral pressure profiles during the simulated gating of MscL. In contrast to previous approximations, we find complex cross-sectional area changes that lead to a 30 $k_{\mathrm{B}}T$ shape contribution to the gating process, significantly higher than previously expected.

II. THEORY

In this section, we give a short overview of the existing theoretical framework used to analyze the contribution of a membrane to the energetics of channel gating. We also provide a new way to decompose the gating energy to contributions that result from different physical factors, in particular highlighting the role of the shape change of a protein.

A. Membrane contribution to channel gating energetics

The ratio between the probability of MscL to be open (P_o) or closed (P_c) can been written as

$$\frac{P_o}{P_c} = e^{-\Delta G/k_{\mathrm{B}}T}, \tag{1}$$

where $\Delta G = G_{\mathrm{open}} - G_{\mathrm{closed}}$ is the free energy cost of channel opening [4, 8, 24, 25]. The free energy cost can be decomposed into an area dilation term $\gamma\Delta A$, a membrane deformation term $\Delta E_{\mathrm{membrane}}$, and a change in protein's internal energy $\Delta E_{\mathrm{protein}}$ [4],

$$\Delta G = -\gamma\Delta A + \Delta E_{\mathrm{membrane}} + \Delta E_{\mathrm{protein}}. \tag{2}$$

Using patch clamp experiments, it is possible to measure the ratio P_o/P_c in Eq. 1 as well as the surface tension γ in Eq. 2 [24, 26]. However, ΔA, $\Delta E_{\mathrm{membrane}}$ and $\Delta E_{\mathrm{protein}}$ are difficult to determine independently. Values for ΔA and $\Delta E_{\mathrm{protein}}$ have been achieved [24, 25] by neglecting $\Delta E_{\mathrm{membrane}}$ and then fitting experimental data for P_o/P_c and γ into Eqs. 1 and 2. The results vary roughly between $\Delta A \approx (6.5 - 20)\,\mathrm{nm}^2$ and $\Delta E_{\mathrm{protein}} \approx (18.6 - 51)k_{\mathrm{B}}T$ depending on the fitting procedure [24, 25]. In an alternative approach the $\Delta E_{\mathrm{membrane}}$ term is also neglected, and the gating tensions and sensitivities to tension are gathered from several different studies. By doing so, one has found an approximative result of $\Delta E_{\mathrm{protein}} \approx 14k_{\mathrm{B}}T$ [26].

The possible significance of $\Delta E_{\mathrm{membrane}}$ has been widely recognized recently [4, 7–12, 14–16, 19–21]. In several studies [4, 7–12], the membrane deformation component has been decomposed to separate contributions that are then approximated from known elastic properties of lipid bilayers. The separate contributions to $\Delta E_{\mathrm{membrane}}$ in these studies are usually the hydrophobic mismatch energy, midplane bending energy due to asymmetric lipid bilayer or protein shape, and curvature frustration energy due lipid spontaneous curvature and protein shape. Using elastic properties these components have been predicted to have a significant contribution on the free energy of membrane protein conformations (for a review, see [4]).

In other studies [14–16, 19–22], the membrane deformation energy has been analyzed using pressure profiles of lipid bilayers. The lateral pressure profile $p(z)$ shows the distribution of lateral pressure across an interface as a function of the normal coordinate z. Due to the inhomogenous nature of a lipid bilayer, the lateral pressure profile of a lipid membrane is markedly non-uniform with a characteristic profile. On the one hand, the water-lipid interface of a membrane wants to shrink due to the interfacial tension between water and hydrophobic lipid parts. On the other hand, headgroup and tail regions want to expand due to entropic, electrostatic, and steric interactions [17, 18]. When embedded in a lipid bilayer, a protein feels the non-uniform pressure from the membrane. If the change in cross-sectional area is known between two states of the protein, the work W done against the pressure profile can be calculated from [14–16]

$$W = \int p(z)\Delta A(z)\mathrm{d}z. \tag{3}$$

If the cross-sectional area $\Delta A(z)$ is expanded using a Taylor series, Eq. 3 can also be written in terms of elastic coefficients [14, 16]. Thus, the elastic deformation model is a lower order approximation of the pressure profile model, instead of being an independent one [9, 14, 16]. It is also important to point out that the work calculated using Eq. 3 contains also the pure area expansion, i.e. $\gamma\Delta A$ in Eq. 2.

Previously, the membrane deformation energy arising from a change in the protein shape has been approximated by taking the pressure profile from simulations and assuming a simple geometrical shape transformation, e.g. from a cylinder to a cone, for the protein [15, 19–21]. The calculated energies for MscL vary between $1 - 10k_{\mathrm{B}}T$, which is in agreement with the approximation from the elastic theory as discussed above.

B. Membrane deformation energy decomposed into area dilation, shape contribution, and hydrophobic mismatch terms

Our goal is to analyze the shape dependence of MscL gating energy without approximations with regard to elastic properties, or any assumptions of a simple shape change. For this purpose we decompose the free energy cost of gating (Eq. 2) in a new way as follows,

$$\Delta G = \Delta E_{\mathrm{pp}} + \Delta E_{\mathrm{mm}} + \Delta E_{\mathrm{rest}}, \tag{4}$$

where ΔE_{pp} is the work done against the pressure profile and ΔE_{mm} is the change in hydrophobic mismatch energy. ΔE_{rest} contains all other energy changes, including $\Delta E_{\mathrm{protein}}$ from Eq. 2, possible midplane bending and any changes in specific lipid-protein interactions. As is shown below, ΔE_{pp} contains area dilation and curvature frustration components.

To calculate ΔE_{pp} we first use Eq. 3 to calculate the mechanical work of creating a cavity with cross-sectional area $A(z)$ into a bilayer having the pressure profile $p(z)$ [14, 19],

$$W = \int p(z)A(z)\mathrm{d}z. \tag{5}$$

Then we decompose the cross-sectional area $A(z)$ into two components: a constant average area A_{o} and a z-dependent

shape variation $\delta A(z)$ around A_o:

$$A(z) = A_o + \delta A(z). \tag{6}$$

Inserting this decomposition into Eq. 5 we get

$$\begin{aligned} W &= \int p(z)[A_o + \delta A(z)]\mathrm{d}z \\ &= A_o \int p(z)\mathrm{d}z + \int p(z)\delta A(z)\mathrm{d}z. \end{aligned} \tag{7}$$

By using the connection [27] between the pressure profile and the surface tension of a membrane $\gamma = -\int p(z)\mathrm{d}z$ and by defining $W_{\mathrm{shape}} \equiv \int p(z)\delta A(z)\mathrm{d}z$ we arrive at

$$W = -\gamma A_o + W_{\mathrm{shape}}(\gamma). \tag{8}$$

The first term gives the work done against a cylindrical inclusion with an area of A_o and the second term the work done against shape variations $\delta A(z)$. It should be noted that since both $A(z)$ and $p(z)$ depend on the total tension γ, also W_{shape} depends implicitly on γ.

To estimate ΔE_{pp} we first have to calculate the mechanical work of insertion for both closed and open state separately using Eq. 5,

$$\begin{aligned} W_{\mathrm{closed}} &= \int p_{\mathrm{closed}}(z) A_{\mathrm{closed}}(z)\mathrm{d}z \\ W_{\mathrm{open}} &= \int p_{\mathrm{open}}(z) A_{\mathrm{open}}(z)\mathrm{d}z. \end{aligned} \tag{9}$$

Then we need to calculate the work $-W_{\mathrm{closed}}$ done when a closed channel is removed from a membrane and the work W_{open} done when an open channel is inserted back into the membrane. ΔE_{pp} is then equal to the net work done in the process, given by

$$\begin{aligned} \Delta E_{\mathrm{pp}} &= W_{\mathrm{open}}(\gamma) - W_{\mathrm{closed}}(\gamma) \\ &= -\gamma \Delta A_o + \Delta E_{\mathrm{shape}}(\gamma), \end{aligned} \tag{10}$$

where the decomposition of Eq. 8 is applied. Now we see that ΔE_{pp} indeed contains the area dilation term of Eq. 2. The second term $\Delta E_{\mathrm{shape}}(\gamma)$ corresponds to the curvature frustration term in elastic models. In this work we calculate these terms from molecular dynamics simulation models without the assumptions underlying the elastic theory. We also estimate the hydrophobic mismatch term ΔE_{mm}. By visual inspection we do not see significant midplane bending and thus we neglegt the midplane bending term. All other energy terms which we do not analyze are joined together and described through ΔE_{rest}. Only ΔE_{pp} and ΔE_{mm} are assumed to depend on tension.

We determine A_o, $A(z)$ and $p(z)$ for both the open and the closed state of MscL using molecular dynamics simulations as described in section III. Then we can calculate $\gamma \Delta A_o$ and ΔE_{pp} using Eqs. 9 and 10. Finally we can also determine the shape contribution using Eq. 10.

III. METHODS

The objective of the work is to study the components of mechanical work in MscL gating using Eqs. 9 and 10. In order to do so, we need to calculate the cross-sectional area $A(z)$ and the pressure $p(z)$ felt by the protein under different tensions γ for both the open and the closed state. We will also need to determine the average change of the cross-sectional area ΔA_o in the closed-open transition.

A. Simulated systems

The MARTINI coarse-grained (CG) model [28, 29] and GROMACS 4.0 simulation package [30] were used for all the molecular dynamics simulations. All simulation systems were coupled to a Berendsen temperature bath at 310 K and surface tension was kept constant by using a semi-isotropic Berendsen pressure coupling [31]. A MARTINI CG model of MscL has been shown to activate when the membrane is subjected to a high enough tension [23, 32]. In this work we have used the model to analyze the release of mechanical energy in a lipid bilayer when a channel is opened.

A closed state MscL from *Tuberculosis Mycobacterium* has been resolved [33] by x-ray crystallography (PDB: 2OAR) and was used as the basis for the CG model. The protein was first inserted into a bilayer of 504 DOPC lipids and the system was solvated with 17565 water beads after which the system was simulated for 12 ns to equilibrate the system. Note that the times reported in this manuscript are scaled by a factor of 4 to account for the faster effective sampling in MARTINI as judged by a higher diffusion rate in the liquid phase [28]. To open the channel, the tension was gradually increased in a stepwise manner from 0 mN/m to 60 mN/m, in 10 mN/m steps. Simulation time in each step was 12 ns. Then the tension was further increased to 65 mN/m and the activation of MscL was observed after simulation of 1.88 μs. The system with the open channel was solvated with 6995 additional water beads (totaling 24560 water beads) to avoid any interaction between periodic images, as the system gets thinner at higher tensions. The final structures obtained at each level of tension were subsequently used as starting points for two sets of simulations; one for the closed (set 1), and one for the open state (set 2).

In set 1, the closed structure was simulated for 2.4 μs at tension levels of 0, 10, 20, 30, and 40 mN/m. Small tension-induced changes in the protein structure were observed during the simulation, but the protein stayed inactive in all cases. By inactive we mean that there is no significant water flux through the channel.

In set 2, the post-activation, i.e. the open state of MscL, was simulated for the same range of tensions (0, 10, 20, 30 and 40 mN/m). The length of the simulation was 1.92 μs for the tensions 30 and 40 mN/m, extended to 3.84 μs for the lower tensions 0, 10, and 20 mN/m due to longer equilibration time. Once more some changes in the protein structure occurred in response to the tension, but the protein stayed active as judged from a significant water flow through the channel.

The systems were considered to be in a metastable state after the area of the membrane and the radius of gyration of the protein converged. This state was reached after approximately 400-500 ns in most cases, except for the open channel at low tension which required (2-2.5) μs equilibration time. The analysis of area and pressure profiles was performed after this time point in each case.

B. Calculation of the area profile

To exploit Eqs. 9 we need the cross sectional area profile which the membrane protein complex occupies from the bulk bilayer. The area (for each membrane normal coordinate value) was defined to contain the protein itself and all the water and lipid beads which are in straight line between any protein bead and the center of the protein.

Using this definition the area as a function of the position along the membrane normal was determined in the following way. First the system was divided into a 3D grid of 0.3 nm cubic cells. Each grid cell was then labeled either as type 0 for empty cells, as type 1 for cells that contain at least one protein bead, or as type 2 for occupied cells that do not contain protein beads. All type 0 cells that were next to a type 1 cell were then switched to a type 1 to include possible empty cells between bulk bilayer and the protein in the protein area calculation. Then for each position z along the membrane normal, the protein-lipid boundary was determined. This was done by tracking the path from the center of the protein to the edge of the grid to locate the farhest type 1 cell. All the cells in this path upto the farthest cell of type 1 were then also marked as type 1. This was repeated for all the edge cells to take all the directions into account. The area of all type 1 cells was then added up and defined as the cross-sectional area of the protein with corresponding z coordinate. This procedure was repated for all values of z.

The constant average area $A_{\rm o}$ defined in Eq. 6 was calculated as the average cross-sectional area over all z considered to be in the bilayer region. In this work "bilayer region" is defined as the region where lipid density is larger than water density.

C. Calculation of pressure profiles

Generally the pressure field of a system is defined as the pressure tensor $\mathbf{P}(\mathbf{r})$, which depends on all spatial coordinates [34]. From geometrical symmetry and the mechanical stability condition $\nabla \cdot \mathbf{P} = 0$ it follows that $\mathbf{P}$ is diagonal, P_{zz} is constant, and lateral components are equal and depend only on the normal coordinates $P_{xx}(z) = P_{yy}(z)$ for a homogeneous fluid bilayer [27]. The so-called lateral pressure profile used in Eqs. 3, 5 and 9 is defined as $p(z) = (P_{xx}(z) + P_{yy}(z))/2 - P_{zz}$ [27].

An inclusion, such as a protein, breaks the symmetry in the (membrane) xy-plane. Protein-lipid interactions generate line tension between the protein and the lipids, which leads to different lateral pressures (and tensions) in the protein and lipid regions [35]. In principle the line tension could be determined from the tension difference between the inside of the inclusion and the bulk bilayer [35]. However, it is not possible to define a clear bulk region inside a realistic protein inclusion due to the small size and the complex structure of the object. Thus, in practice the line tension between a protein and a lipid membrane is hard to define.

Instead, we assume that a protein inclusion is put into a bulk bilayer, where $P_{xx}(z) = P_{yy}(z)$. Then we calculate the pressure in the bulk membrane and use this pressure in Eqs. 3, 5 and 9 to calculate the work done when a protein is included into the membrane. The advantage of this approach is that we do not need to take into account the direction of the membrane-protein boundary because the lateral components are equal and the pressure is equal in all directions on the plane. The protein shape is taken implicitly into account in the calculation of the cross-sectional area.

To calculate the pressure in the bulk bilayer region, the system was first divided into a 3D grid with an edge length of 0.3 nm. The local pressure tensor was then analyzed for each grid point using a recently developed method [34]. The pressure profile in the bulk membrane was obtained by averaging over the x and y coordinates located in the bulk region of the bilayer. The bulk region is defined to start where the thickness of the bilayer is no longer perturbed by the protein inclusion. This condition corresponds to approximately 1 nm from the protein surface. This method is essentially the same as the one in traditional lateral pressure profile calculations for a bulk lipid bilayer [36, 37], with the exception that averages are now taken only over the bulk membrane phase instead of the whole system. In principle, it is possible that one combines a pressure profile from a pure membrane simulation with an area profile from a membrane protein simulation to achieve the same results.

IV. RESULTS AND DISCUSSION

Below, we first describe the different states of the protein together with the calculated shape and pressure profiles. Next, we calculate the work associated with embedding the channel in its different states into the membrane, followed by the calculation of the mechanical energy contribution to the gating process. Further, we move on by dividing the mechanical energy into the area dilation and shape change contributions and by making a link between the shape change and interfacial tension. Finally, we discuss the effect of hydrophobic mismatch.

A. Protein states used in analysis

Since our goal is to calculate ΔE_{pp} as defined in Eq. 10, the relevant properties we need to quantify are the cross-sectional area of the protein and the pressure felt by the protein. The cross-sectional area profiles and the pressure exerted on the protein are shown in Fig. 1 for both the open and closed states at tensions between 0 – 40 mN/m.

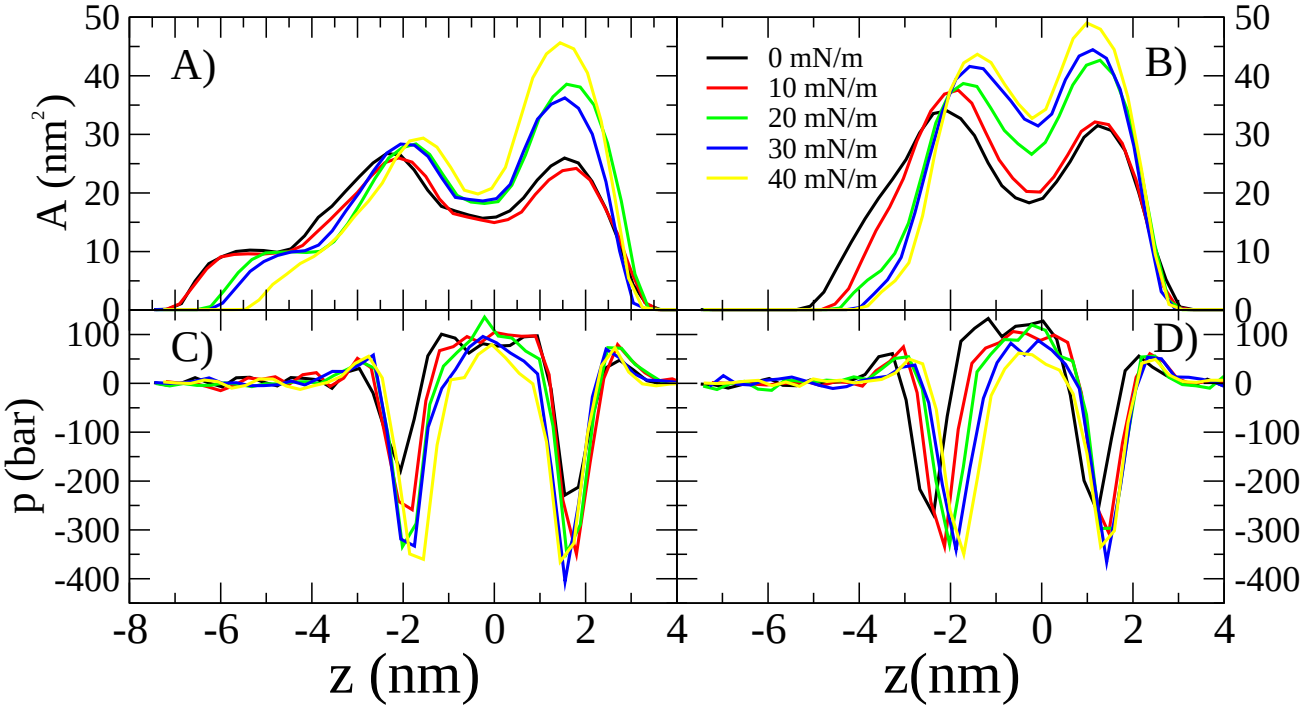

FIG. 1: A) and B) Cross-sectional area profiles for the closed and the open channel under different tensions, respectively. C) and D) Pressure profiles felt by the closed and the open channel under different tensions, respectively. Negative z values denote the cytoplasmic side. The z-axis is set such that the center of mass of the protein is in the $z = 0$ for all the systems.

A first observation is that in both states the largest cross-sectional area is found at the location of the interfacial peak in the pressure profile. Besides the basic shape of the protein, a plausible explanation for this is that the protein adapts to the pressure distribution (exerted by the bilayer) by expanding itself in the interfacial region. This expansion lowers the energy of the bilayer because the area of close contact between hydrophobic parts and water shrinks.

From Fig. 1A we see that the area profile is immediately changed when tension is increased above 10 mN/m even though the channel still remains closed, i.e., there is no significant flux through the channel. In particular, we see a tension dependent area increase on the extracellular side of the protein while the cross-sectional area on the cytoplasmic side is between $25-30\,\mathrm{nm}^2$ for all tensions. Intriguingly, from Fig. 1B we see that the largest cross-sectional area difference between the open and the closed state is on the cytoplasmic side. The cross-sectional area for the open state is between $35-45\,\mathrm{nm}^2$ for all tensions.

These observations suggest that the expansion of the extracellular side is not sufficient for the gating of MscL but that it requires the expansion of the cytoplasmic side as well. This observation is in agreement with the idea of a "hydrophobic lock" located in the cytoplasmic region [38], and with the observation that asymmetric inclusion of lysolipids on the extracellular side opens the channel [39]. When lipids are added to the extracellular side, the relative tension of the extracellular side will decrease and the relative tension on the cytoplasmic side will increase [40]. Increased tension would prefer expansion of the cytoplasmic side of the protein, which according to our results is required for gating.

Inspired by the results shown in the Fig. 1 we divide the tension-induced gating into two steps: 1) an immediate expansion of the periplasmic side that does not open the channel and 2) an eventual expansion of the cytoplasmic side that opens the channel. These steps are illustrated in Fig. 2. The closed state under tension is marked with a star. In the next section we calculate ΔE^1_{pp} for step (transition) 1 and ΔE^2_{pp} for transition 2. This two-stage opening is in full accordance with earlier models suggesting an initial tilting of trans-membrane helices followed by a lateral expansion of the channel core [3, 24].

B. Mechanical work for protein insertion

The pressure profiles and cross-sectional area profiles, shown in Fig. 1, were used to calculate (Eq. 9) the mechanical work exerted by a bilayer when the MscL protein is embedded into a bilayer. Three different states of the protein were considered, namely the closed, closed-expanded, and open (cf. Fig. 2). Values for the closed structure under tensions are calculated using the area profile of the initial closed structure in zero tension and pressure profiles for systems under tension. This corresponds the situation where the bilayer is under tension but the structure of the protein is not changed yet. The results are shown in Fig. 3 A.

The calculated energies are negative. What is more, they

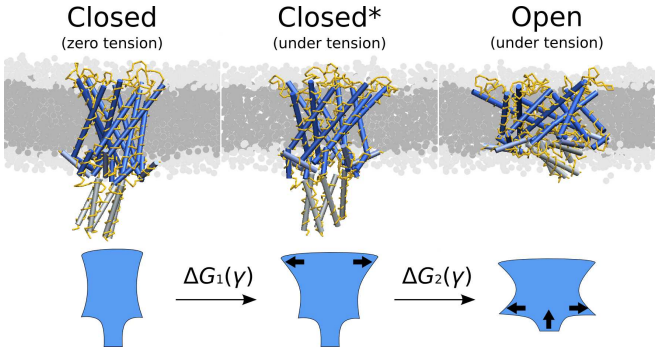

FIG. 2: The gating process divided into immediate deformation after the tension increase (step 1) and actual gating (step 2). A schematic presentation of the shape change of the protein during the close-to-open transition is shown at the bottom.

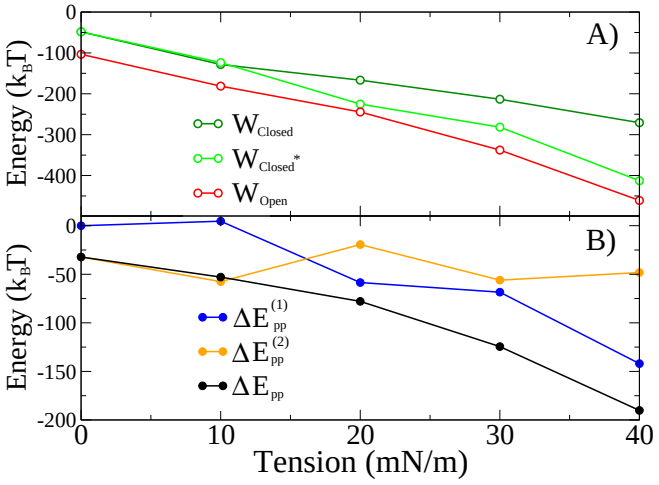

FIG. 3: A) Release of mechanical energy due to an inclusion of MscL in different states under different tensions calculated by Eq. 9. B) Change of mechanical energy between different states under different tensions calculated by Eq. 10.

become even more negative when tension is increased, which means that the bilayer energy decreases when an inclusion such as MscL is inserted. Under tension this is expected because any inclusion that decreases the bilayer area would release energy by γA_0 [8]. However, we see a significant negative energy even without a tension when the area dilation component is clearly zero. This is due to the large area of the protein at the interfacial region which decreases contacts between hydrophobic parts of the membrane and water. Our results suggest that there is a significant decrease in energy if a protein adapts to bilayer stress by increasing its area in the interfacial region. This behaviour might also play an important role e.g. in membrane protein folding, which is known to depend on bilayer properties at least for some proteins [41, 42].

C. Mechanical energy of gating

The results shown in Fig. 3A enable us to calculate (Eq. 10) the mechanical work done by the bilayer in both gating steps, ΔE^1_{pp} and ΔE^2_{pp}. The results are shown in Fig. 3B, along with the total work $\Delta E_{pp} = \Delta E^1_{pp} + E^2_{pp}$. The total mechanical work done by bilayer is always negative because the energy for the open state is always lower compared to the closed state (Fig. 3). Thus, the bilayer energy is always favorable for the open state, even at a state of zero tension.

From Eq. 1 we see that when $P_o/P_c = 1$, then $\Delta G = 0$ and the probability to be in the open state is equal to the probability to be in the closed state. Experimentally the tension for which $P_o/P_c = 1$ is approximately 10 mN/m [24, 25]. By neglecting the $\Delta E_{\mathrm{membrane}}$ term from Eq. 2 and by fitting to experimental data, one has found a result of $\Delta E_{\mathrm{protein}} \approx (18.6 - 51) k_{\mathrm{B}}T$ [24, 25]. Based on our results we can now try to make a more accurate estimate.

While the gating tension is about 10 mN/m in experiments, in simulations with feasible time scales we need higher tensions (65 mN/m) to observe the opening of the channel. If the simulation time scale could be extended considerably, a significant drop in the simulated gating tension would be expected; yet at the moment the current computational resources limit us to enforce gating to take place at the microsecond timescale instead of the natural, millisecond timescale of MscL gating [43], warranting the use of higher tension.

Nevertheless, if we assume a 10 mN/m gating tension and neglect the ΔE_{mm} term from Eq. 4, we see from the results in Fig. 3 B) that $\Delta E_{\mathrm{rest}} \approx 50 k_{\mathrm{B}}T$. The neglect of the hydrophobic mismatch term ΔE_{mm} is justified in section IV F. The ΔE_{rest} contains the change in protein's internal energy $\Delta E_{protein}$ and changes in specific lipid-protein interactions. We do see significant mid-plane bending in simulations by visual inspection thus we assume that its contribution is negligible. Under these assumptions we arrive at a gating energy that is similar to the largest energies achieved by fitting to experimental data. The difference is that our area difference is smaller than previously suggested [25] and that almost half of the energy originates from the shape deformation as detailed in the next section.

D. Gating work divided into area and shape contributions

In experimental studies where the gating energy $\Delta E_{\mathrm{protein}}$ was calculated, it was assumed that the tension-dependent free energy release arises completely from area dilation [24–26]. However, in our analysis we take into account both the area dilation and the shape change contribution as in Eq. 10. Using our results we can calculate both contributions separately.

The pure area dilation component in Eq. 10, $\gamma \Delta A_0$, can be calculated if the change in constant average cross-sectional area is known. Average cross-sectional areas are calculated as described in section III. Average areas for the closed and the open state under different tensions are shown in Fig. 4 A). In Fig. 4 B), the changes in average area for both steps separately

and for the complete gating process are shown.

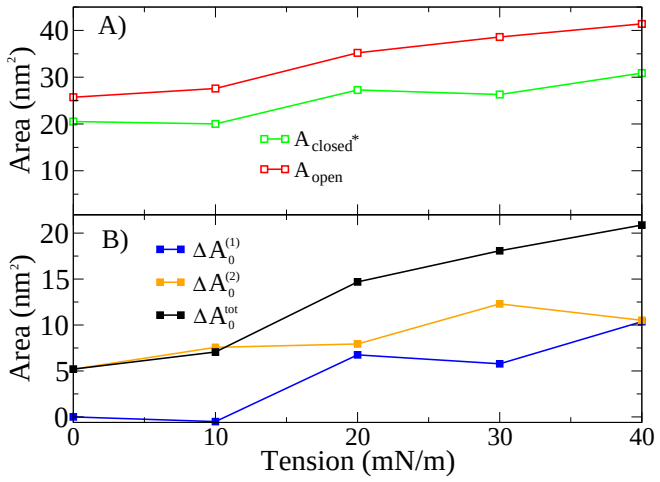

FIG. 4: A) Average areas of closed and open states under different tensions. B) Changes in average areas in different steps.

The left hand side of Eq. 10, $\Delta E_{\rm pp}$, has already been calculated in the previous section (cf. Fig. 3 B) allowing us to extract the shape contribution of the mechanical work $\Delta E_{\rm shape}$. In Fig. 5 we show the area dilation $\gamma\Delta A$, the shape contribution $\Delta E_{\rm shape}(\gamma)$, and the total bilayer mechanical work $\Delta E_{\rm pp}(\gamma)$.

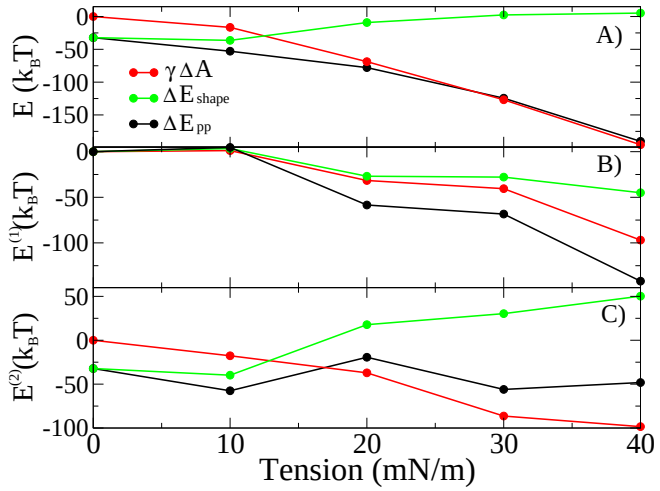

FIG. 5: Gating work divided into area and shape contributions; A) for complete gating, B) for step 1, and C) for step 2.

At zero tension the area component is obviously zero. Thus the $\sim 30 k_{\rm B}T$ preference for the open state under these stress-free conditions must result from the shape contribution as clearly noticed from Fig. 5A. As expected, when tension is increased the area dilation contribution becomes more negative, because tension prefers the open state due to its larger area. However, the shape contribution behaves the opposite. From Fig. 5A we see that with increasing tension the shape preference for the open state decreases and at a tension of 20 mN/m the preference is already practically lost. Due to competition between these contributions the dependence of work on tension is weaker than expected only by looking at the area dilation component. In an experimental fit, this slope is related to the area change in gating [24, 25]. Our results thus suggest that the area change and the gating energy calculated from the experimental fit are too small because the shape energy is not taken into account. The slight non-linearity in tension dependence found recently [25] could arise from the shape dependence of the opening probability.

By comparing Figs. 5B and 5C we see that at 0 mN/m and 10 mN/m most of the work is done in step 2. The reason for this is that the closed state does not deform under these tensions (cf. Fig. 1A). With a higher tension there is an immediate deformation of the closed state (step 1) and also work related to that. In step 1 the area and shape contributions are close to each other, being negative and getting more negative with increasing tension. This is understandable because in step 1 the extracellular side undergoes considerable expansion with higher tensions leading to significant area and shape contributions (cf. Fig. 1). However, the energetics of step 2 behaves differently. The area component decreases almost linearly from 0 to $\sim 100 k_{\rm B}T$ but the shape component behaves almost the opposite, weakening the tension dependence of $\Delta E_{pp}(\gamma)$.

E. Large shape contribution comes from interfacial tension

In the previous section we argued that the energy contribution from a shape change of a protein, in our case MscL, can be as large as $30\,k_{\rm B}T$. This is significantly higher than previous estimates, which vary between $(0-10)k_{\rm B}T$ [9, 10, 19–22]. The main reason for the difference is that in previous studies one assumed simple cylinder-cone-like shape transitions. In our simulations we see large area changes at the location of the interface between the hydrophobic interior of the bilayer and the aqueous surroundings. When the area of protein is increased at this region, it reduces the contact between water and the hydrophobic part of a bilayer, thus lowering the hydrophobic energy of the bilayer.

To give an order of magnitude approximation for the hydrophobic energy change associated with a nanoscopic area change, we calculate the energy release when the area of a interface under a tension of 30 mN/m is decreased by 5 $\rm nm^2$. 30 mN/m is a reasonable approximation for the hydrophobic energy density of the hydrocarbon water interface [17], and 5 $\rm nm^2$ is a realistic local change for the protein area (see our results above and [24, 25]). The released energy can be simply approximated by $\Delta W = -\gamma\Delta A \approx -30\,\text{mN/m} \times 5\text{nm}^2 \approx -35 k_{\rm B}T$. This demonstrates that small area changes at the lipid-water interface can have a significant energetic effect.

F. Hydrophobic mismatch

In previous sections we have omitted the hydrophobic mismatch energy change in gating, ΔE_{mm}. This cannot be neglected without justification because the gating tension of

MscL has been shown to depend on lipid tail length [3]. The hydrophobic mismatch component may be important in tension-induced gating as the bilayer gets thinner when tension is increased. To analyze the significance of this effect we use a simple estimate for the elastic cost of adaption of a lipid bilayer due to hydrophobic mismatch [44],

$$E_{mm} = N_{\mathrm{L}} \times ((6.1 \pm 0.4)\mathrm{nm}^{-1}) k_{\mathrm{B}} T \frac{(l_{\mathrm{L}} - l_{\mathrm{o}})^2}{l_{\mathrm{o}}}, \quad (11)$$

where $N_{\mathrm{L}} = 29$ is the approximate number of lipid molecules in the first shell surrounding the protein, l_{L} is the height of the monolayer next to the protein, and l_{o} is the height of the unperturbed monolayer. This equation has been shown to give the correct dependence of the MscL bilayer partitioning coefficient on lipid tail length close to the optimal one (16 carbons) [44]. As seen below, in our case changes in bilayer thickness are rather small and we are close to the optimal bilayer thickness.

To analyze the hydrophobic mismatch, we calculate the thickness of the lipid bilayer as a function of distance from protein boundary. Deformation in bilayer thickness as a function of distance from the protein boundary is shown in Fig. 6.

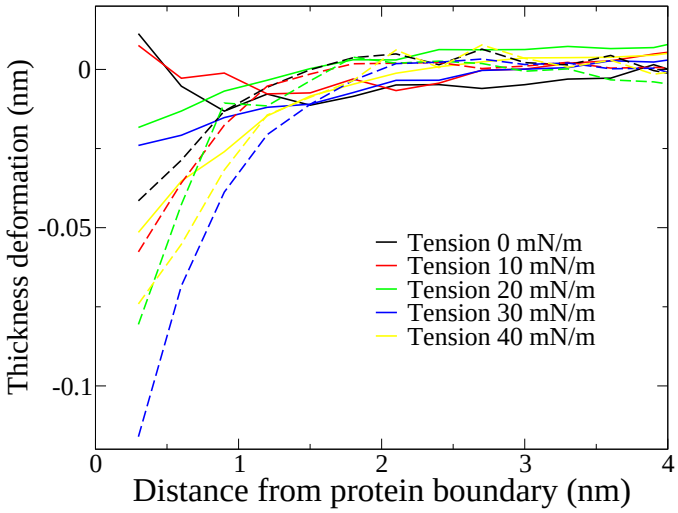

FIG. 6: Thickness deformations as a function of distance from protein boundary. Solid line is for the closed state, and dashes line for the open state.

From Fig. 6 we see that the closed state does not have a mismatch with a tension lower than 20 mN/m, but the open state has a small mismatch with all tensions such that it is always thinner than the membrane. However, the mismatch is very small for each system. The largest thickness deformation is around 0.1 nm, which is in agreement with earlier atomistic molecular dynamics simulations [45–47]. To approximate the largest hydrophobic mismatch energy in our systems, we take the open state at 30 mN/m for which $l_{\mathrm{o}} \approx 2$ nm and $(l_{\mathrm{L}} - l_{\mathrm{o}}) \approx 0.05$ nm. Using Eq. 11 with these values we get $E_{mm} \approx 0.2 k_{\mathrm{B}} T$, which is negligible. This means that the hydrophobic mismatch energy does not contribute significantly to the gating energy in the step 2. To also approximate the order of magnitude of mismatch energy change in the step 1 we calculate the difference between the monolayer thickness in zero tension and under each tension. This would be the maximum hydrophopic mismatch change in the step 1. Then using Eq. 11 we get energies which are always less than 1% of mechanical energies under corresponding tension in fig. 5. This suggest that the hydrophopic mismatch energy is also negligible in the step 1.

V. CONCLUSIONS

Based on coarse-grained simulations of the gating of a mechanosensitive membrane protein, MscL, we calculated the differences in bilayer mechanical energy during the gating process. We decomposed this energy into an area dilation component and a component associated with protein shape. These components were calculated using the cross-sectional area of the protein and the pressure felt by the protein. We found that the bilayer prefers an open state even at zero tension due to a large energetic component of $30 k_{\mathrm{B}} T$ arising from shape changes. This contribution is possibly important when interpreting, for example, patch clamp experiments to any protein which undergoes changes in cross-sectional area. When tension is increased, this component decreases, but then the area dilation component gives a significant preference for the open state.

Our results show that the shape of a protein is likely to have an even larger influence on protein energetics than what has been previously estimated ($(0 - 10) k_{\mathrm{B}} T$ [9, 10, 19–22]). The reason for the difference is the assumption of very simple protein shapes assumed in previous studies. We observed that MscL adapts to the pressure profile of a lipid bilayer by taking a shape which is expanded at the interfacial region. This shape change causes a significant energy release, reducing the interfacial energy between the lipid bilayer interior and the aqueous surroundings.

We conclude that the pressure profile can have an important role in triggering conformational changes of membrane proteins. It is important to note that the analysis performed in this work does apply not only to MscL but also to any protein which undergoes similar conformational changes. Even transformations under zero tension can have significant mechanical energy components due to non-uniform protein shape changes within the bilayer.

Acknowledgements: We acknowledge the support given by the Academy of Finland (OHSO, IV) and the Finnish National Graduate School in Nanoscience (OHSO). The Netherlands Organisation for Scientific Research (NWO) supported this work through Top grant 700.57.303 (SJM, ML). CSC – IT Center for Science Ltd and the HorseShoe computing cluster at the University of Southern Denmark are thanked for computing resources.

[1] A. G. Lee, Biochim. Biophys. Acta - Biomembranes, **1666**, 62 (2004).
[2] M. F. Brown, Chem. Phys. Lipids, **73**, 159 (1994).
[3] E. Perozo, A. Kloda, D. M. Cortes, and B. Martinac, Nature Struct. Biol., **9**, 696 (2002).
[4] R. Phillips, T. Ursell, P. Wiggins, and P. Sens, Nature, **459**, 379 (2009).
[5] R. S. Cantor, Biochemistry, **36**, 2339 (1997).
[6] R. S. Cantor, Toxicol. Lett., **100-101**, 451 (1998).
[7] P. Wiggins and R. Phillips, Biophys. J., **88**, 880 (2005), ISSN 0006-3495.
[8] T. Ursell, J. Kondev, D. Reeves, P. A. Wiggins, and R. Phillips, in *Mechanosensitivity in Cells and Tissues 1: Mechanosensitive Ion Channels*, edited by A. Kamkin and I. Kiseleva (Springer-Verlag, 2008).
[9] D. Reeves, T. Ursell, P. Sens, J. Kondev, and R. Phillips, Phys. Rev. E, **78**, 041901 (2008).
[10] T. Ursell, K. C. Huang, E. Peterson, and R. Phillips, PLoS Comput Biol, **3**, e81 (2007).
[11] O. S. Andersen and R. E. Koeppe, Annu Rev Biophys Biomol Struct., **36**, 107 (2007).
[12] M. S. Turner and P. Sens, Phys. Rev. Lett., **93**, 118103 (2004).
[13] R. S. Cantor, J. Phys. Chem. B, **101**, 1723 (1997).
[14] R. S. Cantor, Chem Phys Lipids, **101**, 45 (1999).
[15] R. S. Cantor, Biophys. J., **82**, 2520 (2002).
[16] D. Marsh, Biophys. J., **93**, 3884 (2007).
[17] D. Marsh, Biochim. Biophys. Acta, **1286**, 183 (1996).
[18] J. N. Israelachvili, *Intermolecular and surface forces* (Academic Press, London, 1985).
[19] J. Gullingsrud and K. Schulten, Biophys. J., **86**, 3496 (2004).
[20] O. H. S. Ollila, T. Rog, M. Karttunen, and I. Vattulainen, J. Struct. Biol., **159**, 311 (2007).
[21] P. S. Niemelä, O. H. S. Ollila, M. T. Hyvönen, M. Karttunen, and I. Vattulainen, PLoS Comp. Biol., **3**, 304 (2007).
[22] H. Jerabek, G. Pabs, M. Rappolt, and T. Stockner, J. Am. Chem. Soc., **132**, 7990 (2010).
[23] S. Yefimov, E. van der Giessen, P. R. Onck, and S. J. Marrink, Biophys. J., **94**, 2994 (2008), ISSN 0006-3495.
[24] S. I. Sukharev, W. J. Sigurdson, C. Kung, , and F. Sachs, J Gen Physiol, **113**, 525 (1999).
[25] C.-S. Chiang, A. Anishkin, and S. Sukharev, Biophys. J., **86**, 2846 (2004).
[26] O. P. Hamill and B. Martinac, Physiological Reviews, **81**, 685 (2001).
[27] J. S. Rowlinson and B. Widom, *Molecular Theory of Capillarity* (Clarendon press, Oxford, 1982).
[28] S. Marrink, H. Risselada, S. Yefimov, D. Tieleman, and A. de Vries, J. Phys. Chem. B, **111**, 7812 (2007).
[29] L. Monticelli, S. K. Kandasamy, X. Periole, R. G. Larson, D. P. Tieleman, and S.-J. Marrink, J. Chem. Theor. Comp., **4**, 819 (2008).
[30] B. Hess, C. Kutzner, D. van der Spoel, and E. Lindahl, J. Chem. Theory Comput., **4**, 435 (2008).
[31] H. J. C. Berendsen, J. P. M. Postma, W. F. van Gunsteren, A. DiNola, and J. R. Haak, J. Chem. Phys., **81**, 3684 (1984).
[32] M. Louhivuori, H. J. Risselada, E. G. Giessen, and S. J. Marrink, submitted to PNAS.
[33] S. Steinbacher, R. Bass, P. Strop, and D. C. Rees, **58**, 1 (2007).
[34] O. H. S. Ollila, H. J. Risselada, M. Louhivuori, E. Lindahl, I. Vattulainen, and S. J. Marrink, Phys. Rev. Lett., **102**, 078101 (2009).
[35] V. S. Markin and F. Sachs, Phys. Biol., **1**, 110 (2004).
[36] E. Lindahl and O. Edholm, J. Chem. Phys., **113**, 3882 (2000).
[37] O. H. S. Ollila and I. Vattulainen, "Molecular simulations and biomembranes: From biophysics to function," (RCS, 2010) Chap. Lateral pressure profiles in Lipid Membranes: Dependence on molecular composition.
[38] K. Yoshimura and M. Sokabe, J. R. Soc. Interface, **7**, S307 (2010).
[39] E. Perozo, Curr. Opin. Struc. Biol., **13**, 432 (2003).
[40] S. Esteban-Martin, H. J. Risselada, J. Salgado, and S. J. Marrink, J. Am. Chem. Soc., **131**, 15194 (2009).
[41] P. J. Booth, Biochim. Biophys. Acta - Biomembranes, **1610**, 51 (2003), ISSN 0005-2736.
[42] C. A. Minetti and D. P. Remeta, Archives of Biochemistry and Biophysics, **453**, 32 (2006), ISSN 0003-9861, highlight Issue on Macromolecular Interactions Honoring Ann Ginsburg.
[43] A. Anishkin, C.-S. Chiang, and S. Sukharev, J Gen Physiol, **125**, 155 (2005).
[44] D. Marsh, Biophys. J., **94**, 3996 (2008).
[45] D. E. Elmore and D. A. Dougherty, Biophys. J., **85**, 1512 (2003), ISSN 0006-3495.
[46] G. Debret, H. Valadi, A. M. Stadler, and C. Etchebest, Proteins: Structure, Function, and Bioinformatics, **71**, 1183 (2008).
[47] J. Jeon and G. A. Voth, Biophys. J., **94**, 3497 (2008), ISSN 0006-3495.

[48] Author to whom correspondence may be addressed. E-mail: samuli.ollila@tut.fi.